SENSOR *and* MODEL INTEGRATION
for the
RAPID PREDICTION
of
CONCURRENT FLOW FLAME SPREAD

Presented by
ADAM COWLARD

For the degree of
DOCTOR *of* PHILOSOPHY

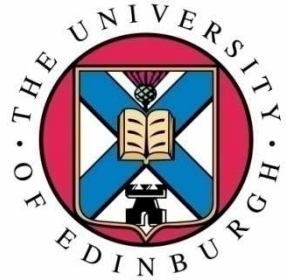

THE UNIVERSITY *of* EDINBURGH
2009

To Mum, Dad, Jonathan and Cecília.

Declaration

This thesis and the work described within has been completed solely by Adam Cowlard at the BRE Centre for Fire Safety Engineering at the University of Edinburgh, under the supervision of Prof. Jose L. Torero, Dr. Stephen Welch, and Dr. Debbie Smith. Where others have contributed or other sources are quoted, references are given.

Adam Cowlard
February 2009

Abstract

Fire Safety Engineering is required at every stage in the life cycle of modern-day buildings. Fire safety design, detection and suppression, and emergency response are all vital components of Structural Fire Safety but are usually perceived as independent issues. Sensor deployment and exploitation is now common place in modern buildings for means such as temperature, air quality and security management. Despite the potential wealth of information these sensors could afford fire fighters, the design of sensor networks within buildings is entirely detached from procedures associated to emergency management. The experiences of Dalmarnock Fire Test Two [15] showed that streams of raw data emerging from sensors lead to a rapid information overload and do little to improve the understanding of the complex phenomenon and likely future events during a real fire. Despite current sensor technology in other fields being far more advanced than that of fire, there is no justification for more complex and expensive sensors in this context. In isolation therefore, sensors are not sufficient to aid emergency response.

Fire modelling follows a similar path. Two studies of Dalmarnock Fire Test One demonstrate clearly the current state of the art of fire modelling. A Priori studies by Rein et al. [65] showed that blind prediction of the evolution of a compartment fire is currently beyond the state of the art of fire modelling practice. A Posteriori studies by Jahn et al. [45] demonstrated that even with the provision of large quantities of sensor data, video footage, and prior knowledge of the fire; producing a CFD reconstruction was an incredibly difficult, laborious, intuitive and repetitive task. Issues of accuracy aside, these models demand heavy resources and computational time periods that are far greater than the time associated with the processes being simulated. To be of use to emergency responders, the output would need to be produced faster than the event itself with lead time to enable planning of an intervention strategy. Therefore in isolation, model output is not robust or fast enough to be implemented in an emergency response scenario.

Fire fighting is therefore left as an isolated activity that does not benefit from sensor data or the potential of modelling the event. In isolation sensors and fire modelling are found lacking. Together though they appear to form the perfect compliment. Sensors provide a plethora of information which lacks interpretation. Models provide a method of interpretation but lack the necessary information to make this output robust. Thus a mechanism to achieve accurate, timely predictions by means of theoretical models steered by continuous calibration against sensor measurements is proposed.

The concept of super-real time predictions steered by measurements is studied in the simple yet meaningful scenario of concurrent flow flame spread. Experiments have been conducted with PMMA slabs to feed sensor data into a simple analytical model. Numerous sensing techniques have been adapted to feed a simple algebraic expression from the literature linking flame spread, flame characteristics and pyrolysis evolution in order to model upward flame spread. The measurements are continuously fed to the computations so that projections of the flame spread velocity and flame characteristics can be established at each instant in time, ahead of the real

flame. It was observed that as the input parameters in the analytical models were optimised to the scenario, rapid convergence between the evolving experiment and the predictions was attained.

List of Publications

- **A. Cowlard**, W. Jahn, C. Abecassis-Empis, G. Rein, JL. Torero, "*Sensor Assisted Fire Fighting*", Fire Technology, In Press 2008.

- **A. Cowlard**, L. Auersperg, J-B. Richon, G. Rein, S. Welch, A. Usmani, JL. Torero, "*A Simple Methodology for Sensor Driven Prediction of Upward Flame Spread*", Turkish Journal of Engineering and Environmental Sciences, 31 (2007), 403 – 413.

- **A. Cowlard**, T. Steinhaus, C. Abecassis-Empis, JL. Torero, "*Test Two: The 'Controlled Fire'*", Chapter 4 - The Dalmarnock Fire Tests ISBN: 978-0-9557-497-0-4. Also a contributing author in Chapters 2 and 3.

- C. Abecassis-Empis, P. Reszka, T. Steinhaus, H. Biteau, **A. Cowlard**, S. Welch, G. Rein, JL. Torero, "*Characterisation of Dalmarnock Fire Test 1*", Experimental Thermal and Fluid Science, 32 (2008), 1334 – 1343.

- G. Rein, C. Abecassis-Empis, A. Amundarain, H. Biteau, **A. Cowlard**, A. Chan, W. Jahn, A. Jowsey, P. Reszka, T. Steinhaus, RO. Carvel, S. Welch, JL. Torero, J. Stern-Gottfried, B. Hume, A. Coles, M. Lazaro, D. Alvear, JA. Capote, S. Desanghere, D. Joyeux, NL. Ryder, C. Schemel, F. Mowrer, "*Round-Robin Study of Fire Modelling Blind-Predictions using the Dalmarnock Fire Experiments*", 5th International Seminar on Fire and Explosion Hazards, Edinburgh, April 2007. (1st Prize FM Global Awards for best papers). Also presented at Advanced Research Workshop on Fire Computer Modelling, Santander, October 2007.

Acknowledgements

First and foremost, I would like to thank Professor José L. Torero my supervisor, friend and the true visionary behind this work, who consistently sees far further than all those around him (and I do not refer to the ridiculous amount of time spent staring out of aeroplane windows).

I would also like to thank Dr Stephen Welch and Dr Debbie Smith whose expertise I surely did not take enough advantage of, together with my sponsors The BRE Trust and EPSRC. I am very grateful for the ever optimistic Dr Guillermo Rein whose valuable advice and encouragement will always be greatly appreciated, as that of Jean-Baptiste Richon who gave much of his time to teach me the art of PIV. Thanks to Lukas Auersperg for helping me to get my experiments off the ground both figuratively and literally, and particular thanks to Tommy, Hubert, Thomas, Pedro, Aitor and all the other (too numerous to name) members of the Fire Group, past and present - we shall surely conquer the world of fire!

Additional to my colleagues in the field, thanks also go out to the Empis' for all their support and kindness over the past few years. Lastly but certainly most importantly, I would like to thank Cecília, Mum, Dad, and Jonathan without whom I would never have gotten this far.

Table of Contents

List of Figures

List of Tables

This page has been deliberately left blank.

Nomenclature

Standard Notation

A	-	Conductive Loss Factor
c_1	-	Constant Forming Part of h_{conv}
c_2	-	Length Scale Relational Constant
c_p	-	Heat Capacity of the Gas Phase
Gr	-	Grashoff Number
h_{conv}	-	Convective Heat Transfer Coefficient
K	-	Group of Constants
k	-	Thermal Conductivity
l_f	-	Flame Length
l_h	-	Heated Length
l_p	-	Pyrolysis Length
L	-	Characteristic Length
m''	-	Mass Loss Rate
n	-	Length Scale Relational Constant
Nu	-	Nusselt Number
Pr	-	Prandtl Number
q''_{conv}	-	Convective Heat Flux to the Solid Surface
q''_e	-	External Source of Radiant Heat Flux to the Solid Surface
q''_{fr}	-	Radiative Heat Flux from the Flame to the Solid Surface
q''_{rs}	-	Re-Radiation from the Solid Surface
q''_s	-	Net Heat Flux at the Solid Surface
Q	-	Net Radiative Heat Flux to the Solid Surface
Re	-	Reynolds Number
T	-	Temperature
t	-	Time
u_∞	-	Ambient Velocity Vector
V_f	-	Flame Spread Velocity
x	-	Length Scale Parallel to the Solid Surface

Greek

α	–	Thermal Diffusivity / Absorptivity
ε	-	Emissivity
μ	–	Viscosity
ν	–	Momentum Diffusivity
ρ	–	Density
T	-	Thickness of Disk

Subscripts

f	-	Referring to the Flame
g	-	Referring to the Gas
ig	-	Referring to Ignition
p	-	Referring to the Pyrolysis Process
s	-	Referring to the Solid Phase
∞	-	Referring to Ambient Conditions
0	-	Referring to Initial Conditions

1 Fire Safety and Emergency Response in the Built Environment

Fire Safety is required at every stage in the life cycle of modern-day buildings. The process begins with the conception and design stage of a building. It then continues to be involved throughout the entire life time of structures, in the construction, approval, operation and decommissioning phases. The various elements of Structural Fire Safety can be broadly separated into three main stages: fire safety design, fire detection, passive and automated suppression systems, and active fire fighting by emergency responders. Despite the intertwined relationship between Fire Safety and buildings in modern day construction, these three main aspects of Fire Safety generally occur independently.

The fire safety design or strategy aims to ensure a safe and rapid means of evacuating the occupants of a building in the event of a fire, whilst minimising its growth, spread, and effect on the structure. This involves the definition of egress paths, signalling, smoke barriers and compartmentation, alarms, structural strengthening / reinforcement, structural fire proofing, suppression and detection systems. The design and planning of these elements generally falls under the jurisdiction of Engineers and Architects, who must demonstrate to a local approval authority (such as the Fire Service) and to the building managers that the various aspects of their strategy will fulfil their requirements of keeping the occupants and the emergency responders safe and unharmed until any fire has either been extinguished or burned out. These elements provide the passive response, the first line of planned defence in the occurrence of a fire emergency. Once a signature of approval is given by the local authority to acknowledge the final provision and assembly of an acceptable passive fire safety system, the role of the Engineers and Architects with respect to the building is usually over, thus decoupling their specific knowledge of the system from any future incidents.

From the inauguration of a building, during its daily usage, the responsibility for evacuation of the inhabitants, maintenance of signage, extinguishers, detectors, sprinkler systems etc., and general compliance with the fire safety strategy falls on the building owner. In the event of a fire, it is expected that detectors, which can be of varying levels of sophistication and sensitivity, will provide early warning of the presence of fires, enabling the building occupants to follow the clearly indicated and possibly pre-rehearsed evacuation routes. Fire and smoke barriers should afford the evacuees sufficient protection whilst containing the fire through compartmentalisation or sprinkler systems. Whether automatically or manually, the Fire Service should be alerted to the presence of the fire and deploy a response team to the scene thus surpassing the role of detection and passive response systems.

When a fire fighting unit arrives at the scene of a fire, responsibility for the building passes to them. With little or no prior knowledge of the building layout, current occupancy, fire location and size, or structural health, they must perform a systematic search of the building for any individuals who may still be inside. Once a search is completed, any information gleaned as to the size and location of the fire, building layout and contents, and general state of conditions within the building is pooled and

assessed, and if deemed safe to do so, an attempt is made to extinguish the fire. In more favourable cases such as those concerning more modern buildings which are generally more sophisticated, there is provision for some information to be made available to emergency responders. In most cases this includes availability of up-to-date blueprints, afore mentioned and possibly implemented emergency management plans, and security camera footage. Alarm panels may indicate which detectors and fire suppression devices have activated, thus establishing in a crude manner, the approximate location and magnitude of the event. Despite these aids, the Fire Service generally operates from a position of little or no information when it comes to fulfilling their duties, thus forcing reliance on intuition and experience in dealing with the specific circumstances at hand. Throughout this whole process there is little or no knowledge transfer between the parties involved. Responsibility for safety is passed on at the various stages of the building's lifecycle, between people from very different backgrounds and knowledge bases, however the individuals' expertise is not.

1.1 FireGrid

Berry et al. [7] have proposed a concept by which the uncertainty and information deficit present at the time of emergency response with respect to fires and structures could be mitigated. Called FireGrid, the project aims to combine sensing and modelling techniques to provide an accurate forecast of live fire events and structural response which can then be used to create and implement a response strategy. The project advocates the use of high performance computing (HPC) over a distributed network to supply extensive and available computational resources to enable the creation of such predictions. Artificial Intelligence (AI) planning techniques could then be implemented to form an intervention strategy based on these predictions, making use of the available resources, both human and mechanical, to attempt to evacuate occupants, fight fires and preserve the structure and its contents. The biggest challenge with regard to fire is the forming of predictions of the fire evolution, which would heavily challenge existing sensing and modelling techniques.

1.1.1 Fire Modelling

Fire models have become widely used in modern day fire engineering. There are many examples of fire modelling being used to model real fires; from the replication of laboratory scale experiments [49], to large scale fire reconstruction for the purposes of forensic studies [54]. The next logical step therefore is the use of fire models in a predictive role. Fire models could be used to anticipate the evolution of a live fire emergency, an innovation that is currently being explored [76]. Current fire modelling practices however, in terms of both the modellers and the models themselves, are not mature enough to be used with the confidence required for this process to be effective.

There are two fundamental elements of the modelling process that leave it, as yet, unsuitable for this application; the accuracy of the output and the time taken to

produce it. The Round Robin study conducted by Rein et al. [65] demonstrated that, time constraints aside, current modelling techniques cannot produce the required level of accuracy. Zone models, although capable of producing results at much higher speeds than the more complex CFD equivalent, do not calculate the detailed physical processes and thus will never be reliable enough for the prediction of the fire spread and evolution. CFD models which including the necessary level of physical detail are far too slow generally taking hours to model seconds [18].

Further compounding the problem are the number of input parameters such as fuel lay-out, material properties, and ventilation, that carry significant uncertainty, are ill-defined or rely on values than may or may not be found in the literature, a flaw that becomes further accentuated the more detailed the model gets. This becomes a critical issue when the output of egress, fire and structural models needs to be combined together to simulate the full event. Models are currently not fast, precise, reliable or robust enough to guide decision making of this nature in the short time frame of a fire emergency. While technological and scientific progress could overcome the issues of speed and precision, given the inherent uncertainty of the input parameters, it is questionable that the output of fire models could ever be robust enough for this purpose.

1.1.2 Sensor Capabilities

Fire, in contrast to other emergencies like earthquakes or floods, is an event that rapidly unfolds in parallel with the intervention. Visually fire fighters have to take in large amounts of complex, changing information and over very short periods of time, and form and reform strategies for intervention based on what they are seeing. As mentioned previously elements of the building systems can sometimes provide some low level information to emergency responders although generally these are not the main purposes of these systems and sensors, which have been designed principally for other things.

Away from fire these and other sensors have evolved rapidly in the last decade and new technologies are being used in building health monitoring, indoor quality management and security of infrastructure [69]. With the development of these technologies research into increasingly advanced methods for the exploitation and adaptation of these sensors has also progressed. Like building systems, some technologies show clear potential for adaptation to aid fire fighters. A practical example is that of video cameras which are already present in many public and private buildings for the purpose of security monitoring. An example of the evolving exploitation of their use is the tracking of people [10]. In controlled situations it has been demonstrated that individuals and groups can be tracked through a sequence of video frames. Bodor et al. [10] highlight the difficulties encountered due to varying lighting conditions. Whilst the authors reported the capabilities of their system to track multiple individuals through a video sequence, they reported its sensitivity to lighting changes such as those caused by sudden cloud cover. While the variation in light intensities occurring during a fire would clearly pose a far greater challenge to such a system, the capability to identify the number and location of occupants of a building and their velocities during an evolving emergency would be of great

assistance to fire fighters and also be of benefit in the seeding of evacuation models [36]. Gavrila et al. [38] take the problem of human tracking a stage further by demonstrating the ability to recognise human gestures and actions. By creating a 3D representation from multiple camera views of a human in a specific pose, this representation can be matched against an existing database to attempt to identify the action being carried out. Obvious applications for such a capability in a fire scenario would be the ability to identify people collapsing or ceasing to move, or individuals that are injured and thus slowing the evacuation of themselves and others.

Mittal et al. [53] and Seitz et al. [68] presented two differing approaches to reconstructing the background scene from video footage, differentiating between the permanent features in the frame and any temporary moving ones. Given the sensitivity of CFD models to the positioning of fuel in the determination of potential fire evolution [45], a resource capable of recreating the initial positions of a fire scene would prove an invaluable tool. Thus it can be shown that through the use of video cameras alone, the amount of information potentially available to an emergency response system is extremely far reaching.

There are examples in the literature where different cameras have been used for the purposes of fire [5][6], but while good punctual results have been obtained, generalization has always proved difficult especially given the complex nature of fire scenarios specifically with regards to the light variation and attenuation. Sensors can track the evolution of physical variables such as temperatures, gas concentrations, light intensity and mechanical stress. These can be interpreted and provide relevant information. Sensors like thermocouples or strain gauges provide punctual measurements of physical variables that in isolation provide data of little value or can mislead conclusions. Tracking of the evolution of physical variables on its own is therefore not a useful option to assist intervention in a fire. An increase in sensor density and complexity however, could provide a greater quantity of useful information that could serve to greatly assist intervention, but could also result in rapid information-overload.

1.2 General Problem Statement

Despite the potential of existing modelling and sensing techniques to provide information to benefit emergency response, several of the required components have been developed for different purposes and thus have never been integrated in a manner that satisfies the needs of the fire service. Sensors have evolved rapidly in the last decade and new technologies are being employed in present day buildings, some of which can already provide potentially useful information for aiding emergency responders. Fire models have become of generalized use in the design of modern buildings and are becoming increasingly accepted by building control, the fire service and building managers, although are still yet to find a role in actual fire fighting activities where operations are still managed on the basis of on the spot information and intuition. Clearly, sensor data and fire modelling can not be independently used for emergency response nevertheless; in conjunction they have

the potential to supplement each other to achieve required speed, precision and robustness.

The ideal tool to assist emergency response to fire would provide accurate forecasts of the evolution of the event. It is envisioned that this capability could be possible through some combination of physical models and live sensor data. These predictions would be used to produce a series of potential outcomes of the evolving emergency given a multitude of potentially viable intervention strategies. The outcomes are then optimized and a preferred intervention strategy is defined. The forecasts would be relayed sufficiently in advance of the reality, such that emergency responders can digest the information, make decisions on, and implement the strategy in the manner that is most effective. Furthermore, the forecasts would be presented in a form that is succinct and appropriate for the personnel receiving it, and also compatible with their specific training and knowledge, thus making interpretation and implementation of the output as effective and operable as possible. Continuous checking of the predictions against a constant stream of sensor data would enable the updating of predictions and thus changes of strategy on the basis of an unforeseen evolution of the event. The information produced by such a tool would need to be punctual, precise, reliable, and robust.

1.3 Lessons Learned from the Dalmarnock Fire Tests

The two compartment tests that form the major parts of the Dalmarnock Fire Tests [1][15] serve to illustrate the current situation, and help establish which aspects of the global objective of a tool to aid emergency response to fire outlined previously, need most research. These compartment tests were highly instrumented with both tests containing more than 400 sensors each. The instrumentation density was designed to provide measurements with time and spatial resolution comparable to that of field (CFD) models.

Both apartments were the same size and shape, with identically arranged furniture. This precise furniture layout was designed to ensure that the fire followed a well defined sequence and thus was as repeatable as possible. A first item, a sofa, was ignited with a strong ignition source provided by a waste paper basket with accelerant, intended to minimize uncertainty during ignition. The flames were allowed to propagate over the sofa until ignition of a secondary item, the bookshelf, occurred. The ignition of the bookshelf was followed by rapid surface flame spread from bottom to top, leading to flashover. The fire was allowed to continue burning almost until burnout in Test One and extinguished after flashover in Test Two.

1.3.1 Lessons Learned from Test One

Dalmarnock Fire Test One comprised a typical compartment fire scenario, characterised by a fuel limited growth phase, flashover, a ventilation limited fully developed fire, and finally extinguished by the fire brigade close to burnout. Test One was seen to be an ideal test of fire modelling capabilities, with studies a priori

[65] and a posteriori [45] demonstrating both the ability of fire models to blind predict compartment fire growth and the model parameters affecting the simulations respectively.

1.4.1.1 A Priori

The Round Robin study [65] alluded to previously, demonstrated clearly the capabilities of current modelling techniques to accurately blind predict a compartment fire. Its objective was to compare the blind prediction modelling results of independent teams, to form a sense of the range of predicted behaviours, thus providing incite into the robustness, consistency and sensitivity of current fire modelling practice. The organisers provided each team with a distinct set of information containing details of the compartment layout, furniture, ventilation, photographs, instrumentation etc. Using any model of their choosing, and any techniques and assumptions they saw fit, the teams attempted to predict key aspects of the fire such as smoke layer temperature evolution, and time to flashover and secondary ignition.

Of the specific components requested from the participants, some of those considered of practical use to the emergency responders are heat release rates, time to flashover and maximum average smoke layer temperatures. The predictions for time to flashover ranged from 77 seconds to 850 seconds to no flashover at all. The actual experimental flashover occurred at approximately 325 seconds and as discussed in the later section on Test Two was shown to be an exceptionally robust figure for this setup. Similarly, the scatter associated to the predicted heat release rates (Figure 1.1), a characteristic deemed extremely important in defining the development of fire growth, was again well outside the experimental error.

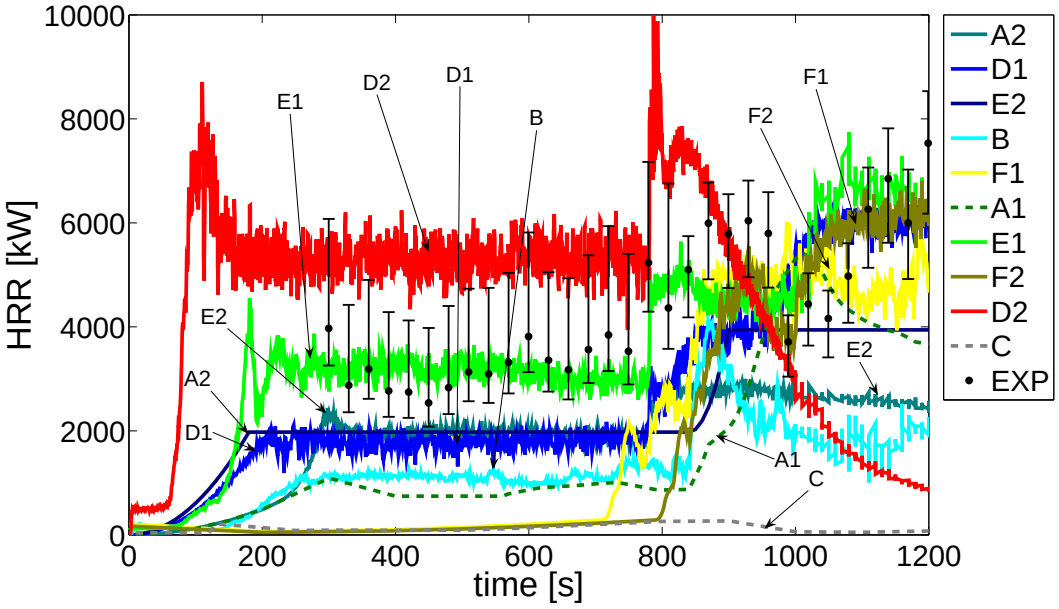

Figure 1.1 – *The predicted heat release rates of Dalmarnock Fire Test One from the a priori Round Robin study [65]. EXP (black dots) indicates the experimental results, dotted lines indicate zone models, and plain lines indicate CFD Simulations.*

The predicted maximum average smoke layer temperatures ranged from 200˚C to 1150˚C with the actual experimental value 750˚C. Despite the information provided to reduce uncertainty, the results when collated clearly show a poor level of accuracy with a very large scatter well outside the range of expected experimental error. In the cases where a model produced a good match of a specific variable to the experiment, it was not necessarily the case for other variables from that same model. It is clear that in its current state of practice, blind predictive modelling cannot provide reliable, robust forecasts that could be trusted to safeguard and benefit inhabitants and emergency responders during and intervention.

1.4.1.2 A posteriori

Jahn et al. [45] conducted a study following the Dalmarnock Tests as a compliment to the blind predictions and in order to establish the sensitivity of a model (FDS v.4) to different input parameters. The overall conclusion of this a posteriori study was that even with prior knowledge of all aspects of the fire, including the initial setup and layout, progression pattern, high resolution sensor data and video footage from the event itself; reproducing the events through modelling was a laborious, non-intuitive, time consuming and repetitive task. At each stage, the model output was compared to the sensor data, and the input file and multiple input parameters were readjusted accordingly. The basic scenario information of fuel layout, geometry and ventilation conditions was found not to be sufficient and only with direct access to the measurements was a satisfactory likeness achieved.

The authors reported that correct assessments of flame spread and the time to ignition of secondary items were crucial to the accurate modelling of the pre-flashover phase. Both of these factors depend heavily on the accurate assessment of flame size and radiation which in turn, the authors found, is extremely sensitive to the correct definition of the size and location of area of heat release, and of the material and thermal properties of the fuel. The findings indicate that while the model was successful in capturing the overall temperature evolution of the room, objects outside of the hot layer did not experience significant heat feed back from it and thus, the benefits of this particular strength of the model was of no use to the prediction of fire spread, secondary ignition and therefore flashover. While this feedback effect may be specific to the particular fuel layout of these tests and will not be the case in all compartment scenarios, the authors highlighted the fact that even given the correct description of heat flux from the sofa to the bookshelf, the flame spread model still was incapable of properly reproducing the heat release rate of the bookshelf. Thus the authors discerned that CFD modelling was not suited to the prediction or reproduction of a pre-flashover fire.

1.3.2 Lessons Learned from Test Two

Dalmarnock Test Two [15] provided two main insights into the potential of a system as defined in the global objective (Section 1.2). Firstly, it lends weight to the conclusions from the a priori and a posteriori studies as it illustrates that the aim of designing a reproducible experiment was met. Secondly it demonstrates the benefits and shortcomings of providing raw sensor data to facilitate emergency response.

The fuel layout and ignition method of Tests One and Two was designed to produce as reproducible a sequence of events and thus robust an outcome as possible given the complexity of the scenario and variation in ventilation conditions. The variation in ventilation conditions was designed to show primarily that an automated system with control of the ventilation could be used to affect conditions in the room, while simultaneously demonstrating the robustness of the experimental design.

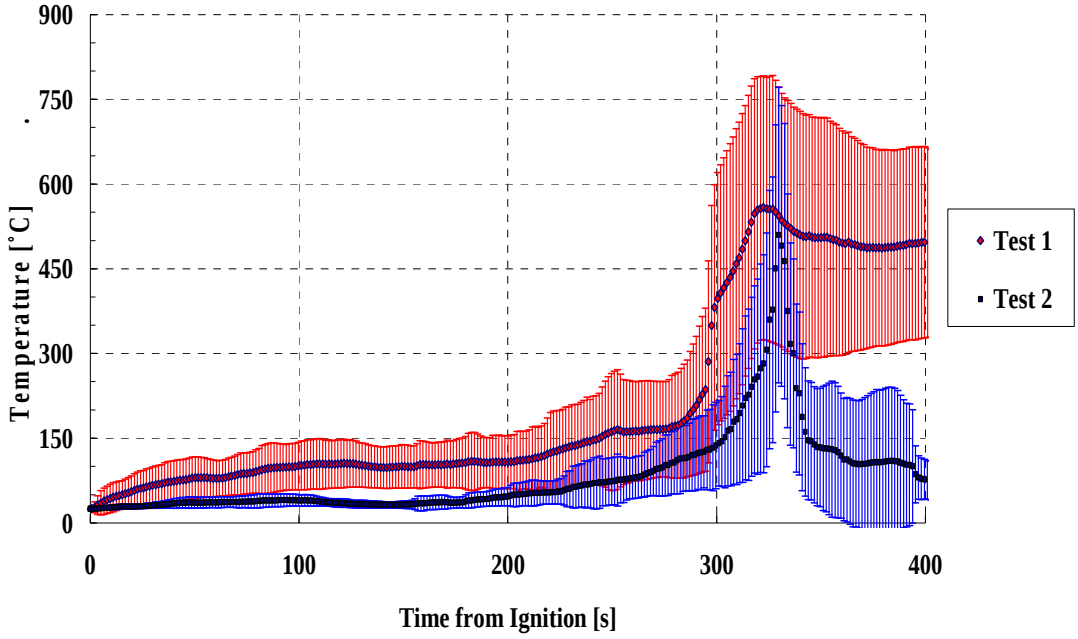

Figure 1.2 – *A comparison of average room temperatures of Tests One and Two. Test Two was extinguished in the later stages of flashover by fire fighters while Test One was left until just prior to burnout.*

The success of the design is clearly shown by the comparison of average room temperatures between the two tests in Figure 1.2. As alluded to previously, Test Two demonstrates that the flashover time of these experiments was very robust to the varied ventilation conditions within the compartment. The flashover events both began within 25 seconds of each other despite the extra ventilation and reduced smoke layer in Test Two. The times of secondary ignition of the bookshelves were within 5 to 10 seconds between the two tests. Thus understanding the reasons behind the variations in the blind predictions both between themselves and the experimental times becomes even more critical; as does the understanding of the difficulties in the post experimental modelling.

During each of the tests, sensor data was being streamed live to a control centre where camera footage and temperature measurements were displayed on multiple screens. Doors and windows to the compartment were fitted with mechanisms allowing remote control of their opening and closing from the control centre. Upon activation of smoke alarms, the windows of the compartment were opened via the remote control to begin the venting of the smoke. The situation was then monitored via the sensors available to observe the build up of the smoke layer. When it was deemed that smoke was beginning to accumulate, one of the compartment doors was opened to provide extra ventilation for the smoke layer. This was then repeated for the final compartment door and for the front door to the apartment itself. The average room temperature, pre-flashover, in Test Two was approximately 50˚C less than in Test One with a greatly reduced smoke layer, yet the secondary ignition and resulting

flashover happened at almost exactly the same time. While initially tenability in the room was maintained and adjacent rooms were kept free from smoke, conditions rapidly deteriorated and from the point of view of the personnel in the control room, the information became both overwhelming in quantity and misleading. It became clear that on the spot interpretation, even of images, was complex and difficult. This is clearly demonstrated by the images in Figure 1.3 where, while both images appear to be showing very different conditions, both images are taken at almost identical times post ignition and just prior to flashover.

a) b)

Figure 1.3 - *Images from a) Test One and b) Test Two show the tests at almost identical times post ignition and pre-flashover, taken from the same locations with respect to the experiments. Even though both scenarios are in the early stages of flashover, the conditions appear very different when just the information afforded by the images is taken into account.*

1.3.3 Summary of the Dalmarnock Test Findings

The first important issue to address are the sources of fire modelling uncertainty. Fire modelling requires many input parameters which can carry significant uncertainty or need values that cannot be found in the literature. In order to successfully match model simulations to real events, a method to enable variables to which the output is extremely sensitive to be properly quantified must be developed. From the point of view of fire forecasting, especially in the growth phase, accurate prediction of flame spread and the order and delay times of subsequent ignitions of other items in the room will make more accurate prediction of the time to flashover attainable. Upward flame spread was identified as one of the critical processes that the CFD tool could not provide adequate results for, even with all other input variables well resolved.

The second issue to address is that of the use of sensors for the benefit of emergency response. The a priori study confirmed emphatically that current modelling practices were not yet mature enough to be used reliably and robustly in the aid of emergency

response in their current incarnation, where as the a posteriori study showed that, given more research into the method of application, the sensor data was essential to attain convergence of modelling and reality. The experiences of Dalmarnock Test Two showed that raw, unprocessed sensor data could be confusing, misleading and could rapidly lead to information-overload for those trying to interpret it. Therefore, the development of a system such as that proposed by Berry et al. [7] that condenses, interprets, and organises output from sensors into a meaningful output for the specific user is essential if sensor technologies are to be exploited to their full potential.

1.4 Specific Project Objective

The goal of this work is to demonstrate the potential value of linking sensor data and models in order to make rapid and accurate predictions of a fire scenario. Due to its fundamental role in the escalation of compartment fires, and the modelling of fire growth; flame spread is taken as the scenario. Modelling flame spread in CFD generally relies on empirical parameters; some extrapolated directly from small scale experiments, and typically implies intensive computational loads. It requires the modelling of physical phenomena encompassing length scales from as small as boundary layer thickness to compartment size, and calculations of heat transfer in the solid and gas phases, flame lengths etc all requiring many input variables and extensive computations. The a posteriori studies of The Dalmarnock Fire Tests [45] have shown that flame spread is a critical phenomena that CFD tools fail to accurately predict and essential for the correct forecasting of the pre-flashover fire.

Optimization techniques exist to minimize the influence of empirical variables and to reduce the volume of computations, and as demonstrated with sensors previously, these techniques have been implemented in other fields, specifically in this case to chemical reactors and many other industrial processes [12], but they have rarely been applied to the study of fire. These optimization techniques rely on empirical measurements that are continuously fed to simplified calculation models until these converge to solutions that can extrapolate the behaviour of the physical process. Torero et al. [73] proposed a method by which flammability variables associated to concurrent flame spread could be directly obtained from stand-off measurements. Later, Rein et al. [64] developed the use of Genetic Algorithms, an optimisation technique, to establish the necessary parameters to model the spread of a smouldering front. In both cases, the direct attempts to obtain parameters from experiments were successful and resulted in simplified analytical methodologies.

This project proposes to conduct upward flame spread experiments over polymethylmethacrylate (PMMA). These experiments will vary in size, inclination, and grade of PMMA but should provide sufficient, relevant data that can be treated with a similar simple analytical approach, thus will be ideal to create and test a methodology. Direct measurements of relevant physical variables pertaining to upward flame spread will be obtained from these experiments and introduced into a numerical tool. Any unknown parameters, normally determined via standard test methods or correlations will be obtained by means of a pertinent optimization

technique. Initial simple experiments, assessed for repeatability and bench marked against the literature, will be used to define the parameters, the methodology, and thus the characteristics of a numerical tool. Subsequent experiments of increasing complexity will be used for testing and validation and to evolve and broaden the applicability of the methodology. It is intended that a resulting methodology could be introduced into flame spread models to speed up computations and at the same time generate reliability and robustness.

2 Literature Review

2.1 Flame Spread

This section of the work presents a summary of information relevant to wall flames, flame spread and flame spread experiments with a view to finding a simple empirical model of the process suitable for the desired application. A brief review of the literature consulted and information derived from it is presented here. (Except where specifically stated, general background information comes from Fernandez-Pello c/o Cox [17] and Drysdale [24])

2.1.1 The Wall Flame

Figure 2.1 shows a two-dimensional representation of a wall flame. The pyrolysis length labelled l_p (or occasionally x_p), represents the length over which pyrolysis of the wall material is taking place. For the purposes of this work the term pyrolysis will follow the definition of Drysdale [24] that describes it as, "chemical decomposition to produce fuel vapours ('the volatiles') which can escape from the surface to burn in the flame."

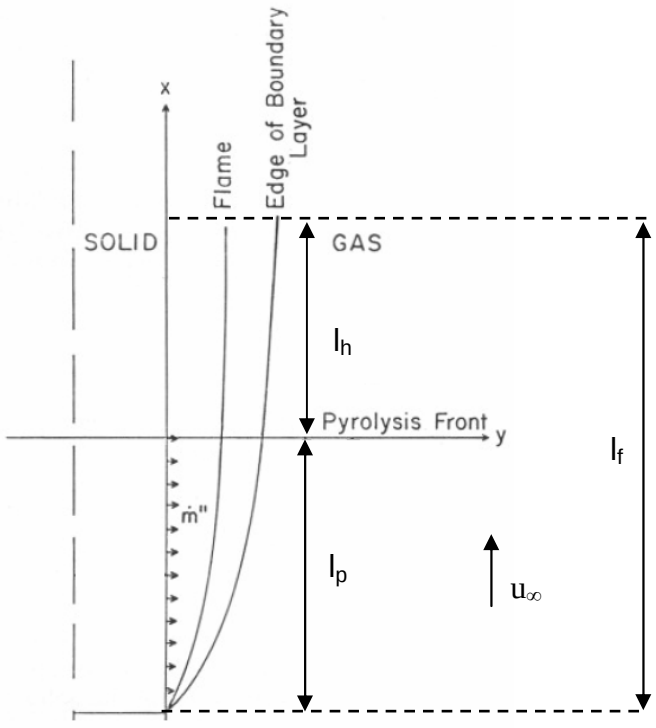

Figure 2.1 – *A two-dimensional representation of a wall flame where l_p is the pyrolysis length, l_f is the flame length, l_h is the heated length, u_∞ is the ambient flow velocity. Diagram reproduced from Fernandez-Pello [29].*

Pyrolysis products of this chemical decomposition resulting from the heating of the solid fuel at or near the surface are released into the adjacent gas phase (m"). Here they mix with the oxidizer (usually air) and form a flammable mixture which if ignited burns as a flame releasing combustion products and heat [24]. The term flame length refers to overall visible length of the flame from the tip to the base and is represented by the notation l_f (or occasionally x_f). The length between the flame tip and the pyrolysis front labelled l_h (the heated length) represents the non-pyrolysing region being heated by the flame.

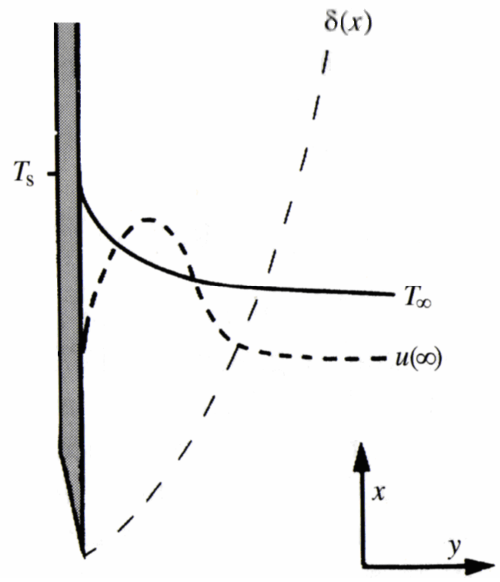

Figure 2.2 – *The diagram shows the vertical velocity profile resulting from the gas phase temperature variation next to a hot solid surface. Diagram reproduced from Drysdale [24].*

The ambient velocity vector is shown by u_∞ and represents the free stream velocity parallel to the solid surface away from the effects of the flame. The velocity profile produced by the gas temperature variation next to and resulting from a hot solid surface is shown in Figure 2.2. The profile caused by a hot flame next to a vertical surface is expected to be similar to this.

2.1.2 Flame Spread

Physical descriptions of flame spread are generally separated in to two categories, concurrent flow and opposed flow. As the names suggest, concurrent flow refers to cases when the direction of spread and the direction of airflow are the same and opposed flow refers to cases where they are opposite. For natural convection wall flames the flow is driven by buoyancy and thus rises. In a wall flame correlation therefore, upward flame spread is characterised as concurrent flow and downward

spread as opposed flow. Flame spread can be defined as the progression of the pyrolysis region over the solid, upward spread being the upward progression of the pyrolysis front and downward spread being the downward progression of the base of the flame or the flame leading edge. For upward flame spread, the pyrolysis front can be equated to rate of spread as defined in Tewarson et al. [70] as: -

$$u = \frac{dX_p}{dt}$$

Equation 1

Where u is the flame spread rate, X_p represents the pyrolysis length and t represents time. For the pyrolysis front to progress, the solid fuel downstream of it must be heated to a point where it releases combustibles which contribute to the reaction in the gas phase. The rate at which this heating and subsequent ignition of the combustion products is accomplished governs the rate of progression of the pyrolysis front and thus the flame spread rate. Therefore another representation of the flame spread velocity (V_f) is simply the length of solid ahead of the pyrolysis front being heated (l_h) divided by the time taken to ignite it (t_{ig}) (Equation 2): -

$$V_f = \frac{l_h}{t_{ig}}$$

Equation 2

This defines the upward flame spread rate as a solid ignition process. The following breakdown of the elements concerned with Equation 2 considers only upward flame spread over thermally thick solids.

2.1.3 Flame Spread as a Solid Ignition Process

2.1.3.1 Time to Ignition

Niikoka et al. [56] demonstrated that the total solid ignition delay time (t_{ig}) is the sum of two parts. The first is the time taken for the solid to pyrolyse (t_p) and the second is the time taken for the resultant combustibles and oxidizer to combine to form a flammable mixture (t_g). These are referred to as the pyrolysis time and the gas induction time respectively. The relationship is expressed as: -

$$t_{ig} = t_p + t_g$$

Equation 3

For the case of upward flame spread where the flame lies against or close to the fuel surface, the buoyancy produced by the heat from the flame pulls the oxidizing air towards the area where the pyrolysate is. The resulting flammable mixture is ignited by the ideally placed flame producing a rapid piloted ignition therefore for this process, the gas induction time is assumed to be negligible [17], and the time taken to heat the solid from its initial temperature to the temperature at which pyrolysis occurs and produce sufficient combustibles for sustained flaming is deemed the ignition delay time for this problem, i.e. $t_p = t_{ig}$. The time taken for the surface of a thermally thick fuel to reach the pyrolysis temperature is found by conducting an energy balance for the surface of the fuel and is shown in Equation 4.

$$t_{ig} = t_p = \frac{\pi k_s \rho_s c_s (T_p - T_0)^2}{4 \dot{q}_s''^2}$$

Equation 4

Equation 4 effectively states that the time taken to heat the surface to its pyrolysis temperature is given by the amount of energy required to heat the surface of the solid from its initial temperature (T_0) to the pyrolysis temperature (T_p), divided by the rate at which energy is being supplied (net heat flux to the surface). This heat flux is assumed to be constant [71] as are the material properties.

2.1.3.2 Heat Flux to the Unburned Surface

As demonstrated by Equation 4, the rate at which heat is transferred to the solid surface governs how quickly it will ignite. Fernandez-Pello [17] writes that heat transfer from the flame to the unburned solid ahead of the pyrolysis front is the controlling mechanism of flame spread. This heat is provided by the flame itself and also possibly from external sources. Upward flame spread is regarded as being the most dangerous form of flame spread due to the high speeds at which it takes place relative to downward and sideways spread. This is mainly due to the positioning of the flame and therefore increased levels of heat production relative to the unburned fuel in the direction of spread. Although hot gases / combustion products downstream of the flame tip do provide some heating of the solid fuel, the literature [17] reports that its effect is minor when compared to the heating provided by the flame itself, thus, the heated length is assumed to finish at the flame tip.

Thomas [71] states that, “Fire has long been regarded as tending to spread upwards by convection and sideways across fire breaks by radiation”, which suggests that the convective component of the heat flux to the surface will be the dominant one in upward flame spread. Fernandez-Pello [17][26] describes the varying influences of each of the forms of heat transfer between the flame and solid fuel, with regard to concurrent flow flame spread both forced and naturally induced. When the flame is laminar in character, occurring both when the flame is small, and when larger, in and just downstream of the pyrolysis region, heat transfer to the solid fuel in this region

is dominated by convective transfer from the flame. Away from the pyrolysis region when the flame is larger and takes on turbulent characteristics, the heat flux to the surface becomes increasingly controlled by radiation, believed to be as much as 80% [59]. As would be expected, there is a transitional region between these two phases where both forms are equally influential on the surface heating. These findings are corroborated by many others including Di Blasi [21] and Hasemi [41] who stresses the importance of the understanding spread of turbulent, radiation driven flames for the better understanding of fire growth in real fire scenarios. Orloff et al. [59] provide more quantitative information regarding this, specifically applied to their studies with natural convection upward flame spread over PMMA. They report that for flames up to approximately 20cm in length, the heat transfer to the unburned fuel is dominated by convection. As the flame grows beyond this and becomes turbulent, radiation gradually takes over. In most physical models conduction through the solid ahead of the pyrolysis front is neglected as the characteristic length associated to it is orders of magnitude less than that of the flame length, which is the characteristic length associated with convective and radiative transfer. The net heat flux to the unburned fuel surface ahead of the pyrolysis front is given by Equation 5: -

$$\dot{q}''_s = \dot{q}''_{conv} + \dot{q}''_{fr} + \dot{q}''_e - \dot{q}''_{rs}$$

Equation 5

2.1.3.2.1 Convective Heat Transfer

$\dot{q}''_{conv}$ is the convective heat flux from the flame to the solid and can be described by Equation 6.

$$\dot{q}''_{conv} = h_{conv}(T_f - T_0)$$

Equation 6

The challenging aspect with regards the definition of the convective flux is in the accurate measurement / optimisation of the convective heat transfer coefficient (h_{conv}). h_{conv} is defined in terms of the Nusselt number which for cases of forced flows parallel to a flat plate, is given by Equation 7: -

$$Nu = \frac{h_{conv} x}{k} = \xi_1 \mathrm{Re}^{\xi_2} \mathrm{Pr}^{\xi_3}$$

Equation 7

where the values of ξ vary depending on the characteristics (laminar or turbulent) of the flow. For convective heat flux in natural convection flows along a vertical plate, the Nusselt number is given by Equation 6: -

$$Nu = \frac{h_{conv} x}{k} = \xi_1 (Gr.\Pr)^{\xi_2} = \xi_1 (Ra)^{\xi_2}$$

Equation 8

again where the values of ξ vary with the flow characteristics.

2.1.3.2.2 Radiative Heat Transfer

$\dot{q}''_{fr}$ represents the radiative heat flux to the solid from the flame and can be approximated by $\dot{q}''_f = \sigma\varepsilon(T_f{}^4 - T_s{}^4)$.

2.1.3.2.3 Surface Re-radiation

$\dot{q}''_{rs}$ represents surface re-radiation and can be approximated by $\dot{q}''_{rs} = \sigma\varepsilon(T_s{}^4 - T_\infty{}^4)$.

2.1.3.2.4 External Radiation Sources

$\dot{q}''_e$ represents external sources of heat flux. In the context of a real fire this would account for other burning items and heat sources in view of the surface.

2.1.4 Length Scales and their Relationships

Figure 2.1, as discussed earlier, shows a two-dimensional representation of a wall flame. There are three specific lengths represented, the pyrolysis length (l_p), the flame length (l_f), and the heated length (l_h). A fourth length that is sometimes included is the burnout length (l_b) which for upward flame spread represents the distance moved by the flames leading edge when the fuel source has been exhausted. Orloff et al. [59] showed that for laminar flow, the flame height is found to be directly proportional to the pyrolysis length (Equation 9) i.e.

$$l_f = c l_p$$

Equation 9

and for turbulent flow the relationship follows Equation 10: -

$$l_f = c l_p^{\ n}$$

Equation 10

where c and n are constants of the given fire situation. The authors proposed a value for n of 0.78 and c of 5.35. Other proposals are by Saito et al. [66] who proposed a value of n = 0.66, Delichatsios et al. [20], who proposed n = 0.8 and Tewarson et al. [70] who also report n = 0.66. The value could be considered as n=1 for laminar spread.

2.2 Upward Flame Spread Experiments and Experimental Techniques

A review of previous works involving upward flame spread experiments and the measurement techniques employed by the authors is presented here. Fernandez-Pello [26] states that, "Experimentally, difficulties are encountered in obtaining accurate measurements of the flame spread rate because the process is unsteady, very rapid, and because the flame bathes the un-ignited surface of the fuel." With this in mind, knowledge of the advantages and disadvantages of previous test methods, setups and measurement techniques that have been tested and reviewed will enable the design of a more robust and reliable test. It is also the intention that by mimicking to some degree a test setup from the literature, the results can be benchmarked and measurement techniques employed can be evaluated, to give an extra assessment of reliability and repeatability.

2.2.1 Sample Material, Size, and Mounting

Saito et al. [66] use Polymethylmethacrylate (PMMA) for upward flame spread tests which showed sustained upward propagation. They report that a sample height of 250mm corresponds approximately to conditions for the onset of turbulence. The authors report that observations of their sample, with a width of 300mm, showed flow and flame propagation characteristics concurrent with a two-dimensional character. This work also reports experiments on Douglas Fir Particle Board of the same dimensions although for this material the authors state that sustained burning was not always seen. The criterion for these experiments was for spread that developed into turbulent flaming over thermally thick materials where the sample was not fully consumed at the completion of the test. In order to satisfy these requirements, a sample thickness of 13mm was deemed sufficient. The authors flush mounted the test specimens to an inert wall material in order to prevent spread to the sides and rear of the specimen and thus maintain a plane wall flame.

Tewarson and Ogden [70] use PMMA for flame spread experiments due to the level of detailed knowledge available on it in the literature. This same reason is also cited

by numerous authors including Consalvi et al. [14] and Fernandez-Pello and Williams [33]. Tsai et al. [74] used specimens of dimensions 70mm wide and 6mm thick with heights ranging from 200mm to 500mm. The PMMA samples were mounted against a 2mm thick steel plate with the intension of preventing flame spread to the sides and rear and also keeping the rear of the specimen sufficiently cool to prevent distortion and sagging.

The setup employed by Fernandez-Pello for both upward [29] and downward [27] spread experiments also used PMMA for its properties when burning. These test samples were 38mm thick and 200mm high. This thickness was chosen by the author to ensure the uniform spread of flames and prevent buckling of the sample during exposure. This thickness also ensured that the specimens could be considered thermally thick. This work sought to isolate the face over which the flame spread took place by mounting the sample in a steel frame. The author went further by insulating the samples from the effects of the steel frame by placing 10mm thick asbestos strips between the sample and the frame. The frame was extended with two baffles aimed at preventing the lateral entrainment of air across the exposed surface and thus maintaining a two-dimensional spread effect. These baffles were angled to prevent re-radiation effects.

Rangwala et al. [62] conducted upward flame spread tests varying the width of the samples. The vertically mounted samples were 500mm high, 12mm thick, and varied in width between 25mm and 150mm. Again the samples were mounted such that the flames were prevented from spread to faces other than the intended one. In other tests on 25mm thick PMMA, the same author [61] places thermocouples on the back of the sample. The author reports that the thermal wave never fully penetrates the sample thus the sample can be considered thermally thick.

Di Blasi [21] indicates through the author's analytical studies of PMMA that a sample is considered thermal thick when the thickness is greater than 2.5mm. The sample is considered thermally thick given that its physical thickness is greater than the depth of thermal penetration [17], i.e. that the rear of the sample remains at ambient temperature.

Orloff et al. [59] used samples 45mm thick, 410mm wide and 1570mm high. This height was to allow the flame to reach a turbulent regime. The authors report the need to ensure a two dimensional spread to the top of the slab. They accomplished this via a similar method to Fernandez-Pello [29] by supplying steel walls running the entire height of the slab along both side edges. The walls were at right angles to the fuel surface and water cooled to prevent radiant heat transfer to the slab. There was a marinate wall at the top of the sample to isolate the face from the top edge and the bottom of the sample sat against the floor thus completely isolating the exposed face from the other edges.

2.2.2 Ignition Methods

Saito et al. [66] used a methane (CH_4) burner with a fixed flow rate, positioned at the centre of the base of the test specimen to provide point ignition of the sample. These authors experimented with removing and maintaining the burner after ignition of the test specimens. Tewarson and Ogden [70] used a rectangular dish containing a methanol (10ml) pool fire to create a uniform pyrolysis front across the length of the bottom of the test sample. A similar method was used by Orloff et al. [59] who provided 3cc of acetone in a narrow tray along the bottom edge. Tsai et al. [74] created a rack to hold the PMMA samples, that could rotate to the horizontal and in such a position a line fire was initiated. A steel plate was held over the sample leaving a 3mm strip of PMMA exposed, which was ignited using a butane-fuelled torch. The rack was then rotated back to a vertical position and the protective steel plate removed in order to start the test. Fernandez-Pello [29] reports the use of an electrically heated Nichrome wire embedded across the lower surface of the PMMA. The wire was tensioned and pulled towards the surface by springs to prevent movement as it underwent thermal expansion. When the current was applied the wire heated the PMMA producing pyrolysis products that were ignited by a small pilot flame thus initiating a line fire. Rangwala [61] used three different methods of ignition with the method employed dependant on the type of fuel. For most solid fuels a wick soaked in methanol attached to the base and ignited using a match was a reliable method. A line gas burner was employed for wider samples to ensure an even line fire was created over the entire sample width. The burner was turned off when an even flame height of 4cm was created over the sample width. For non-dripping fuels a resistively heated Nichrome wire coil was used. Voltage was applied using a variable resistance until the sample ignited.

2.2.3 Measurement Techniques

Analysis of the literature describing upward flame spread identified several measurable physical parameters that evolve with time and are important to the description of the flame spread process. These parameters must therefore be measured by an appropriate sensing technique in order to capture and subsequently predict flame spread using a physical model. In order to define an appropriate technique for each variable, a study of the literature has been conducted to assess the strengths and weaknesses of some existing techniques. The techniques / sensors should be relatively versatile and preferably inexpensive as experiments are expected to vary in nature and in some cases equipment may be damaged.

2.2.3.1 Flame Length Measurement

The simplest method of flame height measurement is through visual estimation during the experiment itself which was employed by Tewarson and Ogden [70]. The authors marked lines at 25mm intervals and recorded times of arrival at each measurement point using a stopwatch. A similar method was employed by Tsai et al. [74] and Orloff et al. [59].

Saito et al. [66] also used a method of visual estimation, inspecting video images taken throughout the experiments. The authors also utilized other methods for comparison. The authors report that a flame height taken from regularly time-spaced frames from video footage performed sufficiently as compared with averaging of measurements from every frame obtained. The same authors also report considering the use of thermocouples to detect the flame tip through defined temperature increases. This was dismissed due to the inability of the technique to distinguish between the flame and the rising hot combustion products produced by the flame. This work reported that although the trend produced by this technique followed that of others, the measurements were generally larger, and a temperature rise of 40˚C above ambient indicating the flame tip presence correlated best with other methods.

Fernandez-Pello [29] used still photography with optimised lens aperture and shutter speed to capture the luminosity of the flame tip. Given numerous tips due to the non-uniform nature of the flame, bounds for the data were defined by the highest and lowest of these visible tips upon inspection of the images. Audouin et al. [5] developed a method by which video footage is treated automatically to produce a measure of the flame height. The experiment consisted of a gas burner simulating a pool fire, thus producing a constant flame. A camera set to a rate of 1Hz captured footage of the fire. By examining the intensity level of each pixel of each image, the author was able to determine a presence probability of flame in each pixel. By setting a threshold presence probability, each pixel was then re-assessed to determine if it contained flame or not. The length of flame in pixels could then be measured and converted to any desired unit of length. Rangwala et al. [62] used a similar method to measure the height and standoff distance of a wall flame.

Consalvi et al. [14] looked at this problem, specifically with the aim of defining flame height in terms of the wall heat flux, thus creating a method convenient for analytic, numerical and experimental studies. The authors found that a correlation existed between the wall heat flux and the non-dimensional characteristic length scale for upward flame spread, and a flame height could be defined via threshold wall heat fluxes.

2.2.3.2 Pyrolysis Length Measurement

Saito et al. [66] employed a method of “surface” temperature measurement with thermocouples to track the pyrolysis front and thus provide a measurement of the pyrolysis length in time. The authors placed thermocouples beads of approximately 0.1mm diameter along the samples vertical centre-line such that the beads of the thermocouples were within ≤ 1mm of the exposed sample surface. A temperature of 320˚C was found to correspond to visually observed ‘bubbles’ in the PMMA and thus the arrival of the pyrolysis front. The history of the pyrolysis length (and also the flame length) for these PMMA experiments was representative of the acceleratory spread. Consalvi et al. [14] used a similar method melting thermocouples to the surface of the PMMA and reporting that the pyrolysis length can be obtained accurately from this method. Rangwala [61] and Fernandez-Pello

[29] also employed a similar method with the later reporting it difficult to obtain accurate results in contradiction to Consalvi et al. [14].

Tewarson and Ogden [70] used a similar method to the one used for flame height estimation. Line markers at 25mm intervals were used to estimate the pyrolysis length with times recorded from a stopwatch. Orloff et al. [59] observed the sample from the rear following the evolution of pyrolysis bubbles at the front surface through the transparent samples. Tsai et al. [74] left a thin slit window in the backing to the PMMA enabling an observer to observe visually and record the time at 10mm intervals. The pyrolysis front was again defined by the presence of bubbles seen at the PMMA's surface.

2.2.3.3 Flow Velocity Measurement

2.2.3.3.1 Point Measurement

2.2.3.3.1.1 Pitot-Static Tube

The Pitot-Static Tube W[9] (Figure 2.3) is a device that correlates pressure to air flow velocity. It consists of a tube filed with air with a diaphragm at one end. The other end is open and placed facing the direction that the airflow is coming from, thus is a mono-directional technique. As the air is stagnated in the tube, the deflection of the diaphragm is correlated to the stagnation pressure. A further measurement of static pressure is made by ports on the sides of the main tube. The dynamic pressure which can be correlated to air flow velocity is simply the difference between the stagnation pressure and the static pressure. The technique is intrusive as it must be placed in the desired measurement location, thus could interfere with the flow. It is also very directional and thus care must be taken to ensure it is aligned with the desired measurement plane.

Figure 2.3 - *The diagram shows a Pitot-Static Tube used to measure air flow as the result of pressure changes. The main central tube is used to measure the stagnation pressure and the ducts to the side measure the static pressure. This diagram has been taken from W[9].*

2.2.3.3.1.2 Hot Wire and Pulsed Wire Anemometry

Hot Wire Anemometry is a technique used for point measurement of air flows W[8]. The technique involves a short length of fine wire placed perpendicular to the desired flow measurement. A current is passed through the wire which causes it to resistively heat to a temperature above ambient. When flow passes over the wire it is cooled and the thus changes the resistance / voltage across the wire. This change in resistance can be calibrated to the flow velocity of the air flow over the wire. As this technique relies on temperature changes to compute the velocity of the air, application to fire and flame spread make this technique potentially unviable. Fernandez-Pello and Williams [32] report that the hot wire can respond undesirably to gas temperature changes and flame radiation and thus is not reliable in these situations. The authors recommend the similar technique of Pulsed Wire Anemometry. This technique uses two wires in parallel at a known distance apart (typically of the order of millimetres), again placed perpendicular to the flow. The first wire receives a pulse of electricity causing it to be heated. The second works similarly to the hot wire anemometer except this time it records an increase in temperature of the gas flowing past. The time delay between the second wire detecting the increase in heat in the air flow caused by the first wire and the actual pulse in the first wire is recorded and a simple distance over time calculation gives the flow speed. The authors still report difficulties with the technique however especially when measuring low velocities as the buoyancy produced by the heated air can obscure the actual required reading. Lower voltages and thus lower temperatures can be used to reduce this problem but this has the adverse effect of producing a very low signal which can make detection difficult. The authors report an optimised design for this system which has been applied to downward flame spread over PMMA. Both pulsed wire and hot wire techniques have the disadvantage of being present in the flow and thus potentially disturbing it. Also the soot content of some flames may become a factor in some locations if there is a build up of soot on the wires themselves.

2.2.3.3.1.3 Laser Doppler Velocimetry

Laser Doppler Velocimetry W[7] is a technique used to measure flow direction and magnitude in both air and liquids. It comprises two beams of coherent laser light that cross at the desired point of measurement. The interference of the two beams creates fringes at a consistent distance which should be aligned with the flow being measured. When particles pass through the focal point of the beams they reflect light towards a receiver and the product of the frequency of the light received and the known difference between the fringes gives the velocity. A discussion of the technique's application to flame spread is given by Fernandez-Pello and Williams [32]. The authors report that it is possible although difficult to obtain both components of the 2D velocity profile associated with flame spread. The technique should be viewed as appropriate for ambitious projects only. The main advantage of the technique is it is generally unobtrusive to the flow although some particle introduction methods may cause some disturbances.

2.2.3.3.2 Plane Measurement

2.2.3.3.2.1 Particle Image Velocimetry

Particle Image Velocimetry (PIV) works on the premise of tracking movements of numerous individual particles between two images taken at a known time interval (Figure 2.4). By evaluating the distance moved by a particle between two images and given the known time difference (δt) between those images a velocity vector can be calculated that describes the particles movement. By tracking many particles between the two images, and averaging the movement of particles in a defined space, a map of velocity vectors can be calculated to describe the overall movement over the period of time, δt.

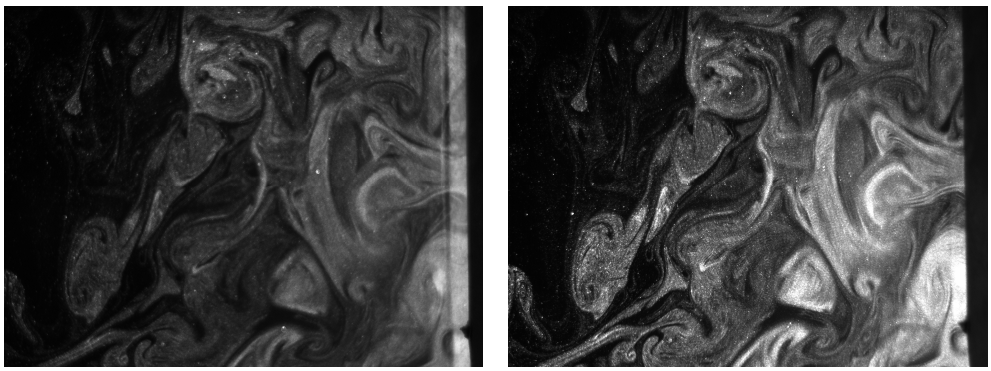

Figure 2.4 – *The images show a PIV Image Pair for an Upward Flame Spread Test.*

There are four main hardware aspects associated with the capture of PIV images: -

- The insertion of particles into the flow (seeding)
- The highlighting of the particles in the flow
- The actual capturing of the image (cameras)
- The electronic timing devices / computers to control all or some of the above

Seeding is the process by which particles are introduced into the flow field. This in itself represents a challenge. The particles must be present in sufficient quantity that there is an adequate number of them present in the two concurrent images for cross correlation, the tracking of particles from one image to the next, to take place. Usually in order to achieve this, the particles must be injected by some means into the flow. Thus the challenge to be overcome is in ensuring the entrainment of sufficient particles without disturbing the flow field that is being measured and thus defeating the point of the exercise. There are various seeding techniques available which are usually tailored to the needs and constraints of the specific application.

The highlighting of particles in most cases is achieved through the use of a high power laser, in many cases a pulsed laser, fitted with a light sheet optic. The laser

produces pulsed beams of high energy light that are diverged into a two-dimensional light sheet which is aligned with the desired measurement plane (Figure 2.5).

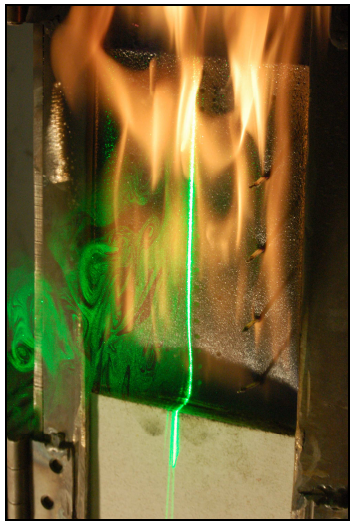

Figure 2.5 – *A laser light sheet highlights the seeding particles around a wall flame.*

A fraction of these pulses of light reflect off the artificially introduced seeding particles towards the camera(s). In the case of application to fire, the laser should be of sufficient power that its light emission is superior to the luminosity of the flame. The cameras are directed perpendicular to the light sheet in order to take images of the particles movement through it. The cameras used for PIV are required to be of sufficient quality that the user can externally trigger numerous aspects of the cameras operation such as shutter speed, exposure time, and frame capturing, and depending on the specific application and measurement requirements, that they can achieve a rapid frame rate and shutter speed. For PIV in the presence of flames, the exposure time should be set low enough such that the luminosity of the flame does not register on the exposure and create ‘noise’ that inhibits the cross correlation process.

The final hardware components are the electronic and computational components that trigger the elements of the image acquisition process. The precise triggering of the laser to coincide with the camera exposure must be controlled to a high degree of accuracy. The downloading and systematic storage of the images from the camera(s) requires varying degrees of data transfer speed and memory capacity. Once the desired image pairs have been acquired, they are post processed to create the desired vector maps. This is done by an iterative process of cross correlation, using an algorithm that tracks the particles between images in a pair, and filtering, the systematic removal of ‘noise’ by various techniques depending on the data in question.

2.2.3.3.2.2 Particle-Track Photography

This process is described by Fernandez-Pello and Williams [32] and employed by the same authors [33] in PMMA flame spread experiments. The process can provide streamline patterns and velocities in flames. Light from a projector is passed through a slit in a rotating disc thus pulsing the light. It is then passed through a lens collimating it to illuminate a central slice along the burning sample. Magnesium oxide particles are injected into the flow and a camera catches their illumination by the projector. The distances travelled by the particles within the pulses can be measured from the images. The duration of the pulses are fixed and were checked in [33] by an oscilloscope reading. The authors report potential sources of error in the system. If the particles are too large their trajectory can be affected by their own inertia, as well as the flow being measured being affected by the method of injection. Heating by the projector also affects the buoyancy driven flow.

2.2.3.4 Heat Flux Measurement

Ingason and Wickstrom [44] report a method by which incident radiant heat flux can be measured using a plate thermometer. The authors describe the results of experiments where the output of plate thermometers are compared to that of water cooled gauges in simple cone calorimeter tests. The authors propose this alternate use of the plate thermometer with field testing in mind due to the non-requirment of water to cool the gauge which may be awkward to supply in some field situations. The plate thermometer according to ISO 834 and EN 1363-1 is constructed using a 100mm x 100mm square, 0.7mm thick steel plate. A thermocouple is welded to the rear centre of the plate and a layer of insulation is applied to the back of the plate sandwiching the thermocouple. The authors report that this setup can be used indirectly with corrections for convective and conductive errors to measure the incident radiant heat flux. Alternative designs (the design outlined above was not designed to measure heat flux) could minimise these errors. The authors suggest reducing the thickness to improve the response time and increasing insulation to reduce conductive errors.

Guidelines for producing a plate thermometer for measuring heat fluxes are given in ASTM E459 – 05. The instrument in this case is referred to as a thin skin calorimeter. The standard outlines the advantages of such a device. It allows for diversity of the construction methods and materials, in order to tailor the design to the specific needs of the situation. The guide lines also allow for an inexpensive instrument making them ideal for situations where exposure levels may be high and the device discarded after use. So long as the device isn't damaged or distorted by temperature it can be regarded as reliable. Calculation methods are similar to those defined by Ingason and Wickstrom [44] and rely on the temperature measurement of the unexposed face of the metal plate and knowledge of the properties of the metal used. A one dimensional heat transfer analysis is used to evaluate the net heat flux for the device. Other users of this technique can be found in [1][2][3].

2.3 Polymethylmethacrylate

Much of the knowledge on flame spread (Section 2.1) and the experimental techniques (Section 2.2) described above has been developed through experiments on Polymethylmethacrylate (PMMA) with many works citing the good understanding of its properties and behaviour as the reason for its use. The main property of interest to this work is the temperature associated to the pyrolysis reaction at the surface. The surface thermocouple method of pyrolysis front tracking (Section 2.2.3.2) relies on a temperature threshold to determine when the front has arrived and also to provide an assessment of spread rate (Equation 1) and as such many practitioners of this technique have defined a Pyrolysis Temperature (T_p) for PMMA. Values for T_p have been approximated for experimental purposes as 329˚C [6], 315 +/- 25˚C [66], 363˚C [59], 390˚C [33]. Fernandez-Pello [17] states that the pyrolysis temperature is not a fixed value and in fact varies with oxygen concentration and ambient pressure. Dakka et al. [19] showed that, rather than there being a single temperature, the pyrolysis process actually occurred over a range. The study looked at piloted ignition of PMMA and showed that prior to ignition there was significant gasification due to pyrolysis. The study demonstrated that the process of pyrolysis is a two phase reaction and is limited by mass transport. The first of the two phases of the reaction is limited by O_2 diffusion into the surface and an increase in O_2 concentration saw the onset of the reaction shift to lower temperatures. Thus the concept of a pyrolysis temperature could be said to be false and rather a pyrolysis temperature range be defined. The range would also appear to be scenario specific, dependant on ambient conditions which would explain the ambiguity in the values reported in the literature.

2.4 Optimisation Techniques

This work envisages the use of some sort of optimisation technique to account for unknown parameters and trend identification in data that cannot be provided directly by sensors. Previous work ([63] [48]) has shown the tremendous adaptability and propensity for a consistently good solution provided by Genetic Algorithms. The use of these techniques in engineering has become increasingly common in recent times. The concepts behind and potential advantages of use of these and other Evolutionary Algorithms will be reviewed along with other potentially viable techniques.

2.4.1 Curve Fitting

Curve fitting or Regression Analysis is the process of fitting a line through a set of data points W[6]. The shape of the curve being fitted is usually described by an equation relating independent and dependent variables using a combination of adjustable parameters and mathematical operators. It is the parameters that must be optimised to create the best fit of the data which is assessed by some criteria such as the least squares method. The minimum number of data points needed for a fit is dependent on the desired shape of the curve and the number of unknown adjustable parameters. These data points to which the curve is fitted act as constraints in the fitting process. The advantages that this technique will bring when compared to other

techniques such as Evolutionary Algorithms will be speed of computation. A description of a fit type in advance specific to this application will be necessary in order that the process be automated according to the FireGrid ethos.

2.4.2 Genetic Algorithms

Genetic Algorithms (GAs) are an optimisation tool inspired by natural genetic variation and Darwinian Theory of natural selection [52] W[5]. GAs are a system of creating a better set of candidate solutions to a problem from a previous set using processes inspired by biological genetics. All candidates fall within a search space (which may or may not be predefined) which represents the area in which all possible solutions can exist and is characterised by a fitness landscape where the highest point is the closest to perfection that a solution within the search space can be.

Genetic Algorithms use data strings called chromosomes as an array to store the bits of information with each bit value known as a gene. Each of the genes represents an unknown in the problem and they can have a predetermined range in which the GA will allow their values to lie. The first stage of the process is to produce a random population of chromosomes with the values of the individual genes being somewhere between defined boundaries. The number of individuals created is problem specific and can span to tens or thousands of candidate solutions. It is expected that there are enough solutions to have a comprehensive coverage of the entire fitness landscape at the start. This ensures that the global optimal solution is not missed with results instead representing a lesser or local optimum. Each member of the newly created population is given a fitness rating. This rating reflects how well the chromosome, with its individual gene values, satisfies the overall problem. The fitness is determined by a fitness function which is entirely problem specific. The correct definition of this fitness function is key to the success of the GA. Candidates go through anyone of a number of selection methods and the likelihood of them being selected is based in some way on their fitness rating. The higher a candidate's fitness, the more likely they are to be selected for creating the next generation. Successful candidates are then 'bred' in pairs using a user specified genetic operator to produce two new offspring.

The genetic operator mimics the natural process of chromosomal crossover, exchanging various genes between the two candidates being bred. When the offspring are produced, there is some probability that one or more of their genes may be mutated. The probability of mutation occurring and to what extent it occurs are determined by the user and to some extent governed by the problem at hand. Crossover and mutation serve not only to move the candidate solutions toward the highest point of the fitness landscape, but also to maintain genetic diversity. This helps prevent premature convergence on a local optimum. By weighting the selection for breeding in favour of the fitter solutions in the population, it is hoped that the average fitness of each successive generation is higher than that of the previous. Once a new generation is produced, the fitness' of the new candidates are assessed and the whole process begins again with selection. This process is looped as many

times as the user decides is necessary by which times it is hoped, the candidates have homed in on the global optimum.

The principle advantage of this technique is its resistance to becoming trapped in local optima coupled with an efficient exploration of the parameter space. It also represents a highly adaptive and versatile method of optimization mimicking the process on which it is styled. The major disadvantages of the technique are that it is not efficient for small numbers of parameters and may not represent the fastest most efficient method. It is also classified as an heuristic method meaning while it will generally produce a good solution (providing a good definition of the fitness function is given) it may not be the absolute optimum.

Others have previously applied GAs to engineering problems [25] [60] and specifically to fire engineering problems [63] [48] with success. Applications involve adaptation of the GA to the specific problem by varying the method of selection, crossover, probability of mutation and some cases by creating a hybrid through combination with other optimisation techniques. An example of this could be a hill climbing (gradient based) optimisation that attempts to improve the candidates of the new population produced at each stage by the GA. For the purposes of this work where optimisation is likely to be performed repeatedly, an adaptation where the process is enhanced by previous solutions is envisaged. Steady State GAs use a specific variation on selection which does not produce a majority of completely new individuals at each generation of the cycle. There is far greater generational overlap with only the weakest individuals being replaced by products of the fittest via crossover etc. This makes them ideal for evolving systems where an element of learning and retention of what has already been learned is desired [52]. In each new optimisation it is possible that the initial population is seeded by the fittest candidates from the previous solution thus further enhancing the retentive nature of this hybrid system. For a system such as that proposed by this work where the variables being optimised are expected to converge at each stage when more sensor information is available, retention of solutions between iterations could reduce the computational demands as the process progresses.

2.4.3 Ant Colony Optimisation (ACO)

The concept behind this method of optimisation is based on the observed behaviour of ant colonies and their methods of guiding other colony members to sources of food via an optimal route W[4] [22]. The algorithm drawn from these observations draws many direct parallels to this behaviour representing ants by autonomous agents that have certain limited tools such as the ability to communicate information locally. Ants initially set out wandering at random. If they find a food source they will return to the nest laying down a trail of pheromones as they go. If another ant searching for food comes across this trail it will be more likely to follow the trail than continue wondering at random. If it then finds food it will return along the trails reinforcing the levels of pheromones making it more likely that subsequent ants will follow. The more a trail is travelled, the denser the pheromone levels become, and the more ants follow it. The process thus has the advantage that it will find acceptable solutions

from the early stages of application which will improve in time through positive feedback.

An important characteristic of this process is that the pheromones evaporate over time and if no ants find the trail or discover food by following it, the trail will eventually disappear. This process encourages the finding of the shortest (or optimal) path as an ant travelling a longer path will take longer to return hence allowing time for the pheromone trail to evaporate. If the trail is short the ant will return quickly and reinforce the still present pheromones of previous ants thus making the path more attractive to others. Evaporation of pheromone trails helps to avoid convergence on local good solutions as otherwise ants would tend to continue to follow the first trails laid and thus always tend to the same location / local optima even after the food source had been consumed / the solution is no longer a good one.

Another important characteristic of the pheromone trail is that the information it provides is only known locally. This also helps to ensure that the search space is explored more holistically as not all agents are immediately influenced by the first solutions found. Only an ant that comes across a pheromone trail will know of its existence and be able to make the choice as to whether to follow it. Other colony members / agents that don't encounter the trail will continue to search randomly until they find a new source of food or a different trail / potentially better solution. Thus while one ant / agent will find a solution, by working together, a number of agents will find a good or better solution by stimulating both themselves and each other based on success and searching a wider area / search space more effectively.

This method of optimisation lends itself to problems where an optimal path must be found but where the optimal path may change during the process. Thus the technique is potentially well suited to real time applications involving fire where the variable nature of fire means that the optimal solution could change as the fire grows and spreads. This particular advantage is explored as part of the FireGrid project (Section 2.5) by French et al. [36] where a conceptual system for routing building occupants in an evacuation using real time planning is proposed. The best evacuation route(s) is optimised given constraints such as current building conditions, predicted fire and smoke spread, occupant locations and pathway capacities etc. Occupants are then directed on the bases of this, by some means, towards an exit. As the fire spreads or the prediction of the fire spread changes, the most optimal route(s) may change with it. It is proposed that an optimisation technique such as ACO could adapt successfully in real time based on evolving information to safely and efficiently evacuate occupants from a building by reacting to actual fire conditions rather than the occupants simply following a pre-proposed strategy.

2.5 Similar Projects and Works

Numerous projects exist that envisage the need for a paradigm shift in the way fires are fought citing the use of computational models in conjunction with optimisation techniques to provide rapid, robust predictions using live sensor data to steer the computations. Thus the need for accurate super real time predictions of fires and structural response will be an essential element to the success of such projects.

The FireGrid project (discussed in Section 1.1) which is the umbrella project under which this work falls brings together many areas of research expertise such as High Performance Computing (HPC), Distributed Grid Systems, Sensing and Digital Communications, Artificial Intelligence (AI), and Fire and Structural Engineering. The projects main goal is the paradigm shift described above and aims to meet this goal through a system where rapid, robust predictions of fires and structural response, inform real time planning of evacuation and emergency response, steered by live sensor data from the emergency itself and a pre-computed database of scenarios. From the point of view of fire and structural engineering, the main challenges to the realisation of this goal are the ability to accurately predict the evolution of the fire and structural response using computational models such as Computational Fluid Dynamics (CFD) and Finite Element Analysis (FE), and the ability to predict these responses rapidly enough to give sufficient lead time to the planning of the evacuation and response. More details on the FireGrid project, the research stemming from it and future work can be found in [7] [16] [45] [75].

Neviackas et al. [55] have proposed a study whose global objective is the paradigm shift mentioned above where sensor data, specifically imaging from regular and thermal cameras of external spill plumes, combined with zone modelling and optimisation techniques are combined to provide information about the fire inside. Initially the project will focus on developing an Inverse Fire Modelling Algorithm using a zone model and genetic algorithm. The input defining the initial population of the GA will comprise output from a database of zone models which will be optimised to provide the closest match between model predictions and sensor data. A concept for Intelligent Evacuation, Rescue, and Recovery (IERR) to aid personnel responsible for making decisions in emergencies such as fires and attacks in and against buildings has been proposed by Miller-Hooks et al. [51]. The authors propose that by integrating blast damage assessment and target vulnerability assessment with online optimisation assisted evacuation software, real time assistance can be provided to emergency responders to enhance the information available to them.

3 Flame Spread Model

The ideal model for this application should encapsulate the physics of upward flame spread primarily so that sensor measured physical quantities can be used to steer it and then subsequently validate predictions made from it given additional sensor data. The model should be simple and practical enough that extensive computation is not needed thereby overcoming one of the major problems associated with CFD modelling. It is desired that as many as possible of the parameters contained in the model be physically measurable, to keep the level of optimisation and therefore computational demands to a minimum thus enabling the rapid and robust prediction of upward flame spread. By correctly capturing the physical aspects of the spread process, the parameters established within the model can aid in the calculation of heat transfer to other objects and prediction of secondary ignition if extrapolated to a more complex scenario.

3.1 Theoretical Model

The model chosen to test the hypothesis is based on the description of flame spread as a solid ignition process. The basic model describing this is given in Equation 2: -

$$V_f = \frac{l_h}{t_{ig}}$$

Equation 2

V_f represents the spread rate, l_h is the heated length being ignited and t_{ig} is the time to ignite l_h. The heated length as described earlier (Section 2.1.4) can be defined in terms of the flame length (l_f) and the pyrolysis length (l_p) which are related using either Equation 9 or Equation 10, the former being a derivation of the later with n = 1.

.

$$l_f = cl_p$$

Equation 9

$$l_f = cl_p^{\,n}$$

Equation 10

Fernandez-Pello [17] states that, due to the nature of the wall flame which is close to the surface, specifically the surface ahead of the pyrolysis front in the direction of flame spread, the heated length can be approximated by the flame length ($l_h \sim l_f$).

Combined with the expression for t_{ig} given in Equation 4, the spread rate can be expressed as: -

$$V_f = \frac{4[\dot{q}_s'']^2 l_f}{\pi k_s \rho_s c_s (T_p - T_0)^2}$$

Equation 11

Equation 11 now defines the spread rate as function of physical parameters, some of which are fairly well defined such as material properties, and others such as temperatures, heat fluxes, and lengths which are potentially measurable parameters. Breaking down the term for net heat flux to the surface into constituent parts as per Equation 5, Equation 11 becomes: -

$$V_f = \frac{4[\dot{q}_{conv}'' + \dot{q}_{fr}'' + \dot{q}_e'' - \dot{q}_{rs}'']^2 l_f}{\pi k_s \rho_s c_s (T_p - T_0)^2}$$

Equation 12

By introducing the expression for convective flux given by Equation 6, Equation 12 becomes: -

$$V_f = \frac{4[h_{conv}(T_{fl} - T_0) + \dot{q}_{fr}'' + \dot{q}_e'' - \dot{q}_{rs}'']^2 l_f}{\pi k_s \rho_s c_s (T_p - T_0)^2}$$

Equation 13

Equation 13 is of the form expressed by Fernandez-Pello [17] for laminar flame spread shown by Equation 14 where the convective heat transfer coefficient is represented by physical parameters and the flame length replaced by the expression given in Equation 9.

$$V_f = \frac{4c_2[(c_1 k_g \rho_g c_p u_\infty / l_p)^{1/2}(T_f - T_p) + \dot{q}_{fr}'' + \dot{q}_e'' - \dot{q}_{rs}'']^2 l_p}{\pi k_s \rho_s c_s (T_p - T_0)^2}$$

Equation 14

The expression for the convective heat transfer coefficient is derived from Equation 7 which is the generic expression of the Nusselt number for laminar flow parallel to a flat plate.

$$h_{conv} = \frac{0.66\,\mathrm{Re}^{1/2}\,\mathrm{Pr}^{1/3}\,k}{x} = (c_1 k_g \rho_g c_p \frac{u_\infty}{l_p})^{1/2}$$

The derivation of this relationship is given in Appendix 1. The type of model given by Equation 14 taken from the work by Fernandez-Pello [17] is referred to by the author in the same work as theoretical models, "which include the dominant controlling mechanisms, but that are simplified enough to provide explicit formulae that can be used in practical applications and overall models of an actual fire with reasonable accuracy", thus identifying the model as fitting the criteria of this work.

3.2 Classification of the Model Parameters

3.2.1 Material and Gas Properties

The material and gas properties in Equation 14 are assumed to be constant throughout the experiments. Typical values are given below.

Thermal Conductivity of Air (k_g) = 0.026 W/m.k
Density of Air (ρ_g) = 1.1 kg/m^3
Specific Heat Capacity of Air (c_p) = 1040 J/kg.K

Thermal Conductivity of PMMA (k_s) = 0.19 W/m.k
Density of PMMA (ρ_s) = 1190 kg/m^3
Specific Heat Capacity of PMMA (c_s) = 1420 J/kg.K

(Values taken from Drysdale [24])

3.2.2 Scenario Specific Constants

There are various temperatures defined in the model. These values are assumed to be constant but are scenario specific, and thus need to be defined through direct measurement during the tests. T_f represents the temperature of the flame, T_p represents the pyrolysis temperature of the material over which the flame is spreading and T_0 represents the initial temperature of the material. The constant c_1 (Equation 15) forms part of the convective heat transfer coefficient. Elements of this constant such as the momentum diffusivity are difficult to define or measure and are thus grouped into this parameter which can be optimised as part of the system being proposed in this work.

$$c_1 = \frac{4}{9}\nu\alpha \,\mathrm{Pr}^{2/3}$$

Equation 15

This particular expression is valid only for laminar flow and the derivation that leads to it is shown in Appendix 1. A system that makes use of optimisation such as the one proposed benefits from a generic term like c_1 as the flame spread expression in Equation 14 is thus more generic and not reliant on individual expressions for each variant of the convective heat transfer coefficient. The constant c_2 is defined in terms of the flame and pyrolysis length by Equation 9 for laminar flames and Equation 10 for turbulent flames. Like c_1, this value can be optimised from measurements.

3.2.3 Time Variant Measurable Quantities

Quantities such as length scales, velocities, and heat fluxes need to be measured throughout the experiments to determine how they vary in time. Sensing and measurement techniques have been adapted from the literature (Section 2.2.3) and are described in Section 4.2.

3.3 Model Assumptions

There are numerous assumptions embedded within the model described by Equation 14 outlined in the literature [17], some of which are outlined here. Heat transfer by conduction through the solid is considered to be one-dimensional and directed into the solid surface and not parallel too it. This means essentially that conduction ahead of the pyrolysis front in the direction of spread can be neglected and hence is not included in the model. This assumption is justified as the contribution made by conduction is orders of magnitude less than the corresponding convective and radiative contributions depending on the conditions of the flame. The contributions from convection and radiation to the heating of the fuel ahead of the pyrolysis region occur only in the region between the pyrolysis front and the flame tip. Heating from combustion products above of the flame tip is neglected as it is of minor influence when compared to the heat provided in the flame region. Heat flux to the unburned surface in the heating region covered by the flame is assumed to be constant over the entire heated length. The heated length is approximately equal to the flame length.

Due to the position of the flame in the wall configuration covering the solid surface, combustibles are ignited rapidly by the flame when produced. Given this strong piloted ignition, the time to pyrolyse the fuel is significantly greater than the time associated with igniting the combustibles once they leave the fuel surface. Thus this later time can be neglected and the ignition time is assumed to be approximately equal to the heating or pyrolysis time (Equation 4).

The model as defined in Equation 14 assumes a non sooty laminar flame with negligible radiation. For this regime the flame and pyrolysis length are assumed to be linearly proportional according to Equation 9. In order to account for a turbulent regime, the relationship should be adjusted to follow a power law correlation as defined in Equation 10. Material and gas properties are assumed not to vary with temperature. Materials are also considered non-charring. The pyrolysis temperature is defined as a single constant value as is the flame temperature.

4 Flame Spread Experiments

Having established a physical model of upward flame spread from the literature, an experiment to reproduce conditions that the physical model describes and from which to collect sensor data to feed the model was designed. The sensing equipment was also developed with the intension of directly providing as many of the model parameters as possible. The setup was based on an established experiment from the literature in order to assess the reliability of the results without excessive repetition and also establish the robustness of the measurement techniques. Based on these experiments a methodology can then be developed to link the sensor data to the model in a form that produces rapid, accurate predictions of the flame spread in conjunction with optimisation techniques. Aspects of the experiments will then change, further complicating the spread scenario to define the limitations of the new methodology.

4.1 Experiment Design

The model taken from the literature shown in Equation 14 describes laminar concurrent flow flame spread over a thermally thick solid surface. The experiments described in Fernandez-Pello [29], of upward laminar flame spread, are deemed compatible with the model. The experiments, described in parts in Section 2.2, use PMMA slabs 200mm high and 38mm thick. Literature suggests that flames will remain laminar in character in the region of the fuel and that the fuel source can be considered thermally thick. Although the bench mark experiments report spread under various levels of external radiation, data is given for spread rates, pyrolysis lengths and flame lengths without external sources of heat flux which will be the conditions for the initial experiments performed in this work. The initial experiments consist of the simplest scenario to be tested in order to adhere best to the analytical model. Upward flame spread will take place on vertical sheets of PMMA 200mm high under closely matched conditions to those of the benchmark experiment. These experiments will be used to construct the methodology and assess the sensing techniques developed. The methodology will then be applied to results of experiments that differ slightly to these initial ones. The baffles used in [29] to maintain a two dimensional flow will be removed, the thickness of the PMMA and the quality/grade of the PMMA will all be varied to assess the robustness of the methodology and the sensitivity of the experiment to these changes. Later the scenario will be complicated further to include concurrent flame spread over tilted PMMA sheets, upward flame spread over longer vertical sheets to allow transition to turbulent flame spread, and a large scale sample undergoing secondary ignition during a compartment fire.

4.1.1 Benchmark 200mm Experiment

Two steel plates as depicted in Figure 4.1 formed a frame in which to hold the PMMA. The design for these plates was based on the description and diagram from

the benchmark experiment. The plates were mounted on a lead screw driven slide so that they could be moved together to clamp the PMMA sample firmly. In order to insulate the PMMA from the steel supports, 10mm thick fire board insulation was sandwiched between the plates and PMMA. Baffles which formed part of the steel framing were designed to maintain a two dimensional flow field and tilted away from the fuel surface to prevent re-radiation back to it. The final exposed surface was 200mm high and 100mm wide. Fireboard identical to that between the PMMA and plates was placed above and below the surface and flush to it in order to create a wall effect. The chosen ignition method was a Nichrome wire running across the surface at the base of the fuel sample. The wire was heated prior to the experiment and pressed into the PMMA to maintain a smooth wall effect. When the sample was placed in the frame, the wire passed through the steel plates and was tensioned by springs on both sides in order to maintain its position after expansion during heating.

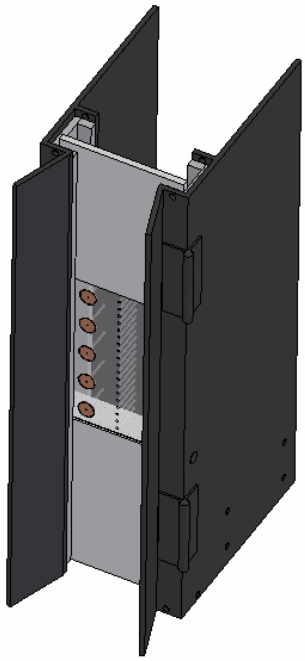

Figure 4.1- *A replication of the PMMA sample holder used in the experiments by Fernandez-Pello [29] based on descriptions in the work.*

The frame was fixed, via the slide, to a versatile aluminium extrusion frame (Figure 4.2) which enabled the experiment to be moved within the overall setup to accommodate the future changes to the scenario. The extrusion frame system enabled easy, rapid fixing and positional adjustment of all of the sensing equipment relative to the experiment. The entire frame was housed in a smoke box, 2.5m x 2.5m x 2.5m high, in order to maintain, as closely as possible, identical environmental conditions throughout all experiments.

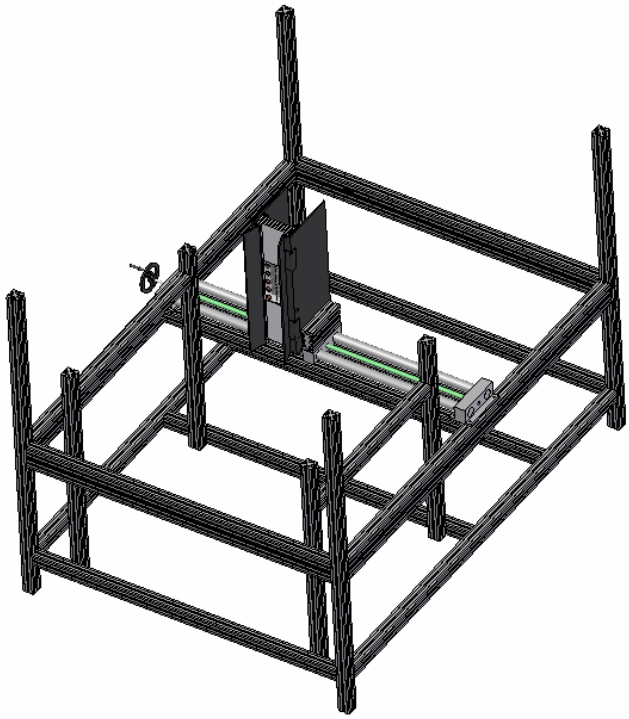

Figure 4.2 – *The diagram shows the housing of the sample holder frame in the aluminium extrusion frame.*

The experiments were initiated by a piloted ignition. Current was passed through the Nichrome wire which heated resistively. Upon the visible observation of combustible gases leaving the sample around the wire, the current was stopped and a butane fuelled blow torch was used to pilot ignite the gases along the length of the wire. If ignition did not occur within a few seconds, the process was repeated. Upon ignition, the door to the smoke box housing the experiment was closed.

4.1.2 Regular 200mm Experiment

The main difference in this first evolution of the initial experimental setup was the removal of the baffles that were used in the benchmark experiment to ensure a 2D flow field at the exposed face. The thickness and quality of the PMMA sample was also varied. Samples identical to the benchmark samples were used for comparison, whilst 25mm thick samples of identical and lower quality PMMA were also used. The sample itself was housed as shown in Figure 4.1 and Figure 4.2 minus the baffles.

4.1.3 Tilted 200mm Experiment

The setup of the PMMA sample in the steel frame with the exposed face isolated was again identical to the benchmark experiments and as with the regular 200mm long samples, the baffles were removed. The PMMA samples themselves were either 40mm or 25mm in thickness, with the 25mm thick samples ranging in quality. 40mm samples consisted only of the higher quality PMMA used in the benchmark experiments. All samples were 200mm high. The major change in this subset of experiments was the angle of the exposed surface which was set at 30˚ to the horizontal as shown in Figure 4.3.

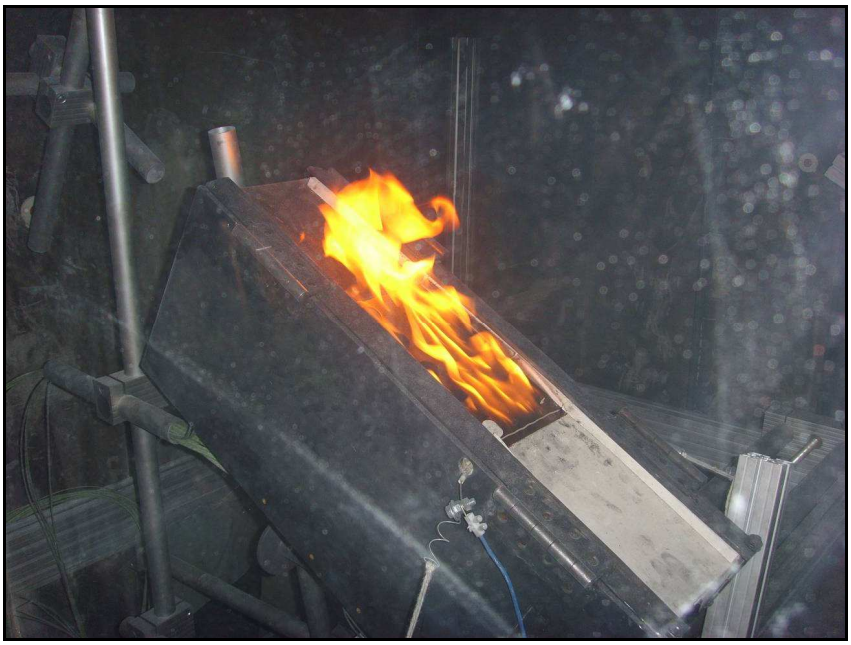

Figure 4.3 – *The image shows the setup of the tilted sample and sample holder within the extrusion frame. All other aspects of the housing of the sample are identical to the regular 200mm experiments.*

4.1.4 500mm Experiment

In order to achieve a more turbulent flame the length of the PMMA sample was increased to 500mm. It was placed into the same steel clamping plates with the baffles removed as used in the regular and tilted 200mm length tests. Due to the increase in sample size, the fire board placed flush with the exposed surface at the top and bottom of the sample was reduced to 50mm in length preserving the isolation of the exposed face and maintaining a smooth wall effect above and below the sample. Two grades of PMMA were used for these tests, both 25mm thick. As before there was a higher quality grade, as used for the initial 40mm thick experiments, and a lower quality grade.

4.1.5 1000mm Sample in a Compartment Fire

This one off compartment fire experiment comprised a PMMA slab, 1000mm high, 30mm wide and 25mm thick, which was placed on the wall of the main experimental compartment of Dalmarnock Fire Test One, with the base one meter above the floor (Figure 4.4). The PMMA was mounted on a larger piece of gypsum plasterboard using Furnace Cement and then mounted on the wall using four screws. The rear face was protected although spread to the outer edges was not prevented.

The sensor wires protruded from the rear of the sample and passed through the plaster board. For this reason the rear had to be protected from any heat damage so spray on insulation was used to prevent the fire from spreading behind the plasterboard. The wires ran down the wall from the plasterboard and were run under the carpet to the data loggers in order to prevent exposure to the severe fire conditions. The wires themselves were individually insulated against the heat and were bunched together and wrapped in rock wool insulation and aluminium foil between the experiment and floor level.

Dalmarnock Fire Test One (discussed in Section 1.3) consisted of a compartment fire in an apartment in Dalmarnock, Glasgow, UK. The fuel was provided by regular living room / office furniture. The furniture in the vicinity of the experiment can be seen in Figure 4.5. Full details of the experiment are available in Abecassis Empis et al. [1].

Figure 4.4 – *The image shows the sample mounted in the compartment fire experiment of Dalmarnock Fire Test One.*

Figure 4.5 – *The photo shows some of the furniture and sensing equipment in the direct vicinity of the PMMA sub experiment.*

4.2 Measurement Techniques

Based on the review of existing measurement techniques and the parameters required to satisfy the model, various sensing techniques were adopted and adapted to meet the requirements of this work.

4.2.1 Pyrolysis Length Measurement

The flame spread model in Equation 14 requires a measurement of the length of the pyrolysis region as an input to the spread-rate calculation. The evolution of the front of pyrolysis bubbles corresponding to the spreading front and thus the pyrolysis length can be visually observed through the transparent PMMA. Under the ethos of FireGrid however it was desired that the process of tracking this front be automated using sensors. For this reason it was decided that a method involving the measurement of sub-surface temperature to track the moving front be used, following loosely the method used by Consalvi et al. [13]. A line of holes at 10mm spacing were drilled along the centre lines of the test specimens, from the rear side to within two millimetres of the front surface where the flame spread was to take place. Thermocouples were inserted into these holes and secured tightly using metal wires such that the thermocouple beads were pressed tightly against the ends of the holes. This set up is shown in Figure 4.6.

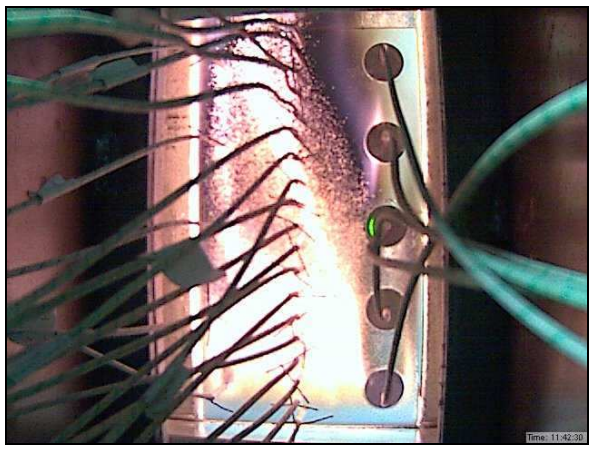

Figure 4.6 – *The image shows a test specimen seen from the rear during a flame spread experiment. The 10mm spaced sub-surface thermocouples can be seen along the vertical centreline of the PMMA slab while the front of bubbles corresponding to the early stages of pyrolysis can also be distinguished, highlighted by the flame.*

The choice of this method introduced the need to establish the temperature corresponding to the arrival of the pyrolysis front when measured by the thermocouples at the ends of the drilled holes. Dakka et al. [19] showed that the pyrolysis temperature is not one fixed value as the reaction rate of the solid differs significantly when conditions are changed. Also it appears that the formation of pyrolysis products below the surface of the PMMA occurs in a two-step reaction where oxygen availability on the surface plays an important role. All these effects mean that the pyrolysis reaction of PMMA occurs over a range of temperatures of approximately 200 to 350˚C. An estimate of the variation of the sub-surface temperature with respect to the proven surface temperature range is not easy to establish and thus a simple approach is followed to determine the temperature indicated by the embedded thermocouples that shows the best correspondence to pyrolysis at the surface. This temperature was evaluated using a combination of video footage and temperature data. The experiments were filmed through the rear of the PMMA samples so that the pyrolysis front movement could be visually observed (Figure 4.6) and pyrolysis length vs. time relationships recorded and plotted from these observations. The evolution of a range of temperatures recorded at the sub-surface thermocouples was also plotted and the visual observations were superimposed over the isotherms (Figure 4.7). The overlap of these data enabled the matching of a specific range of isotherm temperatures with the spread rate corresponding to the camera observations.

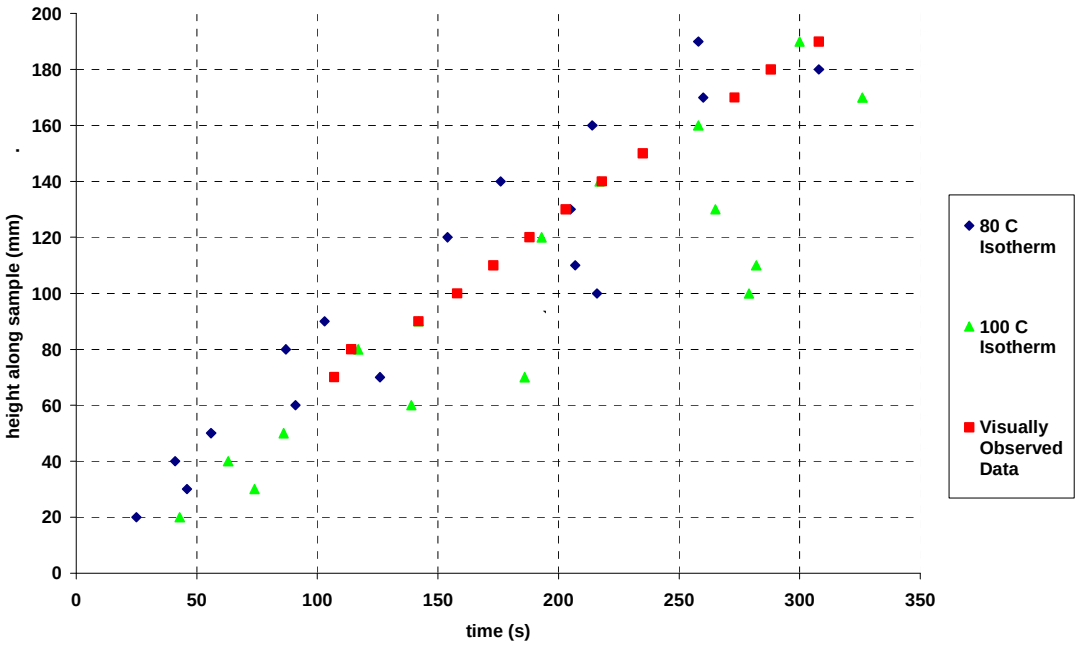

Figure 4.7 – *The plot shows the comparison of isotherm evolution plotted with observations from video footage from a flame spread experiment.*

The results of three benchmark style experiments were analysed in this way and the results repeatedly showed that the visually tabulated data fell into a range of 80˚C to 100˚C. The temperature range defined by Dakka et al. [19] reported above represents the surface of the fuel whereas the sensing method employed here gives readings at a depth below the surface, thus the measurements here appear lower due to thermal lag. It can be seen in Figure 4.7 that the gradients of the lines associated with the isotherms within this temperature range are similar so the implications of the choice of a specific isotherm temperature to represent the pyrolysis front would not have significant impact when extrapolated to a flame spread rate. It is believed that the visual observations corresponded to the initial stages of the overall pyrolysis reaction and thus the lower end of the range of temperature over which this process occurs. The results appeared to correlate best with a measurement of 80˚C so this value was initially chosen as the best representation of the arrival of the pyrolysis front.

4.2.2 Flame Length Measurement

To provide a measurement of flame height, a method was devised similar to that of Audouin et al. [5], Conslavi et al. [13] and Fuentes [37] to extract accurate length scale measurements from video footage of the spreading flame. The process was required to eliminate background noise on the images and measure the height of the flame whilst overcoming the effects of the flickering of the flame.

4.2.2.1 Measurement Method

The flame spread process was filmed from beginning to end with simple webcam style Charge Coupled Device (CCD) cameras. The exposures are broken down into a grid of pixels, each of which is represented by a light sensitive capacitor, that when exposed to light stores charge. For a black and white image, the amount of charge stored equates to a degree of whiteness. For a colour image, each pixel is represented by four such capacitors with band-pass filters, one red, one blue and two green. The combination of the amount of light received, of each of these three colours, relates to the actual colour that the pixel should be. Individual frames were taken from the video chronologically and converted from coloured frames to grey-scale (black and white) images. The data representing a coloured frame is stored in the form of a three-dimensional matrix, equating to the two-dimensional size of the image in pixels, and three values deep representing the amount of red, green and blue light describing the colour in the pixel. The conversion to grey-scale leaves a two-dimensional matrix with each value lying between 0 (black) and 255 (white) which describes a grey version of the colour image (Figure 4.8).

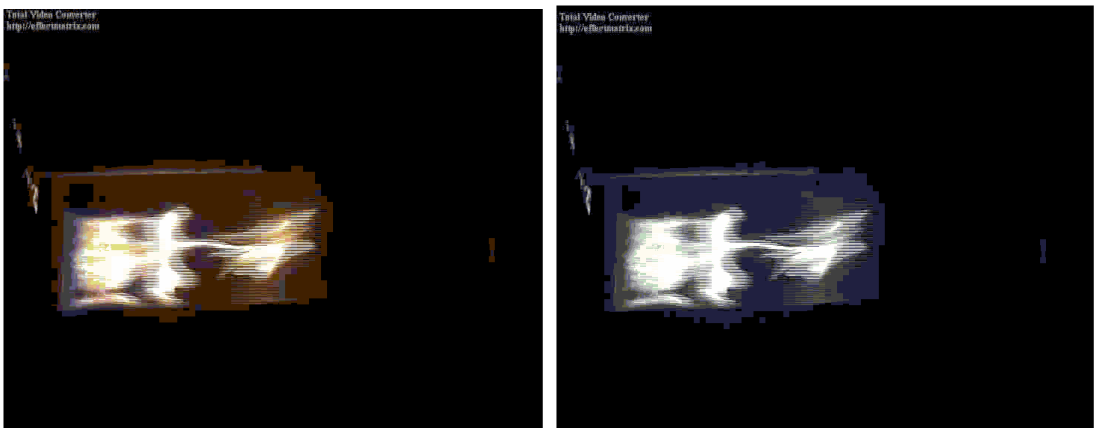

a) b)

Figure 4.8 – *a) a colour image and b) the corresponding grey-scale image.*

In order to measure the length of the flame in the image the background noise must first be removed. This is accomplished by binarising the image i.e. setting the pixel values to either zero (black) or one (white), around a threshold set somewhere between 0 and 255 (Figure 4.9). This takes advantage of the naturally high level of luminosity of the flame compared to its surroundings. The background objects should be less bright and thus by setting the threshold sufficiently high will leave only the bright flame in the image. The threshold level should also be set suitably low so as to minimise the losses of the less luminous edges of the flame in this process. For these reasons, a threshold sensitivity analysis was conducted and is presented in Figure 4.11.

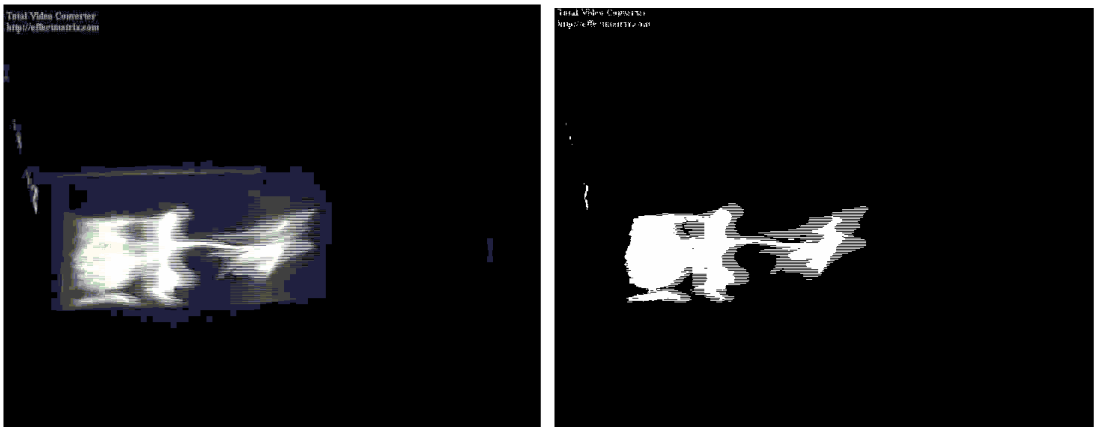

a) b)

Figure 4.9 – The *images demonstrate the changes resulting from the conversion from a) the grey-scale image to b) the binarised image.*

Once this process has taken place for all of the images in a given second, the binary images can be averaged to give a flame presence probability value between 0 and 1 for each pixel during that discreet period of time. A threshold value must then be chosen, again influenced by a sensitivity study, that either side of which the flame is considered to have been present or not present in each pixel over the measurement time. The image is then binarised a second time using this presence probability threshold.

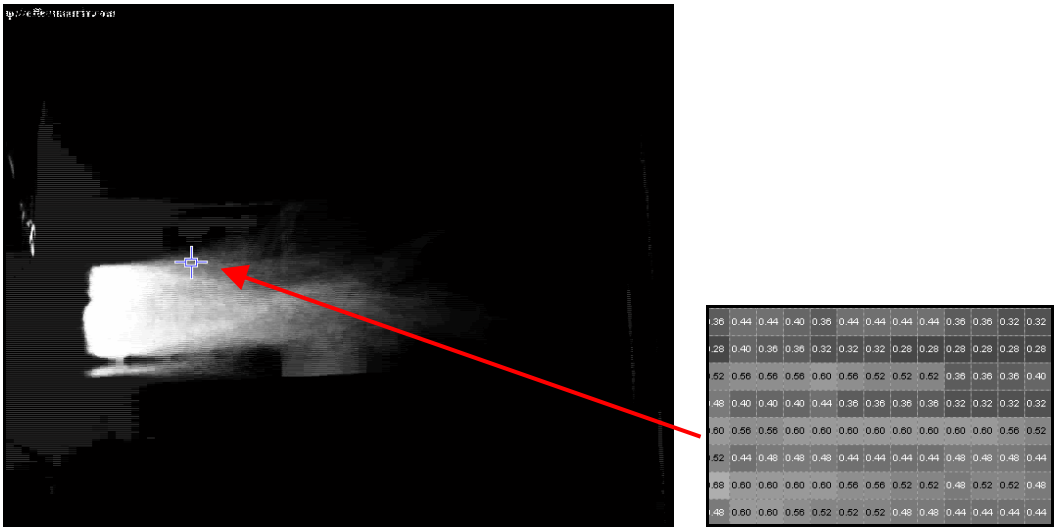

Figure 4.10 – *The presence probabilities for each pixel determined from every frame from a period of one second.*

Once presence is established, a simple search and measurement of the extremities of the flame can be performed and given a known distance per pixel ratio for the images, a physical length can be established at each discreet time period. This entire process took place after the experiment itself by extracting the frames from the stored video footage but it is equally possible to perform it in real time.

4.2.2.2 Sensitivity to Noise Elimination Threshold

The sensitivity of the results to the background noise elimination threshold yielded clear and consistent results (Figure 4.11). Below a value of 50 out of the possible 255, very little of the image background is eliminated and the resulting binarised image shows the presence of a flame equal to height of the image. Clearly this is not the size of the flame itself but simply the non elimination of background noise leaving a white presence zone equal to the height of the image.

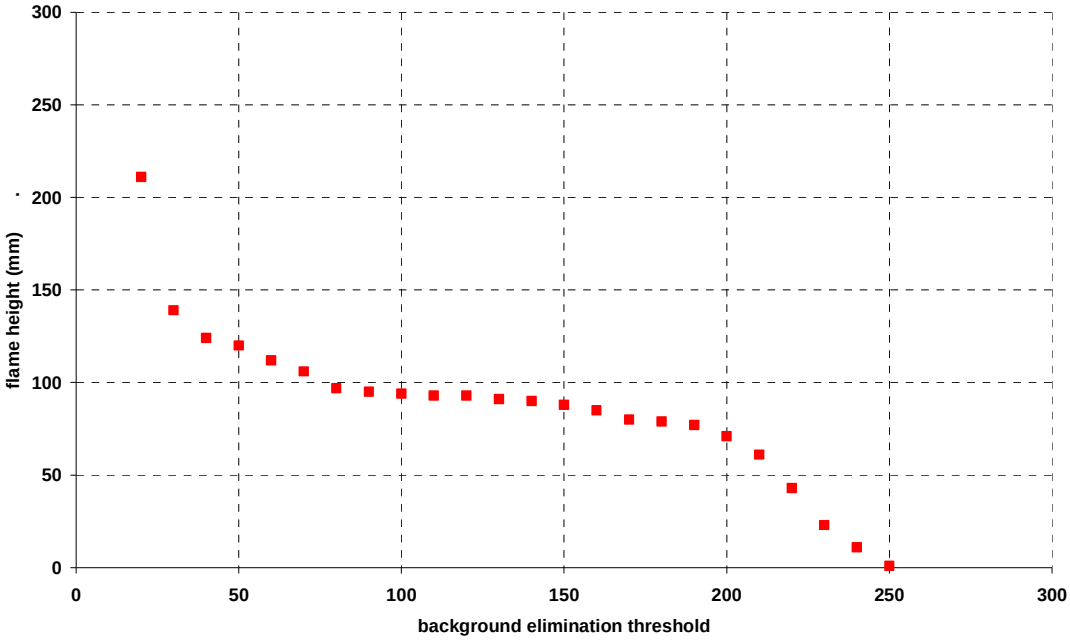

Figure 4.11 – *The graph shows the variation of the resultant flame height with the background elimination threshold. The result was tested for different sets of data and found to be repeatable.*

Between the threshold values of 50 and 100 there is significant sensitivity to a change in the threshold. Toward the lower end of this range where the sensitivity is steepest, this is believed to be simply the progressive elimination of background noise until the flame becomes the sole object of measurement. Beyond this the difference is believed to be indicative of the elimination of the less radiant, outer extremities of the flame shown in Figure 4.12.

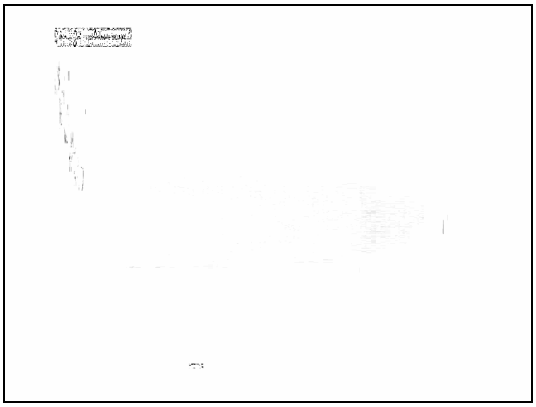

a) threshold = 10

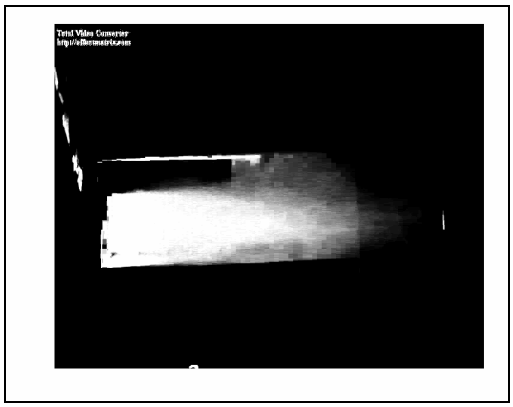

b) threshold = 60

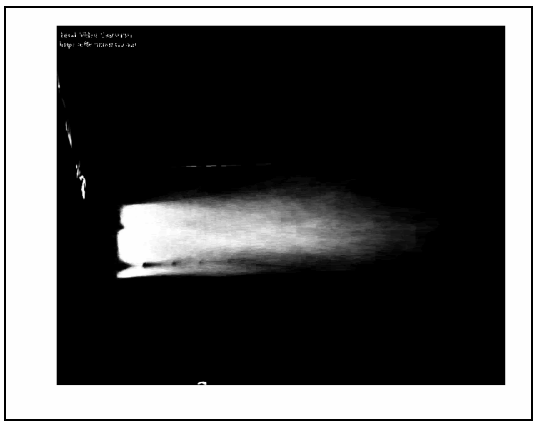

c) threshold = 130

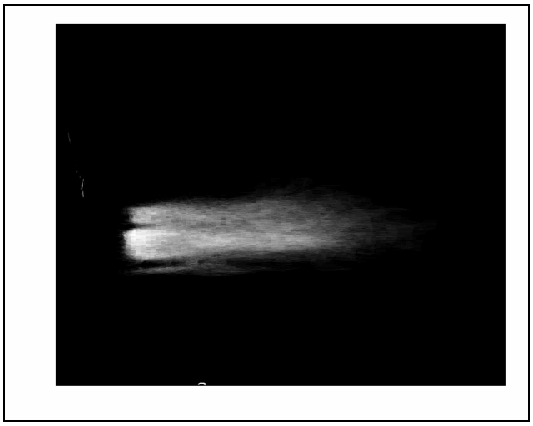

d) threshold = 240

Figure 4.12 – *The resultant images when treated by a range of background elimination thresholds.*

Between a range of approximately 100 and 200, very little sensitivity to the variation in threshold is observed. From this it is concluded that within this range is the optimal value for the threshold and thus a value of 130 is selected. Above this until the maximum possible value of 255 at which value the entire image detail would be removed, we see a gradual shrinking of the flame as only the most luminous inner parts remain in the image.

4.2.2.3 Sensitivity to Flame Presence Threshold

The sensitivity of the results to the flame presence probability threshold showed that for a range from approximately 0.4 to 0.8, the results remained fairly constant (Figure 4.13). Thus a median value of 0.5 corresponding to the flame having been present in a pixel for at least half of the discreet measurement period was chosen.

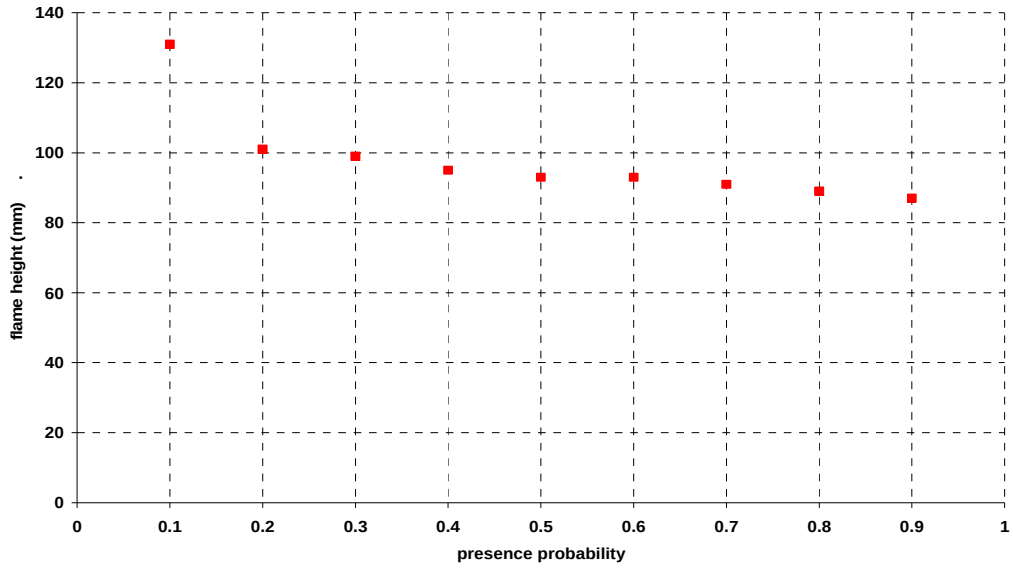

Figure 4.13 – *Results of the analysis of the sensitivity of the flame length measurements to the presence probability threshold. The result was tested for different sets of data and found to be repeatable.*

4.2.3 Heat Flux Measurement

The requirement to measure radiative heat flux to the surface of the unburned PMMA from the flame and potentially from other external sources was carried out through the use of specifically designed thin skin calorimeters.

4.2.3.1 Design and Construction Method

The design used in this work comprised a 20 mm diameter, 2 mm thick copper disc with a small hole drilled through the centre at a 45 degree angle. The diameter of this hole was such that the bead of a type K thermocouple [11] could just be inserted into it. A thin point chisel was then used to close the hole and thus pinch the thermocouple bead tightly into the copper disc (Figure 4.14).

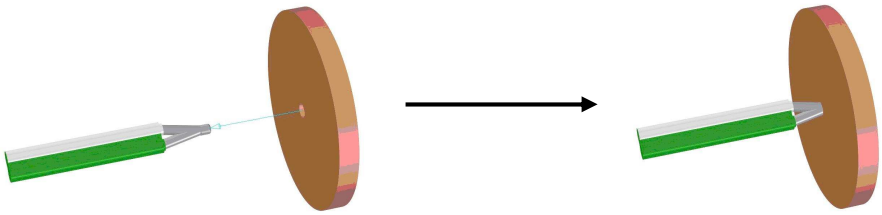

Figure 4.14 - *The thermocouple bead is inserted into the hole in the copper disc and trapped tightly within using a chisel.*

The copper disc was then pressed tightly into a flat bottomed hole of equal dimensions set into, and flush with, the surface of the test sample (Figure 4.15). The thermocouple wire passed through a hole just large enough to accommodate it through to the back of the sample and to the data logger. The exposed surface of the copper disk was coated thinly with matt black paint to achieve an emissivity close to one.

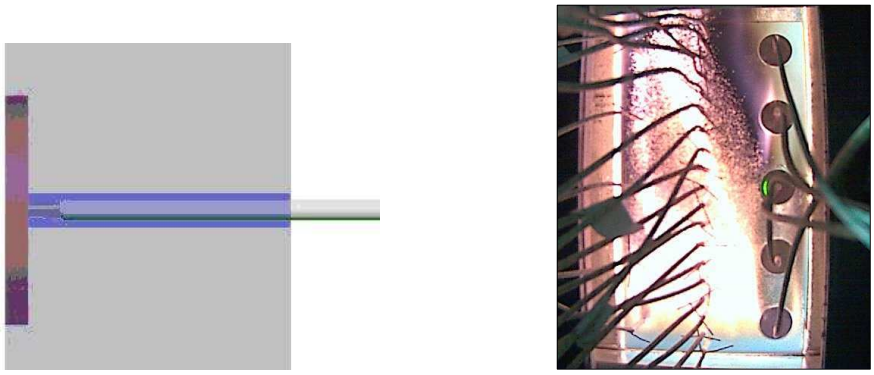

a) b)

Figure 4.15 – *The copper disc is set firmly into a flat bottomed hole of equal dimensions with the thermocouple wire passing through the rear of the sample. They are spaced evenly through the surface of the test specimen.*

The construction of these sensors was relatively simple, rapid and cheap, and was carried out with reference to international standards [4]. The validation of the choice of material and dimensions that comprised the thin skin calorimeters is detailed in [3], the work of which was carried out in parallel with this work.

4.2.3.2 Converting Temperature to Heat Flux

The method for calculating heat flux from temperature was similar to that used by Alston [2]. To calculate the heat flux incident on the disc, an energy balance was performed on the disc as shown below in Equation 16.

$$\rho c \tau \frac{dT_s}{dt} = \alpha_s \dot{q}_i'' - \varepsilon_s \sigma (T_s^4 - T_0^4) - h_{conv}(T_s - T_g) - [(4\varepsilon_b \sigma T_s^3 + h_{cr})(T_s - T_i) + \dot{q}_{klat}'']$$

Equation 16

The term on the left side describes the total heat stored in the calorimeter. The right side describes how heat arrives and leaves. The first term on the right side describes the portion of the incoming heat that is absorbed by the disc, which represents the desired measurement. The second and third term describes the heat that is radiated and convected respectively to the gas phase in front of the disc. The final term describes the heat lost to the back and sides of the calorimeter. The term on the right hand side and both the radiative and convective terms all involve known or measurable quantities. Only the conductive losses prove difficult to measure. For that reason it was decided to lump the conductive losses together into one term and to try to quantify them as a portion of the incoming heat flux (Equation 17). This quantification process, performed experimentally, is described below.

$$\rho c \tau \frac{dT_s}{dt} = \alpha_s \dot{q}_i'' - \varepsilon_s \sigma (T_s^4 - T_0^4) - h_{conv}(T_s - T_g) - [A\dot{q}_i'']$$

Equation 17

4.2.3.3 Calibration Experiments

In order to calibrate the heat losses from the discs to their PMMA surroundings, tests were carried out using a gas supplied radiant panel and a calibrated Gardon Type water cooled heat flux gauge. The radiant panel was turned on and allowed time to heat up. A calibrated Gardon Type heat flux meter was placed in front of the panel during this time to measure the heat flux from the panel and assess when it had reached a steady state regime. Once this point had been reached, the heat flux was noted and the heat flux gauge removed. A set of five Thin Skin Calorimeters, set into PMMA samples using the same production method as outlined above and arranged in a cross pattern as shown in Figure 4.16, were placed at an identical distance to the panel heater as the heat flux gauge had been. The temperatures of the discs were recorded and the test was allowed to continue until the temperatures of the discs had approximately reached a steady state. At this point the panel was turned off and the discs left to cool for a prolonged period of time until they and the PMMA had reached room temperature again. This process was repeated for a variety of heat fluxes using fresh discs whenever they showed effects of the heating so as not to change the boundary conditions being assessed. These effects included the blistering

of the black paint used to coat the exposed surface or bubbles appearing in the PMMA in contact with the disc.

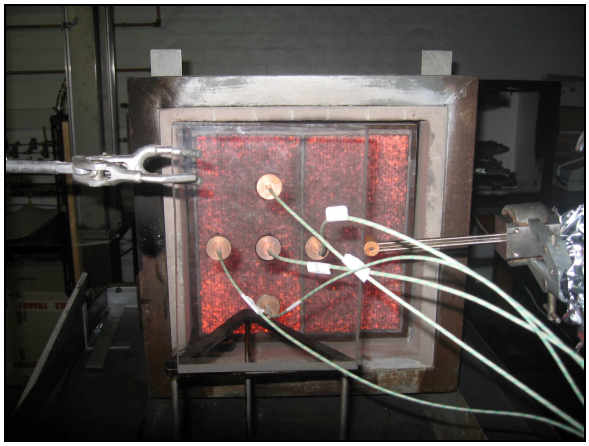

Figure 4.16 – *A sample of PMMA containing five thin skin calorimeter heat flux gauges sitting in front of a radiant panel undergoing a calibration test.*

Once the temperature evolutions of the discs were recorded, they were fed into a rearranged form of the energy balance equation in order to solve for the A value. This A value was then plotted as a function of the temperature for each disk used in the calibration process shown in Figure 4.17.

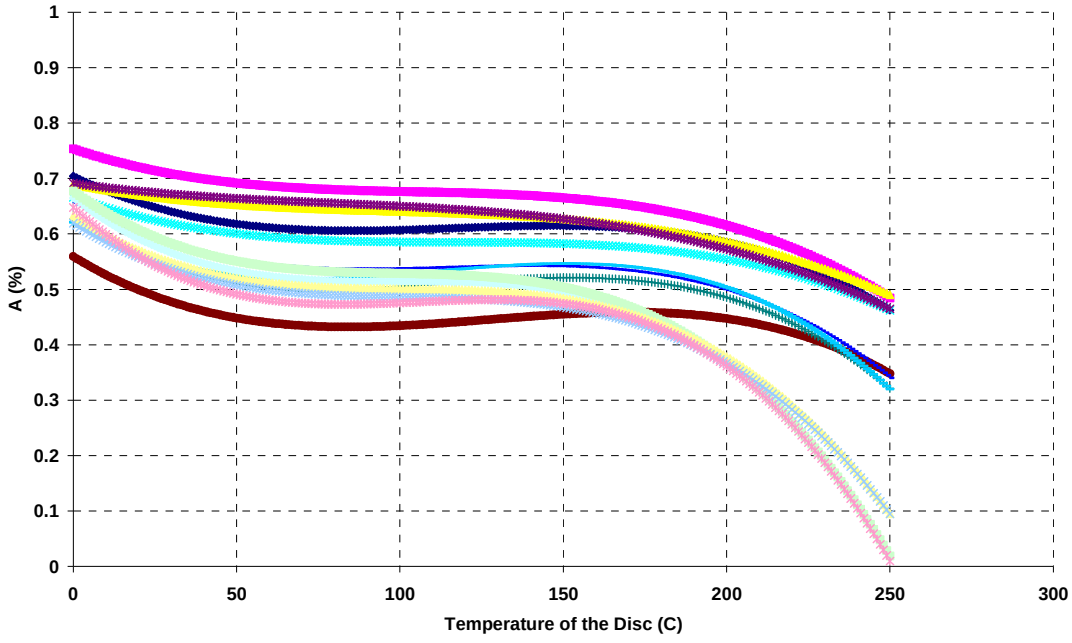

Figure 4.17 - *Plots of the conductive loss factor (A) as a function of the temperature of the disc for the copper discs used in the calibration processes. Heat fluxes ranged from approximately 5 to 15kW/m^2.*

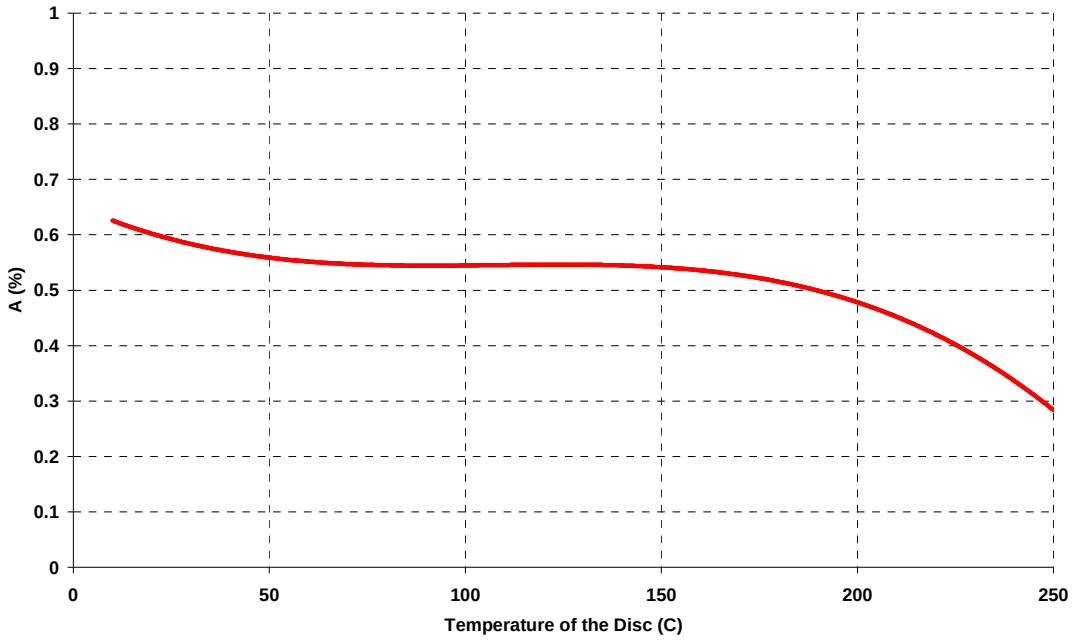

Figure 4.18 – *Plot of the calibration curve for A as a function of temperature for copper disc style thin skin calorimeters in PMMA.*

An average of all the lines plotted in Figure 4.17 was used subsequently to define A as a function of the temperature of the disc. This can be seen in Figure 4.18.

4.2.3.4 Other Parameters in the Heat Transfer Model

For the purposes of the calculation, the emissivity of the surface of the copper disc (ε_s) when painted black is assumed to be one, as was the absorptivity (α_s). As stated earlier, the temperature of the disc (T_s) was measured by a thermocouple as was the temperature of the gas (T_g), used in the convection term, and the room temperature (T_∞), used in the radiation term. The convective heat transfer coefficient h_{conv} was evaluated at each stage in time using Equation 18, with the definition of the Nussalt number (for natural convection in a laminar flow) and subsequently the Grashof number given in Equation 19 and Equation 20 respectively. This is based on the information presented in [42] also adopted in [3].

$$h_{conv} = \frac{Nu_L \cdot k}{L}$$

Equation 18

$$Nu_L = 0.59(Gr.\Pr)^{1/3}$$

Equation 19

$$Gr = \frac{g\beta(T_f - T_\infty)L^3}{\nu^2}$$

Equation 20

Thus given the measurement of the temperature of the copper disc in time, Equation 21 can be used to evaluate the incident radiative heat flux to the surface of the disc and therefore the surface of the PMMA into which the disc is embedded. The incident radiant heat flux to each disc is calculated for each reading. Using the pyrolysis and flame length data, the times at which each flux meter is present in the heated length between the two is established. Then at each moment in time, the heat fluxes from the flux meters present in the heated length are averaged to give the final reading.

$$\dot{q}_i'' = \left[\frac{\rho c \tau \frac{dT_s}{dt} + \varepsilon_s \sigma (T_s^4 - T_0^4)}{(\alpha_s - A)} \right] - h_{conv}(T_f - T_s)$$

Equation 21

4.2.4 Ambient Velocity Measurement

Particle Image Velocimetry was chosen for the measurement of the ambient velocity vector. Laboratory experiments were carried out to determine the capabilities of the system to identify the ambient velocity vector and the potential to automate this process. The setup of the system and the results of the experiments are described and concluded upon below.

4.2.4.1 PIV Setup

4.2.4.1.1 Seeding of the Flow

The Seeder shown in Figure 4.19 comprises a cylindrical container containing seeding particles and a brush mounted on a motor, and with an air inlet and outlet. The seeding particles used in these experiments were titanium dioxide, an inert material with a nominal diameter of 0.5 – 1 μm. The brush rotates thus exciting the

particles into the flow created by the air forced though the container. The air outlet pipe leads to a small section of aluminium tube, the end of which is covered with a wire mesh through which the seeded air is ejected. The entire experiment was housed within a sealed compartment approximately 2.5m x 2.5m x 2.5m (Figure 4.20).

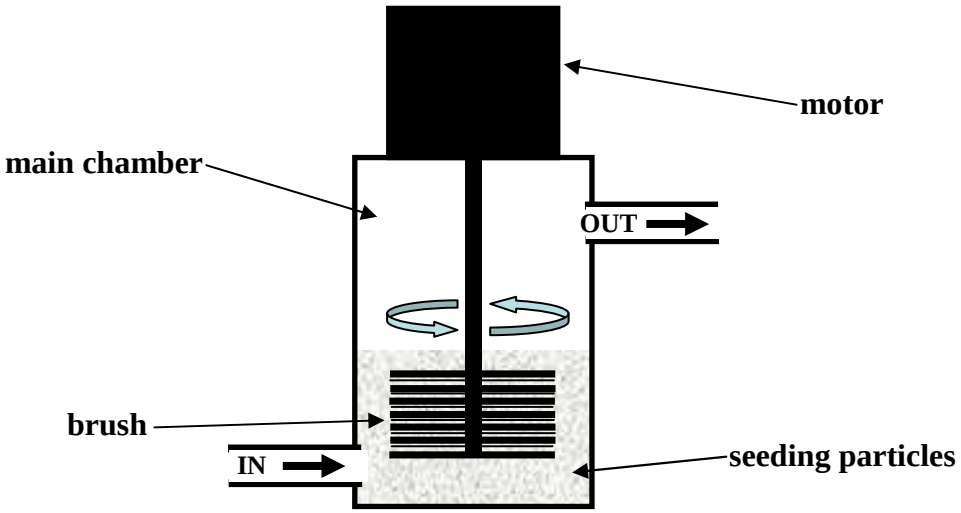

Figure 4.19 – *The diagram shows the seeder purpose built for these experiments. Air is forced in through the lower inlet and entrains the seeding particles that have been excited by the revolving brush. The particle filled air then leaves through the upper outlet to the experimental compartment.*

The compartment had an inlet at ground level in one corner and an extraction duct in the opposite corner a roof level. The seeding was ejected close to the inlet and it was found that this led to the greatest dispersion of seeding throughout the air in the compartment and thus enabled a sufficient amount to be entrained into the measurement zone.

Figure 4.20 – *The compartment in which the experiment was housed was filled as extensively as possible with particle seeding.*

4.2.4.1.2 Illumination of the Measurement Plane

Illumination of the measurement plane was achieved with a Neo 65-15 twin cavity Nd:YAG laser from Oxford Lasers (W[1]) fitted with a light sheet optic. The two laser cavities sat side by side with each producing one pulse per image pair. The pulses were passed through an optic that produced a divergent light sheet which was aligned with the desired measurement plane. The thickness of this sheet was approximately 3mm.

4.2.4.1.3 Target and Camera Setup

A target shown below in Figure 4.21 was designed to fulfil multiple purposes and positioned in the desired plane of measurement. Firstly it allowed for the simple alignment of the light sheet; secondly it enabled accurate focusing of the cameras on the plane of illumination in order that once particles were present they would be in sharp focus; and thirdly it enabled a correction matrix to be established. This need for a correction matrix was introduced by the camera setup.

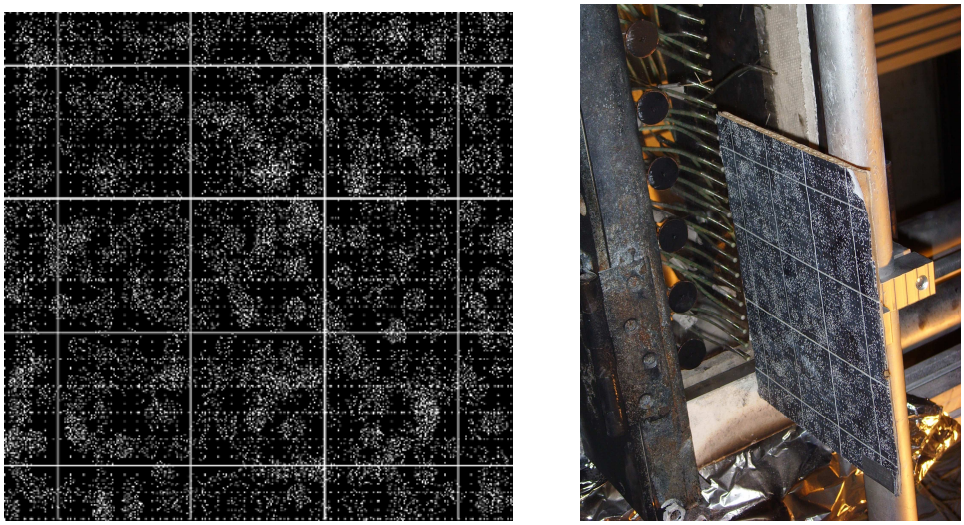

a) b)

Figure 4.21 – *a) shows the target used to focus the cameras on the measurement plane. b) shows the target in-situ in an experimental setup.*

Due to constraints of budget, two cameras were used in parallel in these experiments in order to achieve the required shortness of image exposure time and limit the noise from the radiant flames. When acquiring a pair of images in rapid succession from a single camera, the second exposure cannot finish until the information from the first has been downloaded from the cameras register. Using two separate cameras, one for

each image in an image pair, eliminates this problem but introduces another as in order to correctly assess the distance moved by a particle between two images, the images must be focused exactly on the same place.

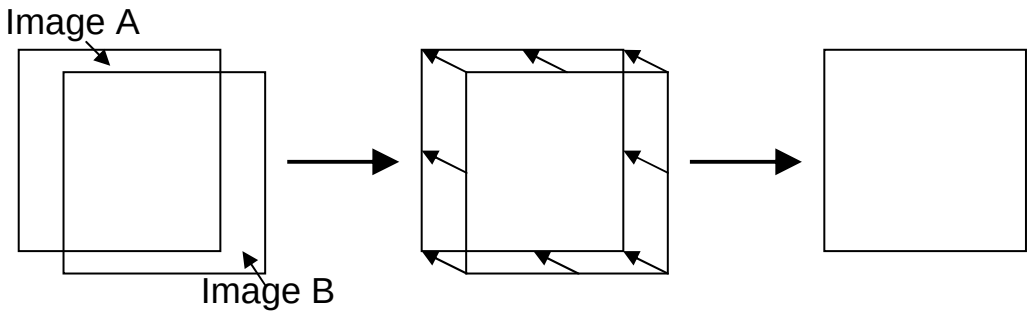

Figure 4.22 – *An illustration to describe the disparity of images viewed using a two camera setup, and how a set of correction vectors can be described to translate one image onto the other.*

As this can not be guaranteed when using two cameras, a matrix must be created that describes the disparity between the cameras views (Figure 4.22). Initially when the image pairs are cross correlated, the resultant vector map will include the difference between the areas that the two cameras are looking at as well as the actual distance moved by the particles. By taking an image of the target from each camera, the matrix describing the disparity can be created and subtracted from the results to leave the true movements of the particles. The cameras used in these experiments were Firewire CCD cameras with a 1392x1040 pixel^2 resolution. No bandpass filters have been used on the optics.

4.2.4.1.4 Image Capture and Synchronisation

The PIV system synchronisation and image recording is performed with R&D Vision HIRIS software and electronics (W[2]). A timing diagram was constructed to ensure that each laser pulse is released during the period of image exposure and that the time delay between pulses (δt) is maintained.

4.2.4.1.5 Post Processing

Post processing the image pairs to calculate the velocity vector maps was performed in two stages, the first using VidPIV software from ILA (W[3]) and the second using Matlab to correct for the difference between the two cameras. VidPIV uses a tree structure which iteratively cross-correlates and filters the results. In this manner the

software is also used to produce the correction matrix. Once the uncorrected results and correction matrix are defined, a Matlab script is used to produce the final vector maps and extract and plot any data required.

4.2.4.2 Assessing and Extracting the Ambient Velocity Vector

The diagrams presented earlier in Figure 2.2 gave an indication of the expected flow patterns and velocity profiles along a vertically inclined flat plate at a temperature greater than that of the surrounding air thus inducing natural convection. In order to assess the capability of the PIV setup to capture these types of characteristic flow profiles and consequently how the u_∞ value might be extracted from a velocity vector map produced by this setup, a set of smaller sub experiments were performed on PMMA wall flames of fixed pyrolysis length. The results of these experiments were collected and processed as detailed above, and plots produced to assess the resemblance of the results to the theory.

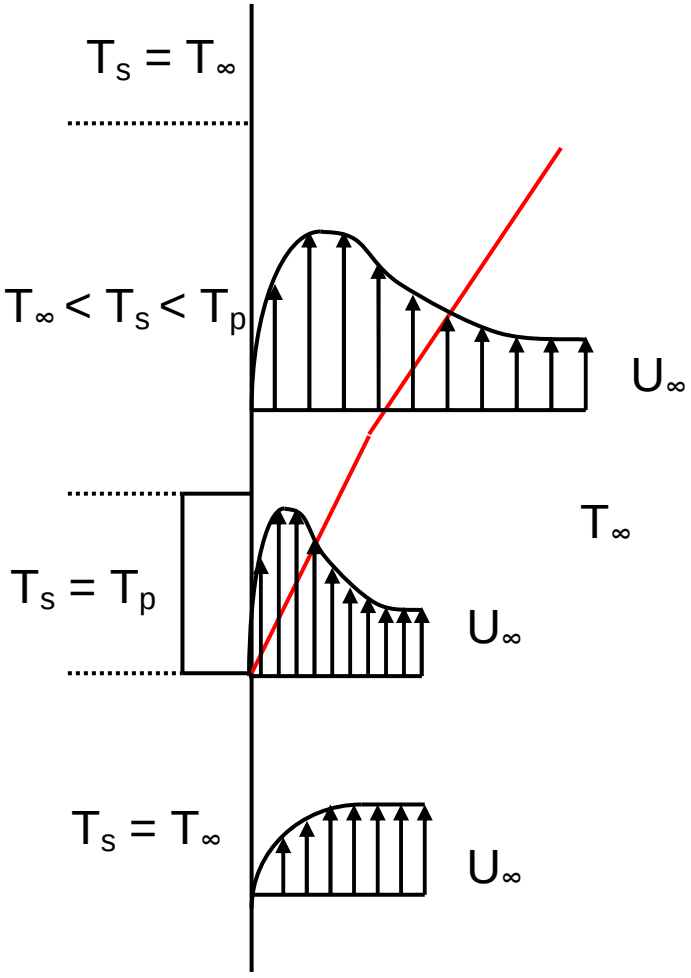

Figure 4.23 – *The expected variation in vertical velocity profile in the regions around the thermal boundary layer shown in red.*

Figure 4.23 shows how the vertical velocity profile is expected to vary in relation to the thermal boundary layer shown in red. Upstream, away from the effects of the flame, there is no acceleration due to buoyancy from heating. The flow is slowed close to the wall by the frictional drag between the wall and the air and subsequently, less so, between the streamline flows until the ambient velocity is reached. Closer to the flame but still upstream of the leading edge, the flow should develop a peak due to the entraining effects of the flame above it and the profile shape will start to transition between the flow profile upstream and the flow profile within the flame. Downstream of the leading edge of the flame, the profile changes rapidly with the addition of the natural buoyancy introduced by the heat from the flame. The velocity profile here can be seen to track what would be the expected temperature profile. A similar pattern of drag close to the solid surface is expected to that of the upstream entrainment region but this is followed by a rapid increase due to the buoyancy induced by the temperature gradient present in the air through the profile of the flame. Further away from the solid surface passing out of and away from the flame region where the temperature drops away towards ambient, the velocity profile follows a similar form. Further downstream into the plume region, as the thermal profile expands laterally, the accelerated portion of the velocity profile is again expected to follow this trend, once again falling away to ambient with distance from elevated temperature of the solid surface.

The sub-experiment created to assess the ability of the PIV system to capture these profiles consisted of a PMMA wall flame of fixed pyrolysis length of 50mm. Like the main experiments, the PMMA was sandwiched between pieces of insulation board to create a smooth transition along the wall from board, to PMMA, to board again (Figure 4.24).

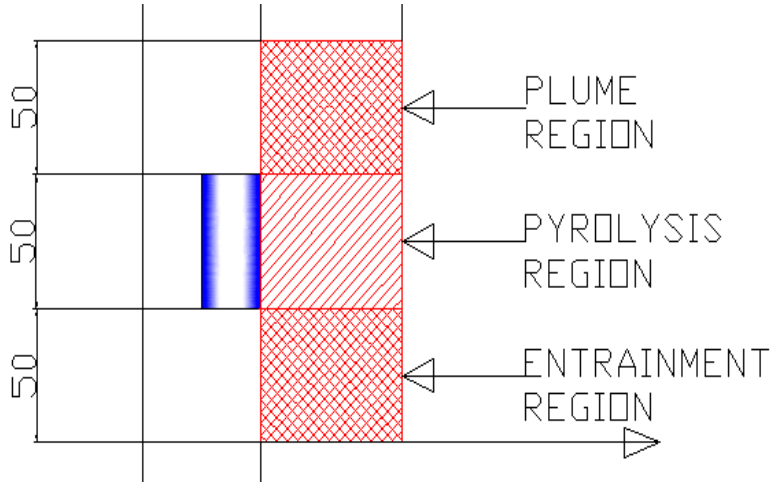

Figure 4.24 – *The setup of the sub experiments creates a smooth wall with a fixed length of PMMA of 50mm shown in blue.*

The experiment was carried out in three parts by separately analysing three distinct regions around the flame; the entrainment region, the pyrolysis region, and the plume region, all highlighted in Figure 4.24. The entire exposed surface of the PMMA was heated and ignited as quickly and evenly as possible using a blow torch. The compartment containing the apparatus was then filled with seeding for the PIV system and measurements taken shortly afterwards. Once regression of the PMMA surface was observed the test was extinguished and the PMMA was replaced.

4.2.4.2.1 Analysis of the Entrainment Region

When characterised, the flow in the entrainment region was not seen to behave precisely as expected. There was significant and erratic fluctuation with respect to direction. The general trend, depicted diagrammatically in Figure 4.25 was that of air flowing / being pulled towards the plate below the flame and rebounding both upwards into the flame and downwards and out away from it. This results in multi-directional flows and recirculation currents in this region. The vertical flow does behave in a similar manner as predicted from the literature although this is not found to be the case consistently.

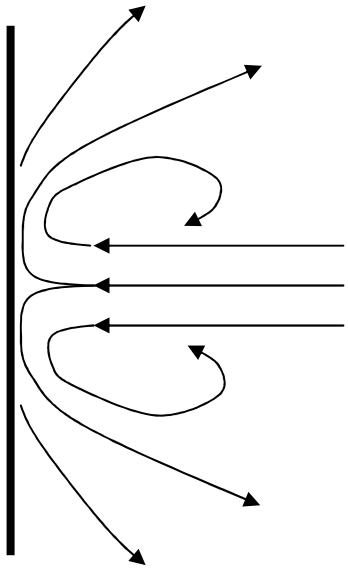

Figure 4.25 – *The diagram shows air approaching the plate beneath the flame and being forced sideways and away from the plate.*

The two sequences of vector maps shown in Figure 4.26 illustrate the observed phenomena. The resultant velocity profiles are thus changeable and unreliable with regard to extracting consistent and representative ambient velocity values.

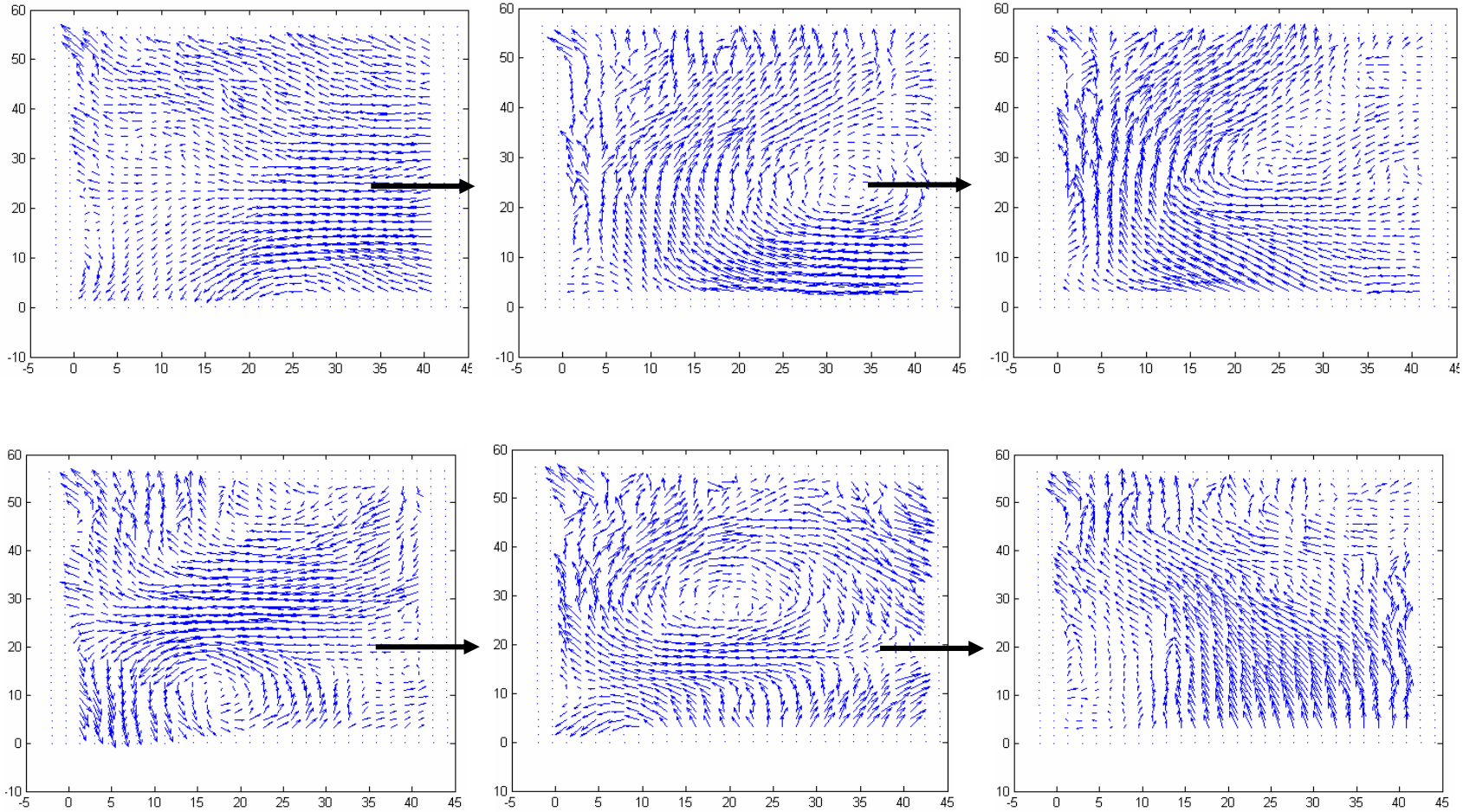

Figure 4.26 – *These two sequences of vector maps show how air is drawn horizontally toward the cold solid surface beneath the flame where upon it is forced either upwards or downwards, and away from the surface. In all maps the surface is positioned at x = 0.*

When the profiles from the entrainment region did resemble the conceptual shape (Figure 4.27), there were two distinct aspects to the profiles. The first was the expected frictional drag profile slowing the air flow closest to the solid surface followed by a rapid increase in velocity over a short distance from the wall. The second was a peak as the drag effects of the wall were overcome followed by the falling away of the velocity towards some ambient value with increased distance from the wall. The peak is the result of the air being entrained in to the flame and thus accelerated beyond the ambient value expected in this cold region. As is shown in Figure 4.28 however, these flow patterns are not consistent.

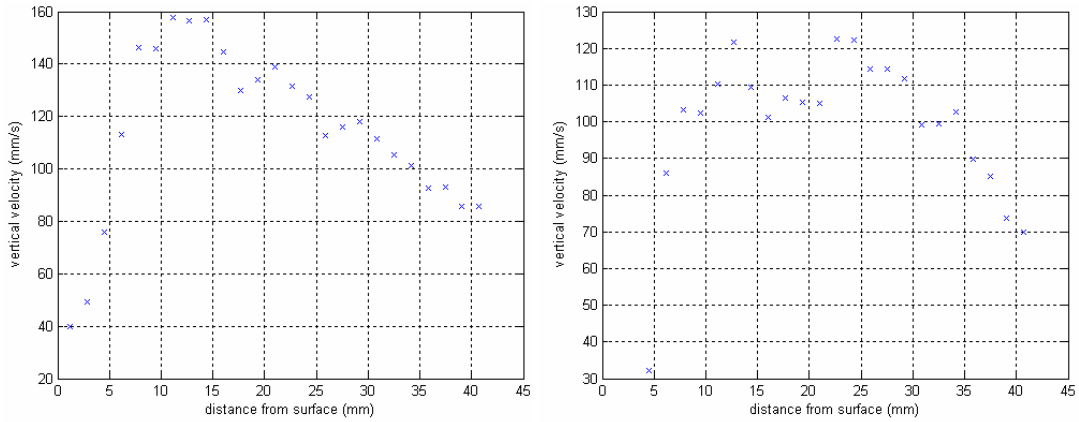

Figure 4.27 – *The two plots show vertical velocity profiles from the entrainment region with a close resemblance to the expected shape as defined by the literature.*

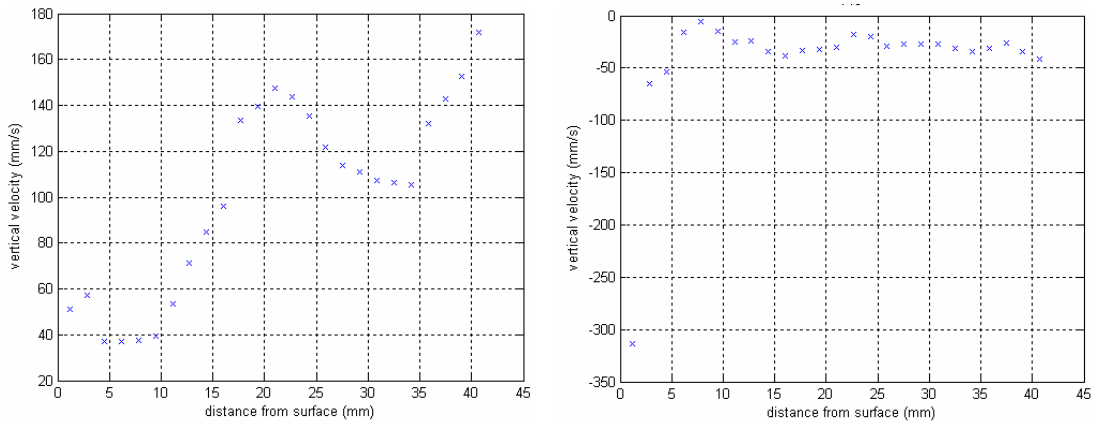

Figure 4.28– *The plots demonstrate the significant fluctuation and inconsistency in the vertical velocity profiles extracted from measurements in the entrainment region.*

4.2.4.2.2 Analysis of the Pyrolysis Region

In general the vertical velocity profiles for the pyrolysis region (Figure 4.29) match the expected profile well and are highly repeatable. There is consistently a peak corresponding to the increased buoyancy produced by the flame which falls away quickly due to the slenderness of the flame and thus the thermal boundary layer. The profile then levels out to a steady ambient flow.

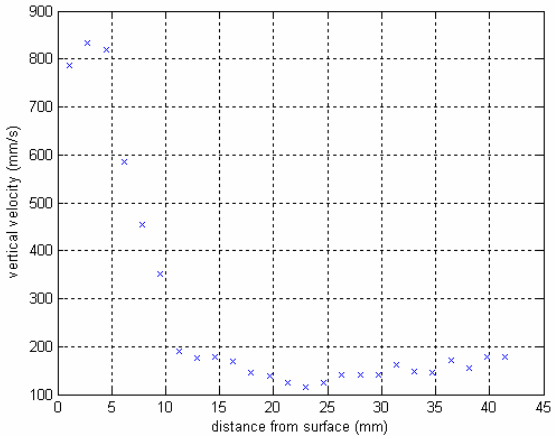

Figure 4.29 – *The plot shows a typical vertical velocity profile in the pyrolysis region.*

The high repeatability and distinct characteristics of these data sets provides a means by which automated identification of the ambient flow velocity may be accomplished. Occasional fluctuations were observed but even with this noise, a level region corresponding to ambient flow is still reached as shown in Figure 4.30.

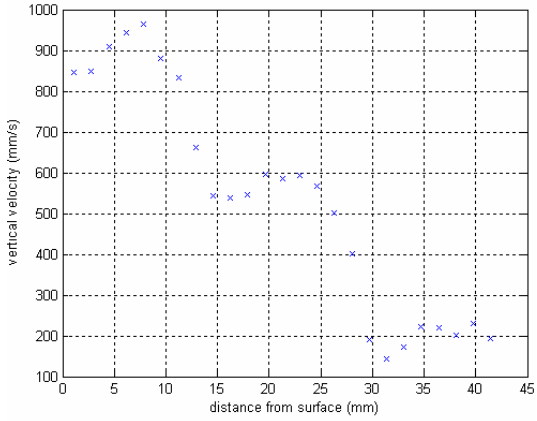

Figure 4.30 – *The occasional profile plots showing fluctuations still exhibit a final flat portion corresponding to the ambient air flow away from the influence of the flame.*

Comparison between the vertical and horizontal velocity profiles revealed a distinct correlation. The horizontal profile would generally cross the x-axis from positive to negative, indicating a change of direction within the flow. The positive direction corresponds to the flow within the flame moving away from the solid surface as the gas expands and rises, and the negative flow represents the cool air being entrained into the flame. The transition between the two, i.e. zero horizontal velocity, was generally observed to occur at or slightly to the hot side of the zone of ambient velocity flow. This correlation can be seen in Figure 4.31 and is very repeatable. Thus it provides a simple method of verifying the boundary between the region of ambient velocity and that of the flame induced buoyancy aiding automated interpretation of the vector maps to produce a value of u_∞.

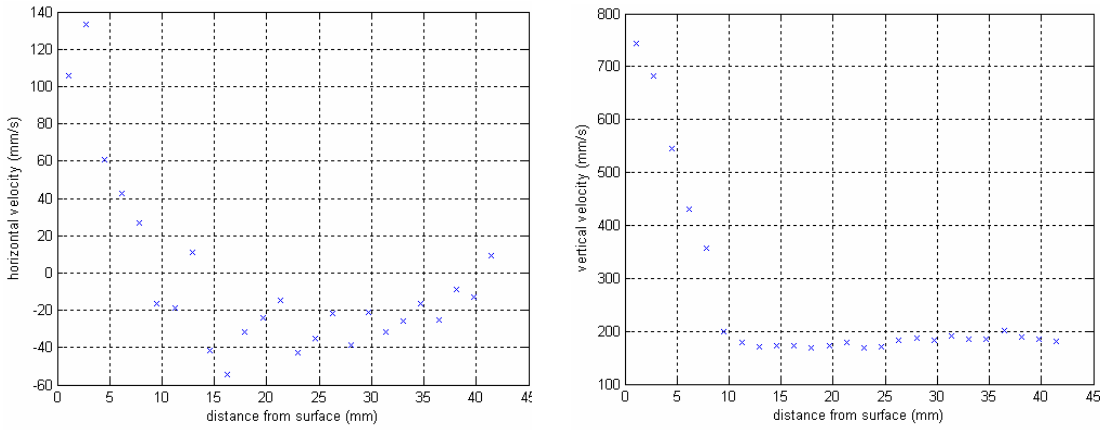

a) b)

Figure 4.31 – *a) the horizontal and b) the vertical velocity profiles taken from the same section through a vector map of the pyrolysis region.*

4.2.4.2.3 Analysis of the Plume Region

Analysis of the plume region further downstream again showed good correlation with the literature. The same pattern of drag region, followed by a peak vertical velocity and then decay down to ambient was seen consistently. With the measurements being further downstream, the hot gases expanding and being forced away from solid surface create a thicker thermal layer. This is clearly evident in the results from this region with the peak typically wider than upstream in the pyrolysis region. A similar pattern demonstrating the clear arrival of the ambient region in the vertical profile coinciding repeatedly with a change of direction of horizontal flow is seen (Figure 4.32).

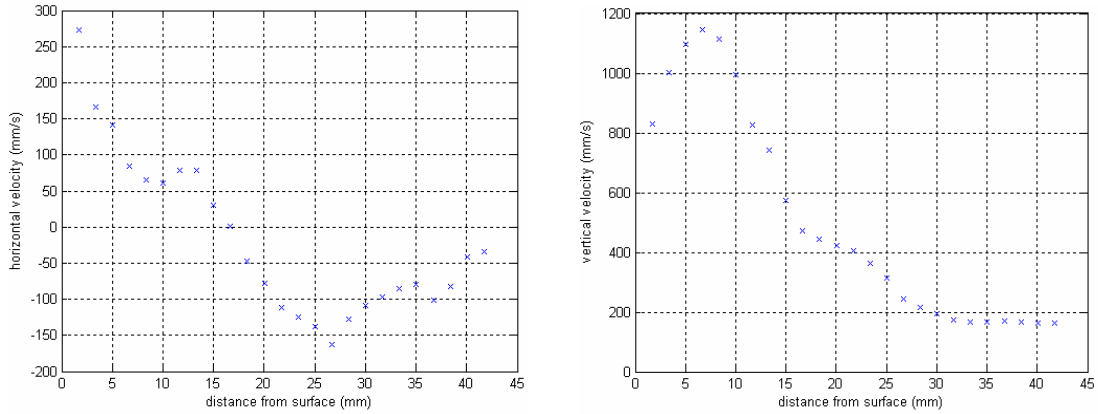

Figure 4.32 – *The plots show typical horizontal and vertical velocity profiles within the plume region of the wall flame.*

4.2.4.2.4 Conclusions

This analysis demonstrates that the PIV system is extremely capable of capturing the characteristics of the flow field around a wall flame. It is also clear from the analysis that the flow patterns downstream of the base of the flame are more robust to fluctuations and thus more suitable to the automated extraction of the ambient velocity vector u_∞. The entrainment area has been shown to be inconsistent and fluctuant even for a small laminar flame. It is evident that when a vector plot is produced that is consistent with the literature model; the ambient velocity value tends to be significantly lower than for areas downstream of the flames leading edge. Thus this region is not considered as appropriate for the measurement of u_∞, particularly when considering an automated process. Downstream of the flames leading edge, the flow profiles are more consistent with the literature and more repeatable and robust to fluctuation. It has also been found that both the horizontal and vertical profiles can be used to locate the edge of the thermal boundary layer and thus the location of the u_∞ input variable to be measured during the flame spread experiments.

4.2.5 Temperature Measurement

All temperatures have been measured using Type KX 7/0.2mm fibreglass insulated thermocouples. The data was collected using an Agilent 34980A data logger.

4.3 Sensor Positioning

The following section describes the setup and sensor positioning of each variant of the flame spread experiments.

4.3.1 Benchmark 200mm Sample Sensor Positioning

The PMMA was clamped between the two plates separated only by the fire board insulation as described previously and shown in Figure 4.1. This setup was fastened to the aluminium extrusion frame as shown in Figure 4.2. Nineteen subsurface thermocouples were inserted into holes spaced at 10mm intervals along the vertical centreline of the fuel sample. These holes were drilled from the back of the sample 38mm, finishing 2mm from the surface. The thermocouple beads were pushed against the inner end of the holes and metal wire was used to hold each one firmly in place. At no time did any of the thermocouples fall out of the holes or indeed appear to come loose during the experiments. Five gas phase thermocouples were inserted from the rear of the samples into holes drilled right through. The beads were positioned 10mm out from the face of the sample and again held firmly in place by metal wire at the rear. The first of these thermocouples was 20mm above the base of the sample, and then at 40mm spacing with the last 180mm above the base and 20mm from the top of the fuel surface. The same spacing arrangement was used for the five heat flux meters, the description of which is given in Section 4.2.3. A view of the top and front of the sample is shown below in Figure 4.33 and Figure 4.34. All drilling work was carried out in a milling machine by lab technicians.

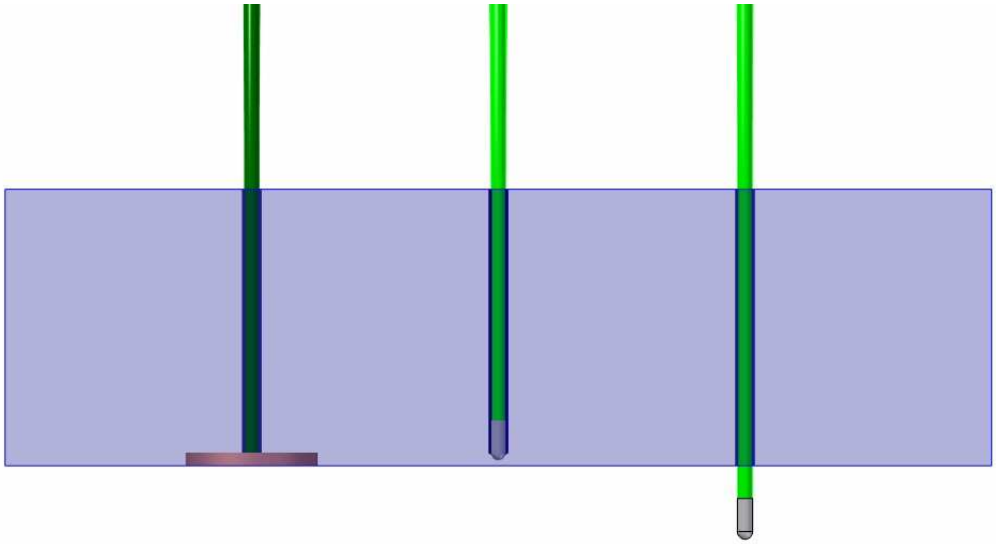

Figure 4.33 – *A top view of the PMMA sample showing the arrangement of the various sensors. The heat flux meters are on the left, the depth thermocouples tracking the evolution of the pyrolysis front are in the centre, and the gas phase temperature measurement thermocouples are on the right.*

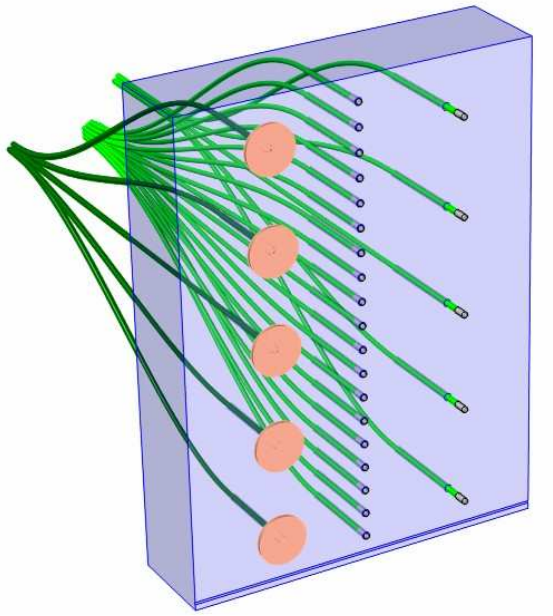

Figure 4.34 – *The image illustrates the sensor arrangement on a 200mm PMMA sample.*

In total four CCD cameras were used during each experiment. The first was positioned behind the transparent PMMA sample and showed images of the pyrolysis bubbles which were then combined and used in conjunction with the isotherm data. Two more cameras were positioned directly in front of the exposed surface to film the flame which was used to measure the flame height. One of these cameras was positioned close to the surface so that it's viewing angle just covered the 200mm of PMMA and the other was positioned further away to capture the flame once it grew beyond the size of the fuel sample. It was intended that the closer camera would more accurately capture the flame height covering the fuel and that the second would capture the whole sequence from a distance but perhaps less accurately. A comparison of the early stages could be made later to discern how much effect the distance of the camera from the flame had on the measurements. The final CCD camera was placed such that it had an overview of the experiment. No measurements were taken from this camera. Figure 4.35 shows in detail the positioning of the CCD cameras with respect to the experiment.

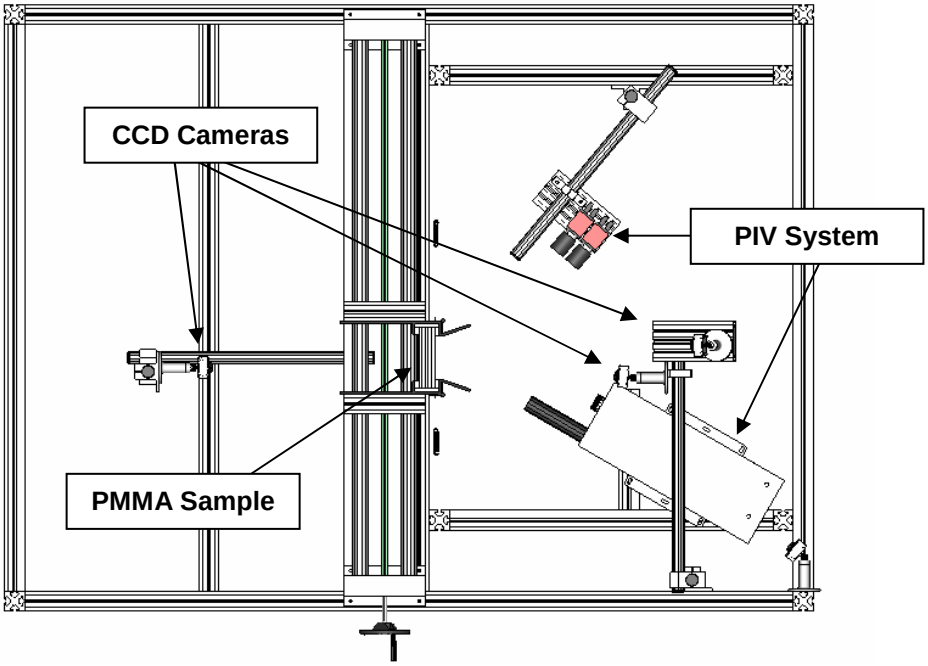

Figure 4.35 – *The plan view of the benchmark style setup shows the positioning of the CCD cameras and PIV equipment relative to the experiment.*

The baffle design taken from the benchmark experiment caused difficulties in the positioning of the PIV system. The desired measurement plane was perpendicular to the surface, starting at the surface and moving out from it. Thus the cameras would need to be positioned at right angles to this plane. The positioning of the baffles meant this was impossible, thus the laser sheet and cameras had to be angled into the fuel surface as shown in Figure 4.35. Once the baffles had been removed for later experiments, the effects of this adjustment, along with the possible effects of the baffles could be assessed.

4.3.2 Regular 200mm Sample Sensor Positioning

The setup for the regular 200mm sample experiments was identical to that of the Fernandez-Pello experiments except with regard to the aspects involving airflow. As the baffles were removed from the plates holding the PMMA in place, the PIV cameras could be positioned at such an angle so as to point parallel to the fuel surface and thus the laser sheet could be aimed perpendicular to it.

4.3.3 Tilted 200mm Sample Sensor Positioning

All thermocouples and heat flux meters for the tilted samples were positioned as per the regular 200mm sample. The CCD camera acquiring images for the flame length measurements was positioned to the side of the sample and aligned with the angle of

the fuel. This was so that the script carrying out the processing technique did not have to be altered and the length produced by it was the length of solid covered and not the height of the overall flame (Figure 4.36). A similar arrangement was made for the PIV cameras, again so that the extracted measurement corresponded to the flow parallel to the fuel surface.

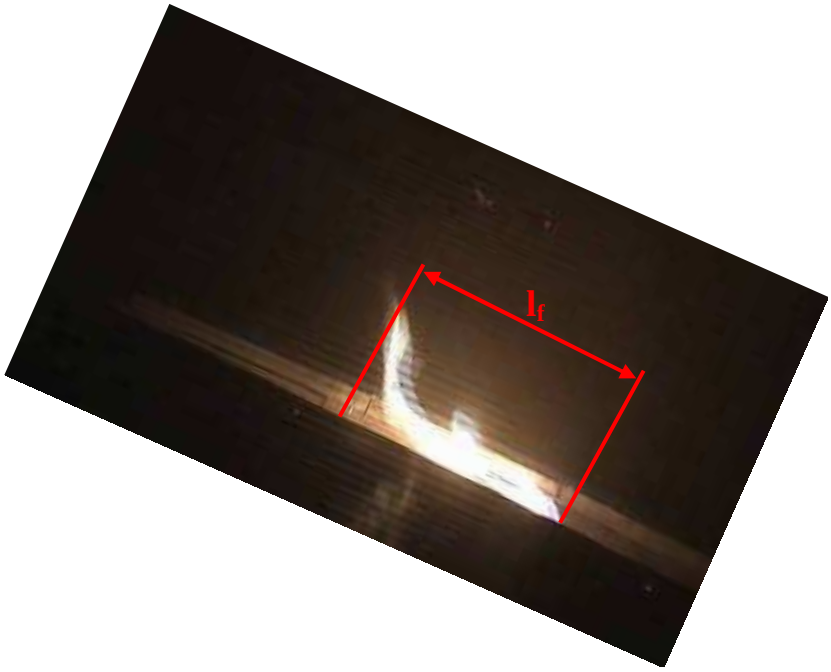

Figure 4.36 – *The image shows the dimension regarded as representing the flame length associated to the flame spread model for a tilted flame spread experiment.*

4.3.4 500mm Sample Sensor Positioning

Surface sensors were identically spaced and fixed as with the 200mm samples thus comprising 12 heat flux gauges, 12 gas phase temperature measurements and 49 depth temperature measurements. The layout is shown in Figure 4.37. Sensor positioning with respect to depth is as per Figure 4.34. In order to capture the entire flame height when at its largest, the CCD camera had to be moved outside of the smoke box housing the experiment and due to restrictions in viewing angles due to windows, captured the side of the flame rather than the front as before. The PIV setup was as per the regular 200mm experimental setup.

Figure 4.37 – *The image shows the increased sensor density for the larger scale laboratory experiments.*

4.3.5 Compartment Fire Sensor Positioning

The sensors employed in this experiment are shown in Figure 4.38. The subsurface thermocouples were placed identically to the lab experiments described above and it is assumed that the same isotherm temperature corresponds to the presence of pyrolysis and surface burning. The characteristics of the heat flux meters are also assumed to be identical.

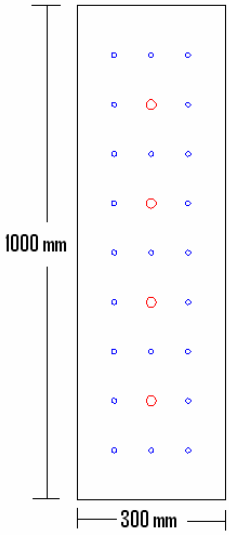

Figure 4.38 – *The diagram shows the layout of surface thermocouples and heat flux meters of the PMMA slab in the main experimental compartment of Dalmarnock Fire Test One. The blue circles indicate the location of subsurface thermocouples and the red circles indicate the thin skin calorimeter style heat flux meters.*

Due to the constraints of the scenario it was not possible to place a video camera directly in front or to the side of the slab to measure the flame height. The slab was in view of two of the CCD cameras however and a scale was drawn on the wall next to sample to aid the assessment of flame height. It should be noted however that the CCD cameras with a view of the slab were at floor height and set to a low frame rate of approximately one frame per second due to constraints in the data transmission rate resulting from the number of sensors present in the overall experiment. Thus the resultant data was not suitable or numerous enough for the same image processing technique employed for the lab experiments. The setup did not directly contain gas phase thermocouples close to the surface of the PMMA although the compartment did contain approximately 240 gas phase thermocouples, and a tree containing 12 of which was within half a meter of the slab. Although a near surface temperature cannot be extracted directly from these measurements, the high sensor density enables iso-slices to be constructed of numerous planes through room and thus provides an assessment of the level of stratification in time during the experiment. It was clearly not possible to include the PIV system within the setup and as such no measure of surface or ambient local flow velocity was taken for this test.

4.4 Results

4.4.1 Comparison With Benchmark Experiment

The results of the initial imitation experiments agree very well with the benchmark experiments [29]. Figure 4.39 and Figure 4.40 show the comparison of the pyrolysis length and flame length measurements. The closeness of the data demonstrates that the measurement techniques that have been adapted for the purposes of this work are capturing the phenomena correctly.

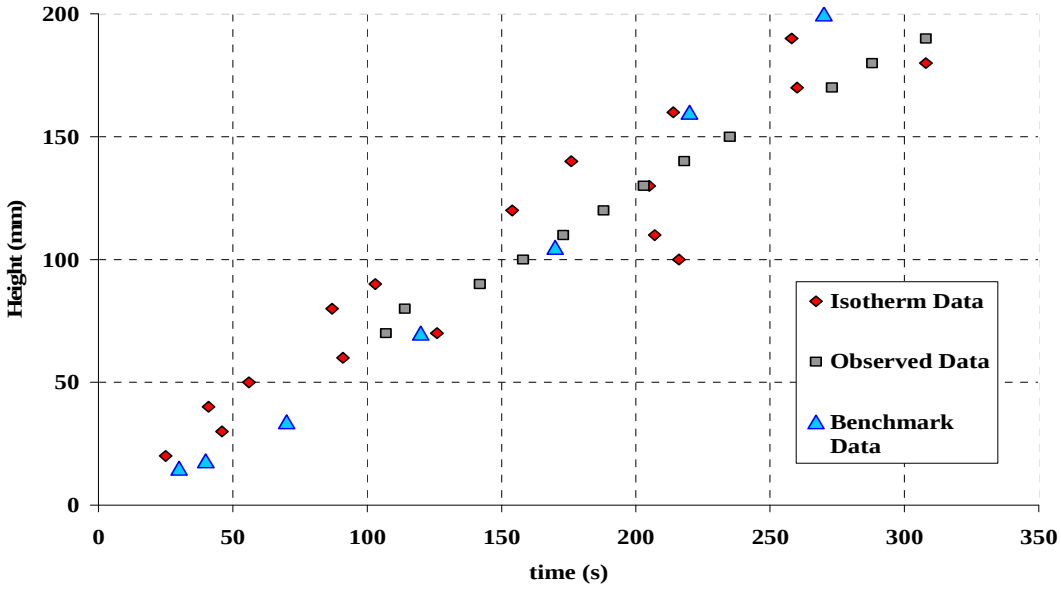

Figure 4.39 – *The plot shows the close match between the evolution of the pyrolysis length in an imitation experiment and the benchmark experiment. The plot shows both visually observed and measured (isotherm) data from the imitation experiment.*

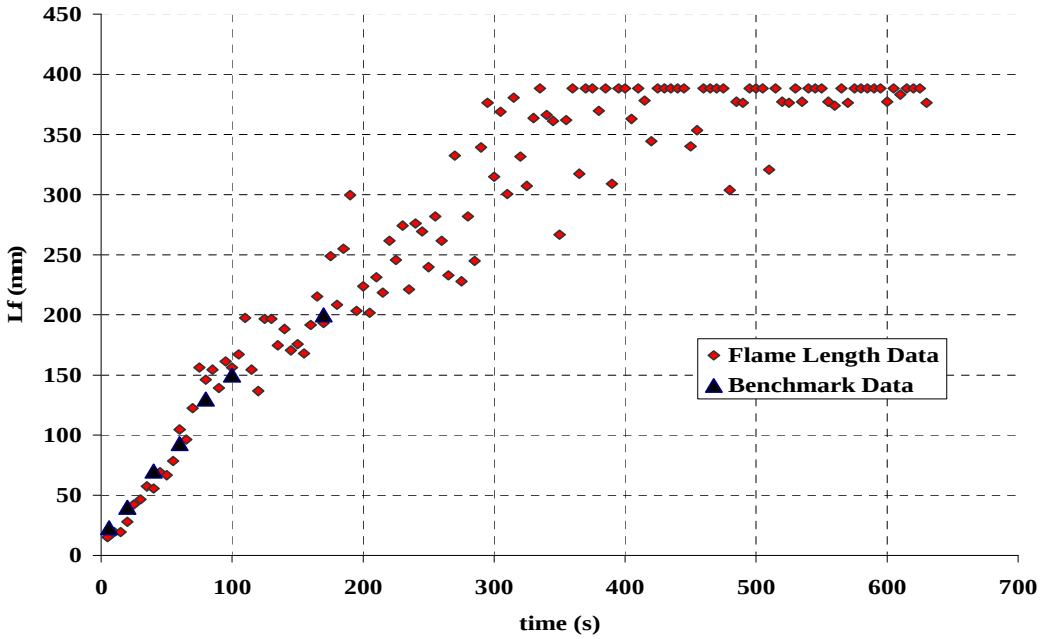

Figure 4.40 - *The plot shows the close match between the evolution of the flame length in an imitation experiment and the benchmark experiment.*

4.4.2 Repeatability of Results

The results for pyrolysis length data from all vertically orientated PMMA samples showed high levels of repeatability. Figure 4.41 shows the data from the vertical 200mm experiments and the initial 200mm of data from the 500mm vertical experiments. There is a good correlation from all data which indicates a range of spread rates between 0.75 and 0.95mm/s. The tilted experiments showed a little more variation with two results matching very closely but one progressing significantly slower. It is believed that these experiments are more susceptible to changes in environmental conditions than the upward flame spread tests as the flame is more exposed and thus moves more relative to the unburned surface affecting the heat transfer to it. The slower spread experiment corresponded to a 25mm thick PMMA sample whereas the two identical experiments both had thicknesses of 40mm. A fourth experiment on 25mm thick lower grade PMMA was conducted but the temperature results were lost and thus cannot be compared to see if the trend was concurrent with the thinner samples in this orientation.

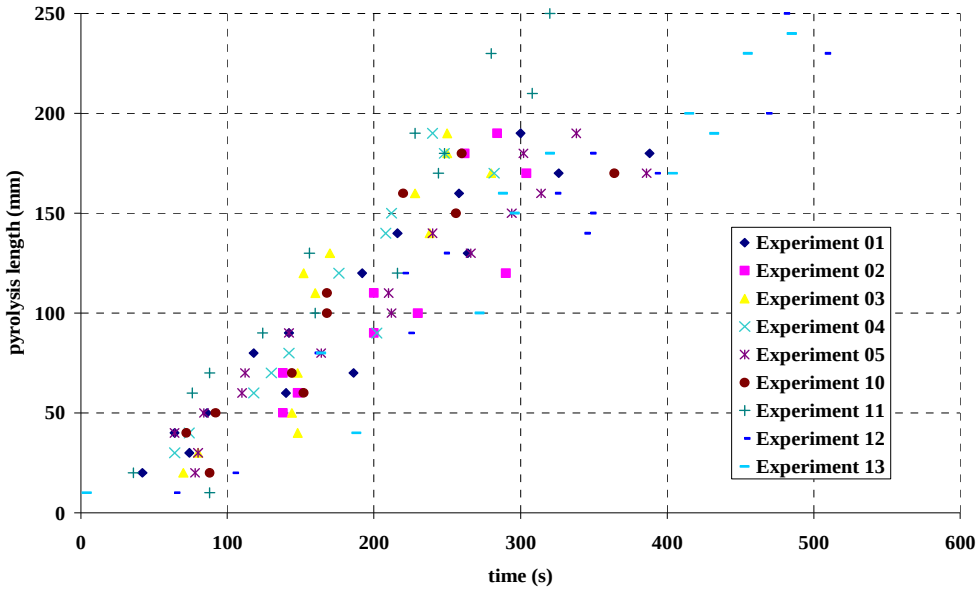

Figure 4.41 – *The evolution of the pyrolysis length for the first 200mm of all vertical specimens demonstrates the repeatability of the initial setup. Spread rates of the flames are approximately between 0.75 and 0.95 mm/s.*

Flame length results again showed good levels of repeatability and comparison to the pyrolysis length data also showed correlations between the two. When the growth rate differed to other experiments of the same type, the difference could in general be seen in both sets of length scale data. The three initial experiments imitating the setup of the benchmark experiment showed almost identical growth patterns, as shown in Figure 4.42. When the baffles were removed there was more variation, shown in Figure 4.43. The flame length results for the tilted experiments were

concurrent with the results for the pyrolysis lengths, with the experiment on a 25mm thick sample resulting in spread far more slow than that over the 40mm thick samples. Flame length data is available for a fourth experiment whose temperature data was lost and showed that the growth rate was very similar to the two 40mm thick experiments indicating that the reduced spread rate may not be linked with the thickness of the material in this case. The flame length data for the slower growth tilted experiment was notably noisier than the others suggesting that environmental conditions had differed in this case. The flame lengths from the vertical experiments also showed similar characteristics. When the flame reached lengths of approximately 200mm, the growth rate of this data slowed and became noisier (Figure 4.42). For the longer experiments the data then proceeded to become less scattered as the flame grew further although was always more scattered than the initial very laminar phases. There was also a curvature evident in the growth trends indicating some level of acceleration present at these increased lengths in all of the 500mm experiments. In all experiments there was also a clear and gradual deceleration as the flame reached the top of the sample and thus its full height. For all lower grade PMMA samples, the flame length data indicated a slower growth rate for all variations of the experiments scenarios.

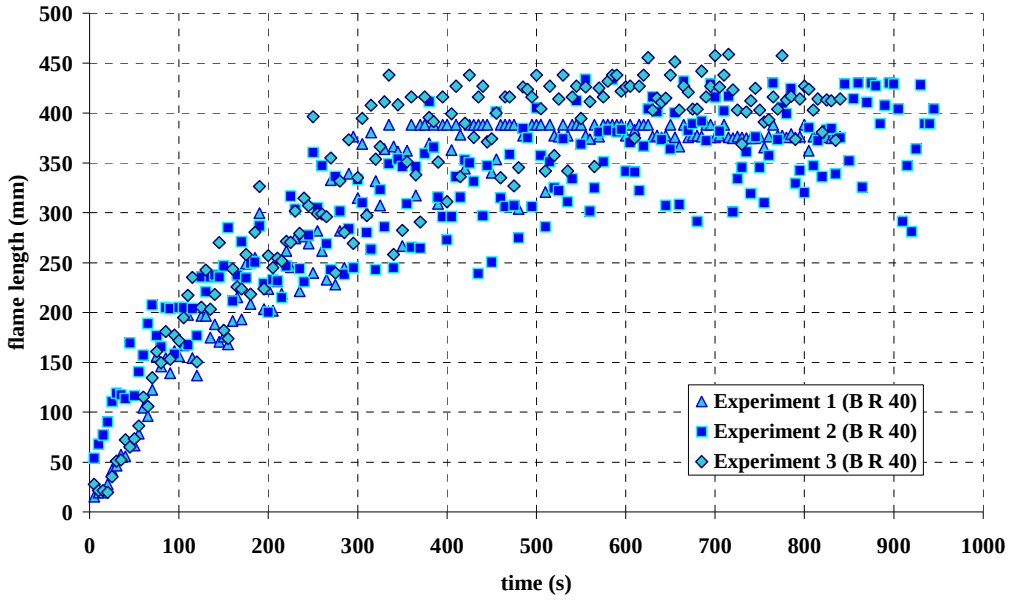

Figure 4.42 - *The evolution of the flame length for Experiments 1 to 3 demonstrates the repeatability of the initial setup.*

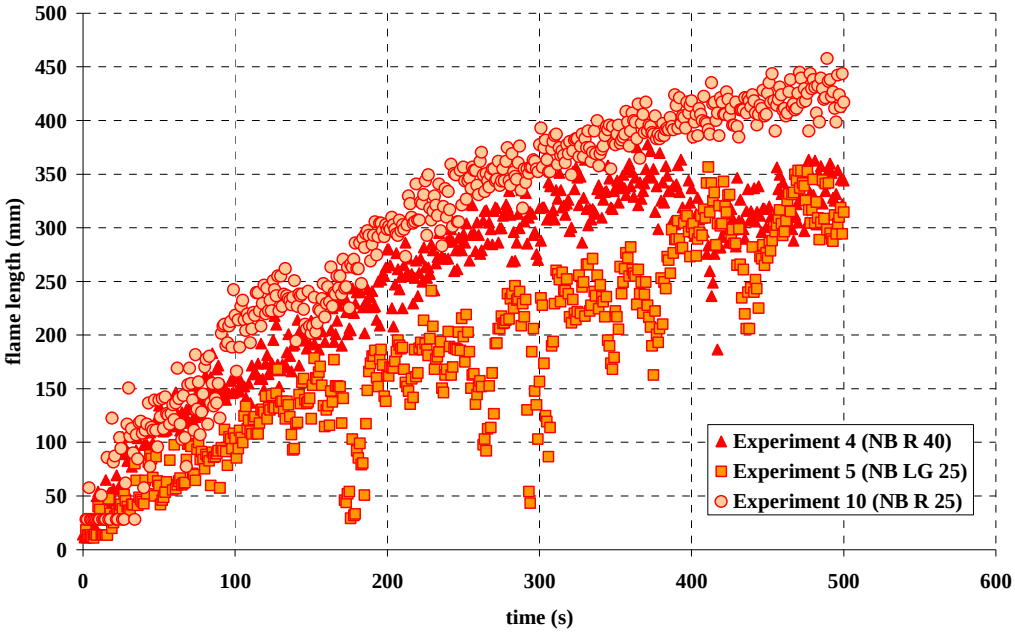

Figure 4.43 – *The plot shows the more varied nature of the flame length growth when the baffles from the benchmark imitation experiments are removed. It also shows the different nature of the flame of the lower grade PMMA (Experiment 5).*

The temperatures measured directly in front of the exposed face showed very consistent results with temperature traces for all vertical PMMA specimens generally hitting a plateau of approximately 700˚C (Figure 4.44, Figure 4.46). Temperatures for the tilted samples levelled off at a slightly lower temperature of approximately 650˚C but again this was consistent for all experiments of this type (Figure 4.45). It was evident from the results when the flame had drawn closer to the vertical surface, as the temperature readings would drop due to the thermocouple beads protruding from the rear of the flame.

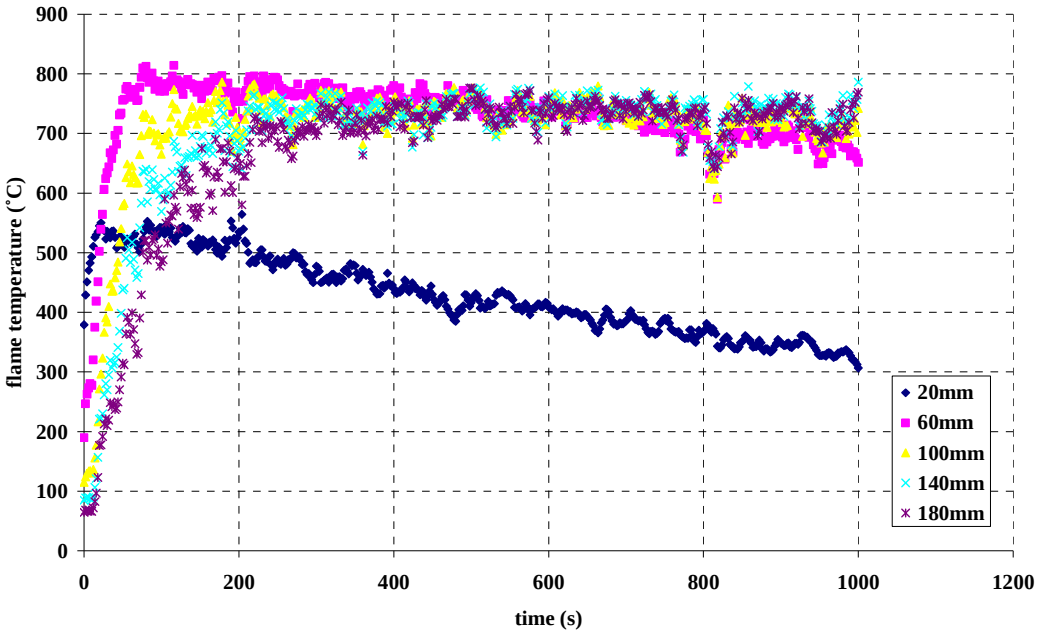

Figure 4.44 – *The plot shows the temperature data for five gas phase thermocouples distributed evenly along the height of the exposed face of a benchmark style vertical spread experiment. The thermocouple beads are 10mm from the surface and their heights above the base of the sample are given in the legend.*

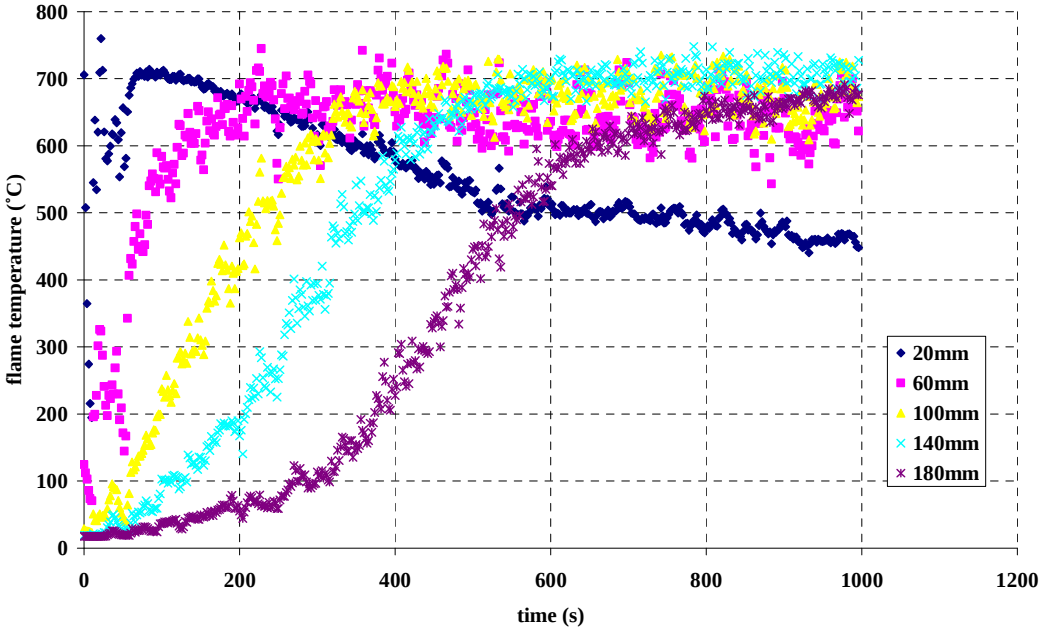

Figure 4.45 – *The plot shows the equivalent data as shown in Figure 4.44 for a tilted experiment. There is a noticeable difference in the time taken for the thermocouples positioned towards the upper end of the sample to come into contact with the hotter gases produced by the flame.*

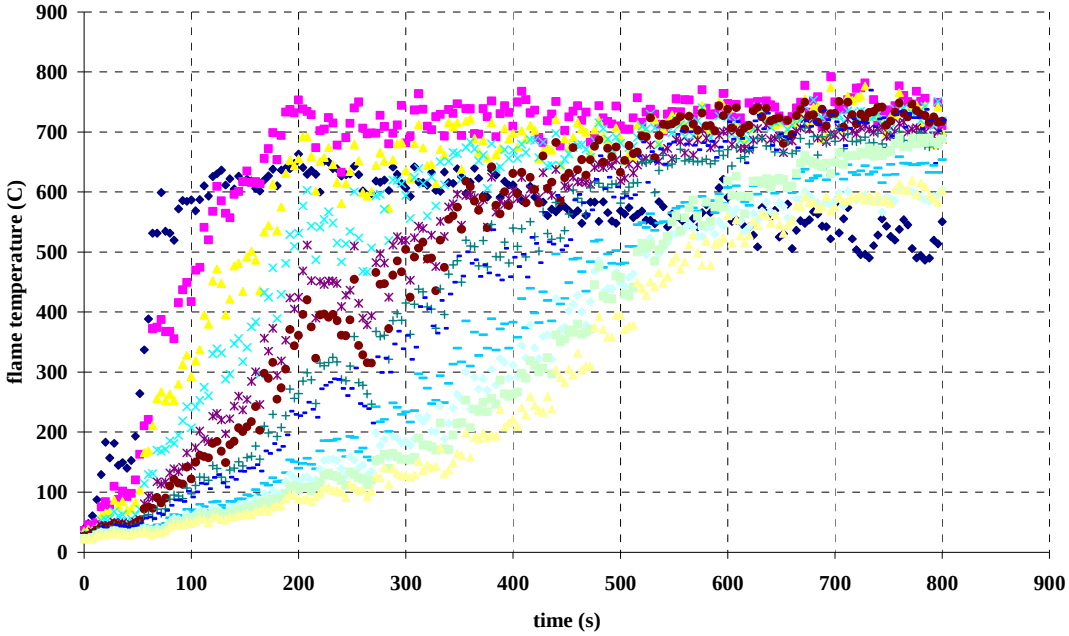

Figure 4.46 – *The graph shows the gas phase temperature measurements from a 500mm high vertical spread experiment.*

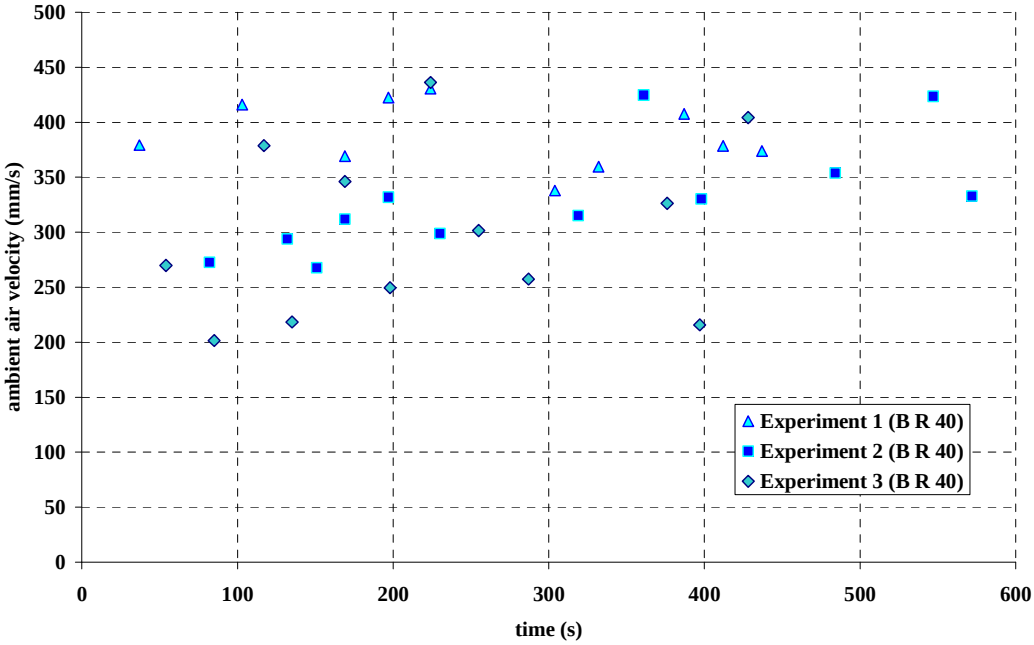

Figure 4.47 – *The plot shows the results for the u_∞ measurements for the benchmark imitation experiments. The results were fairly scattered and ranged between 200 and 450 mm/s.*

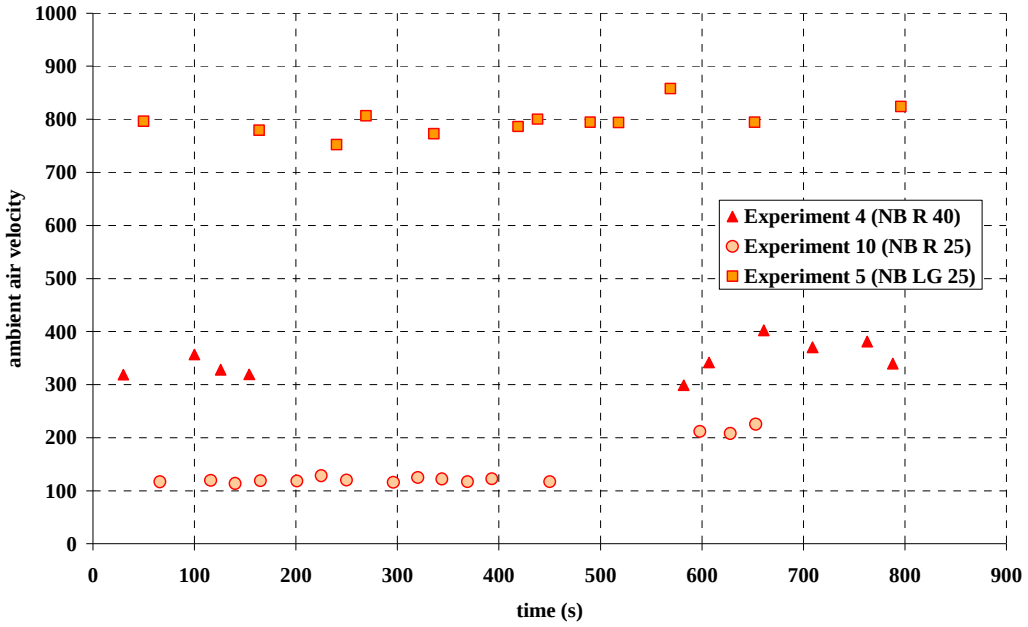

Figure 4.48 – *The figure shows the u_∞ measurements for the regular 200mm experiments. The data was less scattered than was the case with the other tests but spanned the same range of magnitude.*

The ambient velocity (u_∞) measurements made using the PIV system varied across all experiments. The majority of the data showed a more or less constant ambient velocity for the duration of the experiments but ranged from 100 to 1000mm/s between tests. There was no clear correlation between the faster velocities measured and experiments with faster spread rates or vice versa. Neither was there a correlation between the more scattered u_∞ data and similarly scattered l_f data. Comparison of the data for the benchmark experiment where baffles were included (Figure 4.47) to maintain a steady 2D flow, with the data produced when the baffles were removed (Figure 4.48) showed unexpected results. While the data generally spanned similar ranges as would be expected, data from the tests with the baffles was far more scattered than data without, which showed the steadiest results of all the experiments.

The data produced by the heat flux meters was highly scattered and irregular and showed no indication of trends or correlations. The only noticeable feature was the far lower measurements in the tilted surface experiments as compared to the measurements from vertical surfaces (Figure 4.49). The data from all vertical spread experiments was of a similar order of magnitude. The proposed reasons for the highly irregular data are detailed in Section 4.4.3.3.

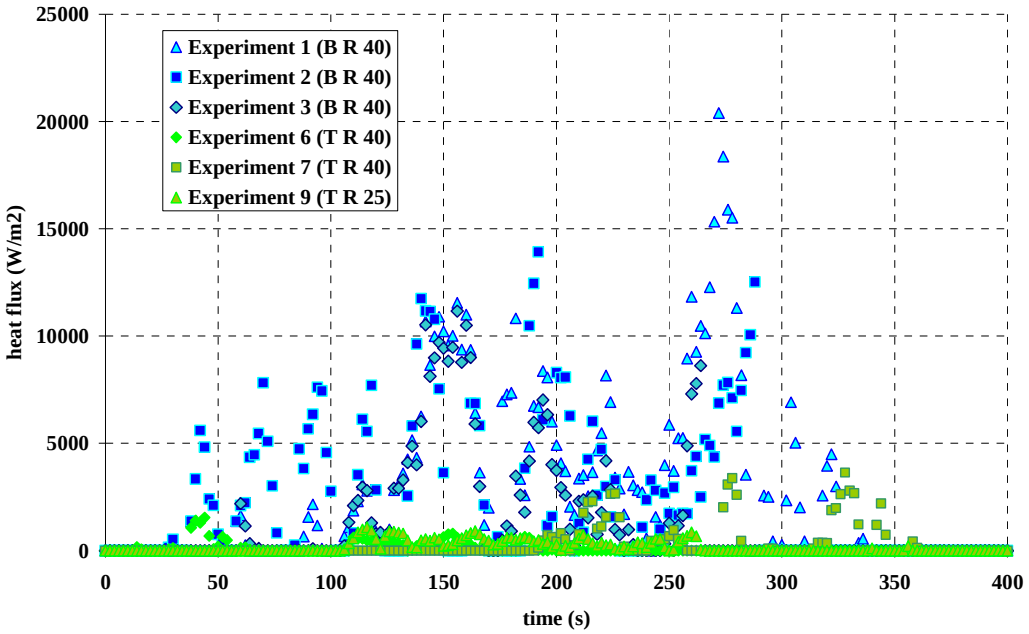

Figure 4.49 - *The figure shows the difference in magnitude of incident radiant heat flux data from the benchmark imitation experiments in comparison with the same data from the tilted PMMA experiments.*

4.4.3 Assessment of Experimental and Measurement Techniques

4.4.3.1 Pyrolysis Length Measurement

The comparison of Figure 4.41 and Figure 4.42 shows a noticeable delay between the measured pyrolysis front reaching the top of the PMMA sample and the flame reaching its full height. This is attributed to the selection of an isotherm temperature corresponding to the earlier stages of pyrolysis as detailed in [19]. At this stage pyrolysis bubbles, although clearly present in the video footage, may not be producing sufficient amounts of gases to sustain flaming at the surface at that location. This can be corrected for by re-plotting a range of isotherms and comparing the times each isotherm indicates as the end of the experiment with that of the flame length plot. Results indicate that an isotherm of 100˚C measured at the thermocouple depth corresponds best with the flame measurements, shown in Figure 4.50 below. The 80˚C and 100˚C isotherm have an approximately 50s difference in their projected experimental end times. As indicated earlier (Figure 4.7), the visual results were initially noted as being within a range of 80˚C to 100˚C from which the former was initially chosen. Given this latest observation however, the upper bound appears to be a more suitable choice and as such, the results given later will be representative of a 100˚C isotherm.

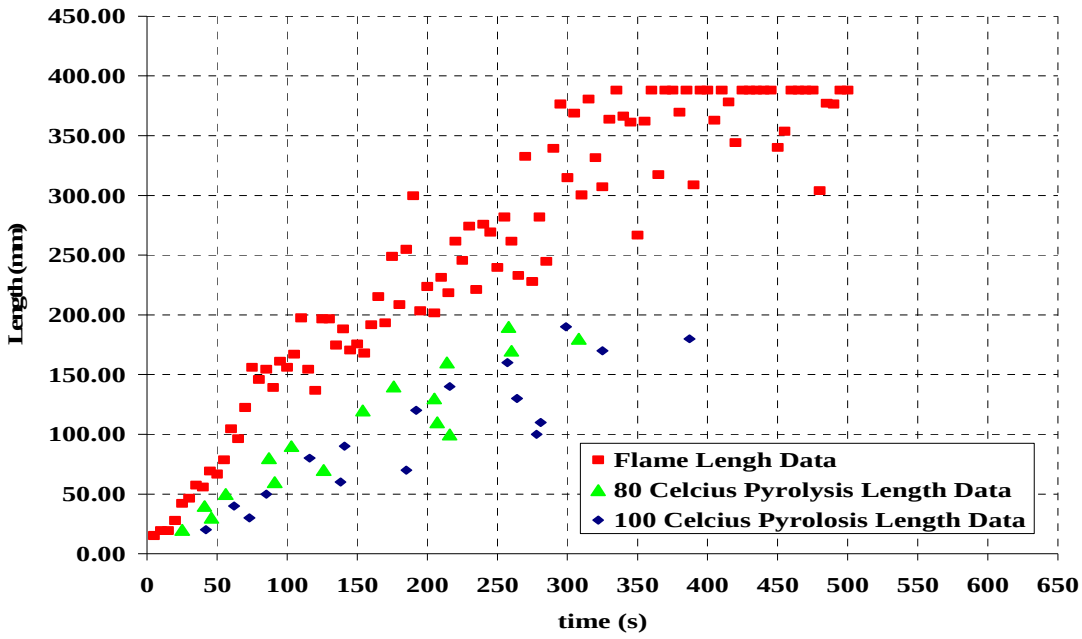

Figure 4.50 – *A plot comparing the pyrolysis length given by a 100˚C isotherm and flame length from the same experiment. The pyrolysis data indicates that the front will arrive at the top of the slab at the same time as the flame stops growing.*

The density of data points provided by this technique is of course limited by the number of thermocouples with one thermocouple providing one data point. With the thermocouples spaced at 10mm intervals there is not significant scope for increased data density in this technique. In the later stages of the experiments fairly accurate trends can be interpreted in the data but early on, trend identification is problematic and reliant on observation of flame length data guided by any available pyrolysis length data points. Thus the data density appears to be at a lower bound with regard to usefulness and practicality. There is noticeable scatter in the thermocouple readings which can be attributed to the condition of the holes in the PMMA. Although effort was made to drill the holes as accurately, consistently, and cleanly as possible, and the holes were cleaned and dried prior to use, it was noted that some holes were not always drilled to within precisely 2mm of the front surface. This would have resulted in some thermocouples being farther from the surface than others and thus having more thermal lag which has a noticeable effect on the results produced. It was also noted that there was occasionally residue left from the drilling process which will have affected the thermal contact with the inner end of the hole and the thermocouple bead. A similar technique was used by Rangwala [61] and Fernandez-Pello [29] who both reported similar problems due to inaccuracy in the thermocouple junction placement. Overall the technique delivers enough information to be usable, much more so in the later stages of the experiments. With more precision and investigation, a very useful technique could be developed for future applications.

4.4.3.2 Flame Length Measurement

The image processing technique is very well suited to this particular problem under the specific environmental conditions. The technique yields a high density of repeatable, reliable and robust data. Some minor changes were made to the positioning of the CCD cameras following the initial experiment as it became clear when the flame has reached the boundary of the cameras view by the repeated results in the data (Figure 4.42) with the coordinate of the upper pixel adjudged to be part of the flame equalling the height of the image. This is distinguishable from the usual steady flame height at the end of the experiments where there is scatter about a mean. The camera positioning was adjusted after noticing this problem after the first experiment performed, and better results were seen immediately in subsequent experiments (Figure 4.42). When the results of the two cameras measuring flame length, one close and one further away, were compared there was little to no difference between the two sets of results. This was the case for all three of the benchmark style experiments. For later experiments only one camera was used at a distance sufficient to ensure the later stages of the experiments were correctly recorded but not so far away as to risk introducing inaccuracy into the results.

Results consistently start to exhibit more scatter as the flame length approaches 200mm and the flame reaches the expected transition to turbulence but this appears to subside once the transition has been made. A data smoothing algorithm can be utilised to reduce this if necessary which should facilitate identification of trends in the data. The processing of images naturally results in the need to analyse larger quantities of data and thus results in increased computational demands than is the case with other techniques. Processing times could be reduced greatly though through more optimised programming and more powerful computational resources. The only doubt remains with respect to the broader applicability to fire scenarios where the levels of light intensity range greatly and the conditions are not as restricted as those that constitute these experiments. These problems are demonstrated by the video footage of the Dalmarnock Fire Tests where visibility is lost at flashover thus depriving the PMMA Sub-Experiment of flame length data.

4.4.3.3 Heat Flux Measurement

In general the data produced by the thin skin calorimeters is noisy and erratic therefore making the identification of trends difficult. In the majority of the experiments the initial readings were negative changing to positive readings as the flame grew and became turbulent in nature. A typical heat flux evolution produced by the calorimeters is shown in Figure 4.51.

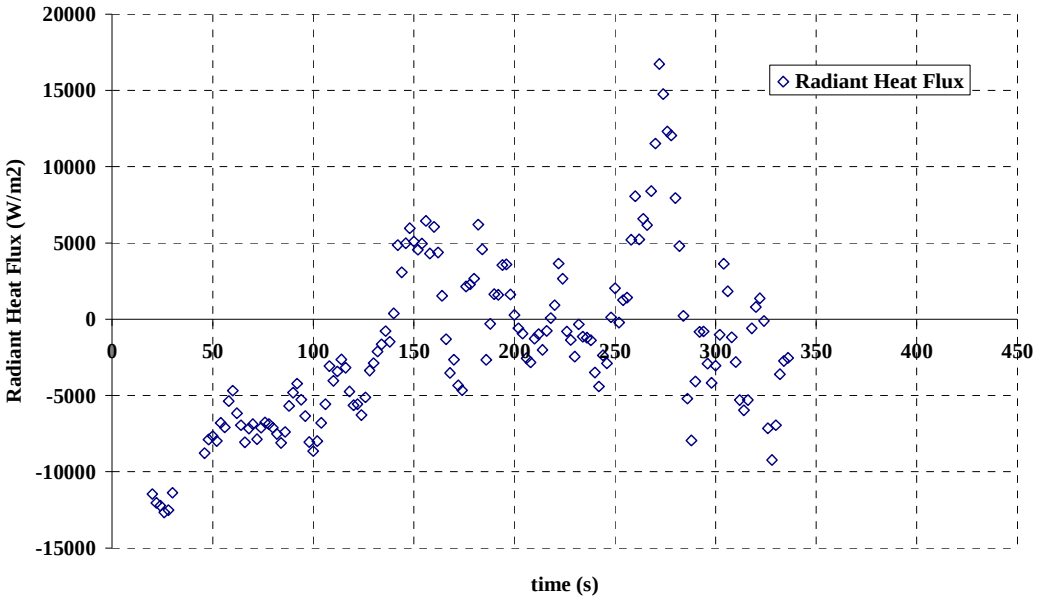

Figure 4.51 – *The plot shows the raw output of incident radiant heat flux (W/m^2) as measured by the thin skin calorimeters and produced by the method outlined in Section 4.2.3.*

As the flame tip becomes level with a disc and the disk is heated and becomes part of the calculation, there is a lag time while the disc responds to the heating effects of the flame and thus until the thermocouple registers that change. In the initial stages, the temperature of the copper disc and thus the energy stored in it is relatively low. The flame temperature however has far less lag time associated with its measurement and is therefore already recorded as being significantly higher than the solid temperature. Thus the first term on the RHS of Equation 21 is approximately zero as the energy stored in the disc and the re-radiation from it are minimal due to the small increase in solid temperature. The second term on the RHS (convective heat transfer to the disc from the flame) is much larger as the flame temperature is quickly established as much higher than that of the disc resulting in this term being much higher than the first and therefore in the negative readings of the radiative heat flux shown in the first portion of Figure 4.51. Due to some difficulties with the reliability of the ignition method (discussed in Section 4.4.3.6) there was sometimes preheating of the lower heat flux meter by conduction through the solid. When the ignition source was removed the temperature of the first disk would then drop slightly as the flame was still very small. This produces a negative value for heat stored in the disc and further reduces the radiative heat flux reading from the calorimeter. As a result of this any negative results have be set to zero to indicate a negligible radiative flux at the time of the reading (Figure 4.52).

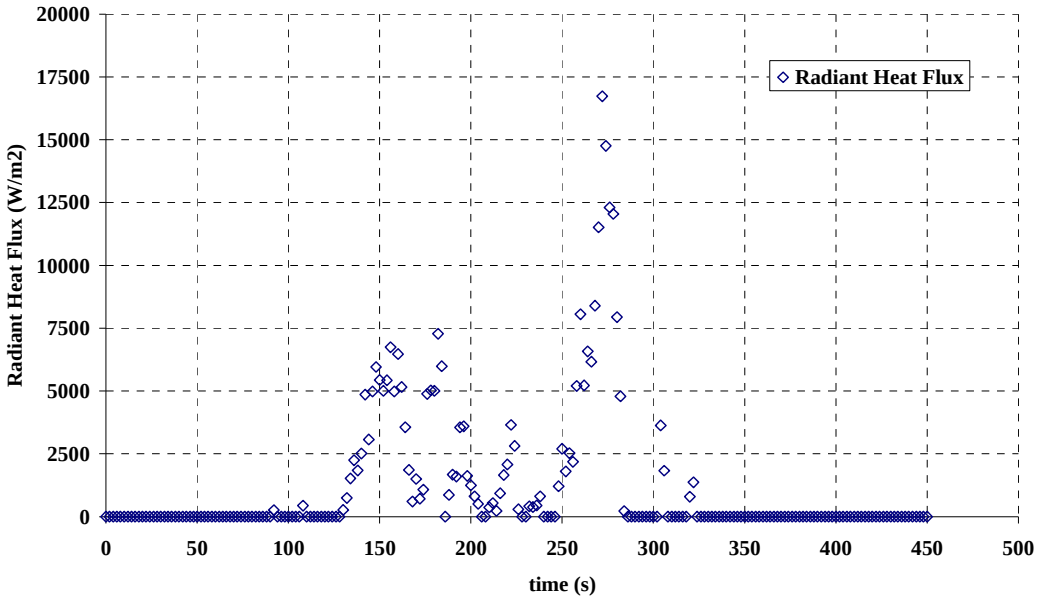

Figure 4.52 – *The plot shows the incident radiant heat flux output from the thin skin calorimeters for a benchmark style experiment with negative values set to zero to indicate a negligible radiant heat flux.*

The data output from this technique tends to evolve in peaks. This appears to be the result of a combination of the method used to ascertain which heat flux meters are in the heated length and the thermal lag described above. As the lowest calorimeter has been in the heated region for the longest period of time, it appears to contribute a greater amount to the value averaged from all the discs in the heating zone contributing to this average. The contributing discs nearer the top of the flame are still displaying the effects of the lag time described above and thus when the pyrolysis front passes the lowest heat flux meter and its contribution becomes invalid, the average falls.

Despite the erratic behaviour of the data there are correlations between this and other data. Figure 4.53 shows a comparison with the flame length data in which trends are very clear. At approximately 100-150s when the flame length data shows a transition to turbulence and reaches the 200mm mark, the levels of radiant heat flux begin to register as non negligible which agrees with previous observations in the literature. At approximately 250s the flame begins to show signs of acceleration with a curvature developing in the flame length data and which corresponds with a spike in the measurements from the thin skin calorimeters. The reading falls away again around 300s as the flame reaches its peak length. This corresponds to the pyrolysis length reaching the top of the PMMA sample and passing the final heat flux meter resulting in no further readings for this data.

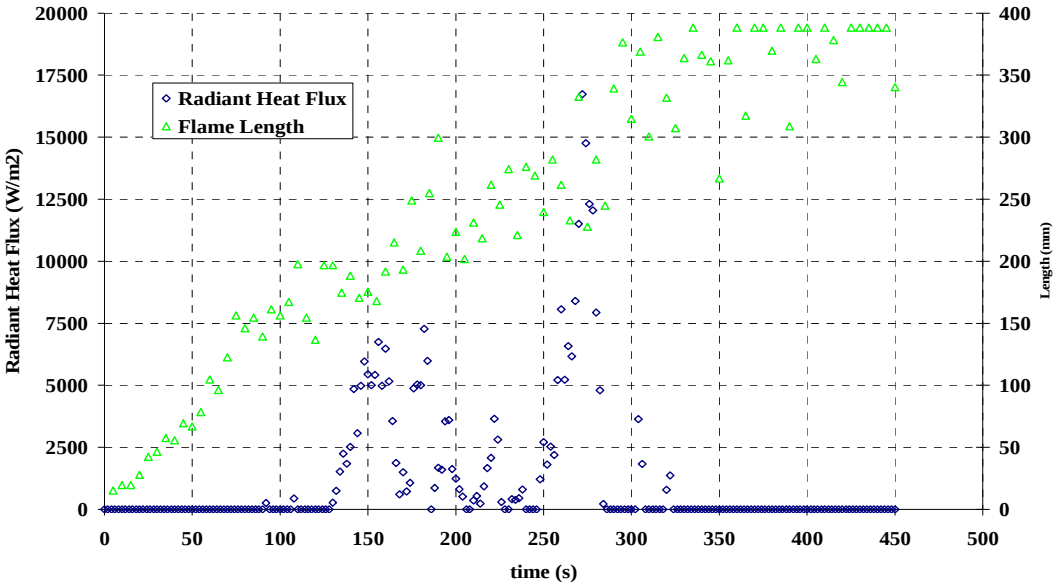

Figure 4.53 - *The graph shows the correlation of incident radiant heat flux measured by the thin skin calorimeters and the flame length for a benchmark style experiment.*

A brief analysis was carried out to establish the ranges of temperatures that the heat flux meters experienced whilst considered to be within the heated length between the flame tip and pyrolysis length. The lower bound temperature was generally around 50˚C and the upper bound at approximately 225˚C for the 200mm high experiments and 325˚C for the 500mm high experiments. The conduction loss factor A (Figure 4.18) was calibrated for temperatures from 0˚C to 250˚C and thus spanning the ranges experienced by the majority of the experiments.

4.4.3.4 Ambient Velocity Measurement

The main advantage of this technique lays in its ability to measure multiple points or more accurately, an area rather than a simple point measurement therefore ensuring that a representative value of u_∞ is measured. The measurement area allows it to adapt to the variable nature of the spreading flame in a way that single measurement point cannot. The data output was very consistent giving confidence in the technique. It also has other potential uses with regards to measurement of thicknesses relating to the flame which were not employed in this work thus yielding a potentially powerful measurement technique.

There were however problems with reliability encountered during testing which have implications for automated use of such a system and also resulted in a less than satisfactory level of data output from the technique. The software proved to be unstable and repeatedly crashed during testing. The time taken to reset the settings upon resumption of the programme wasted valuable measurement time. This problem was not encountered during testing and could not be resolved at the time of testing. A delay was also encountered in refilling the measurement chamber with

seeding. The flow to the seeder was halted during measurements to ensure no interference with the flow being measured and thus levels of seeding were reduced through extraction of the hot gases. The seeder was initially designed to disperse the particles gently in to the direct vicinity of the flame but later adapted to simply fill the entire experimental environment with seeding particles. Had the initial design been focused on the final dispersion strategy, it is believed that more data points could have been achieved during the experiment. It should be noted that the technique, both hardware and software aspects, is not designed for automated use and significant effort would be needed to automate the entire technique from beginning to end. Like the image processing there is a lot of data associated with the images and the cross correlation algorithm necessitates large computational power if it is to be fast enough to be used in real time.

4.4.3.5 Temperature Measurement

Temperature measurements generally gave good consistent results. The gas phase thermocouples gave a good approximation of the flame temperature considering the fairly simplistic method employed. The results from all experiments showed a repeatable consistent plateau in the 700-850˚C region. A more two dimensional array of thermocouples may have been better for tracking the flame temperature and ensuring a peak value was obtained, When the flame grew and drew in closer to the fuel surface later in the experiment, the thermocouples could be seen protruding from the rear of the flame and the corresponding temperature reading fell (Figure 4.54). This proposal does however run the risk of further disturbing the flow and thus interfering with the velocity measurements and potentially the spread process itself.

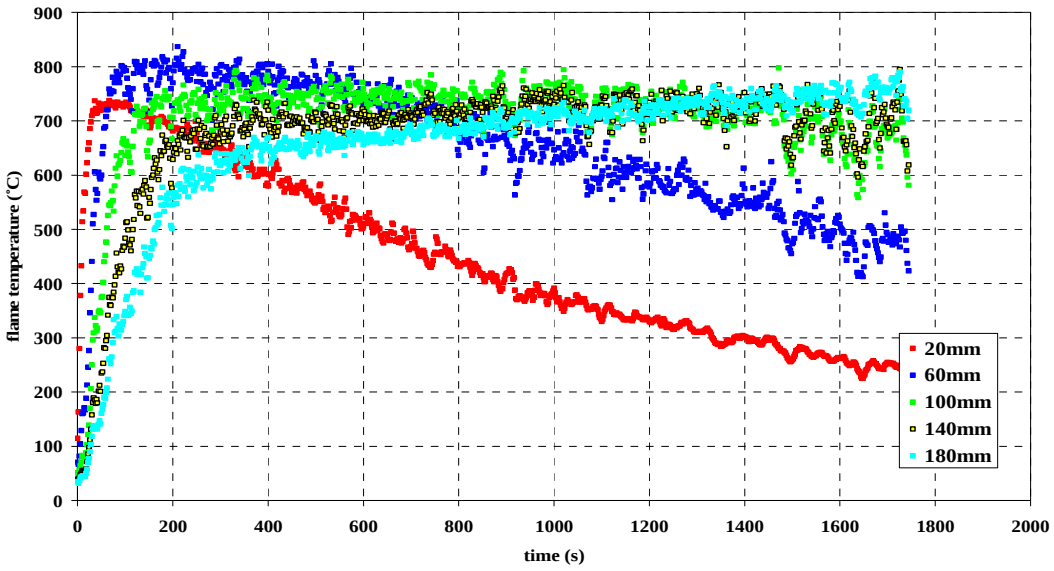

Figure 4.54 – *The plot shows the plateau reached by the thermocouple data during a benchmark experiment. As the flame grows and is drawn closer to the PMMA, the lower thermocouples begin to protrude from the flame and the readings subsequently drop.*

4.4.3.6 Ignition Method

The ignition method successfully fulfilled its purpose of producing a line fire at the base of the PMMA slabs. There was a tendency however for the flame to spread slightly unevenly due to the heat flux meters in the vicinity of which spread was slower than elsewhere across the face. The method was not always completely robust however as frequent power surges caused tripping of fuses for thick wire before a flame could be established while thinner wire tended to break violently when the pilot flame was applied. When the wire snapped it had to be reset into the surface of the PMMA on each occasion which involved removal of the test specimen and thus the embedded and gas phase thermocouples as well. With both outcomes there was preheating of the PMMA followed by a delay due to resetting in which heat could spread through the PMMA sample thus potentially changing the initial conditions once ignition was achieved. These problems led to a balancing act between getting sufficient heat into the solid quickly enough to enable instant piloted ignition without breaking the wire or overloading the fuse. If the heating was performed too slowly with the intension of protecting the wire then there was a risk of preheating the surface ahead of the ignition line which upon ignition would lead to a faster flame spread in this region. Sensor wise this affected the first reading of the embedded thermocouples and the lowest heat flux meter.

4.4.4 Assessment of the Model Assumptions and Correlation to the Literature

4.4.4.1 Dominant Heat Flux Variation

Analysis of the literature regarding the expected heat flux to the unburned fuel ahead of the pyrolysis front (Section 2.1.3.2) indicated that the dominant mode of heat flux would vary with the size and characteristics of the flame. In laminar regions (for small flames or the regions of large flames just ahead of the pyrolysis region) convective flux to the surface should dominate. As the flames grow larger and more turbulent, it is expected that the radiative flux will surpass the convective flux. This is evident in the results of the larger experiments with a sample height of 500mm, and the data output from one such test is used as an example below.

Figure 4.55 shows a comparison of the convective and radiative components of the heat flux from the flame to the surface. The radiative component is measured as detailed in Section 4.2.3 and the convective component is calculated according to the relevant part of Equation 14. Figure 4.56 shows the evolution of the flame length during the spread process and the characteristics of this plot correlate well with the heat flux data (Figure 4.55). Figure 4.55 clearly shows that for the initial 150s post ignition the convective heat flux is the dominant mechanism. Figure 4.56 shows that at this stage the flame is small and video footage shows the flame to be laminar in nature, thus corroborating with the literature. There is a transitional period around 200s where the two components are approximately equal. This corresponds to a flame height in the region of 200mm which agrees with the findings of Orloff et al. [59].

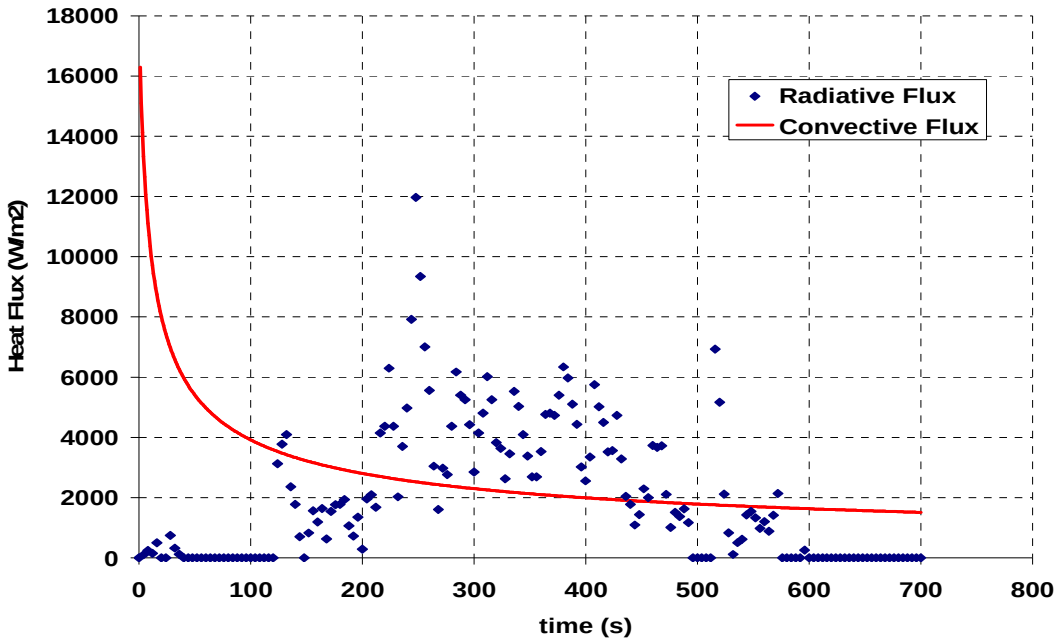

Figure 4.55 – *The plot shows the comparison of the calculated convective and measured radiative heat fluxes during an experiment.*

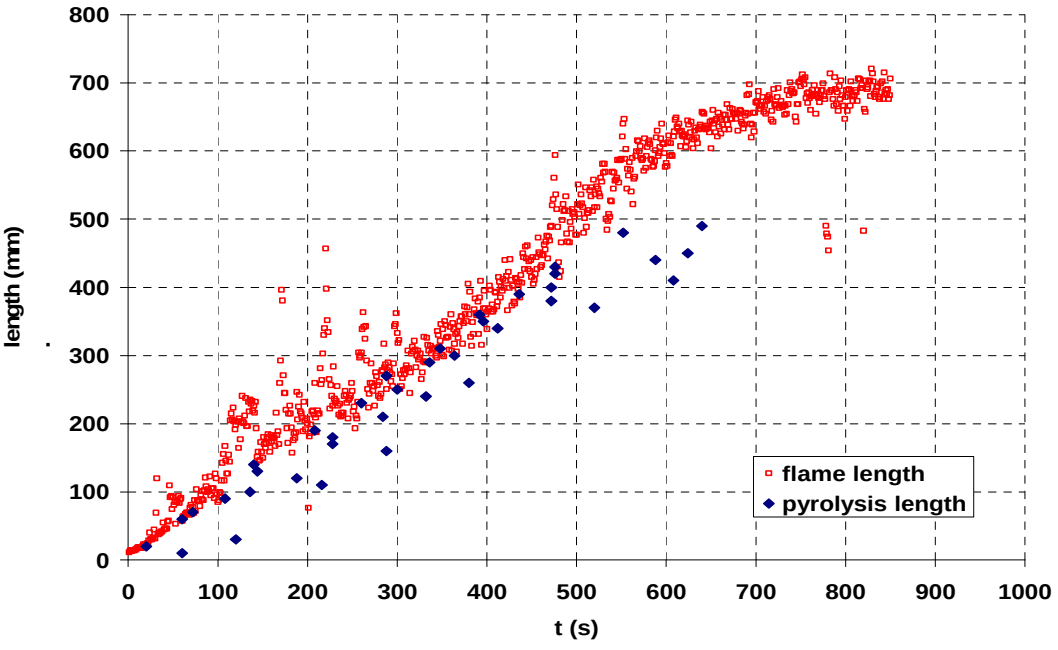

Figure 4.56 – *The gradient of the flame length vs. time plot demonstrates the differing heat transfer processes occurring in the experiment. Pyrolysis length measurement is displayed for reference.*

Between 200 and 500s the radiative portion becomes more dominant, approximately double that of the convective flux and the increase in gradient of the flame height in time represents an acceleration which would be expected in a turbulent regime. From 500s the radiative component then falls away, reaching a negligible value after 600s. At 500s the pyrolysis length composes approximately 420 of the 500mm. Video footage indicates that the region of the flame covering the remainder of the non-pyrolysing fuel is quite laminar in nature. Thus it would be expected that the heat transfer in this region be dominated by convection and the corresponding change in spread rate would show a deceleration. The radiative flux reading can be seen to fall away to zero prior to the pyrolysis front reaching the top of the slab. This is due to the relative positioning of the thin skin calorimeters and the pyrolysis front. The measurement takes into account only flux meters present in the heated length l_h. As the pyrolysis front passes the final meter, in the case of the example experiment 30mm below the top of the sample, the calculation of radiative heat flux ceases, thus the a value of zero for radiative flux is indicated.

4.4.4.2 Heating Ahead of the Flame Tip is Negligible

An assumption of the model is that heating from combustion products ahead of the flame tip is neglected as it is of minor influence when compared with the heat provided by the flame itself. The plot in Figure 4.57 shows the evolution of a selection of the depth thermocouples along side a line representing the approximate evolution of the location of the flame tip.

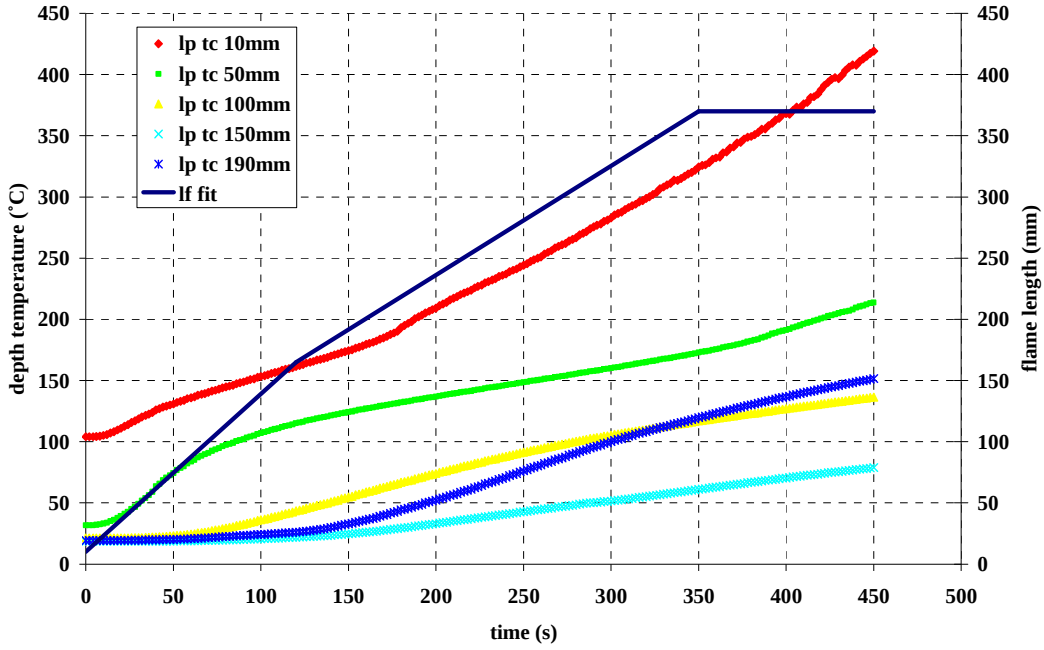

Figure 4.57 – *The figure shows the temperature traces of five of the depth thermocouples spread over the height of the sample and an approximation of the evolution of the flame tip. The lower thermocouples show heating prior to arrival of the flame tip where as the upper ones remain at more or less ambient temperature prior to being considered as being within the heated length.*

Once the flame tip passes the height of the thermocouple it can be considered to be within the heated length and thus any heating from that point on is attributed to the flame. The assumption appears to be justified as demonstrated by the higher positioned thermocouples that in general have not risen above their initial temperature. The lower thermocouples do show preheating but as this has begun prior to ignition it can be attributed to preheating from the ignition source rather than the flame itself. The heat flux meters of the same experiment show a similar trend with all but the lowest at ambient temperature when they become considered as within the heated length and thus valid for measurement.

5 Basic Methodology

Chapter 1 portrayed the need to provide emergency responders with accurate robust information about an evolving emergency to enable them to form an optimised response strategy for each specific emergency they attend. The aim of this work is to demonstrate how combining sensor data with modelling can counterbalance the shortcomings of each of these two entities when used in isolation towards this goal. The model described in Chapter 3 symbolizes the phenomenon taking place in the basic experiments (Section 4.1.1) and thus should be able to predict the future flame spread and flame characteristics if steered by collected data. For this to happen, a process needs to be defined to combine the sensor data recorded by the techniques defined in Chapter 4 with the physical model. The process should attempt to estimate any parameters that remain unknown again steered by the sensor data. The result should be that all the constituent parts of the model are evaluated and are representative of the experiment. By projection forward in time, the conditions at any point in time between the time of forecast and the end of the experiment will be known. The method by which this is accomplished is detailed below and followed by a detailed breakdown of each stage of the process.

5.1 Overview of the Process

The process that has been developed is depicted in the flow diagram in Figure 5.1. There are three main stages to this process which are continuously iterated to provide a dynamic optimisation of the parameters in the model and thus the prediction that it provides. The first phase of the process is data assimilation. The raw data from the sensors is pooled, processed to transform it into a form that is compatible with the model, and filtered to remove error-ness data. The second phase is the population of the model. The parameters contained in the model can be separated into two distinct types at this stage. The first is measured data or predefined constants supplied either as a constant value or a defined time variant relationship. The second type is unknown parameters which are found by means of an appropriate optimisation method. The paths that the methodology can take during the population phase are defined by the transitional stages that the flame will go through as it grows. The methods by which the transient behaviour is described and by which the unknown parameters are optimised are directly related to these transitions. The final phase is the projection of the model and constituent parameters so that the conditions of the experiment can be defined at each point in time between the time of projection and projected end of the experiment. The process then loops back to the first phase, where data is being continuously assimilated, to assess the current data set (original data plus data acquired since) for any changes in conditions. If a condition change has occurred, data prior to it is discarded to exclude it from the optimisation process. All data deemed representative of the current conditions is then sent on to the second phase to populate the model. If the model is truly representative of the experiment and the data processed from the sensor output is an accurate measure of the phenomenon it represents, the output at each iteration should result in convergence of the evaluated parameters as more sensor data becomes available and the error bars

associated with the prediction and each of its constituent parts should shrink. If the parameters diverge, then the physical model is not capable of describing the process in its integrity and needs to be refined.

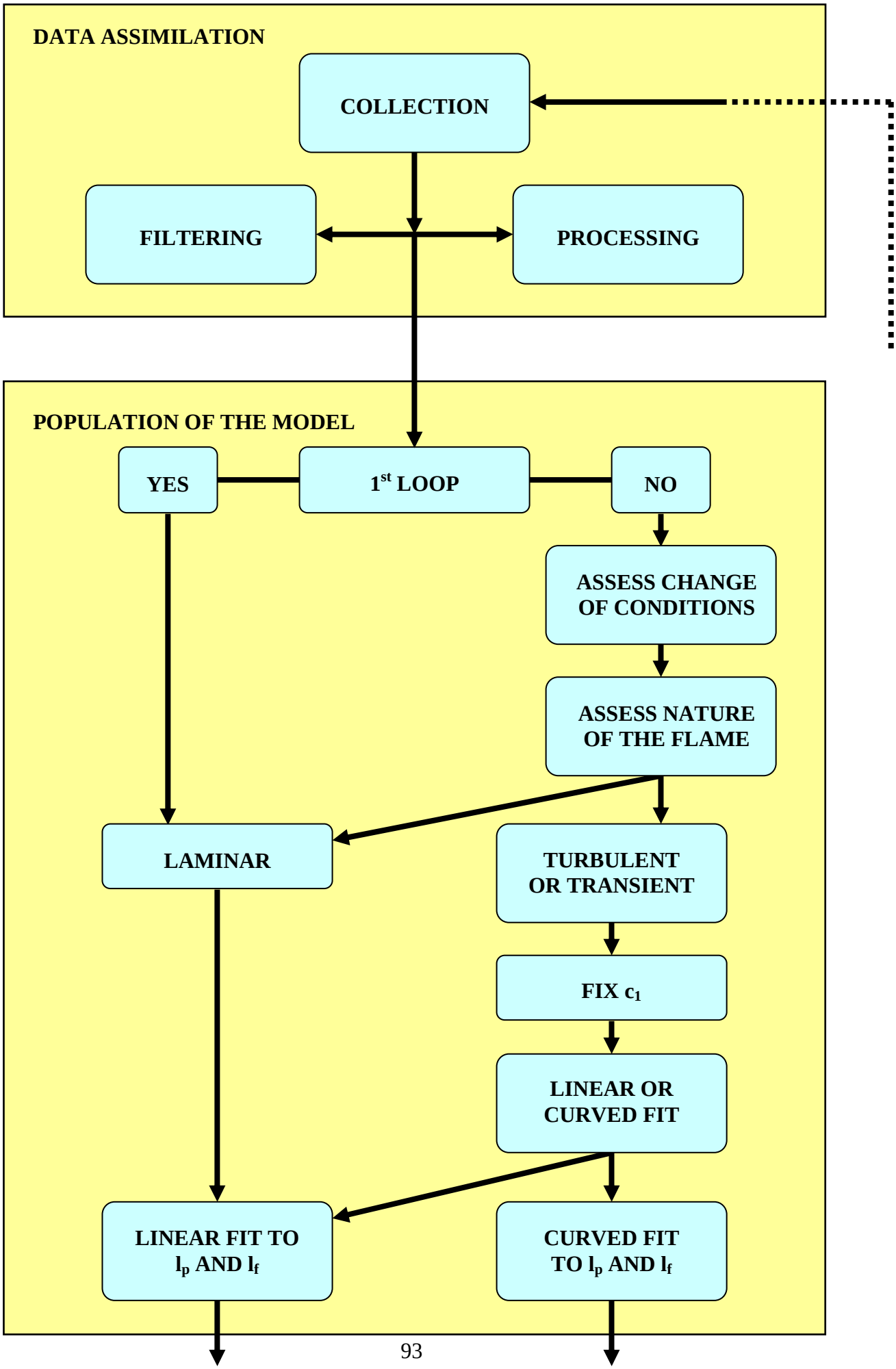
DATA ASSIMILATION
COLLECTION
FILTERING
PROCESSING
POPULATION OF THE MODEL
YES
1st LOOP
NO
ASSESS CHANGE OF CONDITIONS
ASSESS NATURE OF THE FLAME
LAMINAR
TURBULENT OR TRANSIENT
FIX c1
LINEAR OR CURVED FIT
LINEAR FIT TO lp AND lf
CURVED FIT TO lp AND lf

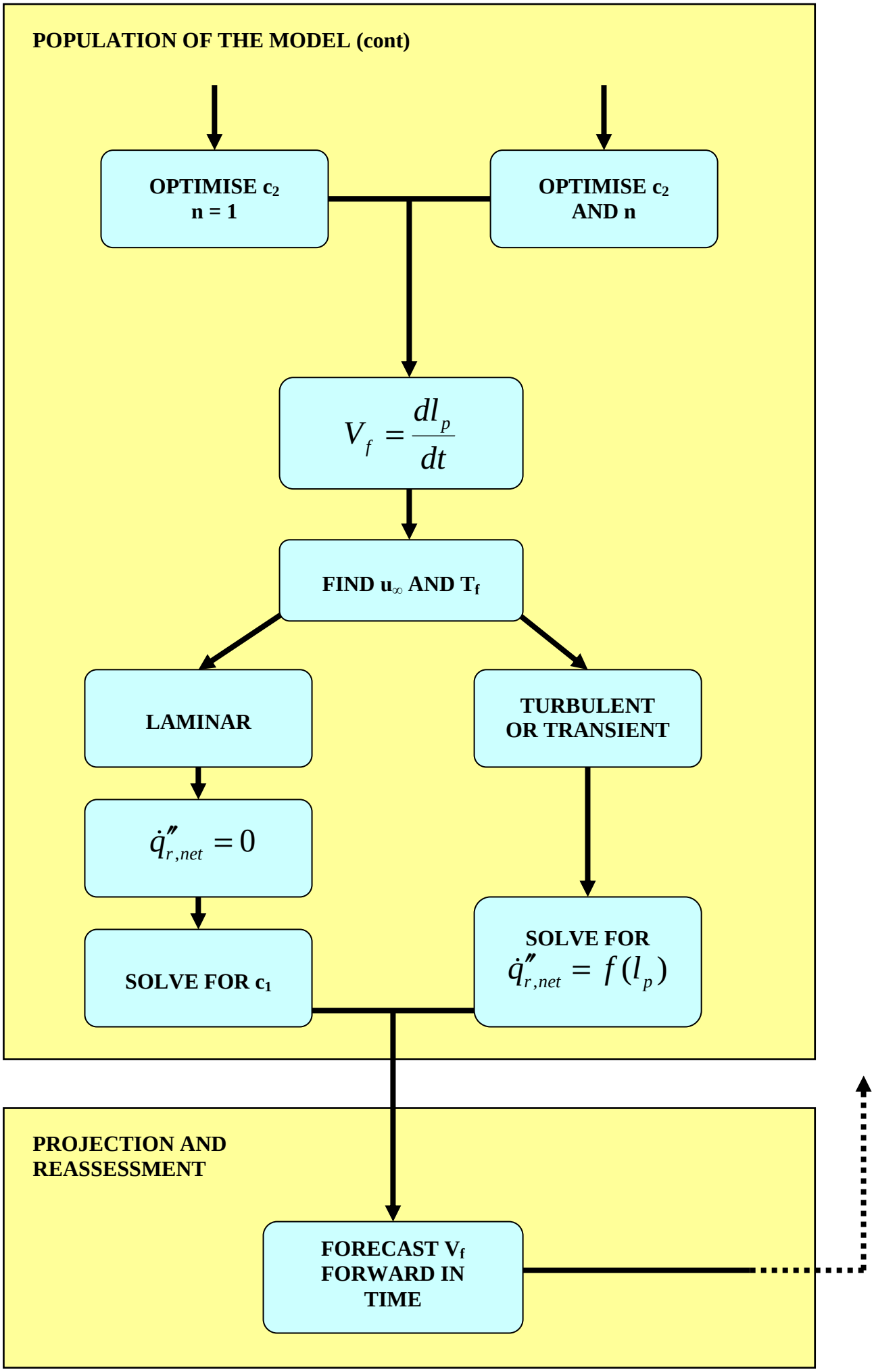
POPULATION OF THE MODEL (cont)
OPTIMISE c2 n = 1
OPTIMISE c2 AND n
$V_f = \frac{dl_p}{dt}$
FIND u∞ AND Tf
LAMINAR
TURBULENT OR TRANSIENT
$\dot{q}''_{r,net} = 0$
SOLVE FOR c1
SOLVE FOR $\dot{q}''_{r,net} = f(l_p)$
PROJECTION AND REASSESSMENT
FORECAST Vf FORWARD IN TIME

Figure 5.1 – *The flow chart shows the relationships between all the elements of the prediction process.*

If conditions within the scenario change, the process effectively starts again, thus convergence of the parameters describing the scenario may take place in numerous phases, each corresponding to a change in conditions. There are three stages expected to be observed during these experiments; an initial laminar phase where convection dominates the heat transfer to the non-combusting fuel, a secondary phase where the regime transitions to a more turbulent flame and radiative heat transfer becomes comparable the convective transfer and finally, a third regime when the flame becomes fully turbulent and the spread velocity shows significant acceleration with radiative transfer from the flame becoming dominant. The simplest scenario will be that the same physical model describes all phases and the differences between phases are encapsulated in the evaluated parameters. Nevertheless, this might not be the case and if a single physical model cannot reproduce all phases, multiple models may need to be constructed and criteria for transition between models need to be defined. Experimental data will be then contrasted with these criteria to establish the physical model to be used.

5.2 Data Collection, Processing and Filtering

The data analysis segment consists of collection of the sensor data from the beginning of the incident / experiment to the present moment in time and the arrangement of this data chronologically and in a form suitable for the model to utilize. While in some cases data can be extracted more or less directly in a form that is useful such as gas phase temperatures, other data such as the flame length and ambient velocity measurements will involve the processing of the raw data to varying extents into a form required by the model. Well defined parameters such as material properties and universal constants are read from a database. For the purposes of these experiments, the techniques that require pre-treatment and the specifics of the individual processes have been detailed in Section 4.2 including the conversion of camera images to flame length data and vector maps to extract relevant ambient velocity vectors, the extraction of isotherm data from depth temperature measurements, and the determination of heat fluxes from temperature measurements within the thin skin calorimeters. With the data in the correct format, it must be also arranged chronologically and in some cases filtered or smoothed before being inputted to the model. Flame temperature measurement for example requires the filtering of the measurements to include only those from thermocouples present in the region of the flame which in turn requires analysis of the flame length data. Once the relevant measurements are isolated a decision can be made as to whether an average or maximum temperature is taken. A similar approach is needed to establish which of the thin skin calorimeters are lying between the pyrolysis front and the flame tip and can be assumed to be measuring the heat flux from the flame to the surface, thus requiring the sensor information from two other sources to make the information usable in the model. The ambient velocity vector once processed from the PIV image pairs and extracted from the correct location in a vector map is

simpler as it is not expected to change significantly and thus is simply averaged as more data becomes available.

5.3 Population of the Model

The second stage of the process is the population of the model. The methods employed in this stage of the process are separated into distinct sets. The set of methods chosen is defined by the characteristics of the flame as are the methods themselves. In order to decide which set of processes to perform, the nature of the flame over the period of time for which data is available must first be defined. If the flame or environmental conditions are adjudged to have changed in nature during the time period represented by the current data, data representing conditions before the change must be discarded. It is important that the data that is used to populate the model and establish which processes are used to accomplish this, represents only the current state of the experiment. This will ensure that, provided the process works correctly, the prediction generated will be a forecast of the current state. Once conditions within the experiment have been established and data relevant to those conditions has been isolated the model can be populated. There are two distinct classifications of parameter within the model; the parameters that are either predefined or directly measured (the “known” parameters), and the “unknown” parameters which have not been directly measured and thus must be optimised from the available data.

5.3.1 Assessment of Current Experimental Conditions

5.3.1.1 Changes of Conditions

Once the data has been assimilated from the sensors, converted to a form concurrent with the requirements of the model, and been filtered to remove data that is clearly error-ness, the data is assessed to spot any significant changes. Changes are indicated by variation in trends and may be representative of a transition of flow regime from laminar to turbulent, or a difference in the environmental conditions. This process is included to ensure that the fits applied to the data in the next stage of the process and the optimised parameters that result from them are representative of the current conditions only and not influenced by non-relevant data.

5.3.1.2 The Nature of the Flame

The nature of the flame determines the shapes of fits and the methods of evaluating unknown parameters, and as such a correct assessment of it ultimately determines the accuracy of the prediction itself. Before fitting and optimisation are performed, the data is inspected and a decision made as to whether the flame is laminar, turbulent or transitioning between the two. The information used to determine this is a combination of the trends shown by the length scale data, the size of the flame, and the amount of incident radiant flux measured by the thin skin calorimeters.

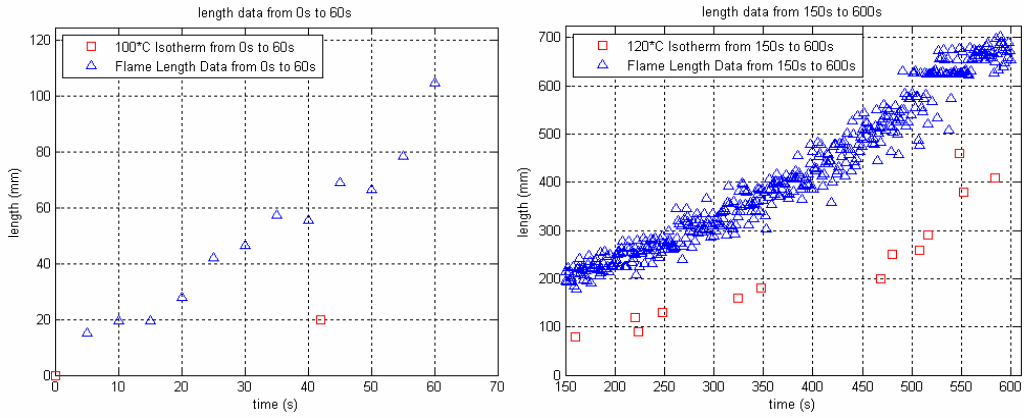

a) b)

Figure 5.2 – *The plots show two sets of flame and pyrolysis length data. (a) a typical laminar flame and (b) a larger more turbulent flame.*

The example shown in Figure 5.2 demonstrates the two flame regimes. The first plot represents a laminar flame where the growth in flame length appears steady and linear. The overall flame length doesn't exceed 200mm which Orloff et al. [59] reported as corresponding to the onset of turbulent behaviour. In the second plot, the flame has exceeded 200mm in length and shows a slight acceleratory trend and thus would no longer be considered laminar.

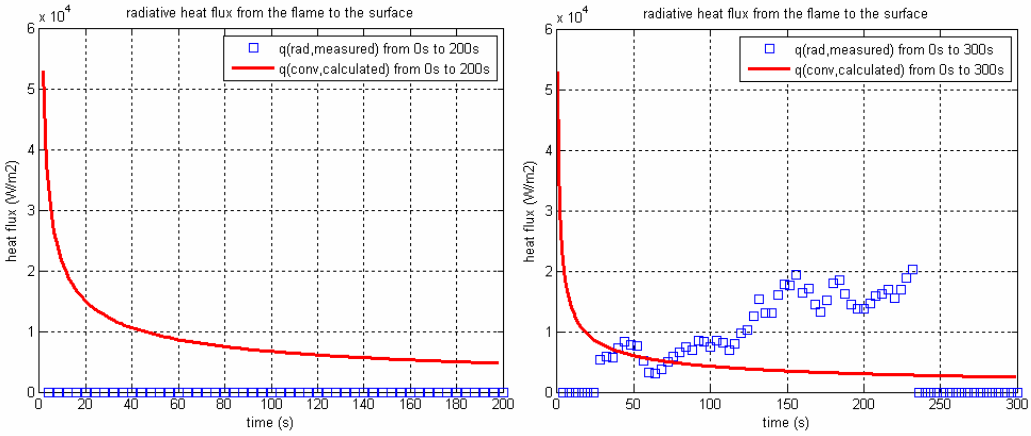

a) b)

Figure 5.3 – *The figure shows two typical examples of graphs comparing the incident radiative flux measured by the thin skin calorimeters (blue squares) and the estimated evolution of the convective flux to the surface based on the c_1 value obtained at the previous iteration. . (a) a typical laminar flame and (b) a larger more turbulent flame.*

The third and final form of data used to make this judgement is the respective levels of convective and radiant heat flux. This data is not available at this stage of the first iteration of the process as provision of both forms of heat flux relies on optimisations made in a previous iteration. The heat flux readings from the thin skin calorimeters rely on a fit of the pyrolysis and flame length data to establish which meters are within the heating region. The estimation of the convective heat flux relies on provision of the c_1 parameter which is optimised later on in the process. Thus, for the first iteration which occurs relatively soon after the ignition, the flow is assumed to be laminar. In subsequent iterations when data is available, plots are produced such as those shown in Figure 5.3 using fits and optimisations from a previous iteration. In the first of the two plots shown in Figure 5.3, the thin skin calorimeter data is registering zero incident radiant heat flux (see Section 4.4.3.3) thus indicating that the flame can be considered laminar. In the second plot, the data from the thin skin calorimeter is comparable to that of the estimated convective flux indicating that the flame is in a transition phase and the relevant levels of radiative flux should be established.

5.3.2 The "Known" Parameters

5.3.2.1 Length Scale Parameters

The values of the length scale parameters, l_p and l_f, vary in time as the flame spreads. To aid the optimisation and prediction processes, a fit is applied to the measured data for each of these two parameters. The fit consists of a function describing how the parameter varies in time. The function used is determined by the nature, laminar or turbulent, of the flame. Length scale data is supplied to the model in the form of these fits i.e. as some function of time, which enables the projection of the trend shown by the data into the future.

Examination of the pyrolysis and flame length data from the experiments and inspection of the literature [17] [59] clearly demonstrates that the two parameters are closely linked and that trends in both sets of data mirror each other to a large extent. This knowledge is important as it suggests that the fits made to these two sets of data should be of the same form i.e. if one set of data is clearly developing linearly, the other should be expected to develop in the same manner and thus linear fit models should be applied in both cases.

This knowledge is also extremely useful in cases where data is sparse as it enables the fitting process to compensate to some extent for a lack of data. This is seen to be the case in the experiments reported here where the number of pyrolysis length data points is limited by the number of depth thermocouples and trends are difficult to identify early on by this data alone. By contrast, the flame length data is generally dense enough to clearly show a trend from the very early stages. The process of applying a fit to the pyrolysis length data is thus more robust as the uncertainty involved in deciphering a trend from the data is removed and the correct style of fit

can be made. In these cases the pyrolysis length data has only to guide the magnitude of the fit thus reducing uncertainty and therefore error.

Inspection of the experimental results has shown there to be two patterns of growth present within the range of conditions encountered in these experiments. In the early stages of the experiments the flame spreads linearly and thus the length scales follow a corresponding trend. As the flames grow, the spread is seen to accelerate portrayed by a curvature in the development of the data in time. The linear growth corresponds to a laminar flame state while the accelerative trend is indicative of a turbulent regime. Thus the method of fitting is predetermined by the result of the assessment of the nature of the flame described above (Section 5.3.1.2) and the application of these fits is described below.

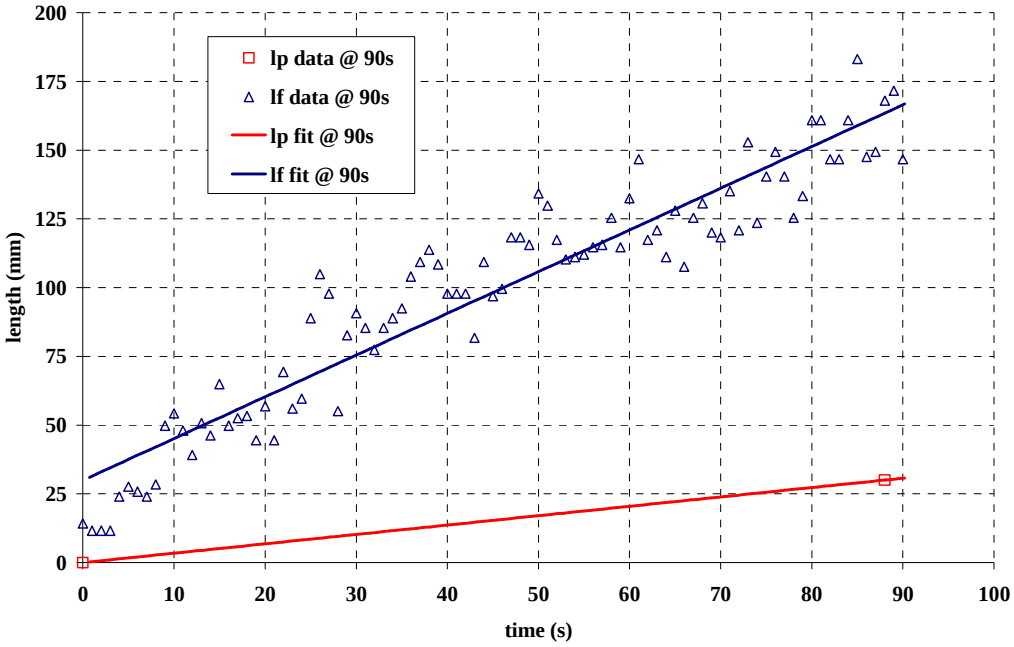

Figure 5.4 - *The plot shows corresponding sets of flame length data (blue triangles) and pyrolysis length data (red squares). The fits made to the data (continuous lines) represent how they are thought to have varied in time up to 90s post ignition.*

5.3.2.2 The Linear Regime

At any stage when the flame behaves in a laminar fashion, a simple straight line fit pattern is prescribed to the pyrolysis and flame length data. This may be in the initial loop or in subsequent loops when the flame is adjudged to be either laminar in nature or in a transition phase but still evolving linearly. As alluded to previously, there is a close relationship between flame length and pyrolysis length which is characterised when the flame is laminar in nature by Equation 22 which states that the two are

linearly related. Equation 22 is identical to Equation 10 with n equal to one for laminar flow.

$$l_f = c_2 l_p$$

Equation 22

If the flame has been deemed to be laminar through inspection of the data a linear fit is applied to both the pyrolysis and flame length data in the form: -

$$l_p = m(t) + c$$

Equation 23

An example of the fits produced by this fit model is shown in Figure 5.4. Inspection of the data in this figure shows consistent growth over this period and it remains smaller than 200mm.

5.3.2.3 The Accelerating Regime

For accelerating spread rates, usually the result of fully turbulent flows, the simple straight line fit can no longer be used to describe the evolution of the data and some form of curve fit must be applied to capture the acceleratory trend for projection into the future.

Initially a set of alternative fit options such as parametric, log and power fits were applied by curve fitting software following inspection of the data. The fit type adjudged to follow the trends in the data best at each iteration of the process was utilized essentially making the process one of trial and error and intuition. This method was discarded because arbitrary fits convey no knowledge of the physical process, and also because based on interpretation of the data at each stage, there could be a tendency to vary the fit type which discourages the convergence of the fits and consequently of the parameters that are subsequently optimised from them. It could be the case that where parabolic curves were prescribed that fitted the immediate data well; when extrapolated into the future; they failed to represent the likely path of the variables in any reasonable way.

Aside from these practical flaws, the ethos of the work was to automate the process as much as possible and this particular system laid too much dependability for success on intuition. Hence a generic fit describing l_p or l_f as a function of time was sort that could be manipulated through the optimisation of its variable parameters to satisfy the expected range of behaviours. The fit was derived from a combination of the focal flame spread model describing flame spread as a solid ignition process, coupled with the definition in the literature [70] that the spread rate is equal to the derivative of the pyrolysis length with respect to time, i.e.

$$V_f = \frac{dl_p}{dt}$$

Equation 24

Equating the two definitions of spread rate the following relationship is established: -

$$\frac{dl_p}{dt} = \frac{4c_2[(c_1 k_g \rho_g c_p u_\infty / l_p^{\,n})^{1/2}(T_f - T_p) + \dot{q}''_{fr} + \dot{q}''_e - \dot{q}''_{rs}]^2 l_p^{\,n}}{\pi k_s \rho_s c_s (T_p - T_0)^2}$$

Equation 25

Grouping of the constants then transforms this into the following form: -

$$\frac{dl_p}{dt} = K_1[K_2 + Ql_p^{\,n/2}]^2$$

Which when rearranged gives: -

$$dt = \frac{1}{K_1[K_2 + Ql_p^{\,n/2}]^2} dl_p$$

This expression can then be integrated to give time as a complex function of pyrolysis length (Equation 26) with adjustable parameters K_1, K_2, K_3 (introduced as the constant of integration), Q, and n to be manipulated to produce the optimal fit of the time – length data.

$$t = \frac{2}{K_1 Q^4 n}\left[\frac{1}{2}(Ql_p^{\frac{n}{2}} - 5K_2)(Ql_p^{\frac{n}{2}} - K_2) + 3K_2 Ln(Ql_p^{\frac{n}{2}} - K_2) + \frac{K_2^{\,3}}{(Ql_p^{\frac{n}{2}} - K_2)} + K_3\right]$$

Equation 26

The full derivation of this Equation is given in Appendix 2. Ideally the expression would express l_p as a function of time allowing the pyrolysis length at any point in time in the future to be calculated directly but the complexity of the expression makes this impossible (at least for this mere mortal) and thus the function is used in this form.

Equation 26 is thus used in the given form to find the optimum fit of time as a function of pyrolysis length for the current isotherm data rather than pyrolysis length as a function of time as was previously the case with the linear fit. The same fit shape is also applied to find time as a function of flame length given that the same model should be applied to both length data according to the justification given previously (Section 5.3.2.1). The fitting process itself is made using commercial curve fitting software optimising the fit with a least squares method. The fit can and has also been made using a Genetic Algorithm. For this application, the curve fitting software was chosen over the GA on the basis of speed of computation, taking far less computational time and effort to derive a good fit. No comparison of the quality of fits derived by the two methods is made here.

5.3.2.4 Flame Temperature and Ambient Flow Velocity

Two constituent parameters of the term expressing the convective heat flux from the flame to the surface are the flame temperature (T_f) and ambient flow velocity (u_∞). Both of these quantities have measurement techniques associated with them. Inspection of the u_∞ data produced by the PIV system shows that, during each experiment, there is very little variation in the magnitude of this parameter and thus a constant value is considered to represent this data sufficiently. The value supplied to the model is thus simply an average of all data points from the current data set.

The flame temperature is taken from the measurements produced by the gas phase thermocouples. These thermocouples are close to the exposed surface of the PMMA and are assumed to be measuring flame temperature when they are enveloped by the flame. Before a choice of temperature can be made, the readings that correspond to a thermocouple within the flame must be segregated from the others. The process that isolates the desired data makes use of the fit made to the flame length data. For a thermocouple to be considered within the flame, the flame tip must be higher than that thermocouple. By substituting the height of the thermocouple into the fit model (Equation 26) in place of $l_{p,}$ together with the values of the adjustable parameters (K1, K2 etc.) produced by the fit of the flame length data, a value of time corresponding to the flame tip arrival at the thermocouple is derived. This process works equally well for the linear fit when the model (Equation 23) is rearranged to make t the subject.

A representation of this is shown in Figure 5.5. Each data point style represents a different thermocouple with the corresponding height shown in the legend. As the flame tip reaches the height of the thermocouple the data changes from grey to coloured. Only coloured data is considered as a potentially valid flame temperature.

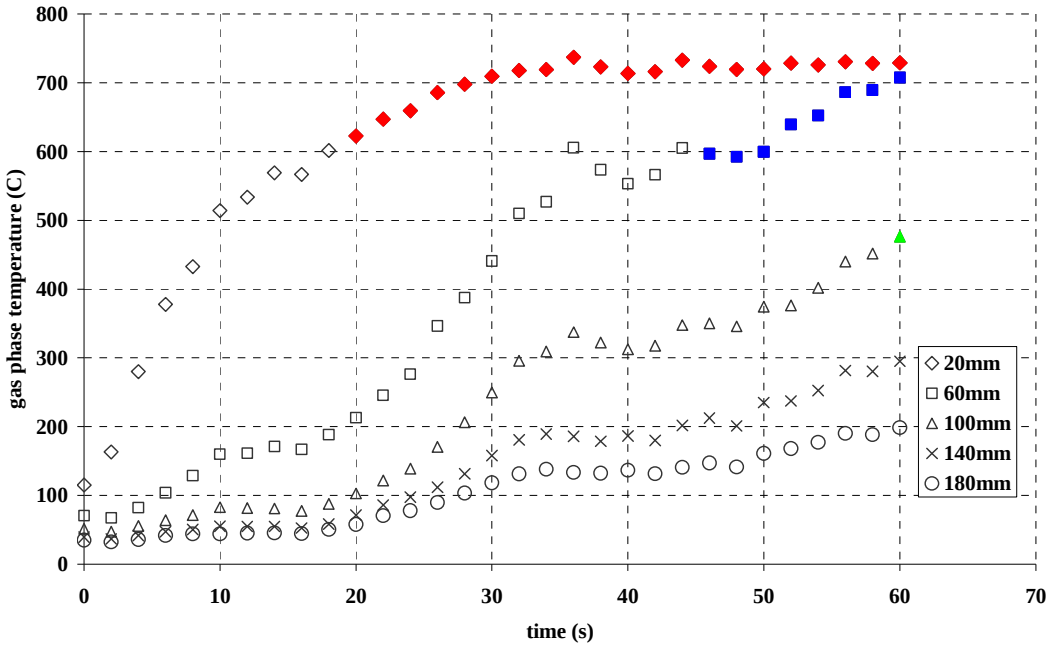

Figure 5.5 - *The plot shows the gas temperature measurements over the first 60s. The readings are only considered for the measurement once the sensors themselves are within the flame. The height of each thermocouple above the ignition location is shown in the legend.*

When the data points produced over the entire duration of the experiment are viewed as a whole, a distinct and consistent trend is observed. As the thermocouples come into close proximity with the flame, the readings they produce rise and level off to form a plateau. The magnitude of this plateau is reasonably consistent for all thermocouple readings in an experiment. A sample of data showing this trend is shown in Figure 4.54. This trend implies that the temperature of the flame is essentially constant and is represented by the value at which this plateau occurs. Thus the flame temperature is calculated and presented to the model as the maximum temperature measured by a thermocouple adjudged to be within the flame.

5.3.3 The "Unknown" Parameters

The ideal scenario would be that all parameters in the model fall into the "known" category, that is, that they are either pre-defined constants (such as material properties or universal constants) or measurable parameters. This scenario would remove much of the uncertainty and calculations associated with the production of a prediction. As this is not always practical or possible, some parameters remain unknown once all data has been pooled and these outstanding parameters must be estimated by some means. The method by which some parameters are optimised is dependent on the earlier assessment of the conditions of the flame, much as the choice of fits applied to the length scale data was. In all cases the method of

optimisation aims to use as much information from the data and literature as possible to remove as much uncertainty from the resulting values as possible.

5.3.3.1 Spread Rate

An estimation of the evolution of the spread rate over the time interval being analysed is required in order to optimise the remaining unknowns. The spread rate can be established from the pyrolysis length data using the relationship described in Equation 24 provided that there is no burnout at the flames leading edge. When the base of the flame remains stationary, the rate of change of the pyrolysis length corresponds to the rate at which the pyrolysis front progresses. The spread rate is derived from the fit as opposed to the data itself as the isotherm data points are too sparse and/or noisy to get a good approximation. This consequently makes the success of the process more heavily reliant on obtaining a representative fit of the pyrolysis length data. The process applies equally well to the linear and curve fits.

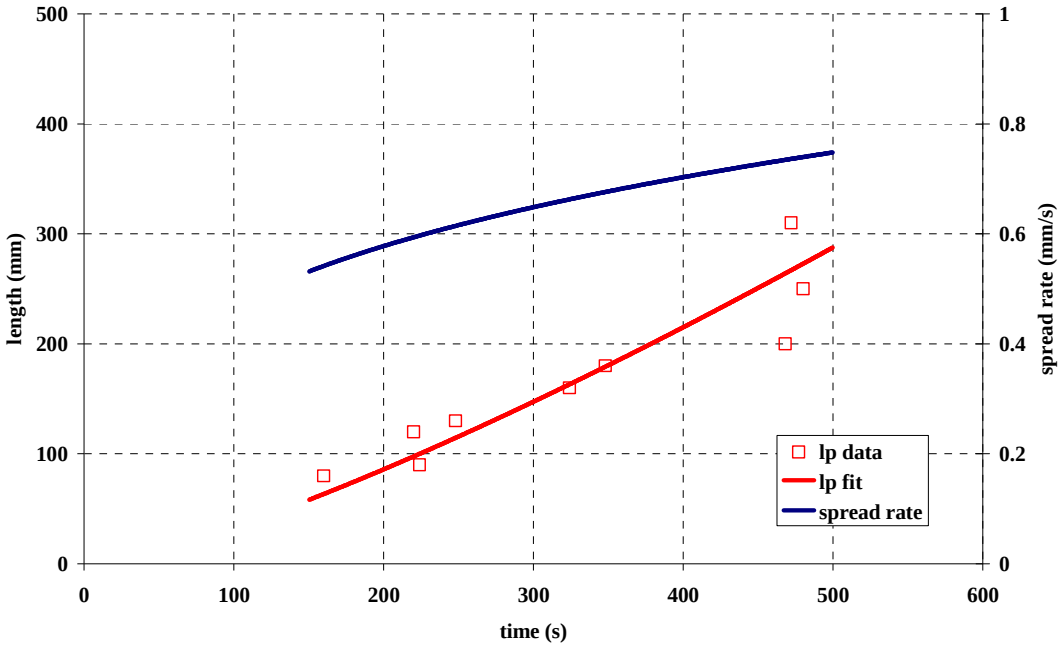

Figure 5.6 - *The plot shows a fit applied to the pyrolysis length data (in red) and the subsequent spread rate derived from it (in blue).*

5.3.3.2 Length Scale Relationship Parameters

The values of pyrolysis length and flame length are related by the parameters c_2 and n according to the correlation defined in Equation 10.

$$l_f = c_2 l_p^{\,n}$$

Equation 10

When the flame is adjudged to be laminar or transitioning towards turbulence but still showing steady linear growth, a linear fit is applied to the pyrolysis and flame length data. The parameter c_2 can be found directly from the ratio of flame length to pyrolysis length (Equation 27) as n is adjudged to be unity (=1) for a laminar flame.

$$c_2 = \frac{l_f}{l_p}$$

Equation 27

The plot of c_2 in time derived from this ratio shows convergence on a single constant value (Figure 5.7) as the initial conditions become less influential on the ratio. This value is taken as representative of c_2 and used to populate the physical model for the laminar, linearly evolving flame regime.

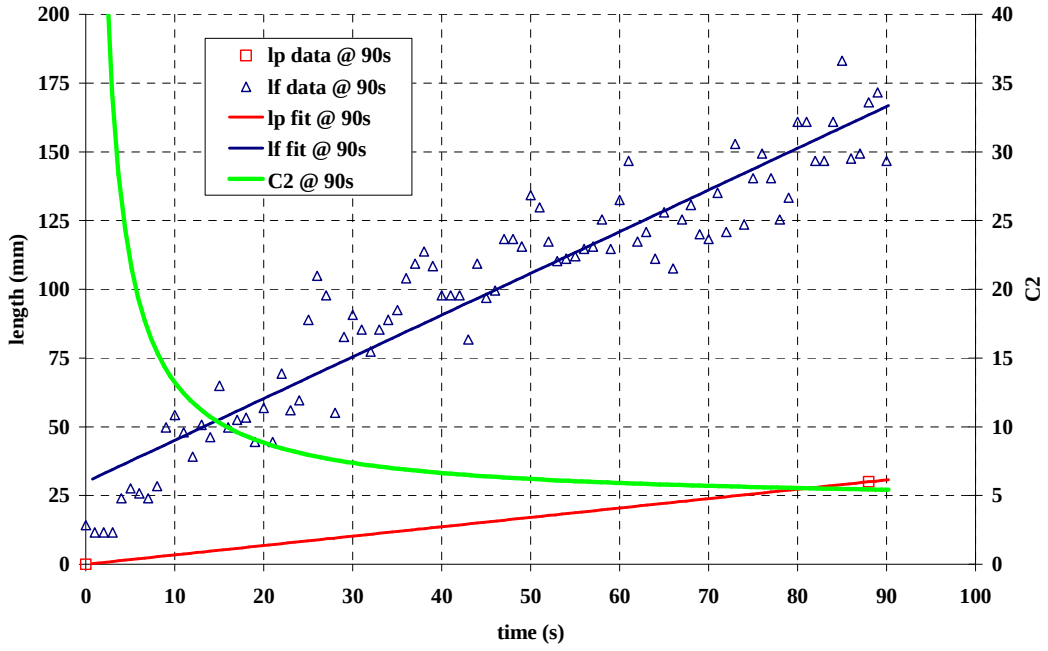

Figure 5.7 - *The plot shows the value of c_2 (green line) resulting from the ratio of flame length (blue line) to pyrolysis length (red line). The value converges on a constant value which is used in the subsequent prediction.*

When the flame has become turbulent and the radiation from it has become the dominant mechanism of heat transfer ahead of the flame front, the spread velocity is seen to accelerate and a curved fit is used to describe the length scale data as outlined in Section 5.3.2.3. In this case the parameter n is not automatically fixed as unity (=1) as for the laminar flame, and the values of c_2 and n must be established in unison and by a different method to that described above for a linear growth situation.

The curve fits applied to the flame and pyrolysis length data (in Section 5.3.2.3) are used as part of an optimisation to determine the values of the parameters c_2 and n as represented in Equation 10. In this case there are only two unknowns and these unknowns have limited ranges. These ranges can be assigned from a combination of the literature (See Section 2.1.4) and the experimental data. A "brute force" method (described below) is used to find the optimum values of each parameter based within these ranges. The optimum is defined as the combination of c_2 and n that minimises the difference between the flame length line fit and the line produced by applying the values of n and c_2 to the pyrolysis length line fit according to Equation 10 i.e. by minimising the value of y in Equation 28 under the constraints of the ranges of its constituent values: -

$$y = \int_{t_0}^{t_{current}} \left| l_{f,fit}(t) - c_2 l_{p,fit}(t)^n \right|$$

Equation 28

The value of t_0 represents the time at the beginning of the current data set from which the fits were made. This could be either the time of ignition of the experiment or the time at which a change of conditions was adjudged to have occurred (see changes of conditions 5.3.1.1). The value of $t_{current}$ represents the time at which the optimisation is being made. The optimal values of c_2 and n are found by a "brute force" method. This means that all possible combinations (within reason) of the values of c_2 and n from their respective ranges are applied to the pyrolysis length fit as per Equation 28 and a value of y is found for each and every combination. The combination that produces the minimum value of y represents the optimum.

The crux of this method thus relies on a good definition of the ranges of the parameters. If the bounds of the ranges are too tight, the optimal solution may lye outside of them and thus may never be discovered. If, on the contrary, the bounds are too distantly spaced, the number of computations that must be performed to adequately cover the search space using a brute force method may make this technique unpractical. A practical set of bounds for these parameters can be defined however through a combination of previous results from the literature and analysis of the available experimental data.

Data for the parameter n is available in the literature (listed in Section 2.1.4) where values are reported ranging from 0.66 to 0.8 for fully turbulent flow and 1.0 for laminar flow. For this work these bounds are widened to allow the process to explore

the possibility that a good solution could lie outside of the conventionally accepted values. The upper bound was set at n=1.5 and the lower bound at 0.5. If the values for the optimum solutions converge on these boundary values, it will indicate that the optimum result most likely lies out with these bounds and that they should be widened further still. If the solution converges within the conventional 0.66-0.8 range then this would give added confidence that the process is working. Given the fairly linear nature of the small flames in most of these experiments, a value closer to 1.0 would seem acceptable.

The bounds of the c_2 parameter are set using a combination of the bounds of n and the maximum and minimum values of $l_{p,fit}$ and $l_{f,fit}$. According to Equation 10, the value of c_2 shifts the value of l_p^n to that of l_f. Using this relationship and given that all of the values of $l_{p,fit}$ and $l_{f,fit}$ are known, the largest value that c_2 could need to be to cover all possible eventualities, and thus the upper bound for this value in the optimisation, is given by the largest value of l_f, the smallest value of l_p and the smallest possible value of n (n=0.5) applied to Equation 29. The minimum bound is given by Equation 30.

$$c_{2,\max} = \frac{l_{f,\max}}{l_{p,\min}^{\,n_{\min}}}$$

Equation 29

$$c_{2,\min} = \frac{l_{f,\min}}{l_{p,\max}^{\,n_{\max}}}$$

Equation 30

A set of candidate values of c_2 and n are then produced that substantially and evenly cover the range between the upper and lower bounds calculated for each of the parameters. Every combination of the candidate values of the two parameters is then applied to Equation 28 and the value of y for each combination is logged. Once all combinations of the candidate parameters have been processed, the combination that produced the smallest value of y is taken as the optimum.

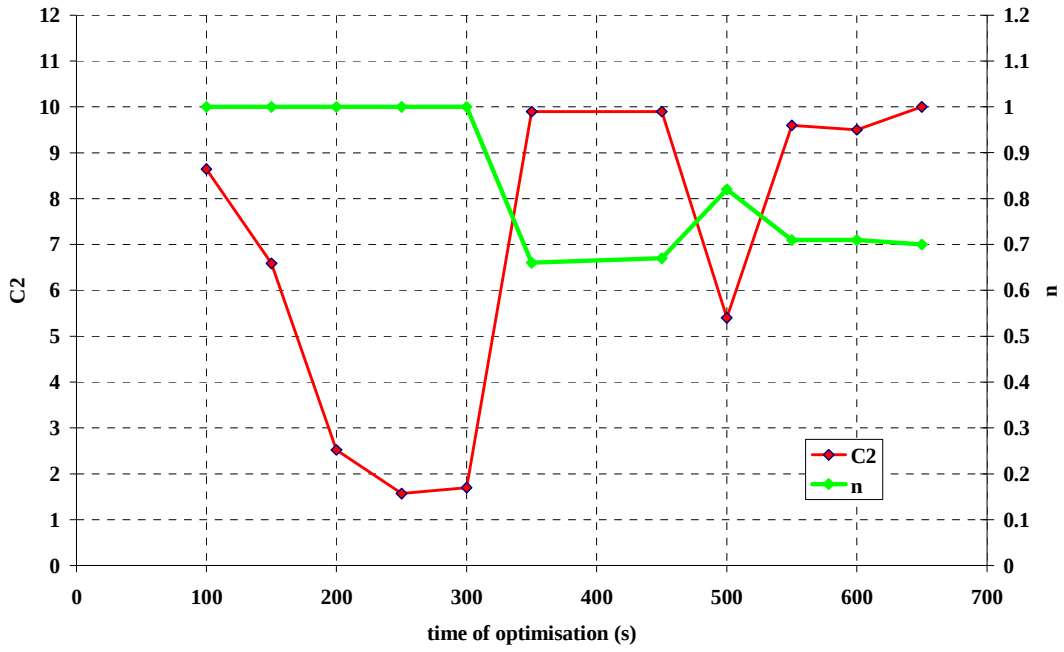

Figure 5.8 – *The plot shown the evolving optimisations of the* c_2 *and n parameters during an experiment where a transition to turbulence occurs. Linear fits are applied until 300s post ignition when enough data is available to demonstrate that a change of conditions has occurred and the fit type switches to the turbulent curve fit.*

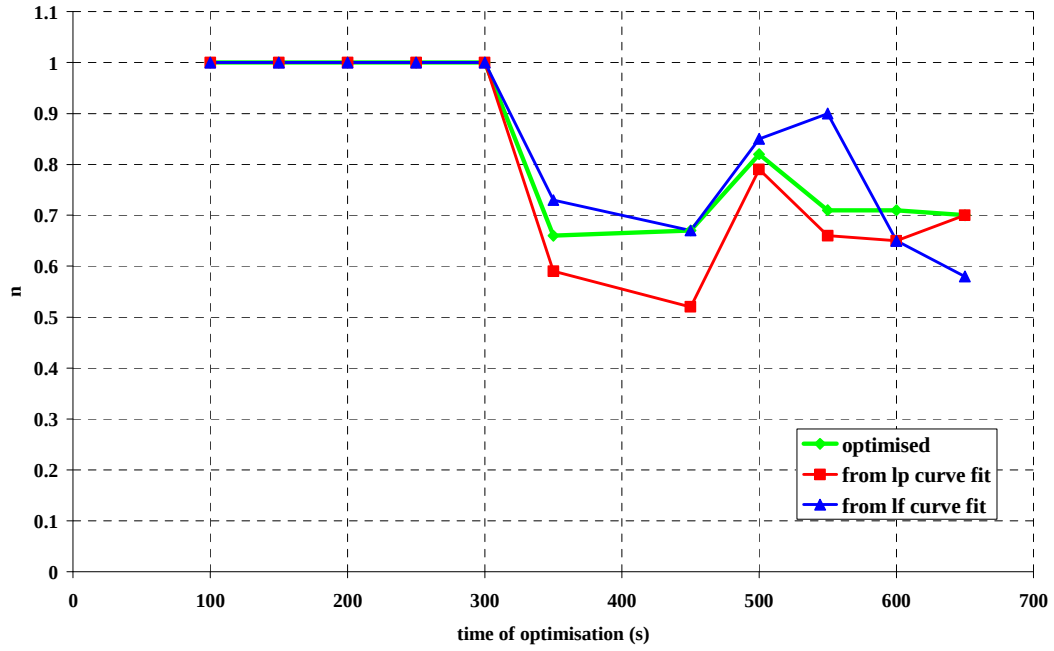

Figure 5.9 – *The plot shows the comparison of the parameter n derived from different components of the optimisation process. The green line represents the value optimised from the curve fits as described. The red and blue lines represent the output from the line fits applied to the pyrolysis and flame length data respectively.*

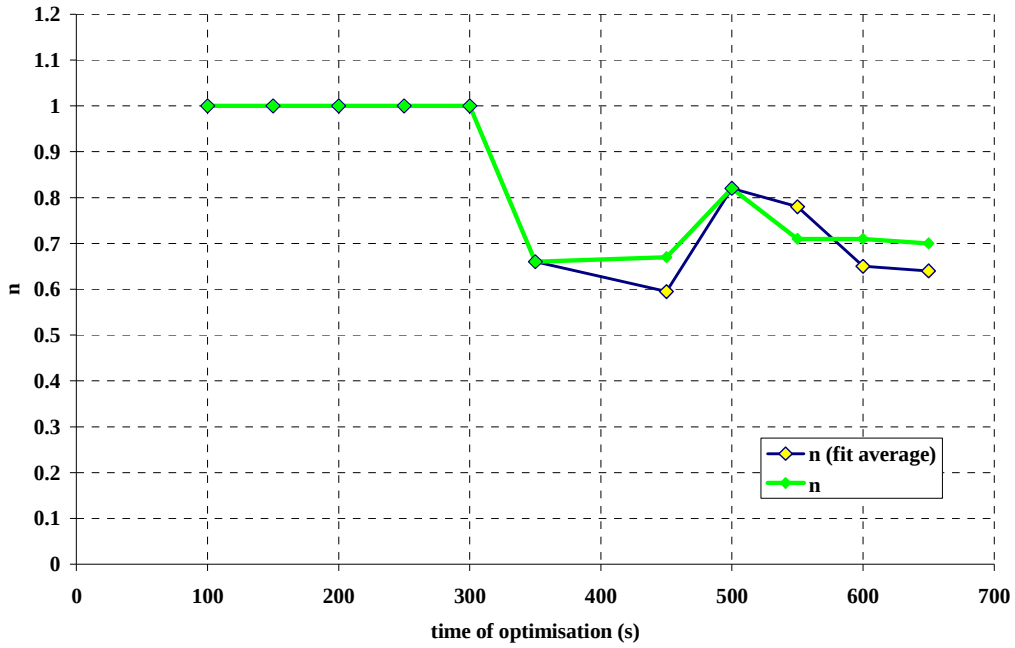

Figure 5.10 – *The plot demonstrates the similarity between the derived value of n and the average of the values derived from the curve fits shown in the previous figure (Figure 5.9).*

Figure 5.8 –shows an evolution of the n and c_2 parameters for a larger scale vertical upward flame spread experiment. Each data point on the chart corresponds to the result of an iteration of the entire process being described. From the first iteration which takes place using data up to 100s post ignition to the iteration comprising data to 300s post ignition, the flame is behaving linearly. The value of n is fixed automatically at 1.0 and c_2 is derived as the ratio of flame to pyrolysis length as per Equation 27. The outputs of the optimisations over this period converge. Post 300s the curve fit is used to describe the data and the brute force optimisation method described above is employed to evaluate the parameters. Once again the parameters can be seen to converge, almost immediately on a final value.

The resultant values of these constants, especially in the case of c_2, are sensitive to the quality of the fits from which the constants are optimised. If the fits do not adequately represent the data, the parameters derived from them will not represent the experiment. If the fits fluctuate significantly between iterations, so will the constants. The flame length data is numerous, and while it can be noisy, it generally provides a robust fit with a low level of fluctuation. The pyrolysis data by contrast is sparser and a single lagging reading by a badly positioned depth thermocouple can affect the shape of the fit more so than a single bad value of flame length data. Thus a fluctuating or non convergent c_2 and or n value output is likely to be the result of a fluctuating or non convergent fit to the pyrolysis length data.

The derivation of the curve fit shape described earlier involved the grouping of constants for ease of calculation to form an expression that was then integrated. The result was the complicated expression shown by Equation 26 that expressed t in terms of lp and some adjustable parameters. These adjustable parameters are the grouped constants and one of these values is n. Thus, each time a curve fit is produced a value for the n parameter is also produced. The three values of n (one produced by the brute force optimisation, one by the fit to the flame length data, and one by the fit to the pyrolysis length data) produced during the same experiment from which the values displayed in Figure 5.8 were drawn, are compared in Figure 5.9 –. The plot shows how the values obtained from the fits track the optimised value fairly closely. The average of the n values resulting from the fits can therefore represent a viable alternative method of deriving n. The average of the n values produced from the curve fits is compared to the optimised value in Figure 5.10.

5.3.3.3 Heat Flux and Constituent Parameters

The final unknown parameters that require optimisation in order to fully populate the model all constitute values pertaining to the heat flux from the flame to the unburned surface. Assessment of this heat flux is complex as it involves the resolution of the total flux to the surface into its constituent convective and radiative portions. While the definition of total heat flux to the surface as a single term might suffice if the aim of the work were simply to predict the spread rate in the future, it is necessary to have this distinction when considering the real life scenarios in which this process could be used. If the overall aim of the process is to better predict a fire growth which requires the accurate prediction of secondary ignition of surrounding items, then the correct proportions of heat transfer by conduction, convection and radiation to other items in the rooms is essential. The resolution of the heat flux into its constituent parts is achieved through the exploitation of knowledge of the dominant heat transfer mechanisms in the flame in its varying states (laminar and turbulent) of growth.

When the flame is laminar, the literature [17][59][71] tells us that convective transfer to the unburned surface ahead of the pyrolysis front is the dominant mechanism of heat transfer and the levels of radiative heat flux to the surface from the flame can be considered negligible in comparison. Indeed examination of the data from the thin skin calorimeters confirmed this as shown in Section 4.4.3.3. The initial iterations of the prediction process generally take place under laminar conditions with a small flame and as such represent the simplest condition with respect to heat flux. This can be exploited to obtain an accurate assessment of the contributions of the convective and radiative components of heat flux from the flame. In these early stages the total heat flux to the surface can be considered entirely as convective and the terms for incident radiation and re-radiation can be neglected. By eliminating these terms from the model, the total heat flux to the surface is expressed as: -

$$\dot{q}''_r = (c_1 k_g \rho_g c_p u_\infty / l_p)^{1/2} (T_f - T_p)$$

Having already established all other quantities in this expression and thus in the model, the only parameter remaining undefined is c_1. Being the only unknown value it can be solved for directly by rearranging the expression of the flame spread model (Equation 14).

In turbulent and transitioning regimes, the radiant heat flux to the surface will become significant and an accurate estimation of its magnitude and how it varies over the course of the experiments is required in order to make an accurate and complete prediction. As stated above, all other parameters in the model have been established by other means, thus the total heat flux to the surface can be solved for by rearranging Equation 11.

$$V_f = \frac{4c_2[\dot{q}''_s]^2 l_p}{\pi k_s \rho_s c_s (T_p - T_0)^2}$$

Equation 11

The total heat flux must then be broken down into its constituent parts. These are shown in Equation 5.

$$\dot{q}''_s = \dot{q}''_{conv} + \dot{q}''_{fr} + \dot{q}''_e - \dot{q}''_{rs}$$

Equation 5

In these experiments there are no significant external sources of heat flux so this term can be neglected. If the terms representing radiative heat flux are grouped to give a term for net radiative heat flux to the surface, Equation 5 can be reduced to: -

$$\dot{q}''_s = \dot{q}''_{conv} + \dot{q}''_{r,net}$$

Thus the only remaining obstacle to be overcome is the fact that $\dot{q}''_{r,net}$ must be derived from one equation with two unknowns. The solution to this problem is achieved by making the assumption that the value of c_1 remains more or less constant throughout the experiment. Having established the value of c_1 early in the process when the entire quantity of heat flux to the surface was convective, and having derived the other constituent parameters of the convective heat flux term by measurement or prior definition of the values, the magnitude of the convective heat flux throughout the remainder of the experiment is deemed to have been established. Thus the net radiative fraction of the total heat flux can be found by deducting the convective fraction from the total. This can be done with confidence of obtaining an good answer provided that the value of c_1 is accurate. Confidence that a representative value has been established for c_1 can be gained when the value of this parameter remains constant or converges in the initial iterations of the process during the laminar stages of the experiments.

Having derived the net radiative heat flux to the surface, the incident portion can be defined by the expression: -

$$\dot{q}''_{rf} = \dot{q}''_{r,net} - \dot{q}''_{rs}$$

The re-radiation term is expressed as: -

$$\dot{q}''_{rs} = \sigma\varepsilon(T_s^{\,4} - T_\infty^{\,4})$$

The surface temperature (T_s) is not directly measured, but is known to vary between T_p and T_0 where $T_0 \approx T_\infty$. Thus the radiant heat flux from the flame to the surface can be expressed as a range by the following expression: -

$$\dot{q}''_{r,net} - \sigma\varepsilon(T_p^{\,4} - T_\infty^{\,4}) \leq \dot{q}''_{rf} \leq \dot{q}''_{r,net}$$

Equation 31

This result hinges therefore on the assumption that c_1 remains constant for the duration of the experiment which must be justified. As discussed, the literature [17][59][71] suggests that while the flame is laminar it is dominated solely by convective flux. When the flame regime transitions to turbulence, the lower portion of the flame still maintains a laminar regime becoming turbulent higher up in the flame (Figure 5.11). This suggests that the dominant heat flux mechanism for a turbulent flame may vary throughout the height of the flame, being dominated by radiation where it is distinctly turbulent but maintaining a laminar convection dominated regime in the region immediately around the pyrolysis front. Toward the end of the experiments when the pyrolysis front is close to the top of the PMMA slab, the turbulent region is no longer contributing to the heating of the final portion of unburned PMMA and convection once again becomes the dominant heating mechanism. The laminar / turbulent nature of a large wall flame can be observed visually from images (Figure 5.11).

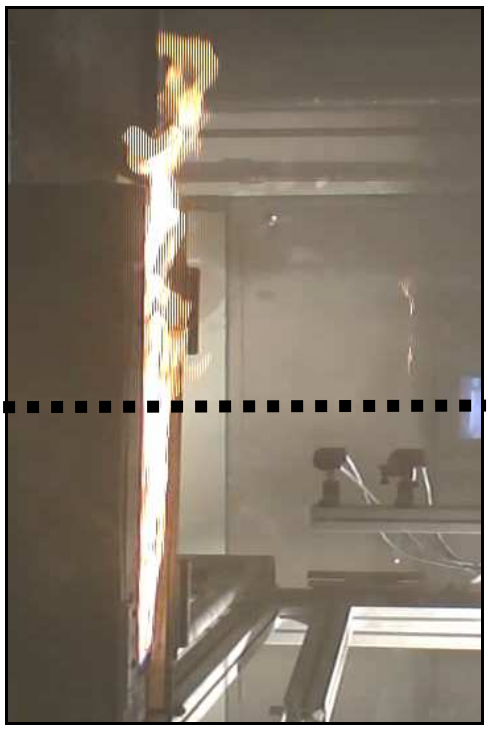

Figure 5.11 – *The image taken from a web camera and used to measure flame length shows the transient behaviour of the larger flame. A more laminar region exists at the bottom (below the line) becoming more turbulent with height (above the line) through the flame.*

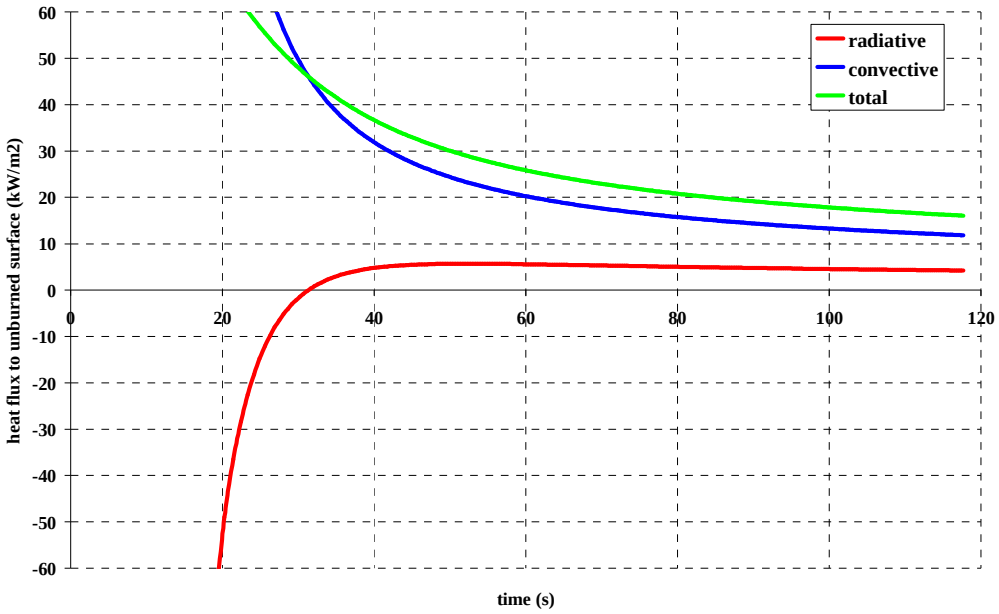

Figure 5.12 - *The plot shows the evolution of the total heat flux to the unburned surface (green line) at the final step of the optimisation process along with a comparison of the breakdown of the individual convective and net radiative components (red and blue lines) estimated by the programme.*

The assumption that the value of c_1 remains approximately constant throughout can be demonstrated by performing this methodology as if the flame remained laminar throughout the entire experiment. When the flame is laminar, the methodology assumes all heat flux to be convective and assumes the net radiation to the surface to be negligible. Thus, the original expression for total heat flux to the surface: -

$$\dot{q}''_s = \dot{q}''_{conv} + \dot{q}''_{fr} + \dot{q}''_e - \dot{q}''_{rs}$$

Can be expressed simply as: -

$$\dot{q}''_s = \dot{q}''_{conv}$$

And the flame spread model becomes: -

$$V_f = \frac{4c_2[(c_1 k_g \rho_g c_p u_\infty)^{1/2}(T_f - T_p)]^2}{\pi k_s \rho_s c_s (T_p - T_0)^2}$$

Equation 32

When this methodology is carried out with this alteration for a larger experiment which makes the transition to turbulence, the value obtained for c_1 follows the evolution shown in Figure 5.13.

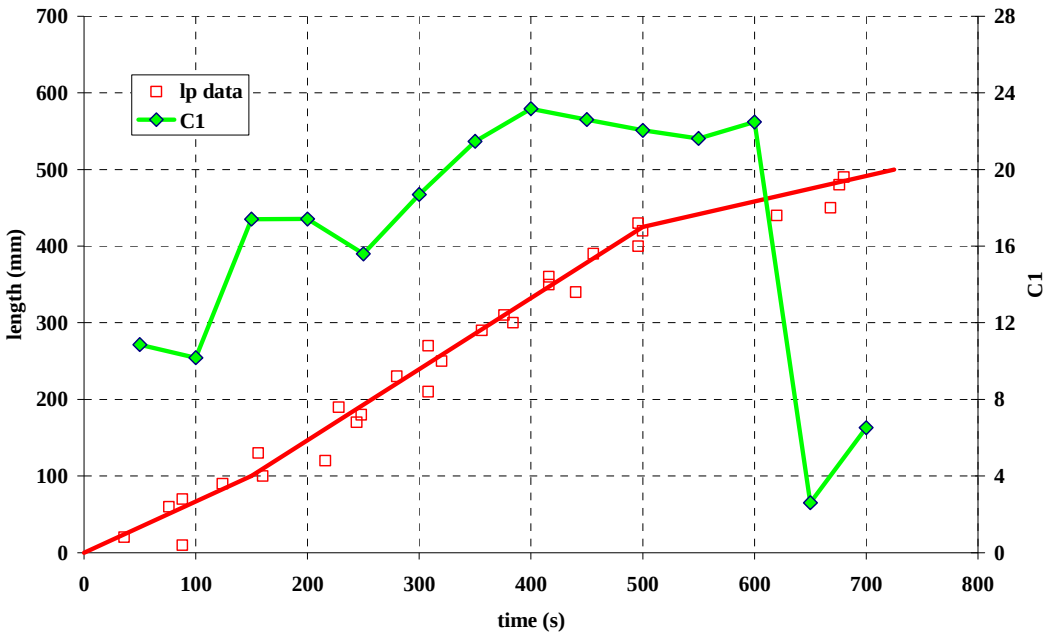

Figure 5.13 - *The plot shows the evolution of the c_1 parameter (right hand axis – green) when the model is forced to consider the flame as laminar. The pyrolysis length data (left hand axis - red) illustrates the growth of the flame over the same period of time for comparison.*

In the initial stages of the experiment the flame is laminar and thus the model described above in Equation 32 can be considered appropriate at this point in the experiment. By extension, the value of c_1 which is converging on a value of approximately 9 to 10, and which is obtained using this model can be considered reasonable. The flame then goes through a period of acceleration which corresponds to a turbulent regime. Throughout this period, the radiative heat flux from the turbulent flame accounts for a significant portion of the total heat flux. The total heat flux in this period must be greater than in the initial period characterised by laminar flaming as the flame is spreading faster. This is due to the extra radiative heat flux from the turbulent flame adjacent to the unburned surface. The model in Equation 32 therefore is no longer valid and the value of c_1 can be assumed to be incorrect. Near the end of the experiment when the pyrolysis front is nearing the end of the PMMA sample, the region of turbulent flaming is no longer adjacent to the little remaining unburned PMMA. At this point the spread rate decelerates. Figure 5.13 shows that the pyrolysis front nears the end of the 500mm PMMA slab at approximately 600s post ignition. Figure 5.14 shows the corresponding flame length data. The increased density of data points in this data shows the trends more clearly. At 600s the growth rate of the flame can be clearly seen to be decelerating. This deceleration is attributed to the loss of the radiative heat flux as the portion of the flame that it is associated with has moved beyond the top of the PMMA slab. The heating regime is now once again dominated by convection as the flaming in the heating region (l_h) is laminar in nature and the model in Equation 32 is valid once more. The corresponding c_1 data is now valid again and is seen to be converging on its original value.

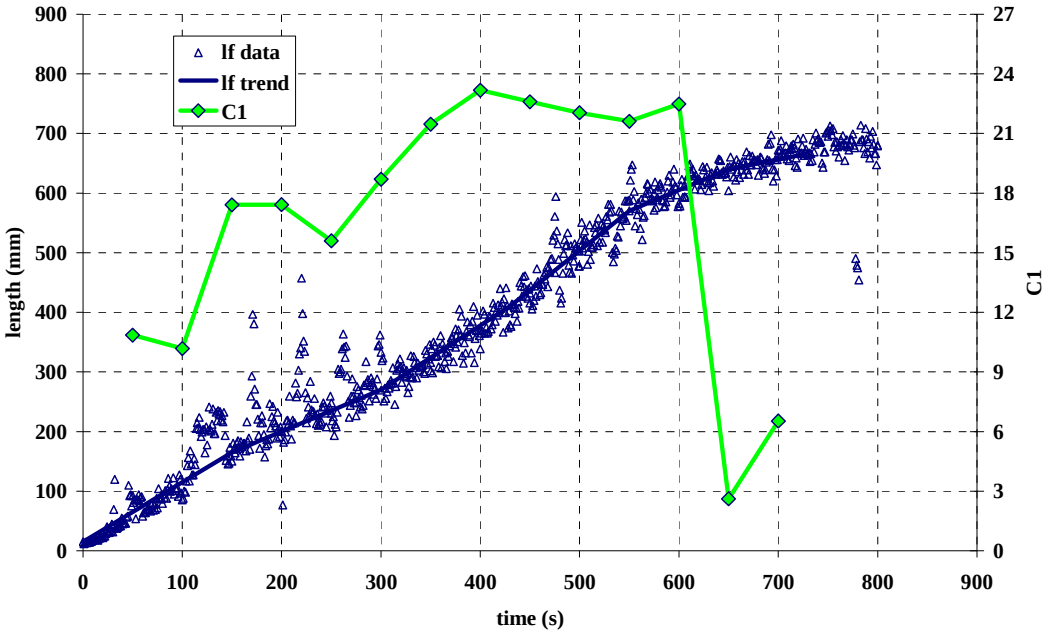

Figure 5.14 - *The plot shows the same c_1 trend as in Figure 5.13 this time compared to the flame length data. The greater density of this data demonstrates more clearly the pattern of the growth corresponding to the behaviour of c_1.*

In the two regions, at the beginning and end of the experiment, where the model is valid and it is believed that the heating is dominated by convection alone, the value of c_1 appears to converge on a similar value suggesting that it remains reasonably constant throughout the experiment. Given a similar analysis, results from other experiments also show a similar result.

5.4 Prediction and Convergence

Once the data is collected and correlated, the unknown parameters established and all parameters of the model established, the spread rate is then forecast forward as a function of the pyrolysis length to establish when the pyrolysis front will reach the end of the slab, and what the size of the flame and level of radiation from it will be. In the case of a prediction made during the laminar stages where the net radiant heat flux term is discarded, the spread rate model becomes independent of pyrolysis length and predicts a continuous constant value as depicted in Figure 5.15. As more data becomes available from the sensors, the accuracy of the prediction and data fits can be appraised and if necessary re-evaluated. With each re-evaluation the interpretation of the spread rate from the start of the experiment or the last change of conditions becomes more accurate and convergent. The same convergence is seen for the curve fits (Figure 5.16) although in this case the predictions are no longer independent of the pyrolysis length.

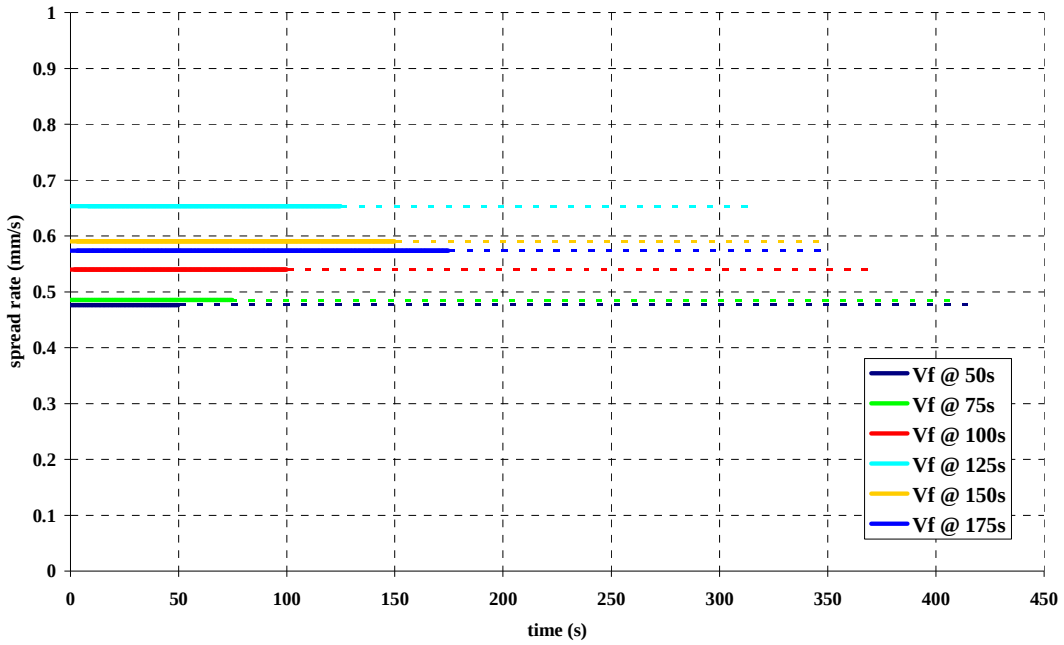

Figure 5.15 – *The solid lines in the plot represent the spread rate from the start of the experiment to the time of prediction give in the legend. The dashed line represents the forecast forward in time based on the data gathered and trends seen up to the present time.*

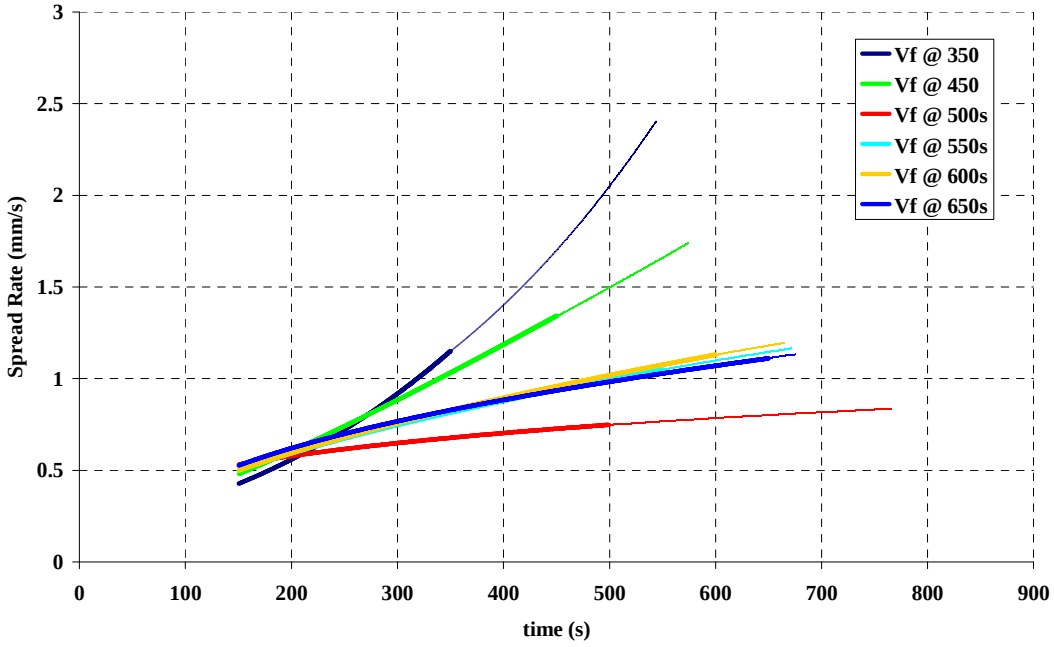

Figure 5.16 - *The solid lines in the plot represent the spread rate from the start of the experiment to the time of prediction given in the legend. The dashed line represents the forecast forward in time based on the data gathered and trends seen up to the present time.*

5.5 Worked Example

To demonstrate the process more clearly, an example is made using Experiment 1. This experiment is an imitation of the benchmark experiment, with a 200mm long, 40mm thick, PMMA slab positioned with the exposed face vertically orientated.

5.5.1 First Iteration

The raw sensor data is collected, transformed into an appropriate form and collated chronologically at 60 seconds post ignition. The flame length data (Figure 5.17) over the first 60s shows a reasonably steady linear growth. The pyrolysis length data (also Figure 5.17) at this stage contains just two readings. The PIV ambient velocity measurement (u_∞) contains only one reading and this is taken as representative of the entire time step. The gas phase temperature data shown in Figure 5.18 shows the readings for all five of the gas phase thermocouples. The programme only considers readings from thermocouples that are currently below the level of the top of the flame (shown in colour). All other readings (shown in grey) are discarded. The value of flame temperature is taken as the maximum single value of those in consideration i.e. taken within the flame. At this stage the thin skin calorimeters do not show any significant incident radiant heat flux.

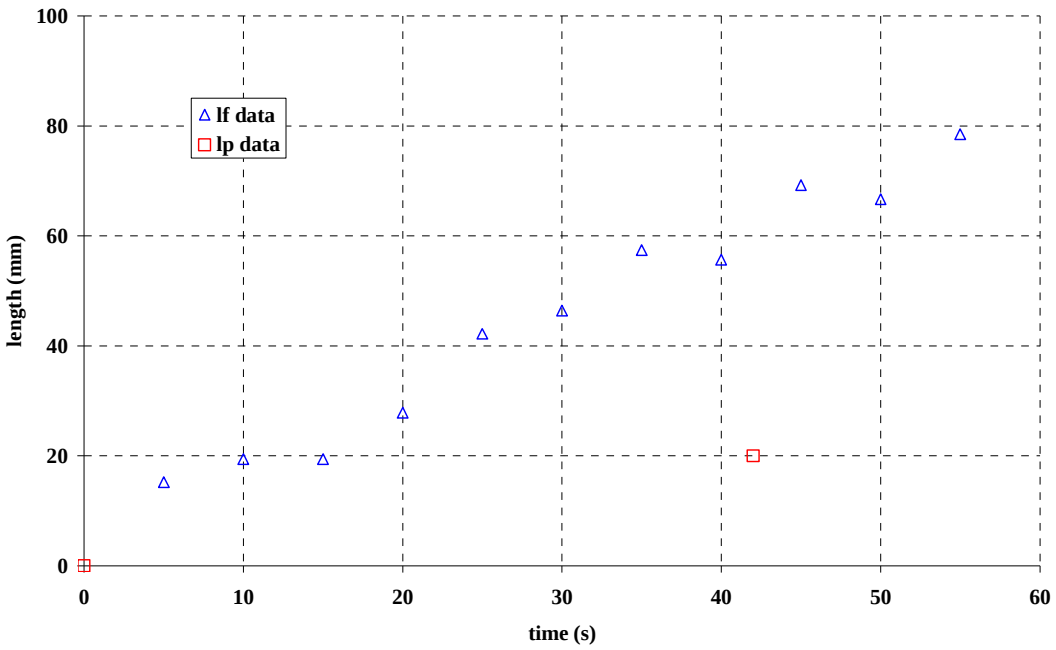

Figure 5.17 – *The plot shows the pyrolysis (lp) and flame (lf) length data collected over the first 60 seconds of the experiment.*

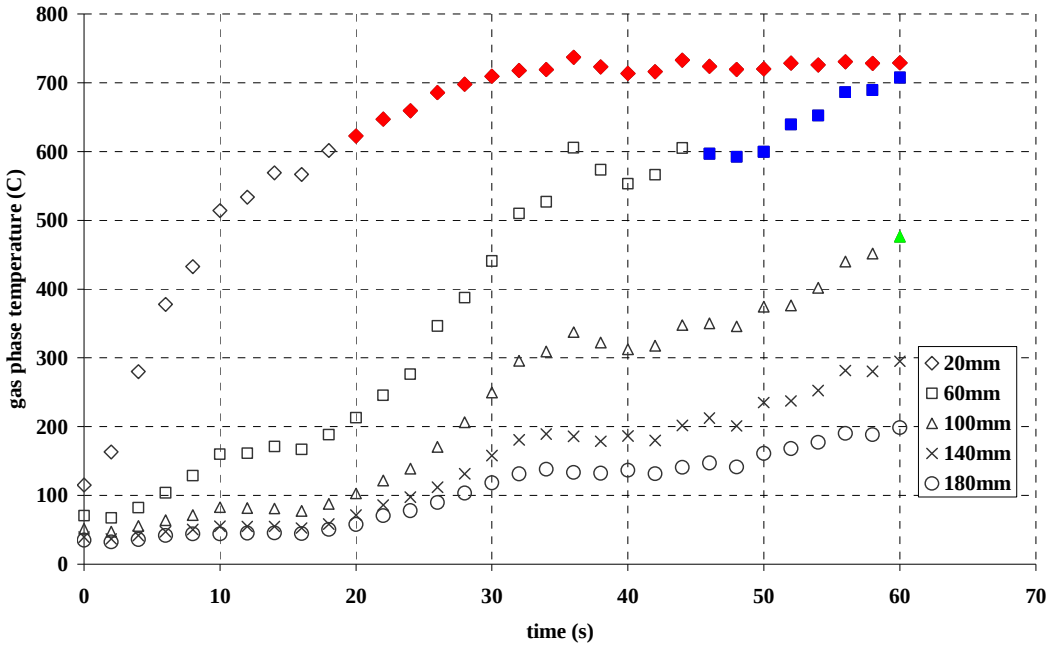

Figure 5.18 - *The plot shows the gas temperature measurements over the first 60s. The readings are only considered for the measurement once the sensors themselves are within the flame. The height of each thermocouple above the ignition location is shown in the legend.*

With the data correlated and displayed, a decision must be made as to whether the flame is laminar or turbulent so that appropriate fits and suitable optimisation techniques can be applied. Inspection of the flame length data indicates a steady linear growth. The flame is also still less than 200mm in length and the level of incident radiant flux is still negligible so the flame is deemed to still be laminar and a linear fit is applied to the length scale data shown in Figure 5.19. The future data, unavailable to the model at the time of prediction, is also shown in this plot to demonstrate the overall accuracy of the fits at this stage given the data available to them. From these fits, the value of the c_2 parameter can be derived from the ratio of the two according to Equation 22 and shown in Figure 5.20. The value converges as the influence of the initial conditions reduces and the final value is taken as a constant to represent the period since the beginning of the experiment. With the trend of the pyrolysis front evolution established, the spread rate over the initial 60s of the experiment can be estimated from the gradient of this line and is shown in Figure 5.21 as a continuous line.

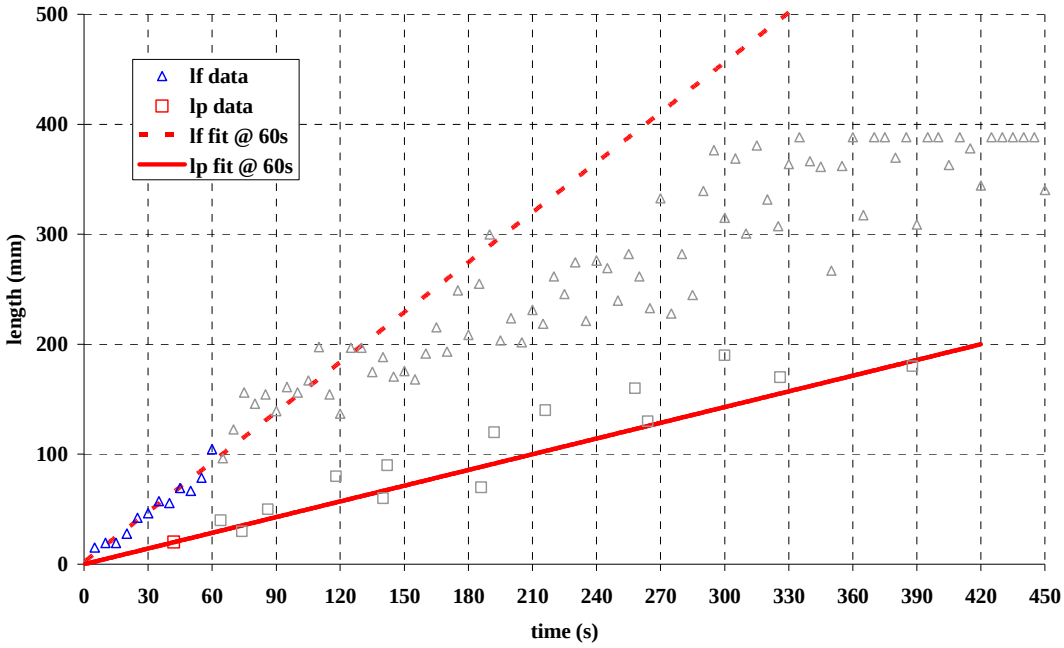

Figure 5.19 – *The flame is deemed to be laminar over the first 60 seconds so a linear fit is applied to the length scale data. The data available to the model is shown in colour on the plot with future data ghosted. The dotted line represents the fit to the flame length data and the continuous line the fit to the pyrolysis data.*

The final set of optimisations concern the heat flux to the unburned surface. As the flame has been deemed fully laminar and the thin skin calorimeters indicate there is no significant radiant heat flux from the flame, only the convective component is considered which leaves c_1 as the final unknown of all parameters needed for the flame spread model. With all other parameters established, the flame spread model is solved for this value. With the evolution of all time variant parameters and all constants established, the spread rate is forecast forward in time. In the case of this first iteration the spread is independent of the time variant values and is simply forecast as a constant in time (Figure 5.21).

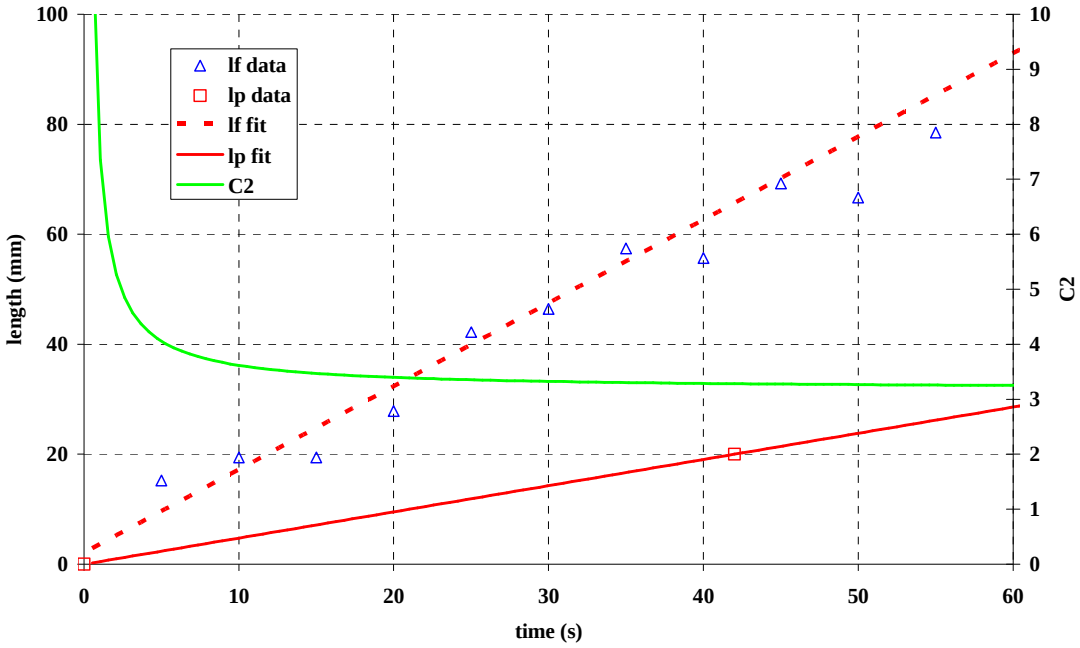

Figure 5.20 – *The plot shows the c_2 parameter (in green) derived from the ratio of flame (dotted red) to pyrolysis (continuous red) length. In time the value converges as the effects of the initial conditions of the plots becomes less influential.*

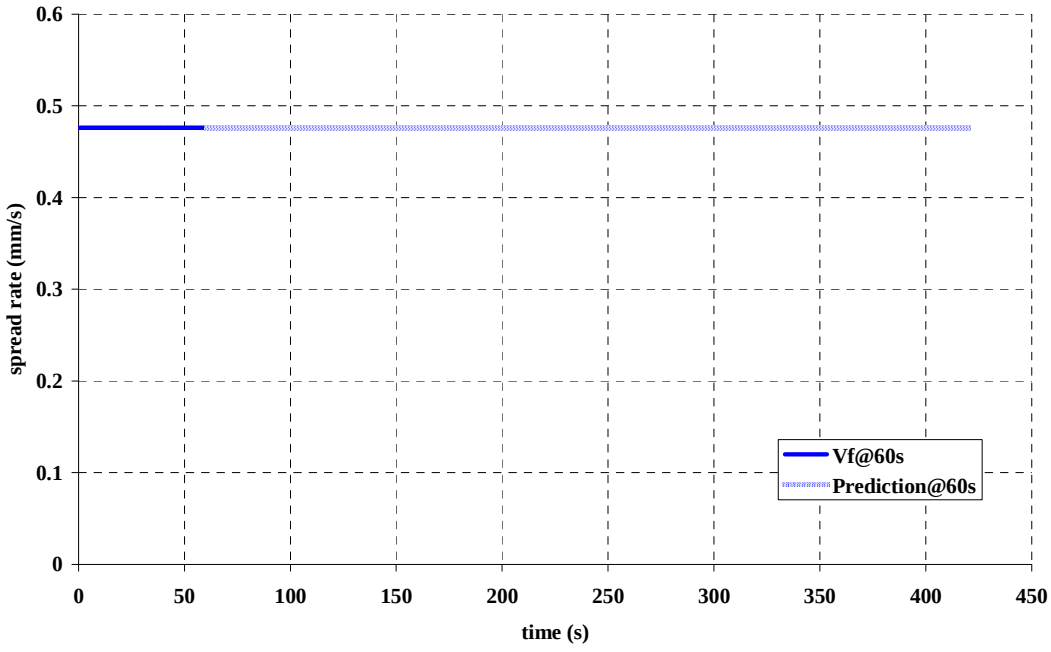

Figure 5.21 – *The plot shows the spread rate estimated from the initial 60s of data and the prediction resulting from it.*

5.5.2 Condition Change and Transition to Turbulence

At the beginning of each iteration, the levels of radiant heat flux measured by the thin skin calorimeters are compared to the convective heat flux derived by the parameters optimised in the previous step. As the flux reading from the calorimeters is averaged from the meters believed to be between the flame tip and pyrolysis front and thus requires knowledge of the position of each over the time step, the fits to the length scales from the previous step are used to provide the radiative flux data. Figure 5.22 shows this comparison at the start of the third iteration at 120s post ignition. The levels of radiative flux have become comparable with the convective flux, and thus can no longer be considered negligible.

Inspection of the evolution of the c_1 parameter at each iteration up to this stage shows that it has remained steady which gives confidence that its value is a good representation of the experiment. Its most recent value is then fixed for the remainder of the process to avoid over-estimation in subsequent iterations as the heat flux can no longer be attributed solely to the convective flux.

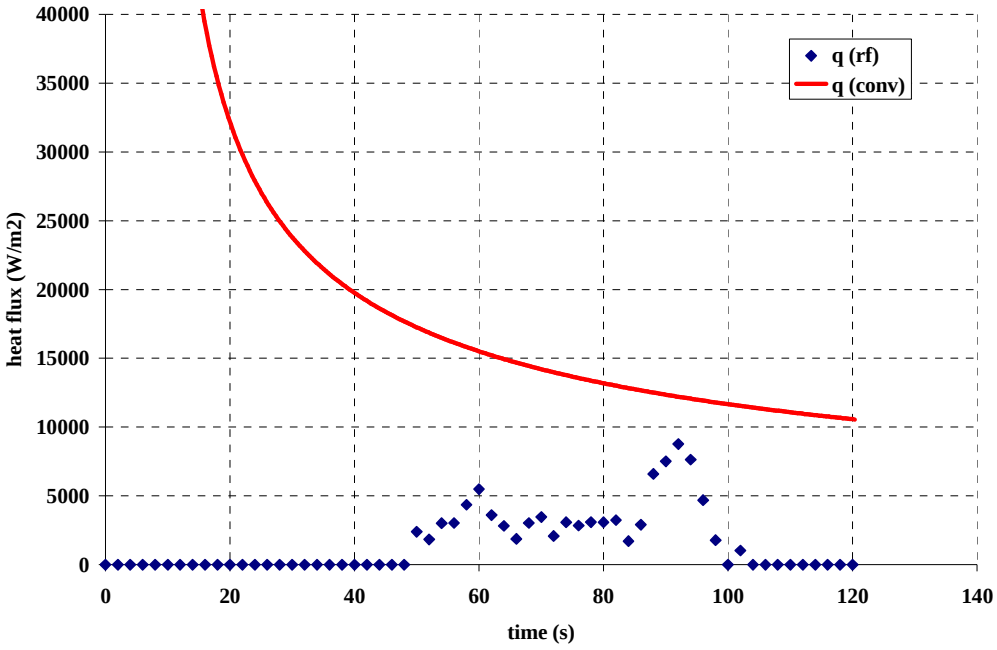

Figure 5.22 – *At the third iteration the level of incident radiant heat flux becomes comparable with the convective flux established with the optimised parameters from the previous iteration. This indicates that the flame has begun to transition to turbulence.*

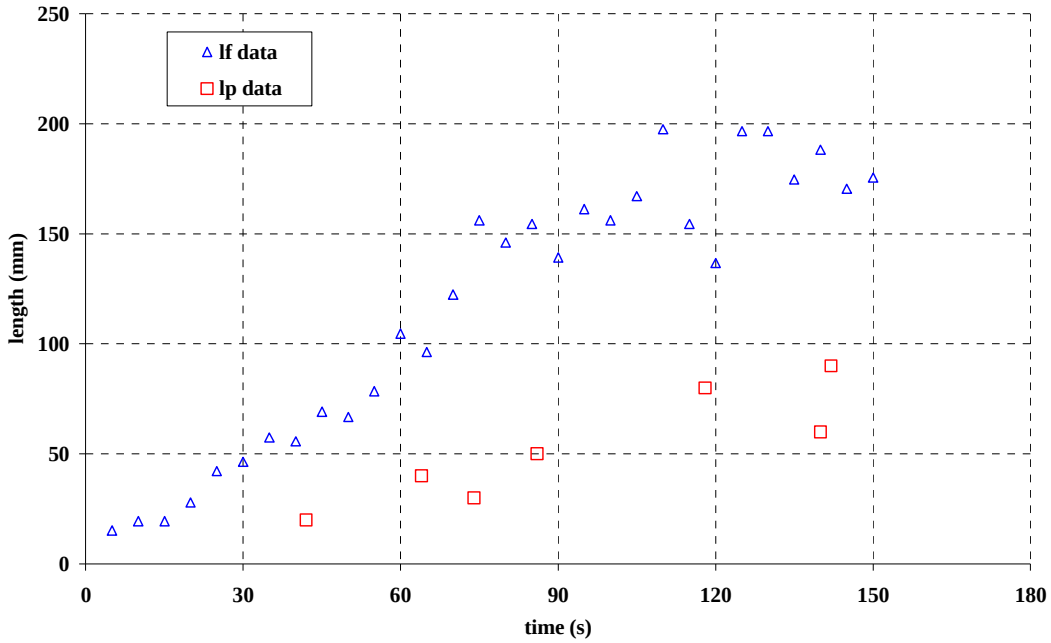

Figure 5.23 – *Inspection of the flame length data at the fourth iteration indicates a change of growth rate beginning approximately at 75 seconds post ignition.*

At the beginning of the fourth iteration, a trend change in growth of the flame becomes apparent (Figure 5.23). Despite the change in growth rate appearing to originate at approximately 75s post ignition, the trend is only obvious given data to 150s. With the flame approaching 200mm and levels of radiant flux increasing, a transition to turbulence is deemed to have begun and data from before the change corresponding to the strictly laminar phase is discarded as not representative of the current regime. The remaining data highlighted in Figure 5.24 is taken forward to form new optimisations based on the data thought to represent the current flame and spread conditions. Initially the data appears linear with the resultant fits shown in Figure 5.25. As more data is accrued the flame length data indicates that the flame is accelerating and from this point onwards, the derived curve fit is applied (Figure 5.26). With a high data density, the fit to the flame lengths converges quickly while the fit to the sparser pyrolysis length data takes longer (Figure 5.27).

With the fit regime now using the curve form, the method of c_2 optimisation must be altered and the n parameter included with it as described in Section 5.3.2.3. With the upper and lower bounds of n, and the lower bound of c_2 prescribed, the upper bound of c_2 is found by maximising its value using an appropriate form of Equation 10 with the maximum value of l_f and minimum value of l_p taken from the fit results and the lower bound value of n. An equally spaced range of values of c_2 and n are established between their respective bounds and every combination of the two is applied to the latest pyrolysis length fit. The combination of the parameters that produces the best match to the flame length fit is selected.

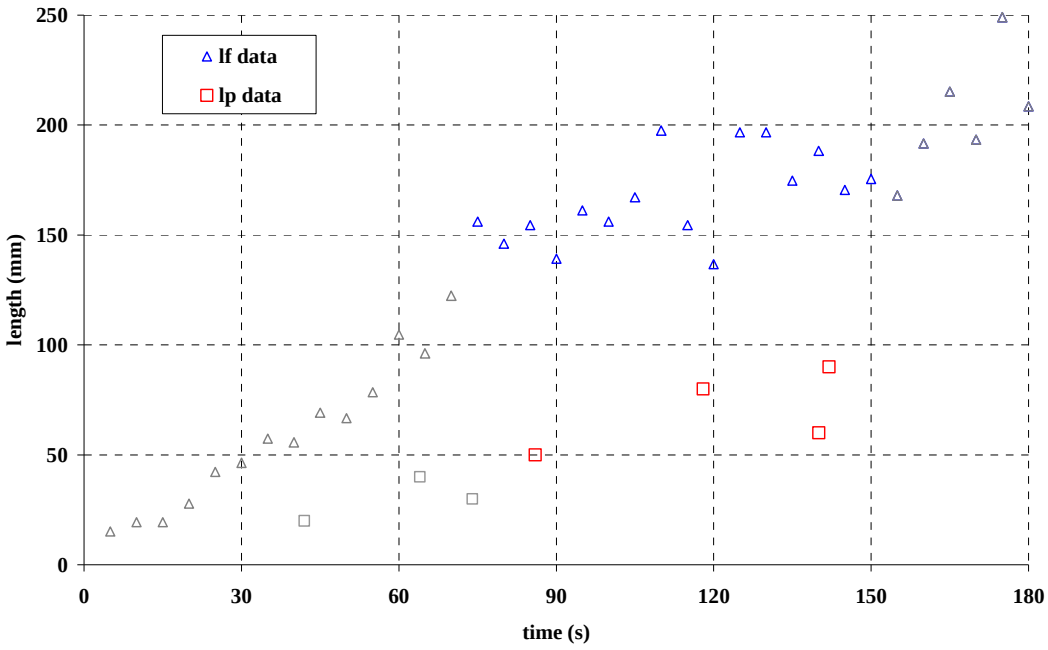

Figure 5.24 – *A decision is made at 150s post ignition that a condition change occurred approximately 75s post ignition. Data from before this time is discarded and only current data (in blue and red) is used for the next set of fits and optimisations.*

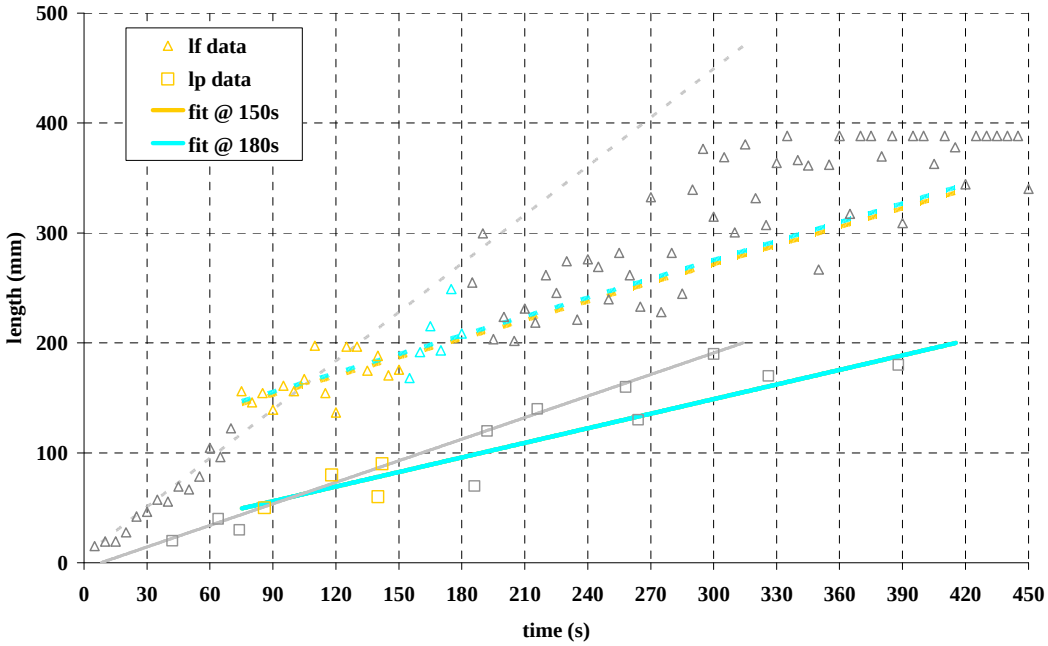

Figure 5.25 – *The plot shows length data fits for the first two iterations following the detection of the change of conditions in comparison to the last fit prior to it. The coloured data represents the information available to the programme when making the new fits.*

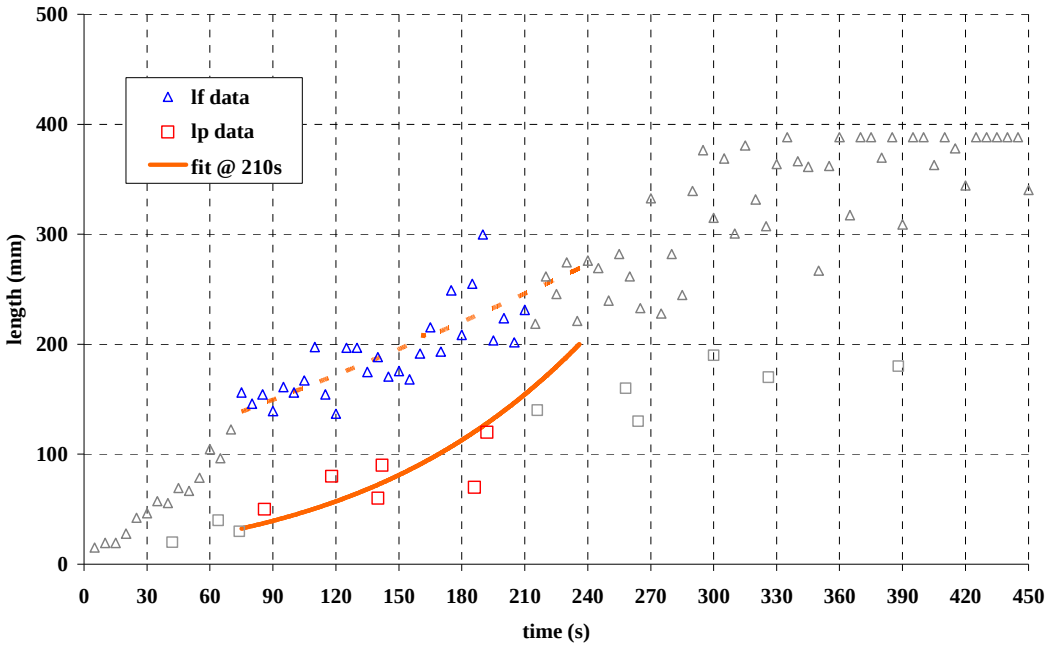

Figure 5.26 – *The relevant flame length data, post regime change, begins to show signs of acceleration prompting a change to a curve fit.*

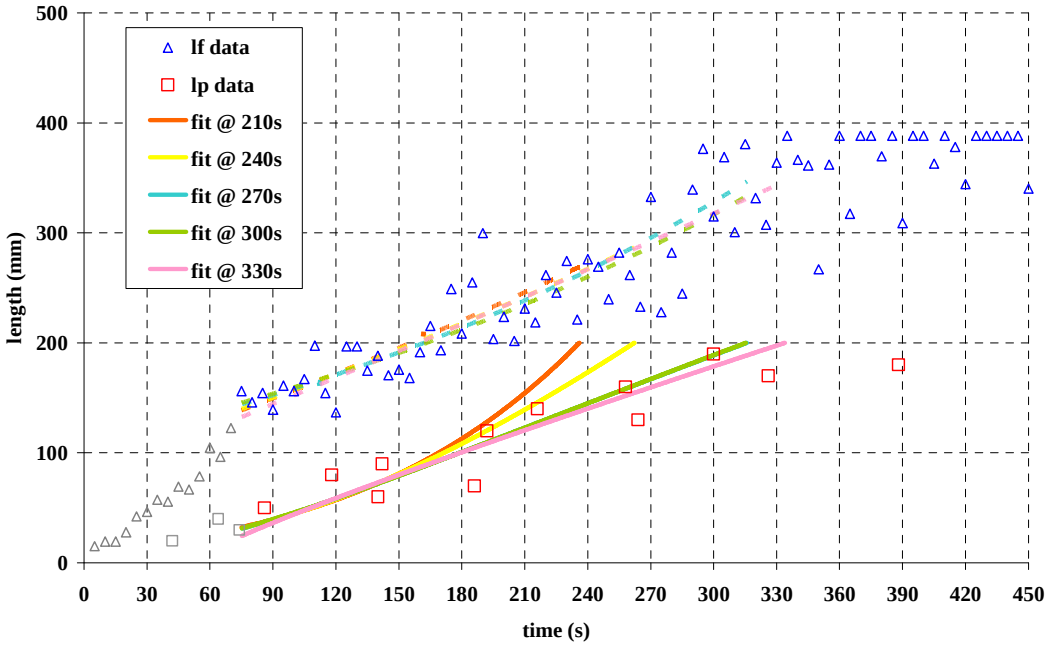

Figure 5.27 – *The plot demonstrates the evolution of curve fits applied in the subsequent steps following the perceived change from linear growth. With a high density of data points the fit to the flame length data converges almost immediately whereas the fit to the pyrolysis length data takes longer due to its sparse nature.*

5.5.3 Reassessment and Convergence

As more data becomes available to the programme this process can be repeated to check the accuracy of the fits, optimisations and prediction. If the output of the previous loop is found to be outside permissible levels of accuracy, it is replaced by the output of the latest loop. The data is also checked for indications that the flame has changed in nature i.e. from laminar to turbulent, or that the environmental conditions have changed in a way that is effecting the spread rate or characteristics of the flame in such a way that necessitates the re-evaluation of parameters pertaining to the flame such as the heat flux from it and expected length etc. At each iteration, providing there has not been a major change in conditions, the optimised parameters and fits should converge if the physical characteristics of the experiment are being correctly measured and representative fits applied.

5.5.3.1 Length Scale Fits and Related Parameters

Examination of the evolution of the n and c_2 parameters in Figure 5.28 demonstrates the changes to each parameter as the flame transitions form laminar to turbulent and the style of data fit changes accordingly. During the initial phase of linear fits, n is automatically set at n=1 but is subsequently evaluated upon the change to curve fitting where it converges quickly on a value of approximately 0.68 which is in line with the lower end of the conventionally accepted range given (and referenced) in Section 2.1.4. The c_2 parameter is also seen to converge rapidly at each stage of the process. It remains constant throughout the early laminar stages and quickly re-converges following removal of data from the laminar phase. Once the fit type becomes curved it again converges quickly.

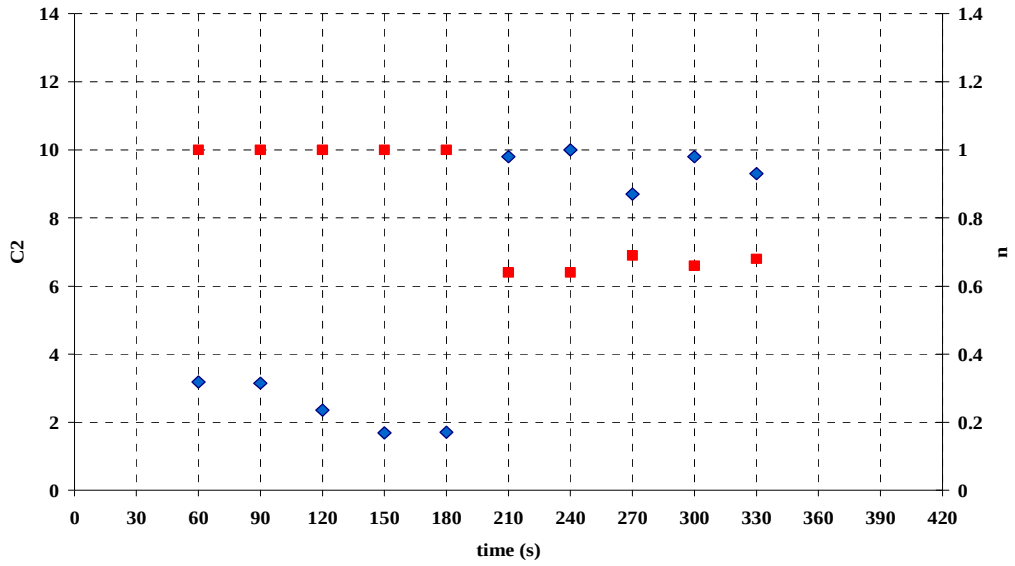

Figure 5.28 – *The plot shows the evolutions of the n and c_2 parameters at each stage of the iteration process. Both parameters are seen to change and re-converge following the change from linear to curve fitted data as the flame began to accelerate.*

5.5.3.2 Heat Flux to the Unburned Surface and Related Parameters

The measured and optimised parameters related to the heat flux segment of the equation all show good levels of convergence. The ambient velocity (u_∞) measurement shown in Figure 5.29 is approximately constant throughout the entire experiment. The flame temperature (T_f) (Figure 5.29) also varies little and approaches a plateau reasonably quickly. With c_1 fixed in the early laminar stages of the experiment the estimated level of convective flux to the surface can be predicted accurately as a function of the pyrolysis length from the early stages of the experiment.

The first estimate of the net radiant heat flux occurs in the next iteration after the c_1 parameter has been fixed, when the thin skin calorimeter measurements indicate that the incident radiant heat flux has become significant. As the experiment progresses the optimised value of net radiant heat flux at the PMMA surface ($q_{fr} - q_{rr}$) converges on a value close to zero shown in Figure 5.30. This is expected as the experiment is small and the most turbulent areas of the flame are generally above the top of the PMMA slab by the time they occur. Also the curvature in the flame spread data that indicated acceleration was slight.

As a confirmation, the same process outlined in Section 5.3.3.3 where the process considers the heat flux solely as convective was carried out resulting in the alternative c_1 evolution shown in Figure 5.31. If the radiative heat flux is more or less negligible throughout the experiment then the value of c_1 and the subsequently derived convective flux should be more less equal for both methods. Inspection of Figure 5.31 shows that the values of c_1 remain reasonably similar. When the maximum difference in c_1 values was selected and convective fluxes calculated from those values were plotted (also Figure 5.31). There was very little difference between the two indicating that the level of radiant flux would indeed have been small.

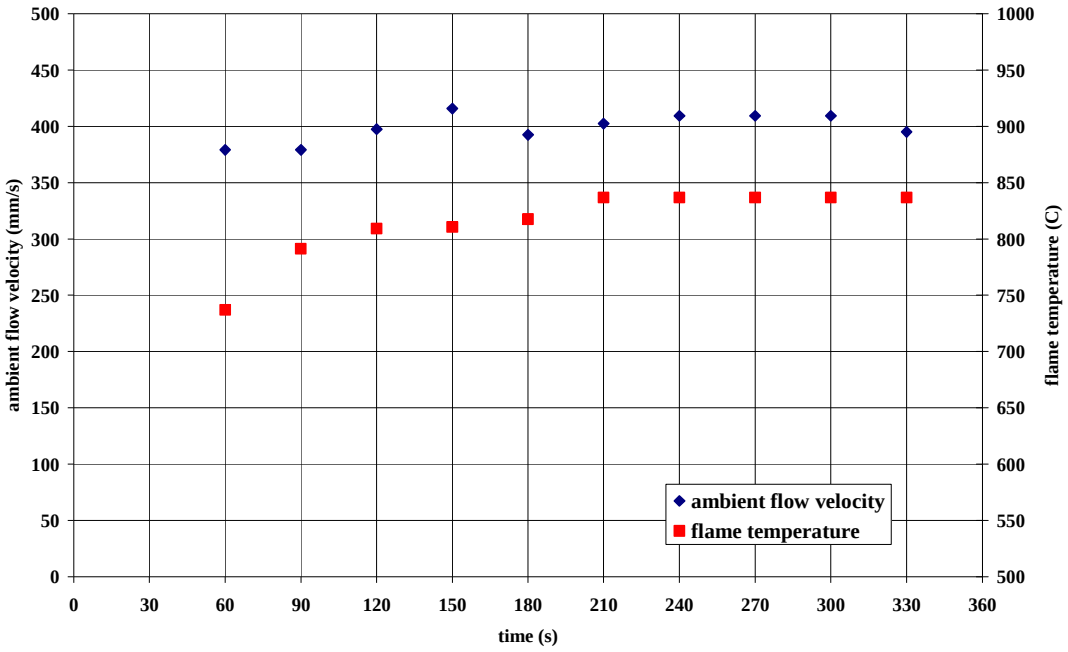

Figure 5.29 – *The plot shows the evolution of measurements of ambient air velocity (u_∞) and flame temperature (T_f) at each iteration. Both remain relatively constant over the whole process.*

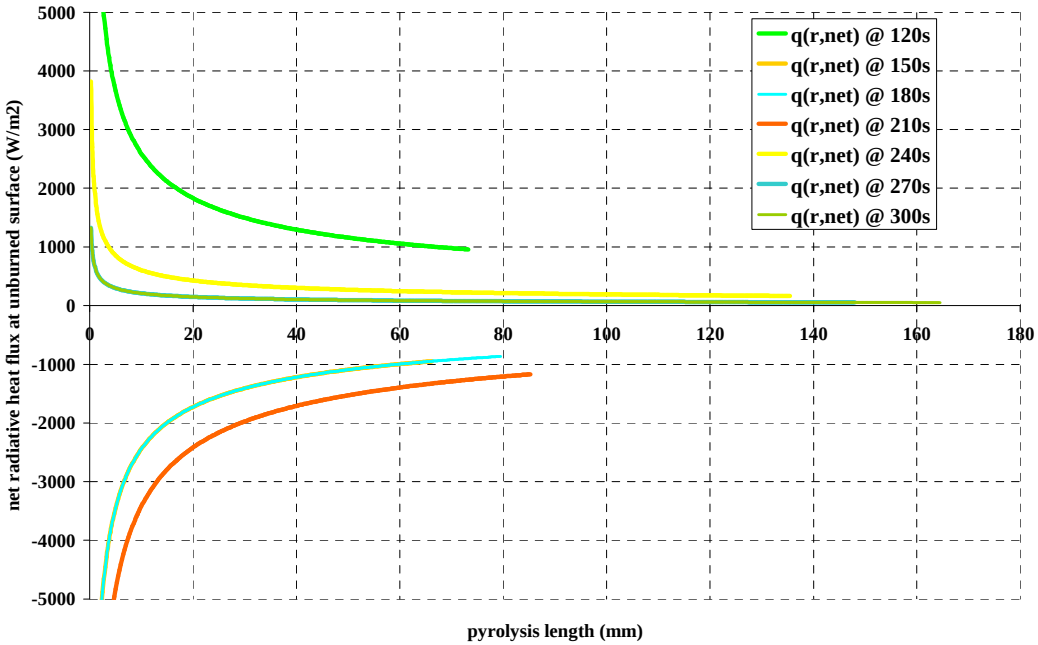

Figure 5.30 – *The plot shows the net radiant heat flux to the flame ($q_{fr} - q_{rr}$) as a function of the pyrolysis length as estimated by the programme at each iteration of the methodology. Prior to the first estimate at 120s, this element of the heat flux was estimated to be negligible and the flame completely laminar.*

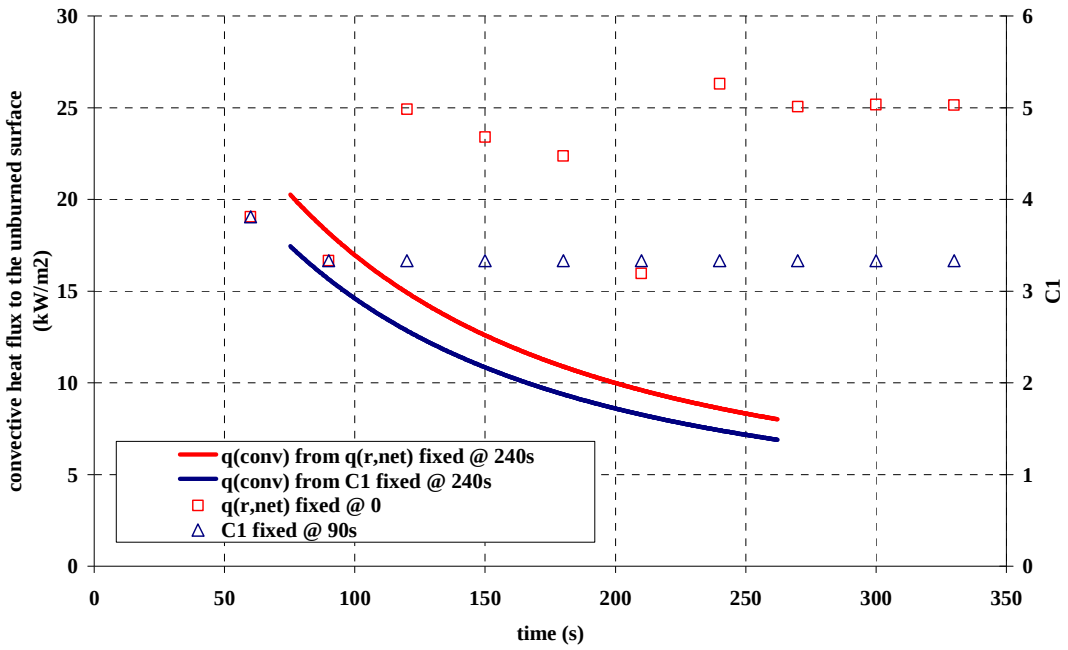

Figure 5.31 – *The plot shows the c_1 evolution when the convective heat flux is evaluated early in the experiment and fixed, in comparison with the value when convection is forced to represent the net heat flux to the unburned surface. The convective heat flux plots produced by the maximum difference between the two at 240s are plotted for comparison.*

5.5.3.3 Spread Rate, Predictions and Experimental End Time

The convergence of the spread rate approximations and experimental end times is essentially a product of the convergence of the pyrolysis length fit. The post condition change spread rates and predictions are shown in Figure 5.32 and show convergence at the same rate and in the same order as the pyrolysis length fits as do the predicted experimental end time shown in Figure 5.33. An accurate answer is obtained at 270s and remains virtually unchanged in subsequent predictions.

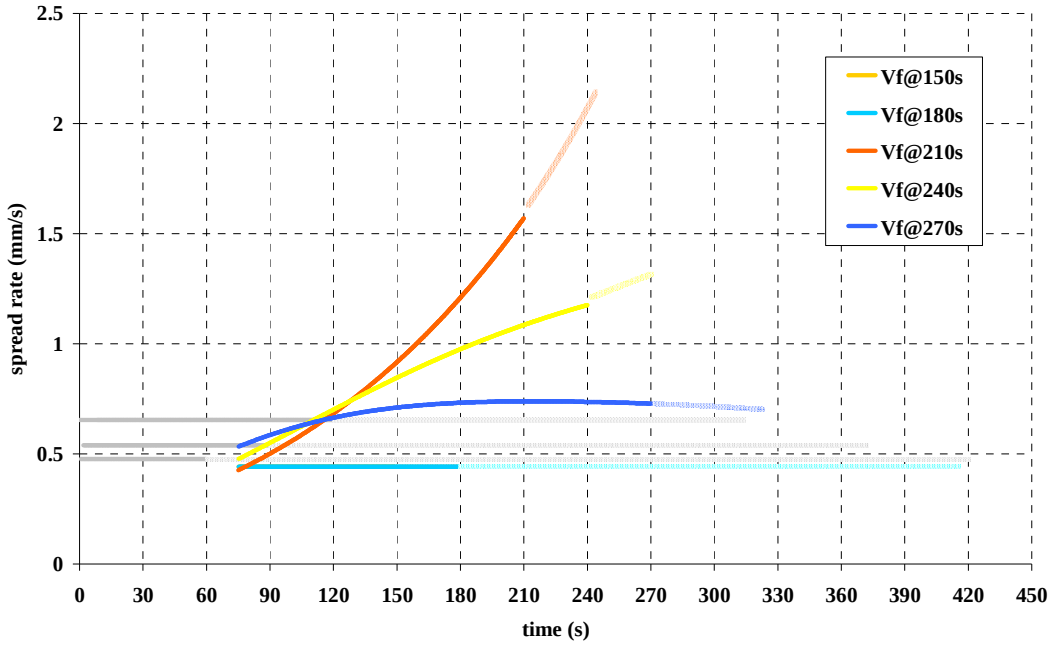

Figure 5.32 – *The plot shows the evolution of the spread rates (V_f) and predictions post condition change. There is a clear convergence of the spread rates derived from the curve fit and of the predictions made from them. Predictions pre condition change are displayed ghosted for comparison.*

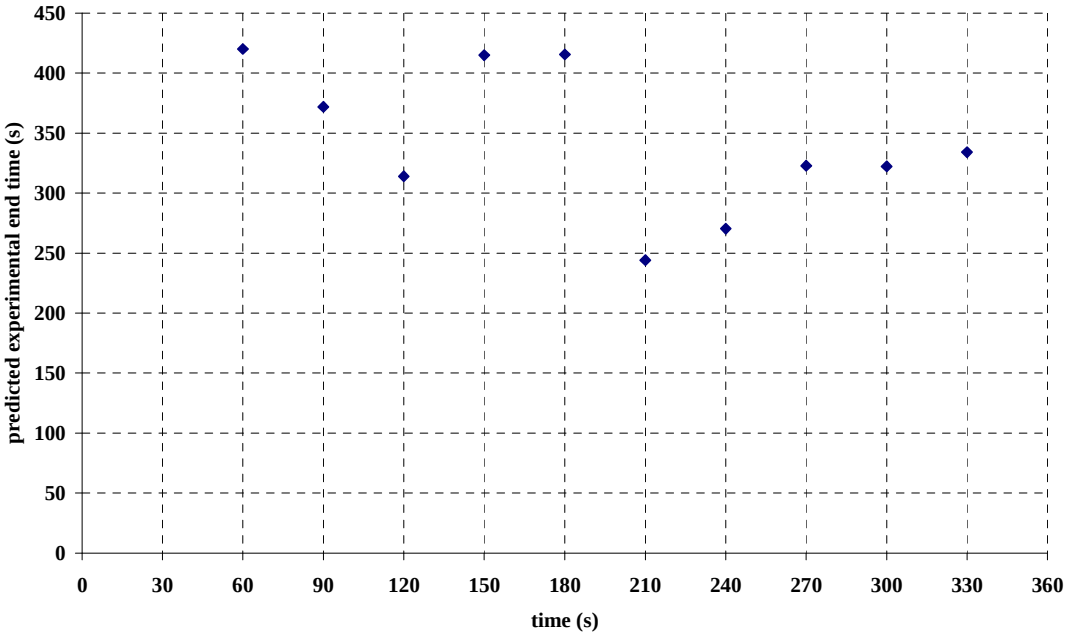

Figure 5.33 – *The plot shows the expected time that pyrolysis front will reach the top of the vertical slab plotted against the time of the prediction. This result is entirely dependent on the quality of the fit to the pyrolysis length data.*

5.6 Summary

A comprehensive methodology has been developed that makes robust rapid predictions of flame spread by combining sensor data and an analytical physical model from the literature. The methodology has been developed and tested with the data from the benchmark style experiments. For these experiments, scenario specific parameters describing the flame were seen to converge rapidly.

It is believed that the chosen model and methods will apply equally well to the other laboratory experiments that have been performed (described in Section 4.1). The versatility of the model means it should be capable of fully encapsulating all of the expected conditions present within these experiments and the methodology should be capable of making accurate spread rate predictions and determining unknown values through the simple optimisation techniques devised.

The methodology has been developed with the ethos of the FireGrid project in mind. It is entirely possible that an automated system based on this methodology could be developed and run in conjunction with the laboratory experiments to produce an accurate and crucially live super real time prediction of an upward flame spread experiment. The next stage in the development of this methodology will be to test its robustness through the application to other increasingly more complex experiments.

6 Application of Methodology

Now that the methodology has been developed linking the model described in Chapter 3 to the measurement techniques described in Chapter 4, the methodology needs to be tested in order to assess how versatile it is and to what range of scenarios it can reasonably be applied without over-extending its capabilities. This is important to prevent over-confidence and future misuse beyond its current capabilities and to assess where future work is required both in furthering its particular range of application and accuracy, and with regard to the overall goal of the project to which this work is linked which is the development of a tool to aid fire fighters. It may be the case that the sensing techniques and optimisation methods that have been developed are heavily tuned to the benchmark experiments on which they were developed and can not be extended further. The other extreme is that the model and sensing techniques are versatile enough to be applied to any surface in any complex compartment fire scenario such as that of Dalmarnock Fire Test One. An attempt has been made to leave the methodology as flexible as possible (within the realm of concurrent flow flame spread) and not to tune it too finely to processes observed in the initial experiments. An example of this are the heat flux terms in the model which were deliberately left in a configuration that could be applied to all concurrent flow flame spread, rather than being derived further to describe natural convection flame spread even though this is generally the case in the experiments performed in this work. It is hoped therefore that the model will be able to operate in most if not all concurrent flow flame spread scenarios. The experimental scenarios carried out to provide data on which to test the methodology are described in detail in Section 4.1. They include a reduction in the restrictions placed on the flow around the flame by the baffles, tilting the PMMA sample over which the flame spread takes place, lengthening the sample to encourage the onset of turbulent flaming and complicating the environmental conditions around the experiment.

6.1 Unrestricted Air Flow

The first test of the robustness of the methodology was to remove the baffles that were part of the initial experiments on which the methodology was formed. These baffles, based on the design of the benchmark experiment [29], were intended to maintain a 2D airflow at the surface. A similar technique was used by other authors [59] for larger turbulent experiments. Other than the removal of the baffles, the setup was as per the benchmark experiments (as described in Section 4.1.2) with an identical PMMA sample. Figure 6.1 shows the convergence of the c_1 parameter for this experiment. The parameter, initially appearing to converge on what is eventually the final value, deviates in the 3rd and 4th iterations. The timing of this deviation appears to correspond to the slowing in growth rate of the flame as it transitions from a weak and very laminar flame, to a more luminous and substantial flame. This trend, shown in Figure 6.2, is seen in all of the vertically inclined experiments and occurs over a short period with flame lengths typically within the range of 100mm to 250mm and corresponds to the start of a transition towards a turbulent flame regime. The growth rate in the flame length slows and is typically characterised by a period

of noisy data, after which the data appears to settle. The growth before and after is usually linear, growing more slowly after the transition.

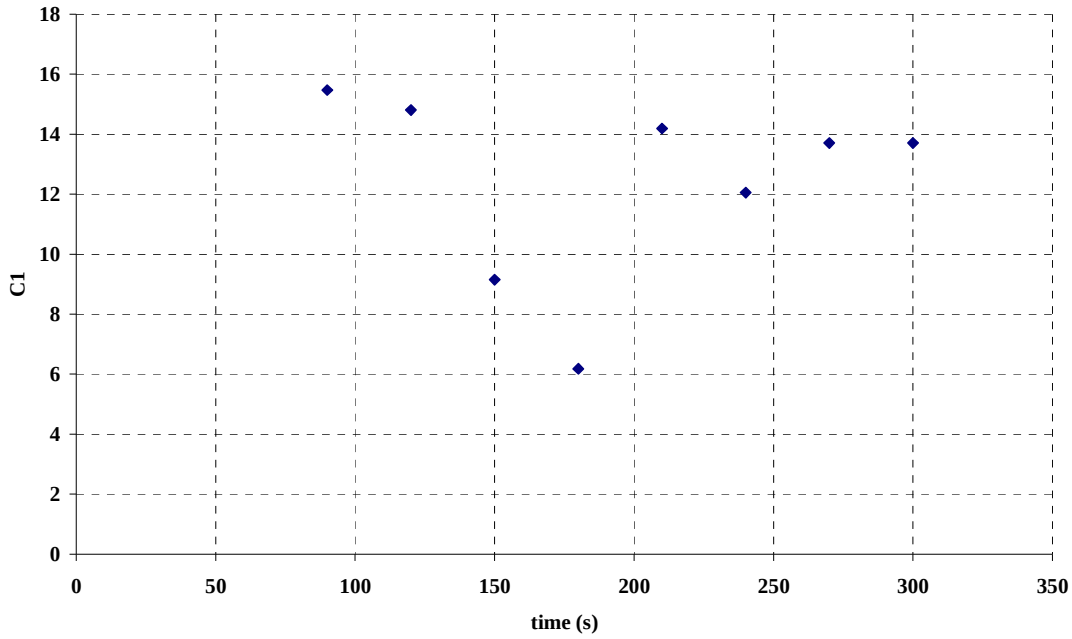

Figure 6.1 - *The plot shows the c_1 values derived for the initial baffle-less experiment. As the flame changes from very laminar to a transition phase the optimised value of c_1 deviates. When the transition is detected and the data from prior to it removed, the optimised values re-converge.*

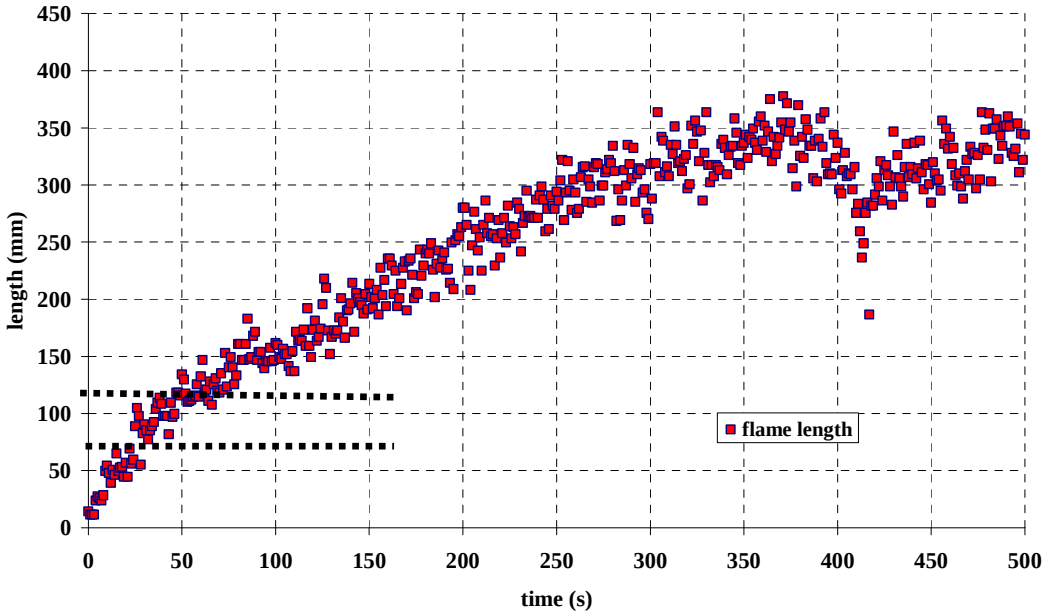

Figure 6.2 – *The plot shows a typical flame length evolution for a vertical experiment. In all vertical experiments there is change in the growth rate of the flame length for lengths in the range of 100 to 250mm. For this particular experiment it occurs at approximately 120mm as indicated on the plot.*

The first two values of c_1 shown in Figure 6.1 are produced prior to the end of the transition. The next two values are produced after the transition but prior to the detection of it. Thus the data used to optimise the 3rd and 4th values represents two different sets of conditions and thus does not produce a valid assessment of c_1. Once the transition is picked up and the data removed, the parameter quickly re-converges. The nature of the growth of the flame in these early stages and the subsequent transition also affects the optimisation of a representative c_2 parameter. During this early, more rapid growth phase, the projections of the pyrolysis length and flame length data are more divergent. Once the transition has been passed however the two sets of data can be seen to parallelise and the c_2 parameter quickly converges. The data presented in Figure 6.3 gives a very clear representation of this as the transition is very abrupt in this case. Up to a time of approximately 80s post ignition, the value of c_2 will change. Once the data corresponding to the time prior to that change has been isolated and removed, and sufficient new data has become available to allow the fits to capture the new trends in the data, the value of c_2 will converge. The c_2 plot for the experiment whose flame length data is shown above in Figure 6.2 and c_1 parameter in Figure 6.1 is given in Figure 6.4.

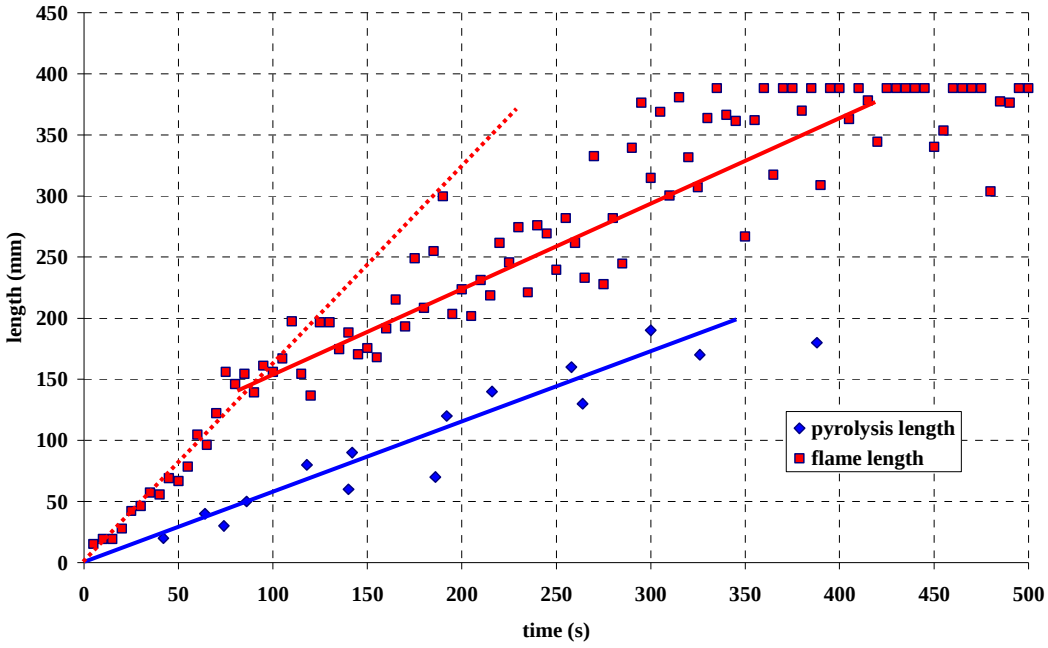

Figure 6.3 - *The plot shows a set of pyrolysis and flame length data for a 200mm long experiment. This data set clearly shows how the change in growth rate of the flame length with respect to the pyrolysis length with cause the value of the c_2 parameter (the ratio of the two lengths) to converge once the transition has passed.*

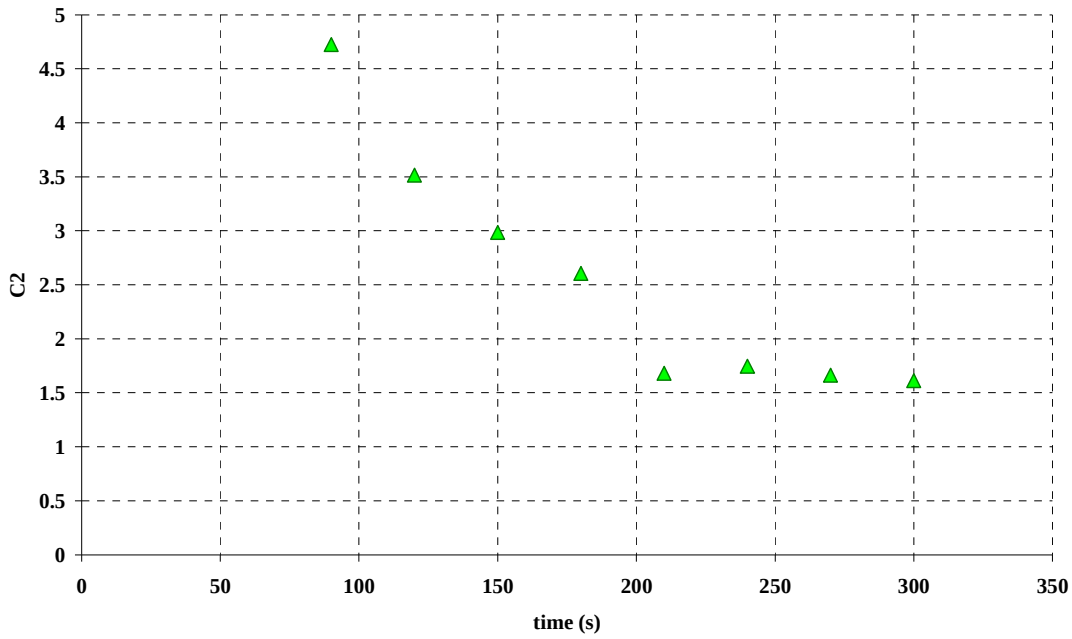

Figure 6.4 – *The plot shows the c_2 values corresponding to the c_1 values shown in Figure 6.1 and the flame length plot in Figure 6.2. Like the c_1 parameter, convergence is reached at the 5^{th} iteration, once the data from prior to the growth transition is detected and removed from the optimisation process.*

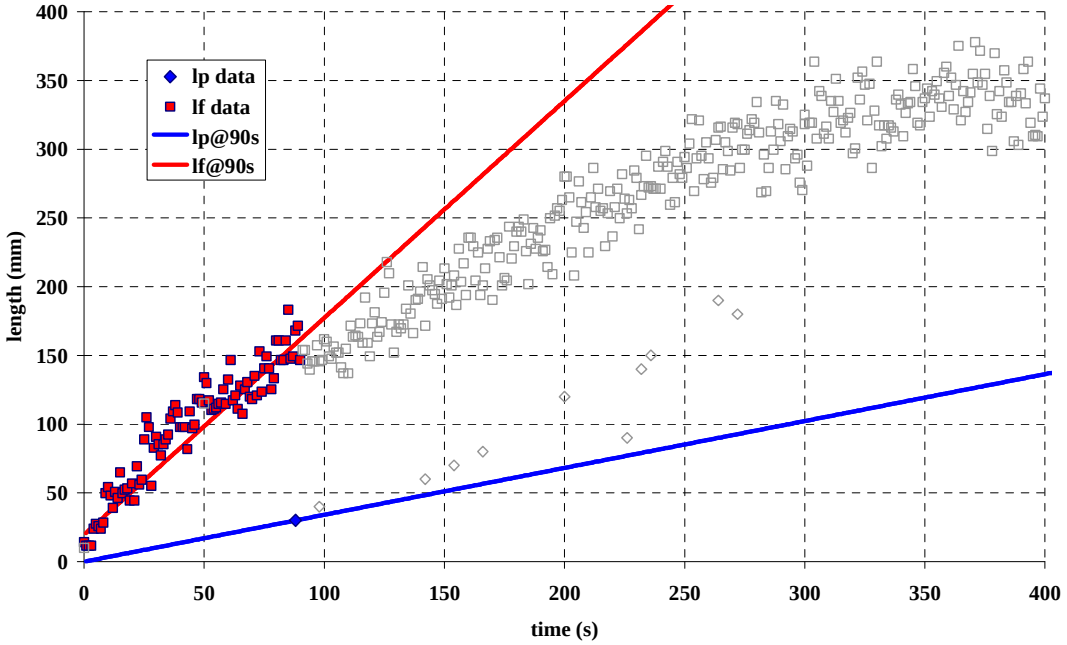

Figure 6.5 – *The plot shows the initial fits applied to the length scale data. As this data represents the immediate growth phase, the fits are not representative of future data and thus the parameters derived form them are also not representative of the future experimental conditions.*

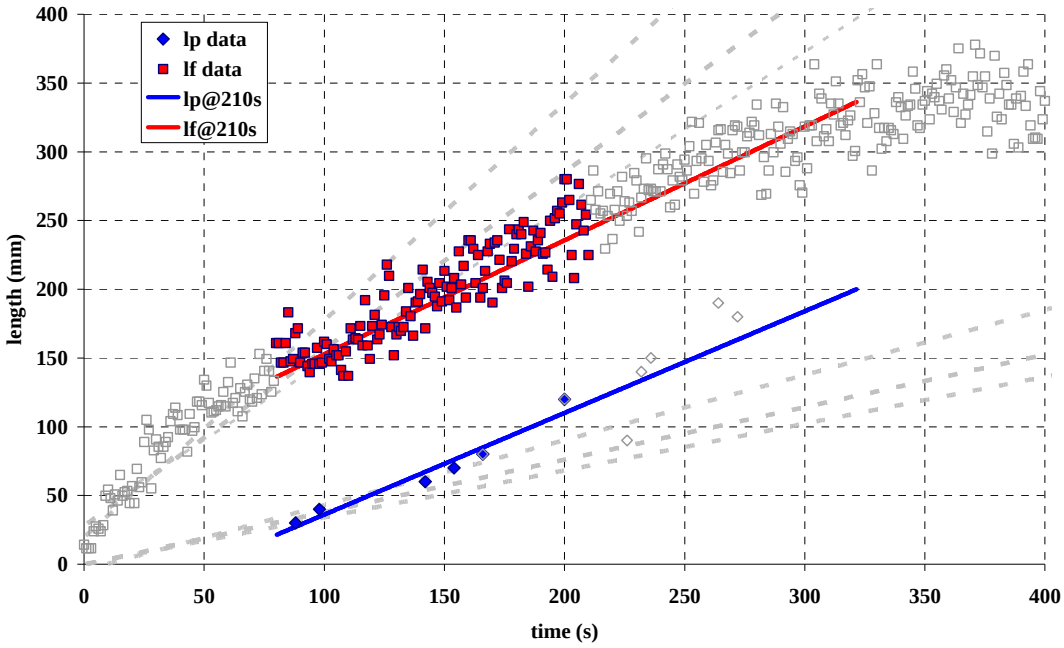

Figure 6.6 – *The plot shows the fits made to the length scale data at 210s post ignition and once the data prior to the growth transition has been neglected from the fitting process. The fits immediately show a much better projection of the future data than the previous ones shown in grey. These fits correspond to the first accurate optimisation of c_2 shown in Figure 6.4.*

The c_2 values (Figure 6.4) follow the same trend as the corresponding c_1 parameter. Once the data prior to the growth transition where the flame length and pyrolysis length are divergent is removed, the parameter converges rapidly. This coincides with the fits themselves converging. The initial fit shown in Figure 6.5 shows how the fits to the initial data diverge and hence give a c_2 value that is not representative of future conditions. When the initial data is removed the fits almost immediately change to project the future trends more accurately (Figure 6.6) and thus to provide a base for accurate parameters to be optimised from. From this stage onwards, the fits vary very little as the future data only confirms their accuracy when it becomes known to and included in the process. As the process remained linear throughout the entire duration of the experiment, the parameter n is automatically set to unity (n = 1) and thus is not an issue.

Two further tests were performed with this same setup but varying the sample, both in thickness and quality. Firstly the sample thickness was reduced from 40mm to 25mm, with all other variables maintained. The second test involved a lower quality PMMA, again 25mm in thickness. This lower grade PMMA had a propensity to drip and degenerate more quickly then the grade used in previous tests. Again, there was an initial growth until a transition to a steady state spread upon which the optimised parameters converged (Figure 6.7).

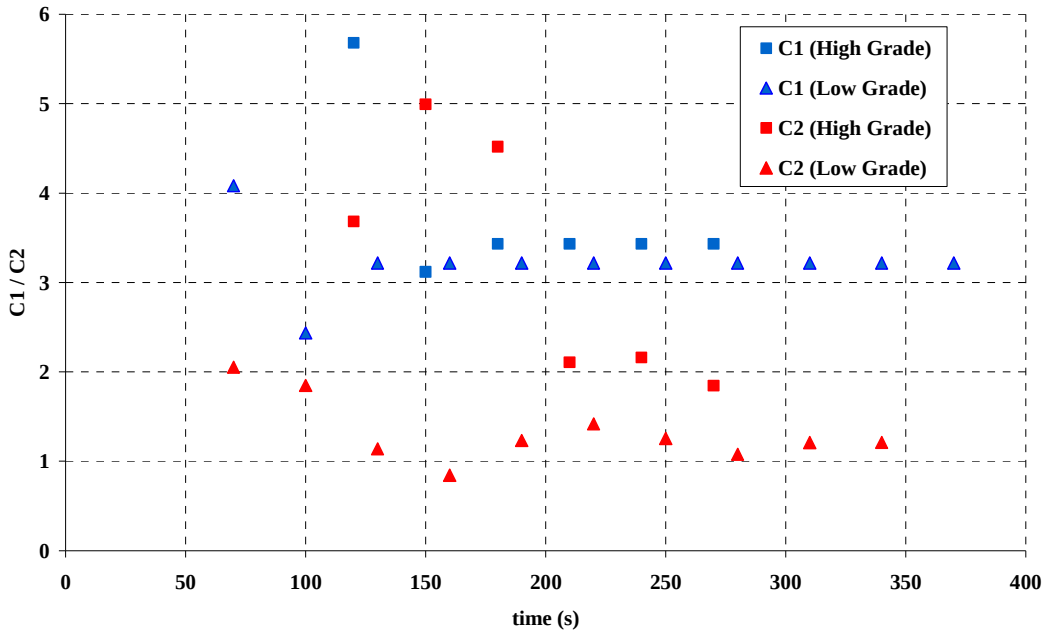

Figure 6.7 – *The c_1 and c_2 parameters for the thinner samples again show good levels of convergence. There is also a similarity between the values of parameters between the experiments.*

6.2 Tilted Surface

Observation of the flame spread in the tilted experiments suggests that the model will be applicable to these experiments. The flame was observed to lye against the PMMA surface in the direction of spread and was generally very laminar in character. Thus the characteristics, especially in the initial stages when the flame was smaller, were similar to those of the benchmark experiment. The literature [24] confirms that spread along an inclined surface will behave concurrently above an angle of 25˚. The samples in these experiments were set to 30˚ to the horizontal. Analysis of the PIV results shows that in terms of the vertical velocity profiles, the two scenarios are very similar. Figure 6.8 shows a typical vector plot and a velocity profile for the component parallel to the fuel surface. The characteristics of the velocity profile are very similar to that of the vertical wall flames presented in Section 4.2.4.2. This implies that the technique used to extract the ambient flow velocity (u_∞) will still be practicable for this scenario.

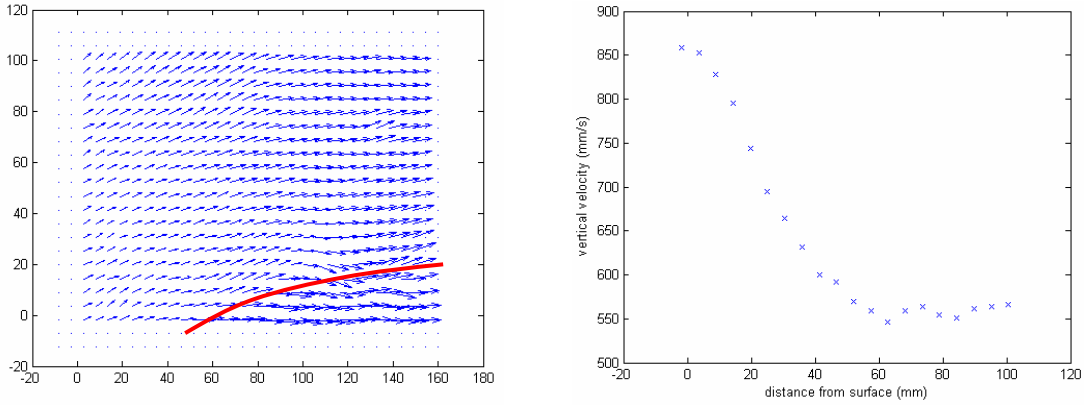

a) b)

Figure 6.8 - *The plot shows results from the PIV measurements on the tilted flame spread experiments. a) shows a vector plot with the position of the flame indicated. b) shows a profile of the velocity component parallel to the surface taken from the pyrolysis zone.*

In terms of the heat transfer to the surface, the flames observed in the tilted experiments behaved more or less like laminar wall flames. The results indicate that the heat transfer to the surface is dominated by convection for the entire experiment. The levels of radiative heat flux to the surface that were measured by the thin skin calorimeters for all tilted experiments were negligible compared to the vertical experiments (Figure 4.49). As the flames got larger towards the end of the experiments they began to show signs of turbulence. A ripple effect was observed intermittently travelling up the flame, being released as a turbulent eddy near the flame tip. The image in Figure 6.9 shows a flame approximately midway through a tilted experiment. The image is taken just prior to the release of the intermittent portion of the flame. The rippling effect is also captured in this image approximately half way up the flame. It was observed through these experiments that when the intermittent portion of the flame was released it moved more or less vertically away from the surface thus at an angle of 60˚ to the PMMA.

As the intermittent parts of the flame are the most luminous and therefore the most radiant portions of the flames, it is believed that this extra separation from the surface in comparison with the vertical flames is partly responsible for the decreased levels of radiative heat flux seen by the thin skin calorimeters. Streamline plots (shown in Figure 6.10) show that as the turbulent ripples pass through the flame, flow conditions near to the surface remain reasonably steady. As the flame nears the end of the experiment it begins to show a more turbulent nature however by this stage the turbulent section of the top of the flame has grown beyond the length of the sample and thus no acceleration is seen in the results. The conditions of the flame at this stage are shown in Figure 6.12.

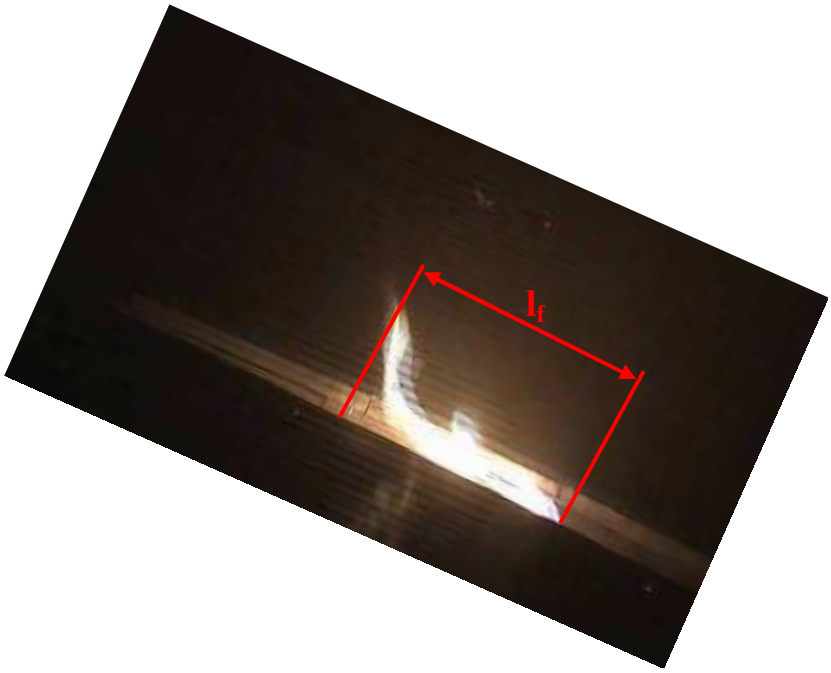

Figure 6.9 - *The image shows a medium sized flame in a tilted experiment. The image is taken just prior to the point of separation of the intermittent portion of the flame. The flame length as would be measured by the image processing software is denoted by l_f. The intermittent part of the flame pulls away from the surface and rises vertically. The persistent part of the flame remains next to the surface.*

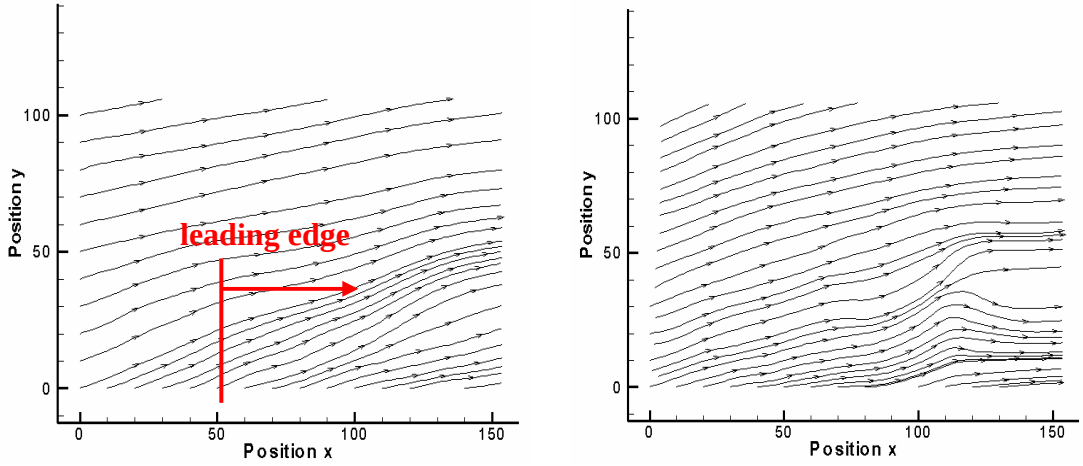

a) b)

Figure 6.10 - *The streamline plots in the figure are both taken from tilted flame spread experiments. a) shows a typical streamline plot from the laminar pyrolysis region and b) shows the effect on the flow when a turbulent ripple travels along the flame. Close to the PMMA surface (positioned approximately at y = -10) the flow profile is not affected greatly. (All dimensions are in mm)*

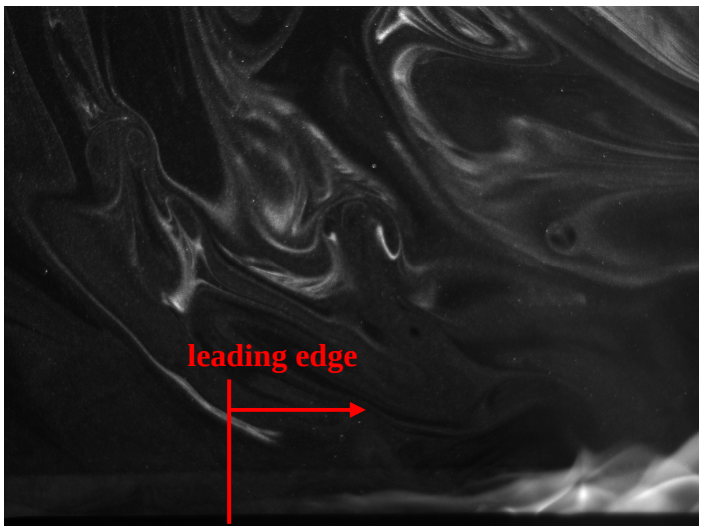

Figure 6.11 - *The image from the PIV cameras demonstrates how the luminosity of the tilted flame increases towards the flame tip. The leading edge of the flame is marked by the red line and the direction of flow and spread is indicated by the arrow. At the flames leading edge where the flow is very laminar and far less luminous the flame does not register on the short exposure. The flame becomes more turbulent and subsequently more luminous further downstream.*

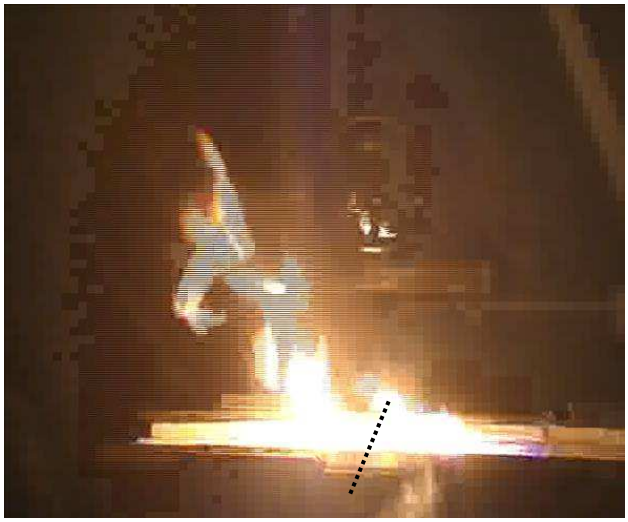

Figure 6.12 – *The image shows the conditions of the flame at the end of the experiments. The flame has become more turbulent in nature however this portion of the flame is situated beyond the end of the slab and thus does not affect the spread rate. (The approximate position of the top of the slab is indicated by the black dotted line)*

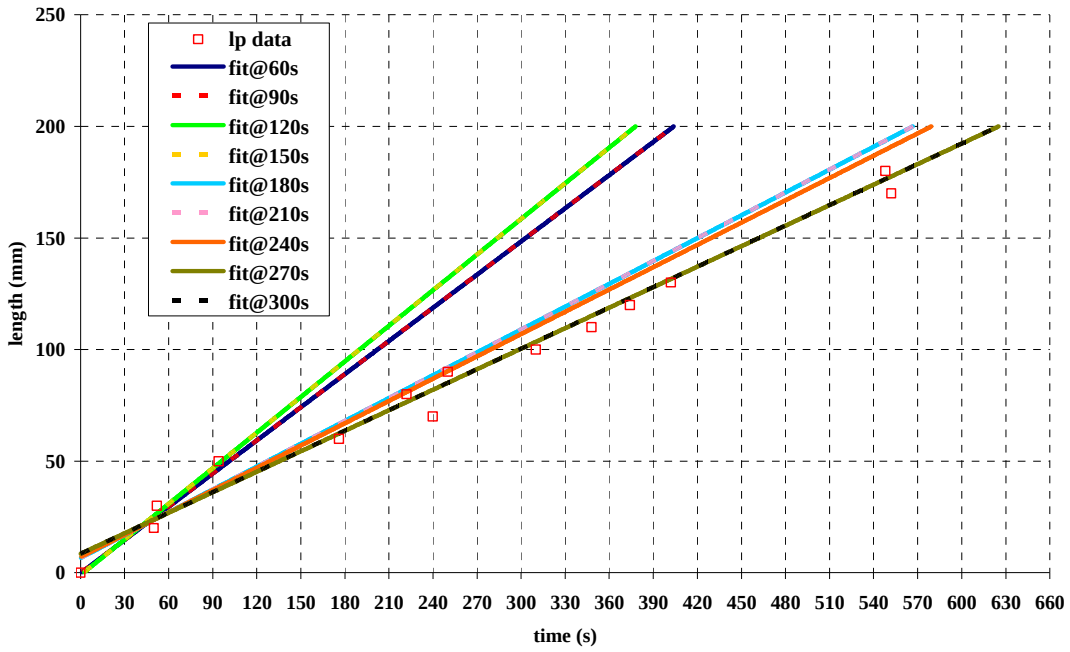

Figure 6.13 – *The plot shows the evolution of the fit to the pyrolysis length data. The fit converges after approximately 300s.*

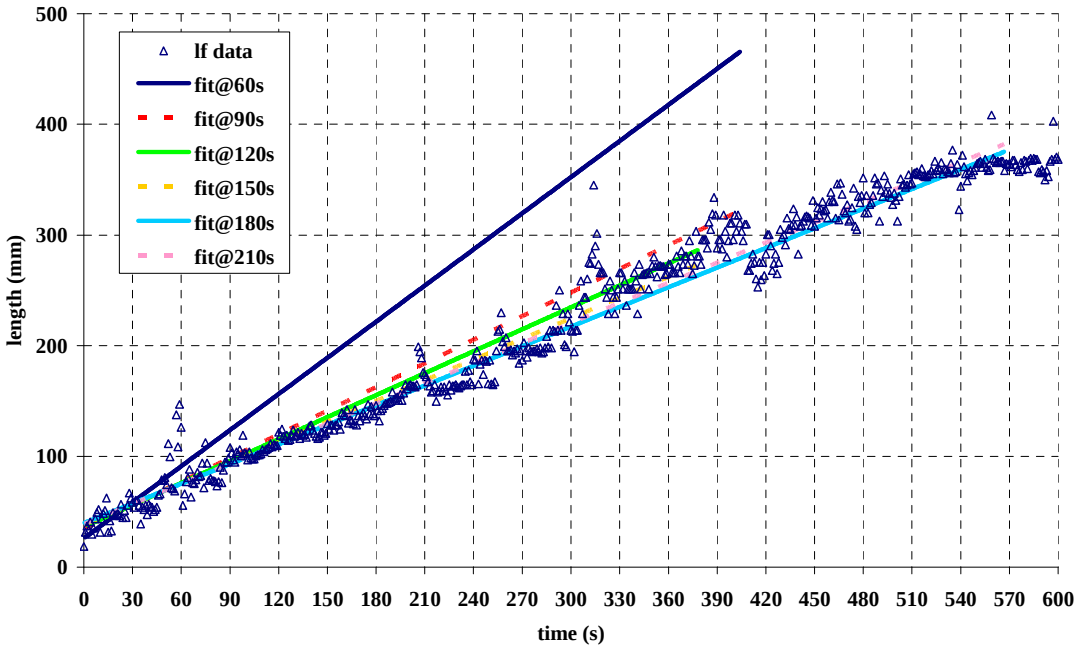

Figure 6.14 – *The plot shows the evolution of the fit to the flame length data. The fit converges after approximately 200s.*

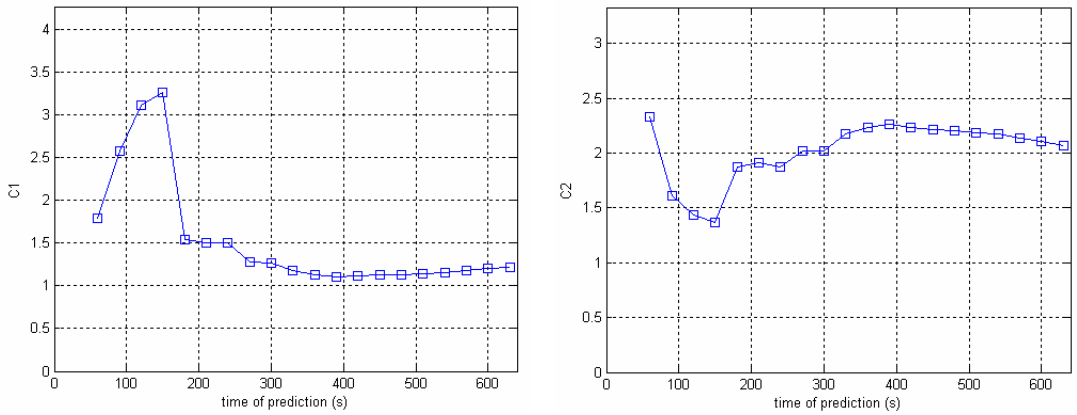

a) b)

Figure 6.15 – *The plots show the convergence of a) the c_1 parameter and b) the c_2 parameter for a tilted experiment.*

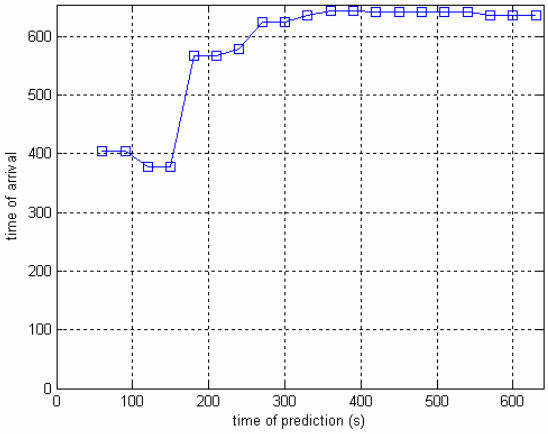

Figure 6.16 – *The plot shows the evolution of the predicted end time of the experiment. The prediction converges quickly and thus gives approximately 300s lead time as to the end time of the experiment.*

In terms of the prediction of spread rate, the scenario presented by the tilted flame spread experiments represents fairly simplistic conditions. The spread rate is essentially constant and the rate of convergence of the parameters concerned with this scenario is only limited by the rate at which isotherm data points become available and thus the fit to this data becomes steady (Figure 6.13). The flame length data which usually provides the greatest insight into conditions in the experiment shows that the flame growth is very steady over the duration of the experiment. The fit to the flame length converges rapidly (Figure 6.14) as do all optimised parameters (Figure 6.15 and Figure 6.16). The methodology is deemed to be more than capable

of providing an accurate prediction of this scenario. Like the previous set of experiments, a variety of PMMA samples were tested in this configuration. All samples were 200mm in length, but as before, thicknesses of the samples varied between 40 and 25mm, and both the lower and higher grade PMMA was tested at 25mm thickness. The results showed equally linear spread and the methodology performed equally well for all samples.

The transition in the flame length growth seen clearly in the vertical experiments is more subtle and prolonged in the tilted setup. It is thought that this is in part due to the slower rates of spread and thus growth of these experiments, and also due to the nature of the definition of the flame length. As Figure 6.9 shows, the flame length is defined as the longest length parallel to the fuel surface for the purposes of the model. The characteristic of the flame in this phase is more turbulent and is exemplified by intermittent buoyant plumes which rise at an angle from the surface, thus the length defined in the model is not always the total length of the flame. This factor can therefore disguise somewhat the true growth of the flame in a more turbulent regime.

Caution should be taken when considering the extrapolation of this result to the bigger picture of, for example, a compartment fire scenario. There is the potential that during this process, information is lost as to the potential effect of the flame on the surroundings. The radiation from the flame that is seen by the PMMA in this case is small and thus neglected in the model. This does not necessarily mean that the level of radiation from the flame to other items will be as insignificant. Linked to this is the assessment and prediction of flame height. When the flame is larger as pictured in Figure 6.12 the turbulent eddies which account for the most radiant parts of the flame are actually angled with respect to the surface. As described above, the length of the flame for the purposes of heat transfer to the surface in the flame spread model is different to the actual length of the flame. The parameters optimised in this process are specific to the goals of the flame spread process and can not necessarily be extrapolated to a wider picture.

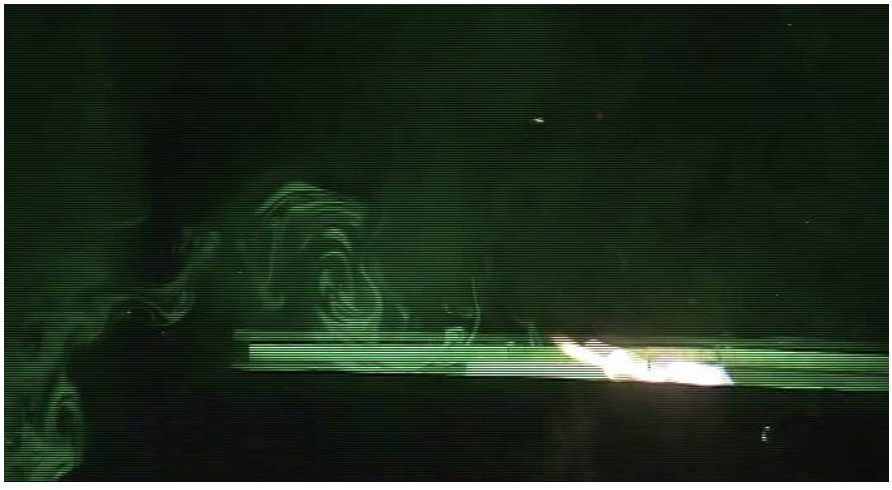

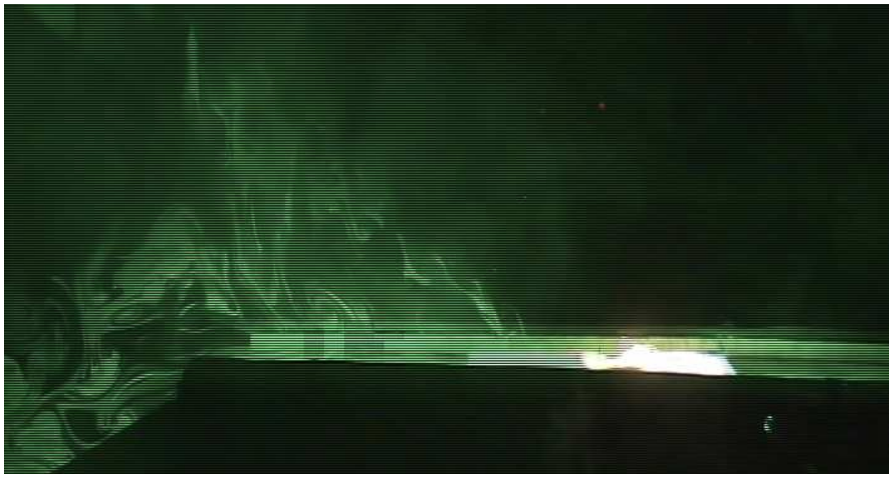

Figure 6.17 – *The images show the highlighted patterns of the seeding particles by the laser during measurements by the PIV system.*

6.3 Transition to Turbulence

The purpose of the larger experiments was to test the methodology's ability to capture the characteristics of a turbulent spreading flame. In Section 5.3.2.3, the derivation of a curve fit designed to capture the trend of an accelerating spread process was described. The previous smaller samples that were tested did not provide sufficient height for the spread to develop into a fully turbulent regime and thus could not be used to assess the capabilities of this aspect of the methodology. Towards the ends of some of these tests the flames appeared quite turbulent so the height of the sample was increased from 200mm to 500mm to provide conditions conducive to turbulence.

In the first example, the initial iterations of the methodology were performed when the flame was smaller and laminar. In these iterations, a linear fit was applied to the data, and the fits and optimised parameters converged very much as the benchmark experiments did. The plot of the c_2 parameter in Figure 6.18 shows convergence up to 300s. Other parameters and fits showed similar convergence. Iterations performed after 300s were performed using the curved fit as inspection of the data available to the model at that time showed a slight acceleratory trend. By this stage the c_1 parameter had been fixed and the model was optimising the values of c_2 and n as well as the net radiant heat flux to the surface.

From the time of change to the curve fit form of the methodology, the optimised length scale parameters, c_2 and n, no longer converged on a single value and instead alternated between two alternative regimes. This is shown in Figure 6.18 for c_2 and Figure 6.19 for n.

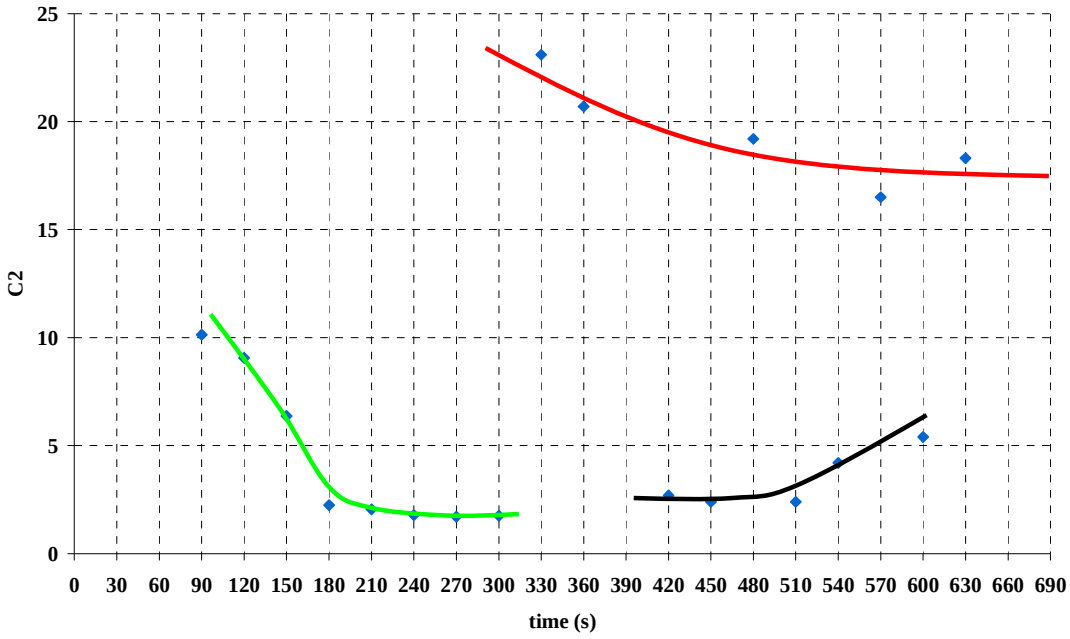

Figure 6.18 - *The plot shows the evolution of the c_2 parameter over the duration of an experiment. When the flow is laminar and a linear fit is applied up to 300s, the value of the parameter converges. When a curve fit is applied to the data post 300s, the value of the parameter alternates between two values. (Corresponding data for n in Figure 6.19)*

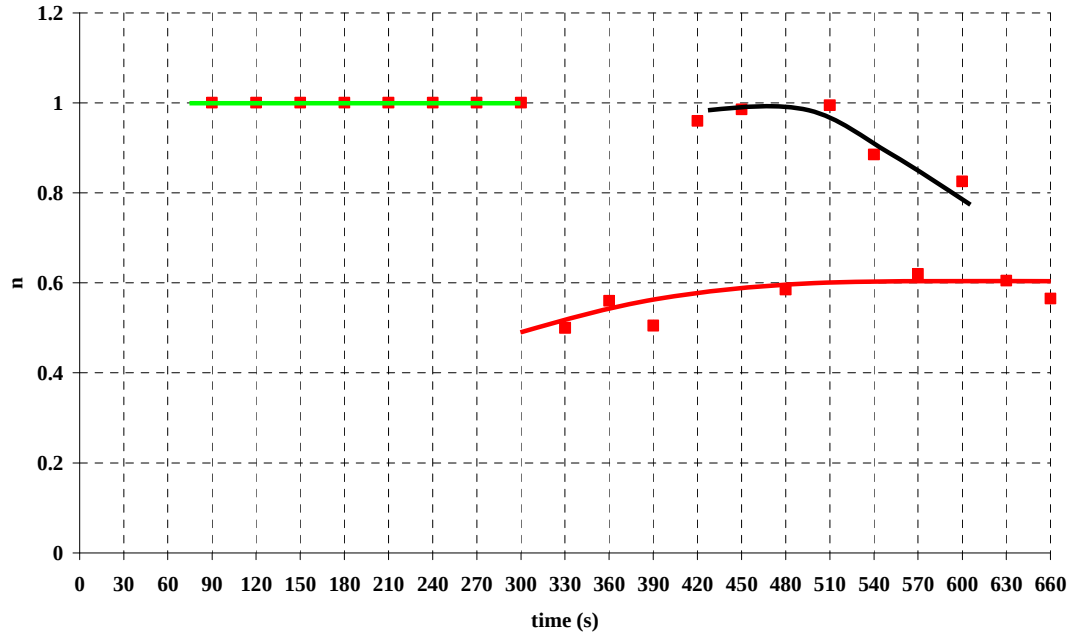

Figure 6.19 - *The plot shows the evolution of the n parameter over the duration of an experiment. When the flow is laminar and a linear fit is applied up to 300s, the value of the parameter is fixed at 1.0. When a curve fit is applied to the data post 300s, the value of the parameter alternates between two values. (Corresponding data for c_2 in Figure 6.18)*

The results of the c_2 and n parameter optimisations show two competing solutions with the results at each iteration falling into one solution or the other. (For ease of description they have been separated into red and black, as depicted by the colour of the lines approximating their trends in the plots.) While this duel solution situation is not an ideal scenario, it does at least show a level of convergence, with two distinct solutions rather than random scatter.

The n value was compared to the other n values that are produced as a result of the curve fits of the flame and pyrolysis length data (Figure 6.20). Both values of the adjustable curve fit parameters converged. Further more the convergence corresponded to the red solution. Further analysis shows that the cause of this 'bi convergence' is related to the behaviour of the curve fit to the pyrolysis data. Figure 6.21 shows the plots of the fits made at each iteration. The lines tend to fall into two distinct trends much like the values of c_2 and n, (again depicted by red and black dotted lines) and furthermore the groups matched.

When the line fits are compared with the entire collection of isotherm data from the experiment, the fits corresponding to the red solution matched the later data most accurately. The fits corresponding to the black solution showed a much slower growth. This characteristic of this later group of fits is due to 'lagging' thermocouple readings when the bead is too far from the surface or in poor thermal contact with the PMMA, with the result that the time associated with the arrival of the isotherm is later than it would have been had the sensor been positioned properly. The time delay results in the trend of the data appearing more linear than it should which is reflected in the fits corresponding to the black solution. When the curvature of the curved fit is very shallow i.e. almost linear, the values of c_2 and n reflect this. The value of c_2 produced by these almost linear shaped fits can be seen to correspond to the value that the early (actual) linear fits converged on. The value of n produced is close to 1.0 which is the default value for a linear fit. When later data from better placed thermocouples becomes available to the fit, the effect is to pull the curve back towards the red solution and the corresponding values of c_2 and n move away from the linear values. In this case, the values of n fall around the more 'acceptable' range as defined in Section 2.1.4.

The optimised fits of the net radiant heat flux to the surface (Figure 6.22) support this explanation. The fits corresponding to the black solution converge on a lower and seemingly constant value. This is consistent with a linear fit as a near constant heat flux would lead to the near linear spread rates extrapolated from the pyrolysis fits of the black solution. The heat flux fits corresponding to the red solution converge on a more or less constant rate of growth which is consistent with an acceleratory spread rate.

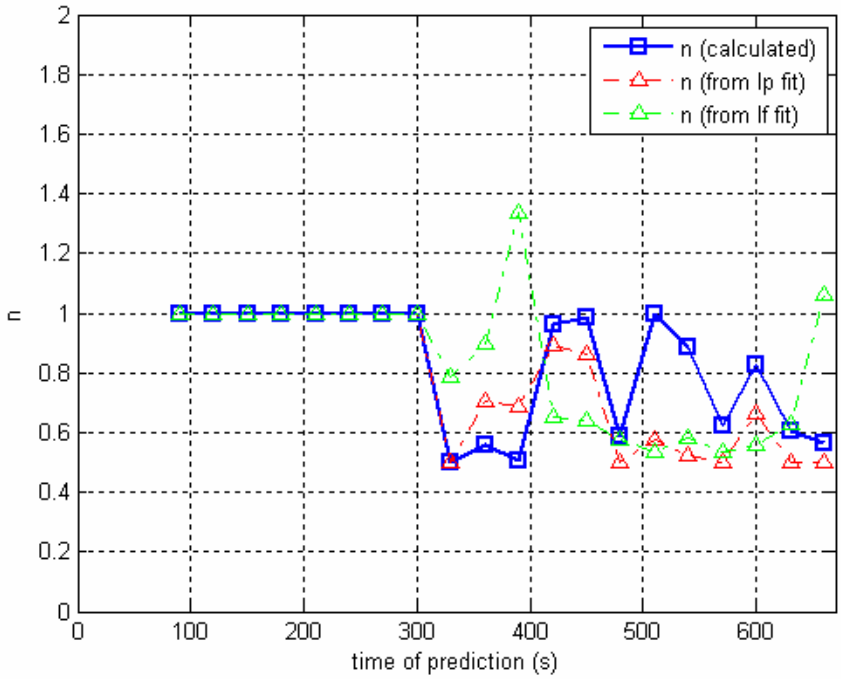

Figure 6.20 - *The values of n produced by the optimisation process (blue squares) alternate between two positions, n ≈ 0.6 and n ≈ 0.9-1.0 suggesting two potentially good solutions. The values of n corresponding to adjustable parameters in the curve fitting process converge on the lower of these solutions.*

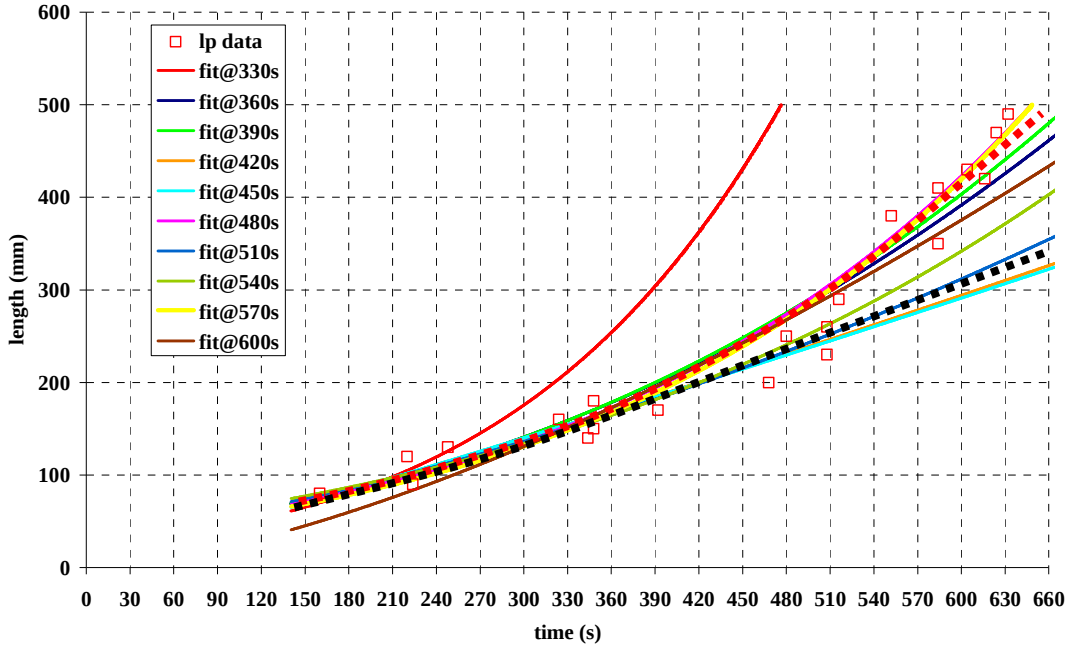

Figure 6.21 – *The plot shows the evolution of the fits made to the pyrolysis length data. There are two main groups of fits, indicated by the dotted lines. Each group corresponds to one of the two alternatives in the convergence in the c_2 and n data.*

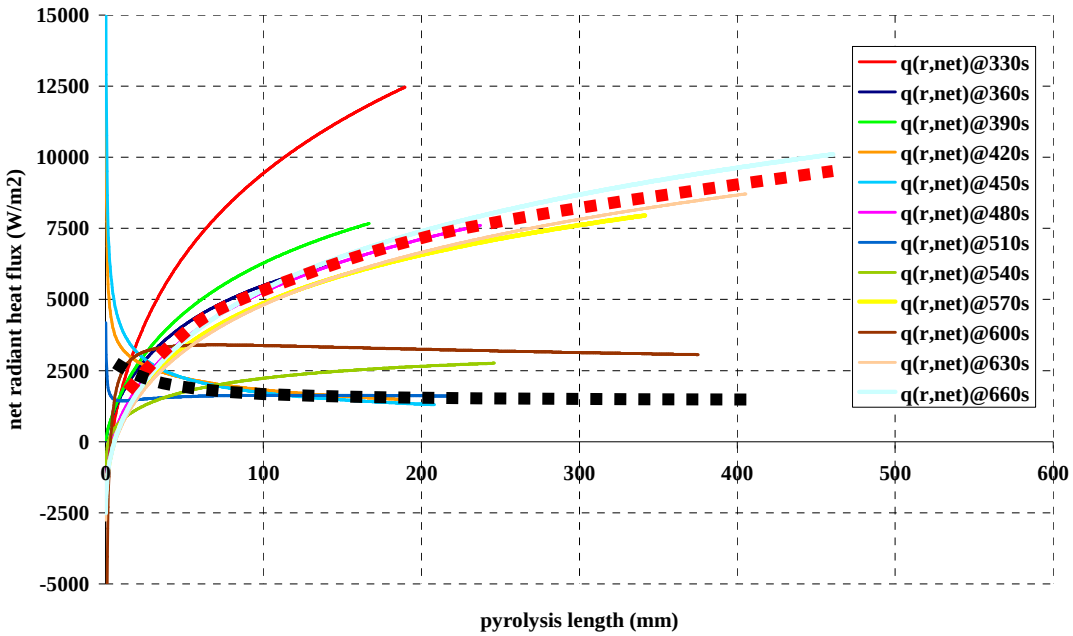

Figure 6.22 – *The plot shows the estimation at each iteration of the net radiant heat flux to the surface from the flame. Again there are two main groups within this plot each corresponding roughly to the trends shown by the dotted lines. The group of lower values correspond to the more linear fits of the pyrolysis length data. The group of higher values correspond to the more acceleratory curved fits of the pyrolysis length data.*

Two further experiments were carried out in this setup, one with an identical setup to the example just discussed, and another with lower grade PMMA. All samples for this setup were 25mm thick. The second experiment did produce a good convergent solution. The test began as per the previous vertical tests in a laminar spread regime and changed in nature, transitioning to a more turbulent steady spreading flame when the flame height reached approximately 150 - 200mm. As seen before, at this stage the parameters and fits converged. Later the data began to show a slight acceleration and the process changed to the curve fitting version of the methodology. On this occasion the optimised parameters settled on one solution. Later when the pyrolysis front approached the top of the plate, the spread appeared to slow and the parameters, although still being estimated from the curve fit type, re-converged on the values seen at the beginning of the experiment. The length scale data and the corresponding n and c2 values are shown in Figure 6.23 and Figure 6.24 respectively.

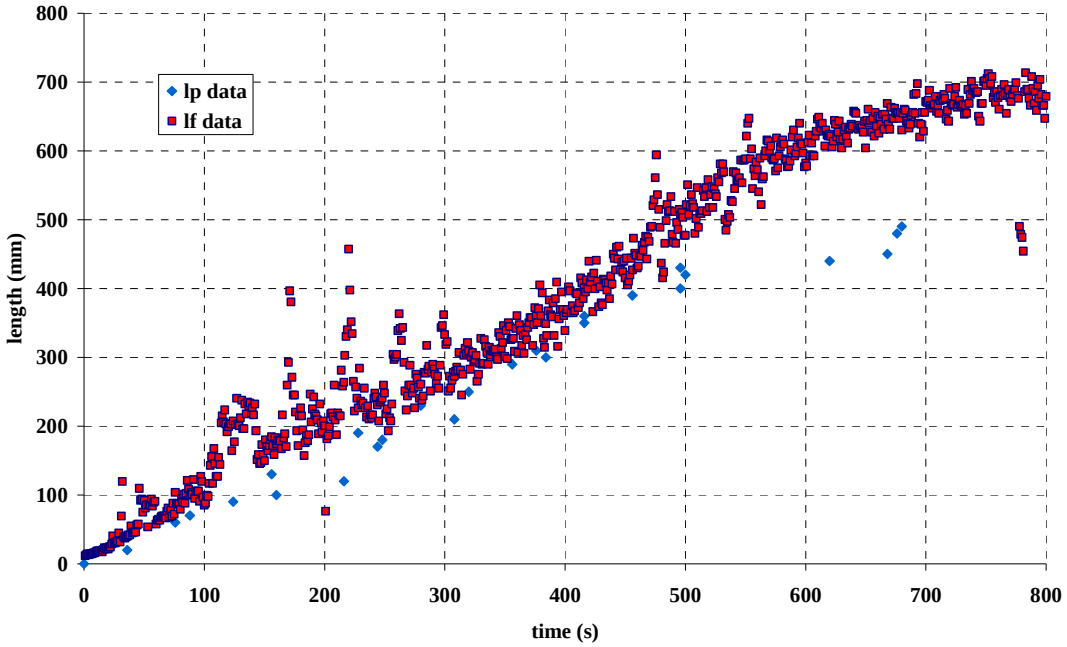

Figure 6.23 – *The plot shows the pyrolysis and flame length data for the second example experiment. Initially the flame grows quite linearly and from approximately 250s begins to accelerate slightly. Around 500s it begins to slow again.*

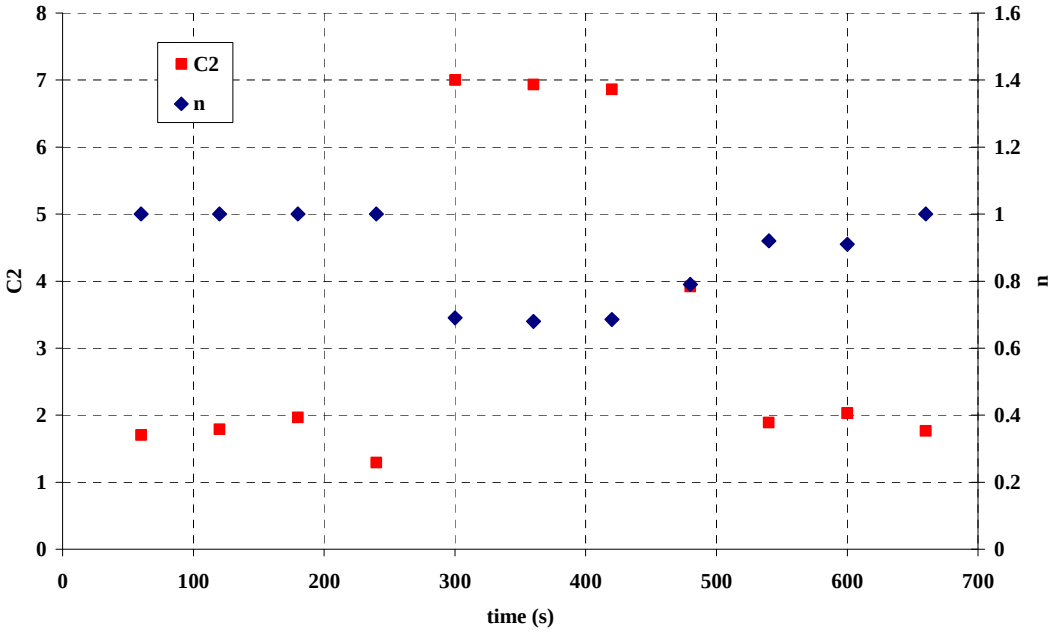

Figure 6.24 – *The plot shows the evolution of the length scale relationship parameters of the second example of the larger scale experiments. In the initial steady spread regime the parameters converge. In the middle of the experiment the fit switches to the curve fit type and again the parameters converge. As the spread rate slows at the end of the experiment, the parameters revert back to their original values corresponding to a more constant spread velocity.*

The results from this second analysis coupled with the alternating convergence seen in the previous example indicate that the sample height may not be sufficient to produce a significantly turbulent accelerating flame spread. The acceleration seen in these experiments is very slight and only really evident for a short period prior to the ends of the tests. The results do appear to show however that the methodology is capable of capturing the trends and optimising reasonable parameters from the data. A longer experimental sample may afford a more comprehensive look at the turbulent regime and the parameters associated with it. The results of the analysis of the third experiment of this type did not show any notable acceleration in the spread rate to justify the application of the curve fit type. It was found that the linear fits provided a good description of the data to the end of the experiment. The c_2 and c_1 parameters converged well in the early stages and were seen to describe the data from later in the experiment well. While not an ideal test of the second part of the methodology, the results from the application of the methodology to these experiments indicate that the derived curve fit will produce a good solution. The results show that the fit will give answers in the same range as those reported from turbulent experiments in the literature (Section 2.1.4). The results of the first example of these experiments also show that the optimisation using this fit style will derive parameters that describe linear data with the equivalent values to those derived from direct linear fits. Thus should the situation arise where a premature application of this fit is performed with data that is not fully turbulent, this misapplication will not necessarily force the optimised parameters to resemble those concurrent with turbulent flame spread. Nevertheless, a larger experiment would be needed to fully ascertain the proficiency of this methodology when applied to turbulent spread.

6.4 Complex Compartment Fire Environment

A PMMA sample was placed in the main fire compartment of Dalmarnock Fire Test One [1]. Due to the timing of the tests, this experiment was setup and carried out prior to the other experiments described here and thus without the hindsight of their findings. In the best case it was intended that the data from this test could be used to demonstrate that the methodology, then still to be developed, could be used in a complex fire scenario such as the scenario in Dalmarnock. In the worst case though, the inability to produce a prediction of spread rate and optimisation of scenario specific parameters would serve to highlight the current limitations of the technique and future work requirements which in reality turned out to be the case.

The main obstacle to the successful application of the methodology in its current state was a lack of relevant sensor data which posed many problems. Although there were hundreds of sensors present in the experimental compartment, only a handful of them were directly tailored to the PMMA experiment in the way the techniques outlined earlier in Chapter 4 were. The first problem was the difficulty in defining an ignition time which was not a calculation included in the original methodology where the time of ignition was simply observed and noted. Studying the video footage after the ignition of the waste paper bin in the compartment, the fire was seen to spread on to the sofa where it grew in size and eventually ignited the base of one of the two bookshelves. The fire quickly spread up the bookshelves which were set in

a corner configuration and were loaded with combustible items leading to flashover in the compartment. At this point a thick black smoke layer descended obscuring the various cameras views of the PMMA which had not ignited by this stage (Figure 6.25). At no point during the experiment while the cameras were functional could flames be seen coming from the PMMA although inspection afterwards showed that half of its thickness had been consumed. Not only does this obscuration prevent simple definition of the ignition time and location on the slab, it also precluded any measurements of the flame heights using the image processing techniques defined in Section 4.2.2 which provided the greatest source of information previously.

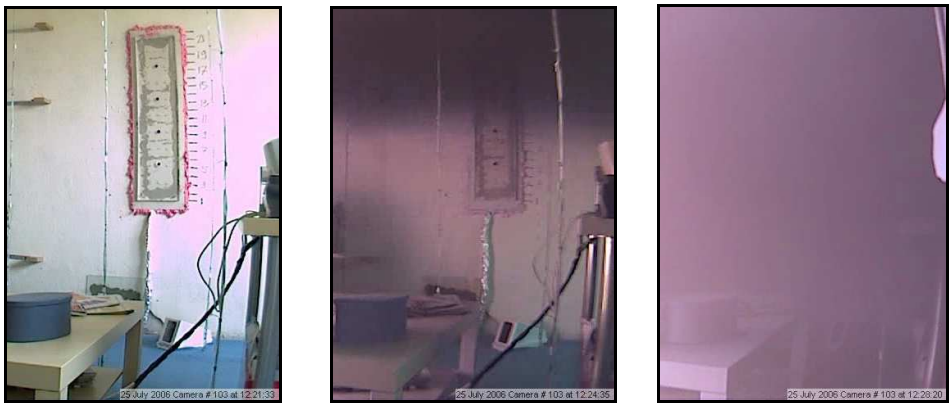

a) b) c)

Figure 6.25 – *The images taken from a webcam within Dalmarnock Fire Test One demonstrate the issues with using camera footage for measurements in a fire scenario. a) shows the PMMA slab prior to the experiment, b) shows the slab during the pre-flashover growth phase of the fire, and c) shows the obscuration of the camera as the smoke layer descends during the flashover event.*

The PIV measurement of the ambient flow velocity (u_∞) was not present in the test. Aside from the fact that the equipment is too valuable to be risked in such a hazardous environment, the tricky nature of the measurement technique and the impracticalities of providing seeding to the flow make it unviable for such an experiment. There were only 23 depth thermocouple measurements spread two-dimensionally over the face of the PMMA sample rather than the line distribution of the laboratory experiments. This arrangement was due to the undefined location of the ignition and the extra width of the slab in comparison with the laboratory experiment. There were also only four thin skin calorimeters spread over the centreline of the sample. The sensor density of the surface sensors was thus less than the laboratory experiments. The comparatively low density of sensor data prevented both the clear definition of an ignition time and the obtaining sufficient information to fully populate the model to make a prediction. Also with only one set of results no assessment could be made of the repeatability of the test.

The sensor data that is available however can help to demonstrate the required adaptations of the methodology and experimental techniques necessary to overcome the extra challenges brought on by the complexities of this environment. An ignition criterion needs to be defined most likely based on a combination of depth thermocouple readings, gas phase thermocouples, and heat flux meter readings. The simplest would seemingly be the use of gas phase thermocouples close to the surface to detect a large temperature gradient that would be expected from the sudden presence of the flame. This may be complicated by the presence of a hot upper layer but a distribution of thermocouples in the compartment could be used in conjunction with the thermocouples close to the solid surface, by indicating the likely height and uniformity of the hot layer throughout the compartment as was performed with the results from Dalmarnock in other works [1] [15]. The method of measurement of radiant heat flux to the surface must be improved either through the development of the thin skin calorimeter technique or by another method if it were to be used to this purpose. This technique may be complicated however as the levels of radiant heat flux in a small laminar flame may be difficult to detect.

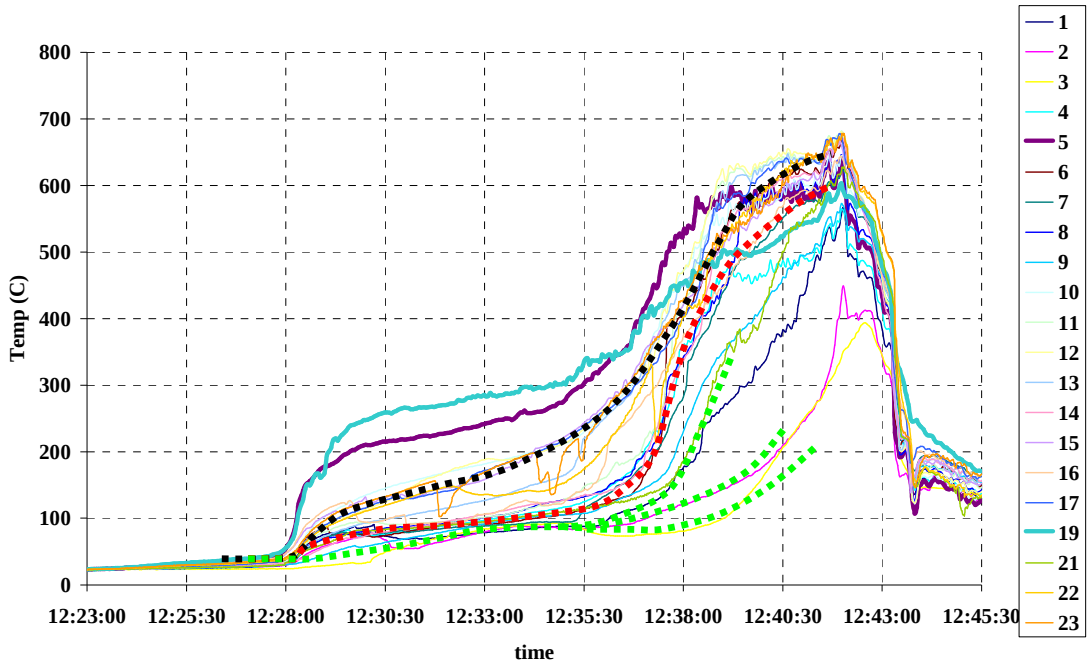

Figure 6.26 – *The plot shows the temperature output from the thermocouples embedded within the PMMA slab in the Dalmarnock sub-experiment. Flashover occurred at approximately 12:28:00. Thermocouples 5 and 19 were partially exposed to the gas phase hence a more rapid rise in temperature is seen.*

The third option would be through the tracking of the depth temperature as was used to define the arrival of the pyrolysis front in the laboratory experiments. This is complicated though by the preheating that the sample is exposed to both through radiation from the fire and the hot smoke layer prior to ignition (Figure 6.25 b)). The thermocouple traces from the depth sensors are shown in Figure 6.26. The temperatures remained relatively low prior to flashover which occurred at

approximately 12:28:00 at which stage three trends emerged in the data which are indicated by the thick dotted lines in the plot.

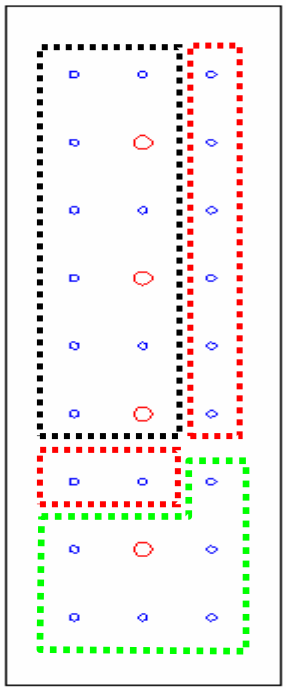

Figure 6.27 – *The diagram shows the positioning of the surface sensors in the Dalmarnock PMMA sub-experiment. The blue markers represent the positions of thermocouples below the surface and the red markers the positions of thin skin calorimeters. The sensors grouped in coloured boxes correspond approximately to the groups of thermocouples represented by dotted lines in Figure 6.26. (The diagram is not to scale)*

The temperatures of the thermocouples in the group corresponding approximately to the black dotted line appeared to have ignited not long after flashover (12:28:00) and increase steadily from this point. These are mainly in the upper region of the specimen (surrounded by the black dotted line in Figure 6.27) that will have experienced more preheating due to the hot smoke layer prior to flashover (Figure 6.25 b)). The readings from the lower thermocouples in this group lagged slightly behind the reading from the upper ones but their trends are still distinct from the thermocouple readings corresponding to the red and green dotted lines. The remaining thermocouples corresponding to the red and green dotted lines rose to a plateau of approximately 100˚C. Due to the length of time they remained at this plateau it appears that there may not have been an ignition in these regions at flashover but that ignition occurred later. The group of thermocouples corresponding to the red dotted lines in both Figure 6.26 and Figure 6.27 showed a sudden rise in temperature at approximately 12:36:30. Other sensors in the room indicate that this coincides with the ignition of a collection of paper items on a nearby desk. This may

have acted as a strong piloted ignition given that this area of the surface would most likely have been producing pyrolysis products due to heating from the post flashover smoke layer and possible flaming in the region denoted by the black box in Figure 6.27. The remaining thermocouples are heated by the descended smoke layer then show ignition trends separately. These are generally the lowest thermocouples in the sample (denoted by the green dotted lines in Figure 6.26 and Figure 6.27) and the trends indicate the occurrence of downward flame spread over the lower portion of the sample.

This information serves to demonstrate that the definition of an isotherm temperature is not as clear cut as before due to the lack of a flame acting as a pilot for the combustion products produced by heating of the sample. Though at times the PMMA may have been pyrolysing, there may not necessarily have been any flame spread. This emphasises the importance of being able to define the ignition both in terms of time and location. It also serves to demonstrate that the pyrolysis front tracking technique may not be applicable, at least in its current state to these types of scenarios. These approximate and qualitative trends appear to show that due to heating effects typical of the compartment fire scenario, the ignition of the top of the sample was abrupt due to preheating and the flame spread over the remainder of the PMMA sample was more downward. Thus in order to test the methodology in an upward flame spread regime, future tests of this nature should consider carefully the placement of the specimen with respect to other items in the room to try to force an ignition near the base of the sample earlier on.

Overall this experiment demonstrates that the most limiting factor is the amount and quality of sensor data available that is specific to the purpose defined by the methodology and that the evolution of future experiments should be guided by the end use scenario, be it a compartment fire or other wise. Measurement techniques should be developed with anticipation of worst case environmental scenarios to prevent gaps in potentially crucial data sets brought about by previously unforeseen severe environmental conditions.

6.5 Assessment of Findings

It has been demonstrated that the methodology in its current form works well for lab scale concurrent flow experiments where the ignition is well defined and the flame is the only source of heating. The predictions made converged on accurate solutions predicting future conditions well. These solutions were obtained rapidly providing good lead time. Also the majority of the process for these simple scenarios has been automated to tie in with the ethos of the FireGrid project.

The quantity and quality of pyrolysis length data points proved to be a significant factor affecting the success of the methodology in predicting the outcome of an experiment and in obtaining convergence in the optimisation of parameters describing the data. Specifically the successful convergence of the length scale parameters n and c_2 in this scenario is governed by the quality of the depth thermocouple technique. This may also be a result of the somewhat heavy reliance of

the methodology on the quality of the assessment of how this measurement is evolving. The pyrolysis length is the essential piece of information that connects the goals of the prediction. The aim of the work is to provide an accurate prediction of the spread of the flame over the surface, an accurate prediction of heat transfer to other items and thus an accurate prediction of the growth phase of a fire. The way the methodology is set out places a heavy reliance on the accurate measurement of the pyrolysis length to achieve these goals.

All lab scale experiments ignited with the ignition wire method showed a similar development process at the beginning of the experiments. There is an initial growth phase as the flame establishes itself, whereupon it transitions to a steady state linear growth. At this stage the relationship between the flame length and pyrolysis length (c_2) is quickly established. The comparison of the c_2 values for all vertical experiments expressed as a function of the flame length is shown in Figure 6.28. This plot represents the 200mm high experiments and the first 200mm of the longer experiments. The values for this parameter derived for all experiments shows convergence on a value of approximately 1.8. The plot indicates that before the convergence i.e. during the initial small growth period, the flame will be governed by the conditions resulting from the ignition such as preheating by conduction.

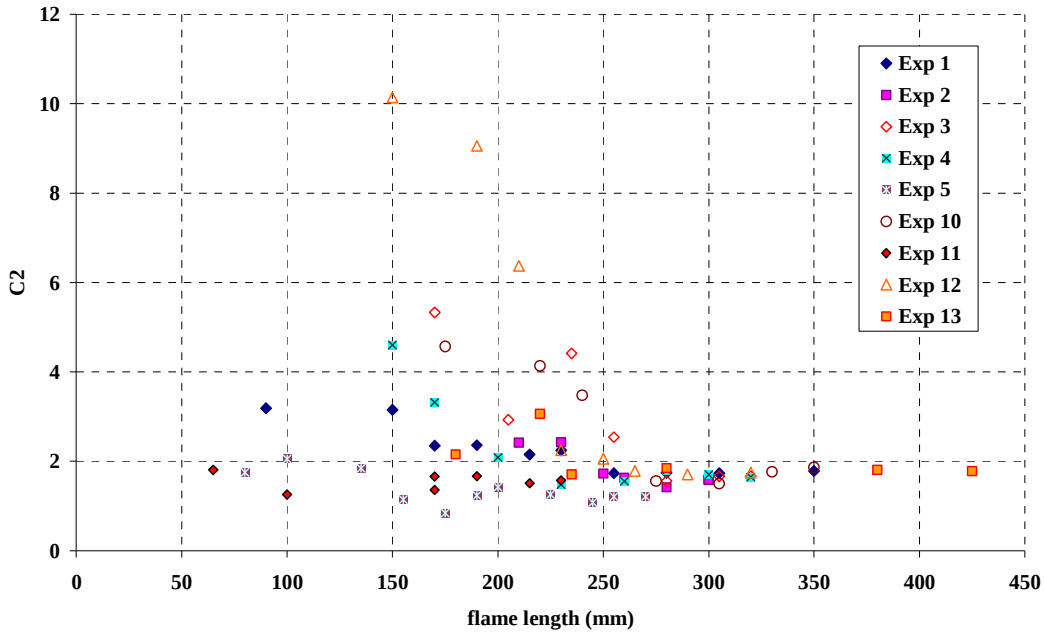

Figure 6.28 – *The plot shows the c_2 values for all vertical experiments established from the relationship $l_f = c_2 l_p$ using the methodology established in this work. In the early stages of transition away from a completely laminar regime, the values converge.*

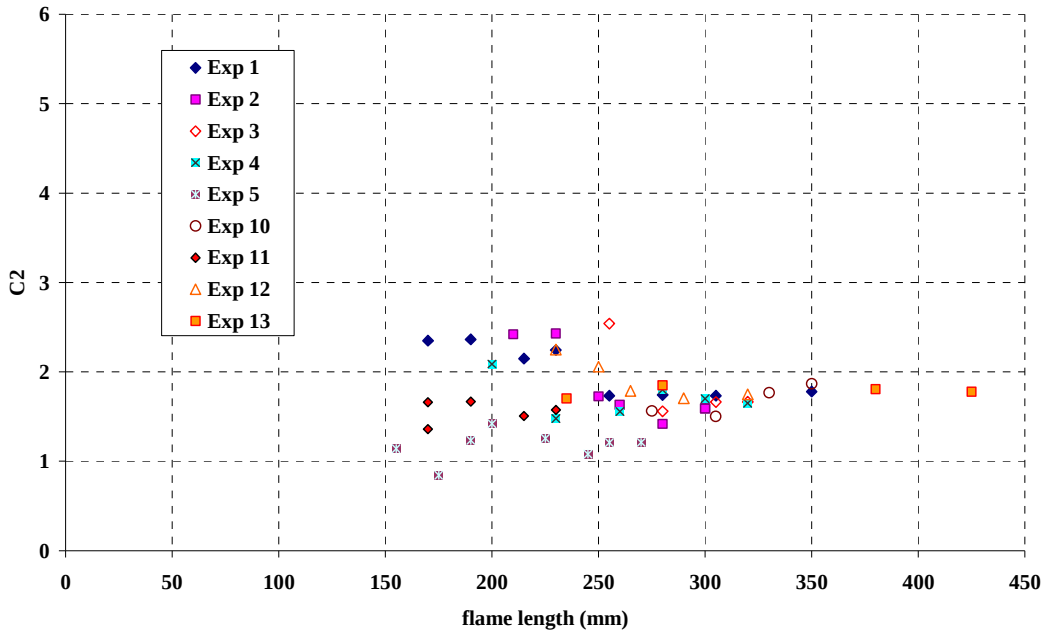

Figure 6.29 – *The plot shows the data presented above Figure 6.28 with the values removed that corresponds to data from before the change in flame length growth rate shown in Figure 6.2. All experiments show convergence on a value of c_2 of approximately 1.7 to 1.8.*

Once the flame has grown to a certain size however, it will become independent of the initial conditions and heat transfer from the flame to the solid will be completely dominant in the spread process in comparison to any effects brought on by the ignition method. When c_2 data corresponding to optimisations performed prior to the transition is removed, the remaining data is far less scattered as shown in Figure 6.29. This plot shows a correlation exists throughout these experiments showing the value of c_2 is equal to approximately 1.8 under constant spread conditions when the flame is the dominant mechanism of heat transfer.

A correlation also appears to exist throughout the experiments for the value of the c_1 parameter. For most of the successful applications of the methodology, the flame spread was entirely or at least in part steady state or constant. While this is the case, the spread can be shown to be independent of the pyrolysis length and the radiative heat flux to be negligible and thus the model in Equation 14 can be reduced to the following expression by the grouping of other constant parameters: -

$$V_f = K.c_1.u_\infty$$

Equation 33

Where the value of the introduced constant K is given by: -

$$K = \frac{4c_2 k_g \rho_g c_p (T_f - T_p)^2}{\pi k_s \rho_s c_s (T_p - T_0)^2}$$

Equation 34

Thus, through rearrangement of Equation 33 the value of c_1 should be linearly proportional to the ratio of spread rate to ambient flow velocity according to: -

$$c_1 = \frac{1}{K} \cdot \left(\frac{V_f}{u_\infty} \right)$$

The plot in Figure 6.30 shows that the data does show adherence to this model except for one of the experiments. Analysis has shown that the u_∞ measured for this experiment is the lowest of all experiments and a factor of 10 increase would bring it to a magnitude in line with other experiments and also into adherence with the correlation as indicated by the triangular turquoise data point on the plot. It is possible that the dt between PIV images was under-prescribed in the original vector map calculations but for now the data point is neglected.

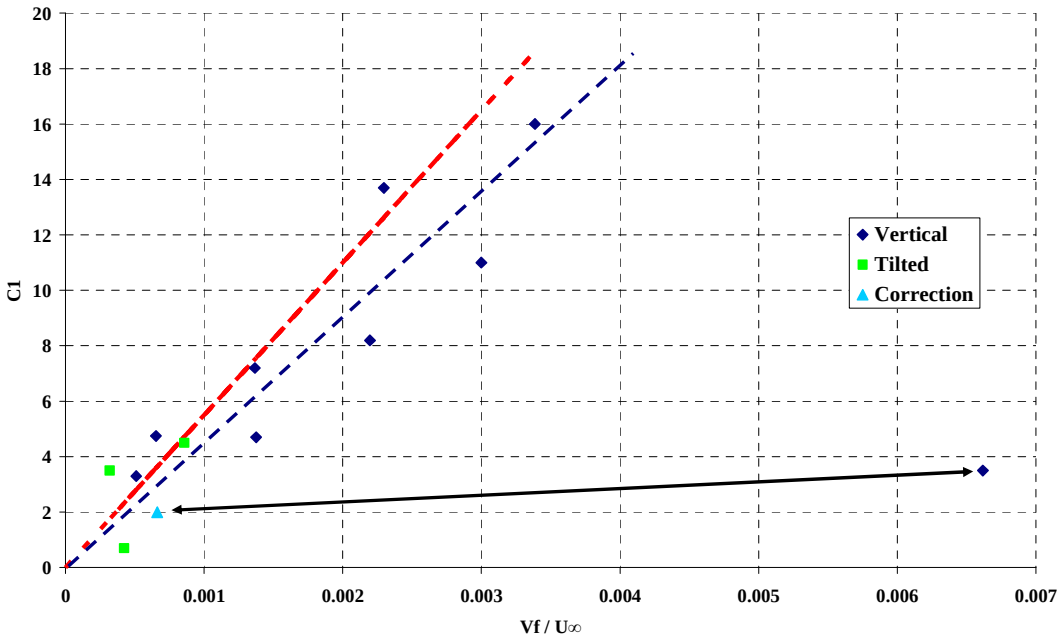

Figure 6.30 – *The plot shows the correlation for data taken from all of the lab experiments that the methodology could be successfully applied to. The slope of the dotted blue line corresponding to the inverse of the constant K in Equation 33 is 4500 which corresponds to a c_2 = 2.2. The red line represents c_2 = 1.8.*

The blue dotted line on the plot corresponds to the best fit of the results of the experimental data. According to the definition of the constant in Equation 34, the value of c_2 resulting from this best fit is $c_2 = 2.2$. The red line represents the result of $c_2 = 1.8$ that the correlation in Figure 6.29 indicates. The trends shown in Figure 6.29 and Figure 6.30 demonstrate that there is continuity in the optimised parameters resulting from the laboratory experiments. This would be expected given the high levels of repeatability in the sensor data and thus shows that there is also a level of repeatability inherent in the methodology.

Extrapolation to the more complicated scenario provided in the Dalmarnock Fire Test Sub-Experiment was not possible. Conditions within the scenario prevented some of the measurements techniques used in the lab such as PIV measurements from being used. The test also demonstrated the vulnerability of other techniques that were used, such as video footage and pyrolysis front tracking by temperature, to the complex conditions of a real fire scenario. Other parameters and methods must therefore be defined and included within the methodology to provide ignition time(s) and location(s). Future experiments should follow an evolution that gradually spans the gap between the laboratory experiments reported here and the conditions present in the Dalmarnock Tests.

Overall for application of the current methodology to concurrent flow flame spread, the limiting factor when extrapolating to more real fire scenarios is the amount and quality of sensor data. While the model should be sufficient for all concurrent flame spread scenarios, both new and current sensing techniques will need to be developed to make them more versatile to overcome the challenges provided by the more complex scenarios and environmental conditions.

7 Conclusions

This work has demonstrated that prediction of concurrent flow flame spread and properties of the spreading flame can be performed accurately and rapidly (faster than the event itself) by using a combination of data from purpose designed sensor techniques and 'simple' physical models that are representative of the processes being forecast. A methodology has be developed that performs this process using data from laboratory scale experiments involving concurrent flow flame spread ignited from a single ignition source. As data was collected from the sensors, the predictions generated and the scenario specific parameters optimised were seen to converge on accurate solutions. As the flame spread process evolved and the flame changed in nature, the output from the methodology re-converged to capture the new conditions and make fresh predictions based on them. An assessment has also been made of the limitations that must be overcome to make this technique viable in an end use scenario such as the compartment fire of the Dalmarnock Fire Tests.

The physical model adopted in this work proved ideal for this specific application. It describes the level of physics of the flame and spread process in terms of physical properties that are measurable by relatively simple and inexpensive sensors without the need for excessive, time consuming computation. The model used here is applicable to concurrent flow flame spread over various lengths, inclinations, and grades of 'thermally thick' PMMA. It is simple enough that calculations do not necessitate significant computational power. At the same time it captures the relevant phenomena for both the accurate calculation of flame spread and parameters that could be used in the assessment of heat transfer to the surroundings in conjunction with a larger prediction scenario.

The real crux of the method is the quality of measurements and density of measurement points. High quality and high density of data ensures that the conditions within the fire are captured rapidly and accurately. The evolution of the experiments has shown that sensing techniques can accurately capture the conditions of the experiments but need to be further developed to make them more robust to the variety of potential environmental conditions under which they may be needed to function. An entire range of qualities of sensing techniques were seen in this work. The heat flux gauges, although producing frequent data, were not suitable for a heat flux as weak as the ones present in the experiment and thus could only provide a qualitative assessment of when the radiant flux from the flame might have become significant. At the other extreme, the image processing of the flame length was high in quality and data density and provided a very clear indication of the evolution of the flame and likely conditions of the experiment. Somewhere between these extremes, the pyrolysis length measurement technique provided a magnitude and a basic trend when more data became available but after a change of conditions, time was required to accrue enough data points to make an accurate assessment of the new conditions. This technique was limited by the number of sensors and thus the number of data points produced. This shortcoming was counteracted slightly by the known relationship between this length and the flame length mentioned previously. It is important to understand and include such relationships in such methodologies to

ensure that physical characteristics are being captured correctly and enhance the knowledge of the situation being evaluated.

Despite the small role played by the Particle Image Velocimetry system in the actual application, it served as a good example of the balance needed between high quality data from complex measurement systems and the need for robust regular measurements. While the data it provides is highly detailed and affords high levels of information to a minute scale, the process of obtaining the measurements and condensing the output to a useful form is complex, highly intuitive and occasionally unreliable. Thus the robustness and reliability concerned with performing the actual measurement comes into question rather than output itself. The study of the Dalmarnock sub-experiment showed that the measurement techniques need to be robust to the range of expected fire conditions and thus should be designed with these conditions in mind. The most pertinent example of this is the image processing of camera images to measure the height of the flame which, in the controlled conditions of the lab experiments, provided reliable, robust, frequent data but was rendered useless in the compartment fire scenario due to the smoke layer build up. Thus the broader scope of application environments should be considered when designing measurement devices in future work.

The methodology developed here successfully coupled the sensor data from the lab scale experiments to the physical model. It produced predictions of flame spread rates and scenario specific parameters that converged in time on accurate solutions as more data was assimilated. In this respect it fulfilled its requirements well. The convergence showed that the adopted measurement techniques were capturing the physical characteristic of the scenario and the methodology was interpreting the data correctly with the use of an appropriate model.

The methodology makes use of existing knowledge of flame spread and flame characteristics to define the evolution of the time variant parameters and to optimise the scenario specific parameters. The knowledge of the relationship between pyrolysis and flame lengths in the spread process enabled the methodology to define the length being heated as part of the ‘flame spread as a solid ignition’ model from the data sets. This information also played an important role in evaluating the evolution of the pyrolysis front as the pyrolysis length data alone was not sufficient for this. The flame length data being far more populous depicted the trends of the growth of the flame far more clearly and when coupled with the pre-defined relationship between the length scales, could be used to define the like shape of the fit to the pyrolysis length data. This fit could then be extrapolated to give the spread rate over the period of time represented in the data.

The flame exhibits both laminar and turbulent characteristics in the experiments and knowledge of the heat flux composition in each of these regimes enables the methodology to separate the contributions of the convective and radiative portions due to the flame. This will be important when the scenarios are extended beyond a single burning item and knowledge of heat transfer between surfaces and surrounding mediums becomes important to successful prediction of fire growth. In

the current methodology the separation of the heat flux components allows for the optimisation of unknown parameters associated with a particular type of flux.

For the experiments analysed in this work, convergence of the scenario specific parameters and the predictions was highly reliant on the fit applied to the pyrolysis length data. More data points and a more robust method of measuring this would make the overall process more rapid and robust. More heat flux sensors and crucially for this application, a more accurate measurement of the various components of this parameter would help considerably, especially with the separation of convective and radiative heat flux to the unburned surface. Overall the methodology strikes a fine balance between the use of existing knowledge of the processes involved while not being reliant on existing correlations for provision of unknown parameters. Quantitative data is extracted from the sensor data by making use of pre-defined relationships but at the same time is not dependent on them.

Having established the nature of the disparity between the successful application of the methodology to the laboratory experiments described in this work and the failure to apply this methodology to the conditions observed in Dalmarnock Fire Test One, an evolution of experiments can be anticipated that will enable the methodology and sensing techniques to be developed to the level required for use in a scenario like Dalmarnock. Linear spread in a concurrent flow regime has been comprehensively covered here and concurrent turbulent flame spread has also been undertaken with some success. Longer experiments to provide longer periods of turbulent behaviour and confirm the models ability to capture the radiant heat flux and acceleration during a turbulent regime should be conducted. A collection of downward or sideways flame spread experiments at laboratory scale should be conducted to ensure that the methodology extrapolates to similar scenarios at this scale when used with an appropriate model. Once simple scenarios have been comprehensively covered and methodologies developed to encapsulate these basic spread processes, the experiments should progress in complexity toward the scenario observed in Dalmarnock Fire Test One. This could be achieved through the complication of the surrounding environment with radiant panels or pool fires providing external sources of heat flux to the surface other than simply the heating produced by the flame itself. This could then be extended to predictions of multi-item ignition and subsequent surface flame spread. In order for these experiments to be successful, the measurement techniques would also need to evolve to ensure that sufficient data is available to the models. The end use scenario should be kept in mind when developing the techniques to ensure they are not as specific to the experimental scenario as the techniques developed in this work proved to be.

In summary, this work has demonstrated the potential of integrating modelling and sensing techniques to achieve rapid robust predictions of fire scenarios which would support fire fighters in mitigating an evolving fire emergency. Sensing techniques alone can provide huge quantities of data but lack appropriate interpretation. Models provide a method of interpretation but lack the information and data to make their output robust and reliable. Combining the two in the form of theoretical models steered by continuous calibration against sensor measurements will compensate for the deficiencies of the individual tools when used in isolation.

8 References

[1] Abecassis-Empis, C., Reszka, P., Steinhaus, T., Biteau, H., Cowlard, A., Welch, S., Rein, G., Torero, J.L., "*Characterisation of Dalmarnock Fire Test 1*", Experimental Thermal and Fluid Science, 32 (2008), 1334 – 1343.

[2] Alston, J., *Room/Corner Fire Calibration Data: Marine Composite Screening Specimens*, Master's Thesis, Worcester Polytechnic Institute, May 2004.

[3] Amundarian, A., *Assessment of the Thermal Efficiency, Structure and Fire Resistance of Lightweight Building Systems for Optimized Design*, PhD Thesis, University of Edinburgh, April 2007.

[4] ASTM E459 - 05: Standard Test Method for Measuring Heat Transfer Rate Using a Thin-Skin Calorimeter

[5] Audouin, L., Kolb, G., Torero, J.L., Most, J.M., *Average Centreline Temperatures of a Buoyant Pool Fire Obtained by Image Processing of Video Recordings*, Fire Safety Journal, 24 (1995), p167 – 187.

[6] Arakawa, A., Saito, K., Gruver, W.A., *Automated Infrared Imaging Temperature measurement with Application to Upward Flame Spread Studies - Part 1*, Combustion and Flame, 92 (1993), p222 – 230.

[7] Berry, D., Usmani, A., Torero, J.L., Tate, A., McLaughlin, S., Potter, S., Trew, A., Baxter, R., Bull, M, Atkinson, M., *FireGrid: Integrated emergency response and fire safety engineering for the future built environment*, (2005).

[8] Biran, A. and Breiner, M., 1995, *Matlab for Engineers*, Addison-Wesley, ISBN 0-201-56524-2.

[9] Brehob, E.G and Kulkarni, A.K., *Experimental Measurements of Upward Flame Spread on a Vertical Wall with External Radiation*, Fire Safety Journal, 31 (1998), p181 – 200.

[10] Bodor R, Jackson B, Papanikolopoulos N (2003) *Vision-based human tracking and activity recognition*. In: Proceedings of the 11th Mediterranean conference on control and automation.

[11] BS EN 60584-1:1996, IEC 60584-1:1995. Thermocouples. Reference tables

[12] Carvalho, M.G., Proc. Of the 1st Mediterranean Combustion Symposium, 1999

[13] Conslavi et al., *Diffusion Flames Upwardly Propagating over PMMA: Theory, Experiment and Numerical Modelling*, IAFSS Proceedings, (2005).

[14] Consalvi, J.L., Pizzo, Y., Porterie, B., Torero, J.L., *On the Flame Height Definition for Upward Flame Spread*, Fire Safety Journal, 42 (2007), 384 – 392.

[15] Cowlard, A., Steinhaus, T., Abecassis-Empis, C., Torero, J.L., "*Test Two: The 'Controlled Fire'*", Chapter 4 - The Dalmarnock Fire Tests ISBN: 978-0-9557-497-0-4.

[16] Cowlard, A, Jahn, W., Abecassis-Empis, C., Rein, G., Torero, J.L., *Sensor Assisted Fire Fighting*, Accepted for publication in Fire Technology (Nov 2008).

[17] Cox, G. et al, 1995, *Combustion Fundamentals of Fire-Chapter 2-The Solid Phase - Fernandez-Pello, A.C.*, Academic Press Ltd, ISBN 0-12-194230-9.

[18] Cox, G. & Kumar, S., Modelling enclosure fires using CFD modelling, in DiNenno (ed.), SFPE handbook of fire protection engineering, 3rd ed., NFPA, Quincy, MA, 2002, pp. 3-194 to 3-218.

[19] Dakka et al., *Mechanisms Controlling the Degradation of Poly(methylmethacrylate) prior to Piloted Ignition*, Proceedings of the Combustion Institute Vol. 29.

[20] Delichatsios, M.A., *Flame heights in turbulent wall fires with significant flame radiation*. Combustion Science and Technology, 39 (1984), p195 – 214.

[21] Di Blasi, C., *Influences of Sample Thickness on the Early Transient Stages of Concurrent Flame Spread and Solid Burning*, Fire Safety Journal, 25 (1995), p287 – 304.

[22] Dorigo, M., Socha, K., An *Introduction to Ant Colony Optimisation*, IRIDIA Technical Report Series, No. TR/IRIDIA/2006-010, April 2006, ISSN 1781-3794.

[23] Dorigo, M., Maniezzo, V., Colorni, A., The Ant System: Optimisation by a colony of cooperating agents, Submitted to Transactions on Systems, Man and Cybernetics.

[24] Drysdale, D.D., 1998, *An Introduction to Fire Dynamics 2nd Edition*, Wiley and Sons, ISBN 0-471-97291-6.

[25] Elliott, L., Ingham, D.B., Kyne, A.G., Mera, N.S., Pourkashanian, M., Wilson, C.W., Genetic Algorithms for Optimisation of Chemical Kinetics Reaction Mechanisms, Progress in Energy and Combustion Science, 30 (2004), p297 – 328.

[26] Fernandez-Pello, A.C., *A Theoretical Model for the Upward Laminar Spread of Flames over Vertical Fuel Surfaces*, Combustion and Flame, 31 (1978), p135 – 148.

[27] Fernandez-Pello, A.C., *Downward Flame Spread Under the Influence of Externally Applied Thermal Radiation*, Combustion, Science and Technology, 17 (1977), p1 – 9.

[28] Fernandez-Pello, A.C., *Flame Spread in a Forward Forced Flow*, Combustion and Flame, 36 (1979), p63 – 78.

[29] Fernandez-Pello, A.C., *Upward Laminar Flame Spread under the Influence of Externally Applied Thermal Radiation*, Combustion, Science and Technology, 17 (1977), p87 – 98.

[30] Fernandez-Pello, A.C., Hirano, T., *Controlling Mechanisms of Flame Spread*, Combustion, Science and Technology, 32 (1983), p1 – 31.

[31] Fernandez-Pello, A.C. and Mao, C.P., *A Unified Analysis of Concurrent Modes of Flame Spread*, Combustion, Science and Technology, 26 (1981), p147 – 155.

[32] Fernandez-Pello, A.C. and Williams, F.A., *Experimental Techniques in the Study of Laminar Flame Spread over Solid Combustibles*, Combustion, Science and Technology, 14 (1976), p155 – 167.

[33] Fernandez-Pello, A.C., Williams, F.A., *Laminar Flame Spread Over PMMA Surfaces*, Fifteenth Symposium (International) on Combustion, The Combustion Institute, p217 – 231.

[34] Foley, M., Drysdale, D. D., *Heat transfer from flames between Vertical Parallel Walls*, Fire Safety Journal, 24 (1995), p53 – 73.

[35] Foley, M., 1995, *The Use of Small Scale Fire Test Data for the Hazard Assessment of Bulk Materials*, PhD Thesis, University of Edinburgh.

[36] French, T., et al., In Production, (2009).

[37] Fuentes, A., PhD Thesis, (2007).

[38] Gavrila, D.M., Davis, L.S., *Towards 3-D Model Based Tracking and Recognition of Human Based Movement: a Multi-View Approach*, Int Workshop on Face and Gesture Recognition, Zurich, 1995.

[39] Goldberg, D.E., 1989, *Genetic Algorithms in Search, Optimisation, and Machine Learning*, Addison-Wesley Publishing Company, Inc., ISBN 0-201-15767-5.

[40] Hahn, B.D., 2002, *Essential Matlab for Scientists and Engineers 2nd Edition*, Butterworth - Heinemann, ISBN 0-7506-5240-3

[41] Hasemi, Y., *Thermal Modelling of Upward Flame Spread*, Fire Safety Science – Proceedings of the First International Symposium, p87 – 96

[42] Incropera, F.P., DeWitt, D.P., 1996, *Fundamentals of Heat and Mass Transfer 4th Edition*, Wiley and Sons, ISBN 0-471-30460-3

[43] Ingason, H., De Ris, J., *Flame Heat Transfer in Storage Geometries*, Fire Safety Journal, 31 (1998), p39 - 60.

[44] Ingason, H., Wickstrom, U., *Measuring Incident Radiant Heat Flux Using a Plate Thermometer*, Fire Safety Journal, 42 (2007), p161 – 166.

[45] Jahn, W., Rein, G., Torero, J.L., *The Effect of Model Parameters on the Simulation of Fire Dynamics*, Fire Safety Science (in press), 2008.

[46] Kulkarni, A. K., *Upward Flame Spread of Vertical Walls*, NIST-GCR-89-565.

[47] Kulkarni, A. K., Kim, C. I., Kuo, C. H., *Turbulent Upward Flame Spread for Burning Vertical Walls made of Finite Thickness*, NIST Grant No. 60NANB8D0849.

[48] Lautenberger, C., Rein, G. and Fernandez-Pello, A.C., *The Application of a Genetic Algorithm to Estimate Material Properties for Fire Modelling From Bench-Scale Fire Test Data*, Fire Safety Journal, 41(3) (2006), p204 – 214.

[49] Lewis, M.J., Moss, J.B., Rubini, P.A., *CFD Modelling Of Combustion And Heat Transfer In Compartment Fires*, Fire Safety Science 5, (1997) p463 – 474.

[50] Meacham, B., Sarkis, J., Dembsey, N., *Adaptive Management in Fire Regulation and Emergency Response*, Fire Safety Science – Proceedings of the Ninth International Symposium.

[51] Miller-Hooks, E., Krauthammer, T., *An Intelligent Evacuation, Rescue and Recovery Concept*, Fire Technology, 43 (2007), p107 – 122.

[52] Mitchell, M., 1996, *An Introduction to Genetic Algorithms*, Massachusetts Institute of Technology, ISBN 0-262-13316-4 (HB), 0-262-63185-7 (PB), http://mitpress.mit.edu.

[53] Mittal, A., Huttenlocher, D., *Scene Modelling for Wide Area Surveillance and Image Synthesis*, IEEE Press, 2000.

[54] National Institute for Standards and Technology (NIST), *Final Report on the Collapse of World Trade Centre Building 7*, Federal Building and Fire Safety Investigation of the World trade Centre Disaster, NIST-NCSTAR-1A.

[55] Neviackas, A., Trouve, A., *Sensor-Driven Zone Modelling of Enclosure Fire Dynamics,* Abstract Only, Corresponding Author: atrouve@umd.edu.

[56] Niioka, T., Takahashi, M., Izumikawa, M., Gas Phase *Ignition of a Solid Fuel in a Hot Stagnation-Point Flow,* Proceedings of the 18th Symposium (International) on Combustion, (1981) p741 – 747.

[57] Ohlemiller, T., Cleary, T., Shields, J., *Effect of ignition conditions on upward flame spread on a composite material in a corner configuration*, Fire Safety Journal, 31 (1998), p331 – 344.

[58] Ohlemiller, T. J. Cleary, T.G., *Upward flame spread on composite materials*, Fire Safety Journal, 32 (1999), p159 – 172.

[59] Orloff, L., De Ris, J., and Markstein, G.H., *Upward Turbulent Fire Spread and Burning of Fuel Surface*, 15th Symposium (International) on Combustion, The Combustion Institute, (1974) p253 – 264.

[60] Park, T.Y., Froment, G.F., *A Hybrid Genetic Algorithm for the Estimation of Parameters in Detailed Kinetic Models*, European Symposium on Computer Aided Process Engineering – 8, pS103 – S110.

[61] Rangawala, A., *Flame Spread Analysis using a Variable B-Number*, PhD Thesis, University of California at San Diego, 2006.

[62] Rangwala, A.S., Buckley, S.G., Torero, J.L., *Upward Flame Spread on a Vertically Orientated Fuel Surface: The Effect of Finite Width*, Proceedings of the Combustion Institute, 31 (2007), p2607 – 2615.

[63] Rein, G., Lautenberger, C., Fernandez-Pello, A.C., Torero, J.L., Urban, D.L., *Application of Genetic Algorithms and Thermogravimetry to Determine the Kinetics of Polyurethane Foam in Smouldering Combustion*, Combustion and Flame, 146 (2006) p95 – 108.

[64] Rein et al. (Combustion Science and Technology, 2004)

[65] Rein, G., Abecassis-Empis, C., Amundarain, A., Biteau, H., Cowlard, A., Chan, A., Jahn, W., Jowsey, A., Reszka, P., Steinhaus, T., Carvel, RO., Welch, S., Torero, J.L., Stern-Gottfried, J., Hume, B., Coles, A., Lazaro, M., Alvear, D., Capote, J.A., Desanghere, S., Joyeux, D., Ryder, N.L., Schemel, C., Mowrer, F., "*Round-Robin Study of Fire Modelling Blind-Predictions using the Dalmarnock Fire Experiments*", 5th International Seminar on Fire and Explosion Hazards, Edinburgh, April 2007. (1st Prize FM Global Awards for best papers). Also presented at Advanced Research Workshop on Fire Computer Modelling, Santander, October 2007.

[66] Saito, K., Quintiere, J.G., Williams, F.A., *Upward Turbulent Flame Spread*, Fire Safety Science - Proceedings of the First International Symposium, p75 – 86.

[67] Schmitt, L.M., *Theory of Genetic Algorithms*, Theoretical Computer Science, 259 (2001), p1 – 61.

[68] Seitz, .S.M., Dyer, C.R., *Photorealistic Scene Reconstruction by Voxel Coloring*, Univ. of Wisconsin, Madison Report, 1998.

[69] Sohn, H., *A review of structural health monitoring literature 1996-2001*, Proceedings of the Third World Conference on Structural Control, Volume 2 (2003), p9 – 15.

[70] Tewarson, A. and Ogden, S.D., *Fire Behaviour of Polymethylmethacrylate*, Combustion and Flame, 89 (1992), p237 – 259.

[71] Thomas, P. H., On *Concurrent Upward Surface Spread of Flame*, Fire Safety Journal, 22 (1994), p89 – 99.

[72] Thomson, H.E., Drysdale, D.D. and Beyler, C.L., *An Experimental Evaluation of Critical Surface Temperature as a Criterion for Piloted Ignition of Solid Fuels*, Fire Safety Journal, 13 (1988), p185 – 196.

[73] Torero et al. (Combustion Science and Technology, 2001)

[74] Tsai, K-C., Turnbull, J., Will, G., Drysdale, D., *Upward Flame Spread: Heat Transfer to the Unburned Surface*, Fire Safety Science – Proceedings of the Seventh International Symposium, p117 – 128.

[75] Upadhyay, R., Pringle, G., Beckett, G., Potter, S., Han, L., Welch, S., Usmani, A., Torero, J.L., *An Architecture for an Integrated Fire Emergency Response System for the Built Environment*, Fire Safety Science – Proceedings of the Ninth International Symposium.

[76] Upadhyay, R., Beckett, G., Pringle, G., Potter, S., Han, L., Welch, S., Usmani, A., Torero, J.L., *A System Architecture for Technology Integrations in FireGrid: An Integrated Fire Emergency Response System for the Built Environment*, Fire Safety Science, (in press) (2008)

Web pages

W[1] Oxford Lasers, United Kingdom, www.oxfordlasers.com

W[2] R&D Vision, France, www.rd-vision.com

W[3] ILA, Germany, www.ila.de

W[4] Ant Colony Optimisation, Wikipedia Online Encyclopaedia, http://en.wikipedia.org/wiki/Ant_colony_optimisation [Last accessed 30 Jan 09]

W[5] Gentic Algorithms, Wikipedia Online Encyclopaedia, http://en.wikipedia.org/wiki/Genetic_algorithms [Last accessed 30 Jan 09]

W[6] Regression Analysis, Wikipedia Online Encyclopaedia, http://en.wikipedia.org/wiki/Regression_analysis [Last accessed 30 Jan 09]

W[7] Laser Doppler Velocimetry, Wikipedia Online Encyclopaedia, http://en.wikipedia.org/wiki/Laser_Doppler_Velocimetry [Last accessed 02 Feb 09]

W[8] Hot Wire Anemometer, Wikipedia Online Encyclopaedia, http://en.wikipedia.org/wiki/Hot-wire_anemometry#Hot-wire_anemometers [Last accessed 02 Feb 09]

W[9] Pitot Tube, Wikipedia Online Encyclopaedia, http://en.wikipedia.org/wiki/Pitot_tube [Last accessed 02 Feb 09]

Appendix 1. - Derivation of h_{conv} Term for Equation 14

Equation 14 introduces a term for the convective heat flux to the surface that describes it as a function of physical parameters: -

$$\dot{q}''_{conv} = h_{conv}(T_f - T_p) = (c_1 k_g \rho_g c_p \frac{u_\infty}{l_p})^{1/2}(T_f - T_p)$$

Eq. 1

The value h_{conv} is the convective heat transfer coefficient which through comparison, can be seen to take the following form: -

$$h_{conv} = (c_1 k_g \rho_g c_p \frac{u_\infty}{l_p})^{1/2}$$

Eq. 2

Equation 3 shows the Nusselt number for laminar flow, parallel to a flat plate of length x which is also product of the heat transfer coefficient.

$$Nu = \frac{h_{conv} x}{k} = 0.66 \mathrm{Re}^{1/2} \mathrm{Pr}^{1/3}$$

Eq. 3

where the Reynolds number is defined by; -

$$\mathrm{Re} = \frac{x u_\infty \rho}{\mu} = x u_\infty \nu$$

Eq. 4

And the Prandtl Number is defined by: -

$$\mathrm{Pr} = \frac{\alpha}{\nu}$$

Eq. 5

Thus substituting Eq. 4 into Eq. 3: -

$$h_{conv} = \frac{2}{3}[x u_\infty \nu]^{1/2} \Pr^{1/3} \frac{k}{x}$$

$$h_{conv} = \left[\frac{4}{9}\right]^{1/2} \nu^{1/2} \left[\Pr^{2/3}\right]^{1/2} \left[k^2\right]^{1/2} \frac{u_\infty^{1/2}}{x^{1/2}}$$

$$h_{conv} = \left[\frac{4}{9} \nu \Pr^{2/3} k^2 \frac{u_\infty}{x}\right]^{1/2}$$

Eq. 6

Given $\alpha = \frac{k}{\rho c_p}$ and thus $k = \alpha \rho c_p$

Eq. 7

Substituting Equation 7 into Equation 6 gives: -

$$h_{conv} = \left[\frac{4}{9} \nu \Pr^{2/3} \alpha k \rho c_p \frac{u_\infty}{x}\right]^{1/2}$$

$$h_{conv} = \left[c_1 k_g \rho_g c_p \frac{u_\infty}{l_p}\right]^{1/2}$$

Where c_1 is a constant of the form: -

$$c_1 = \frac{4}{9} \nu \alpha \Pr^{2/3}$$

Eq. 8

Appendix 2. - Derivation of Pyrolysis Length Curve Fit

The curve fit defined in Chapter 5 is derived from the flame spread model defined in Chapter 3 with the expression relating the flame length as a power function of the pyrolysis length substituted in: -

$$V_f = \frac{4c_2[(c_1 k_g \rho_g c_p u_\infty / l_p{}^n)^{1/2}(T_f - T_p) + \dot{q}''_{fr} + \dot{q}''_e - \dot{q}''_{rs}]^2 l_p{}^n}{\pi k_s \rho_s c_s (T_p - T_0)^2}$$

Grouping the constant terms as: -

$$K_1 = \frac{4c_2}{\pi k_s \rho_s c_s (T_p - T_0)^2}$$

$$K_2 = (c_1 k_g \rho_g c_p u_\infty)^{1/2}(T_f - T_p)$$

$$Q = \dot{q}''_{fr} + \dot{q}''_e - \dot{q}''_{rs}$$

And also substituting the following expression for V_f: -

$$V_f = \frac{dl_p}{dt}$$

The following relationship can be defined: -

$$\frac{dl_p}{dt} = K_1[K_2 + Ql_p^{n/2}]^2$$

Which when rearranged gives: -

$$dt = \frac{1}{K_1[Ql_p^{n/2} + K_2]^2} dl_p$$

By substituting, rearranging and differentiating to form an expression for dl_p: -

$$dt = \frac{dl_p}{K_1 u^2} \text{ - (1)} \qquad \text{where} \qquad u = Ql_p^{n/2} + K_2$$

$$l_p^{n/2} = \frac{1}{Q}[u - K_2]$$

$$l_p^{n} = \frac{1}{Q^2}[u - K_2]^2$$

$$l_p = \left[\frac{u^2 + K_2^2 - 2uK_2}{Q^2}\right]^{1/n}$$

$$l_p = y^{1/n} \qquad \text{where} \qquad y = \left[\frac{u^2 + K_2^2 - 2uK_2}{Q^2}\right]$$

$$\frac{dl_p}{dy} = \frac{y^{1/n-1}}{n} \qquad \text{and} \qquad \frac{dy}{du} = \left[\frac{2u - 2K_2}{Q^2}\right]$$

$$\frac{dl_p}{dy}.\frac{dy}{du} = \frac{dl_p}{du} = \frac{y^{1/n-1}}{n}.\frac{2}{Q^2}.[u - K_2]$$

$$\frac{dl_p}{du} = \frac{2}{Q^2 n}.[u - K_2].y^{1/n-1}$$

$$\frac{dl_p}{du} = \frac{2}{Q^2 n}.[u - K_2].\frac{1}{Q^2}.[u - K_2]^2$$

$$\frac{dl_p}{du} = \frac{2}{Q^4 n}.[u - K_2]^3$$

$$dl_p = \frac{2}{Q^4 n}.[u - K_2]^3.du$$

And substituting the resultant expression for dl_p into (1): -

$$dt = \frac{dl_p}{K_1 u^2} \qquad \Rightarrow \qquad \int dt = \frac{2}{K_1 Q^4 n} \int \frac{(u - K_2)^3}{u^2} du$$

$$\int dt = \frac{2}{K_1 Q^4 n} \int (u - 3K_2 + 3K_2 u^{-1} - K_2{}^3 u^{-2}) du$$

Integrating gives: -

$$t = \frac{2}{K_1 Q^4 n} \left[\frac{u^2}{2} - 3K_2 u + 3K_2 Ln(u) - \frac{K_2{}^3}{u} + K_3 \right]$$

Substituting: -

$$u = Q l_p{}^{n/2} + K_2$$

And rearranging gives: -

$$t = \frac{2}{K_1 Q^4 n} \left[\frac{1}{2} (Q l_p{}^{\frac{n}{2}} - 5K_2)(Q l_p{}^{\frac{n}{2}} - K_2) + 3K_2 Ln(Q l_p{}^{\frac{n}{2}} - K_2) + \frac{K_2{}^3}{(Q l_p{}^{\frac{n}{2}} - K_2)} + K_3 \right]$$

Appendix 3. – Experimental Results

Pyrolysis and Flame Length Measurements

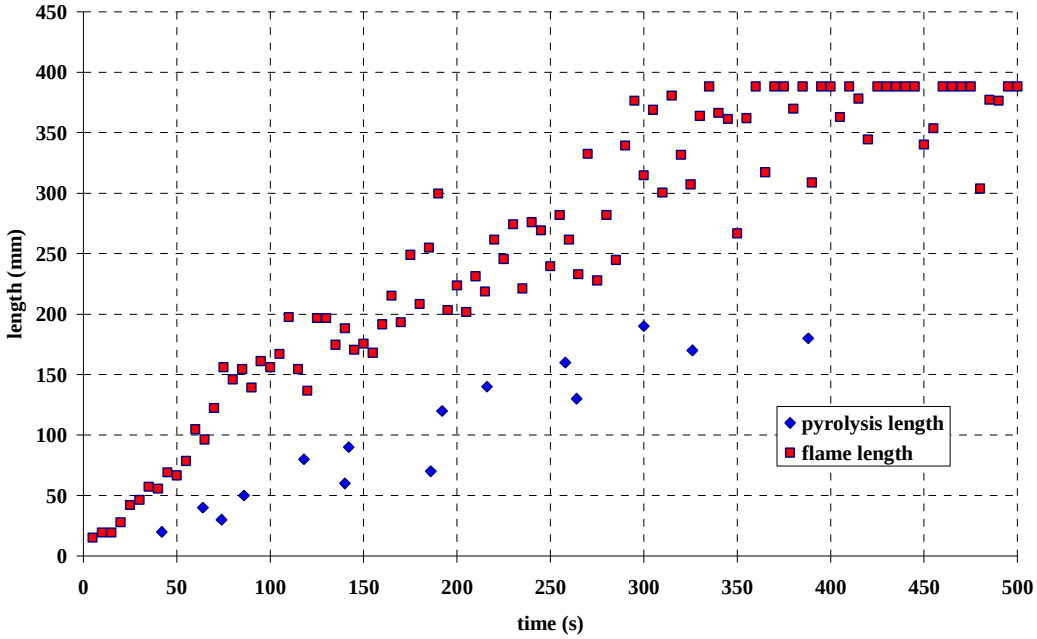

Experiment 1

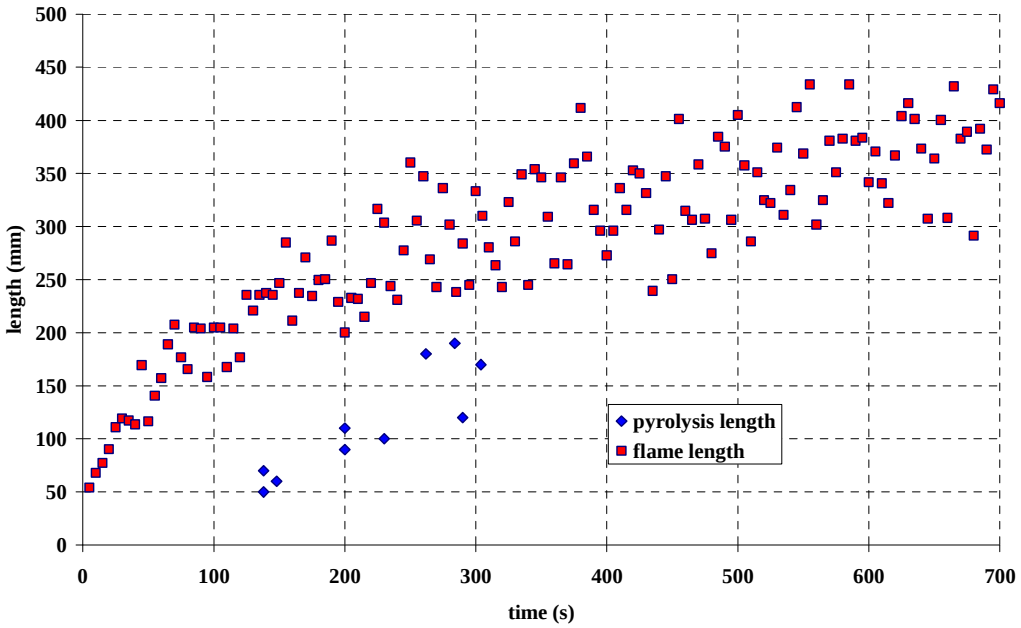

Experiment 2

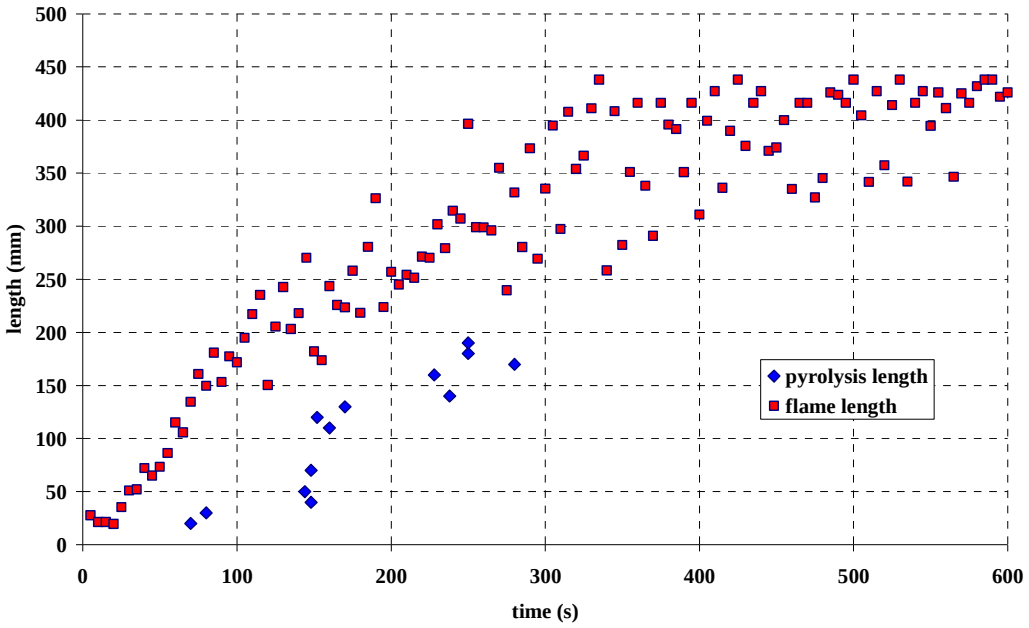

Experiment 3

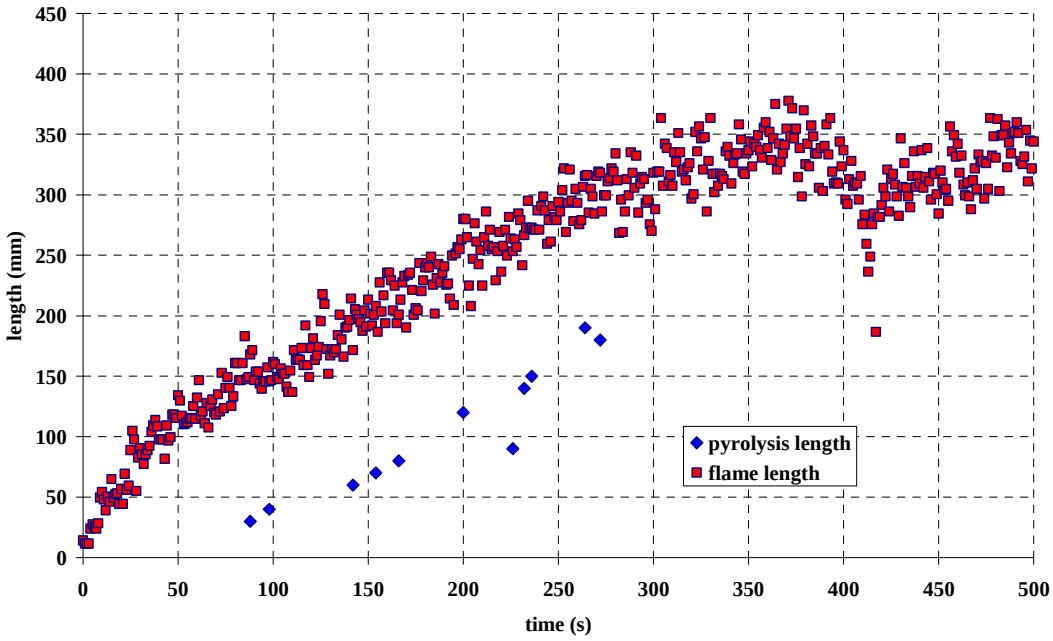

Experiment 4

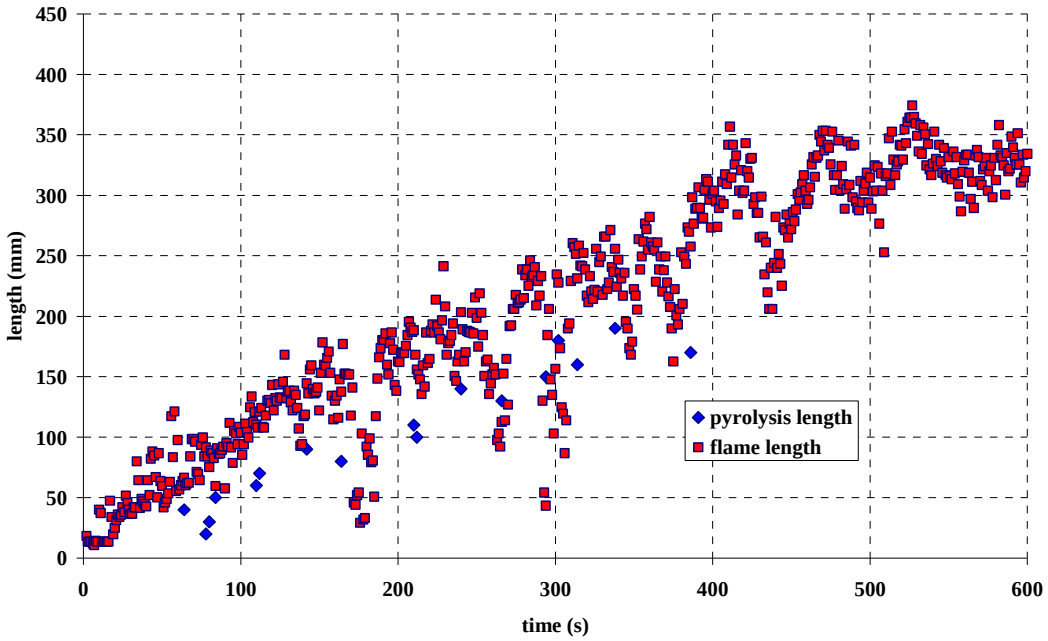

Experiment 5

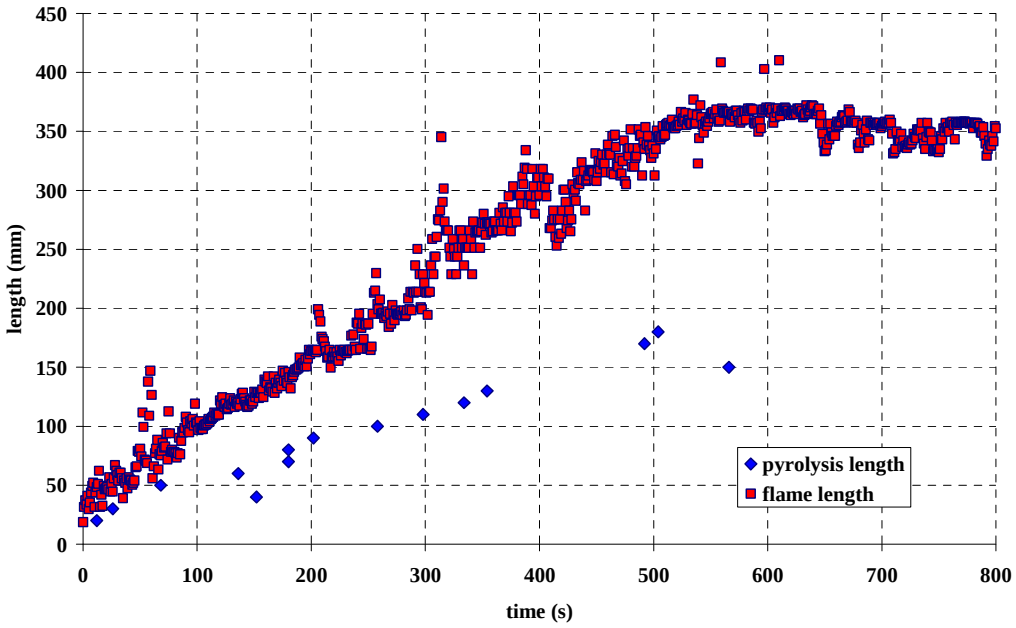

Experiment 6

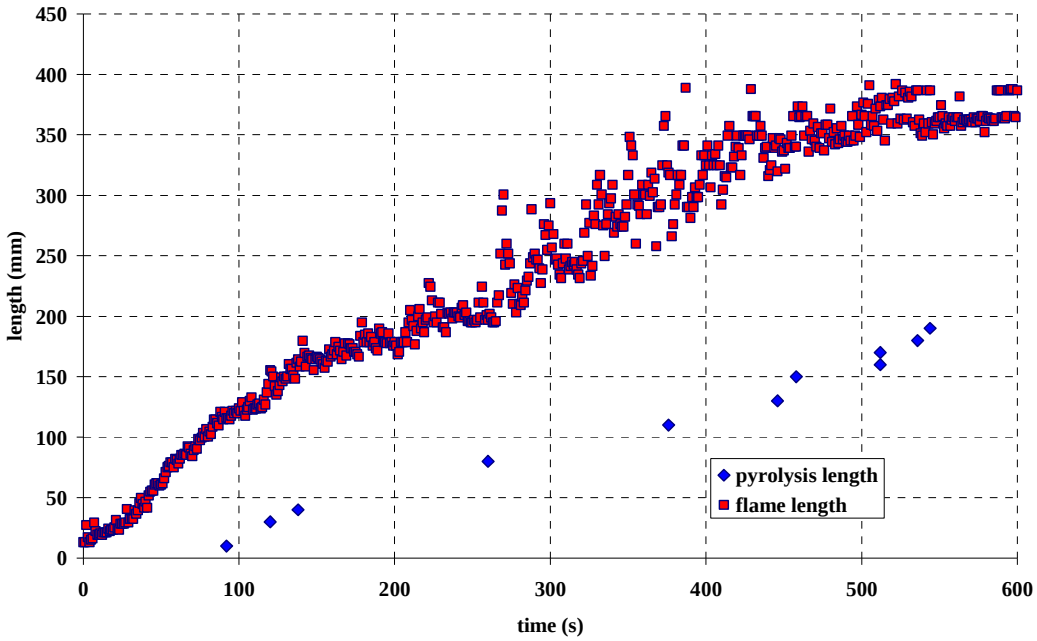

Experiment 7

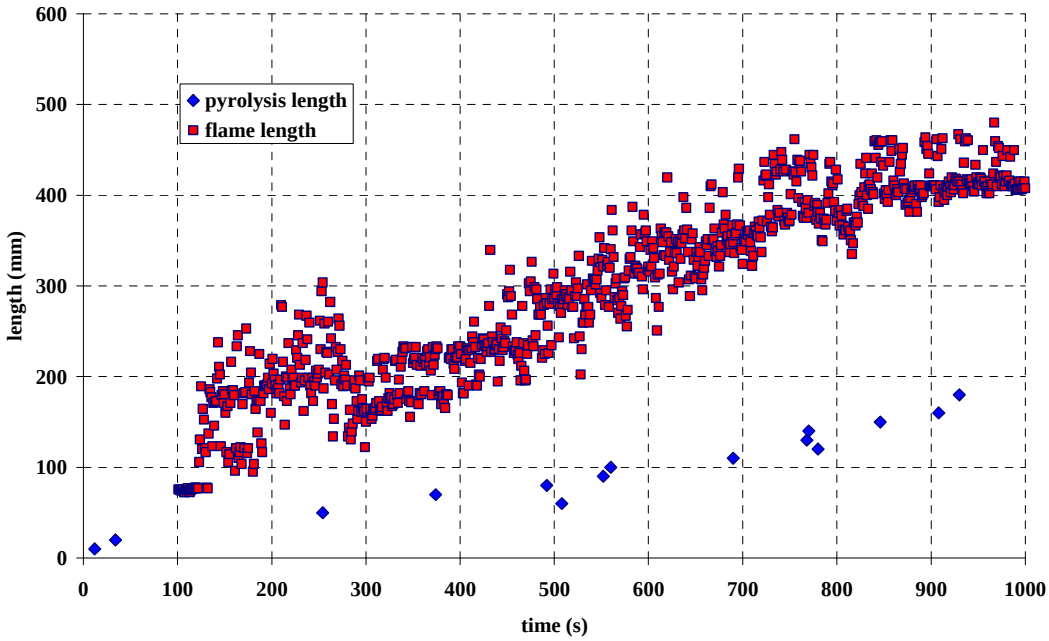

Experiment 9

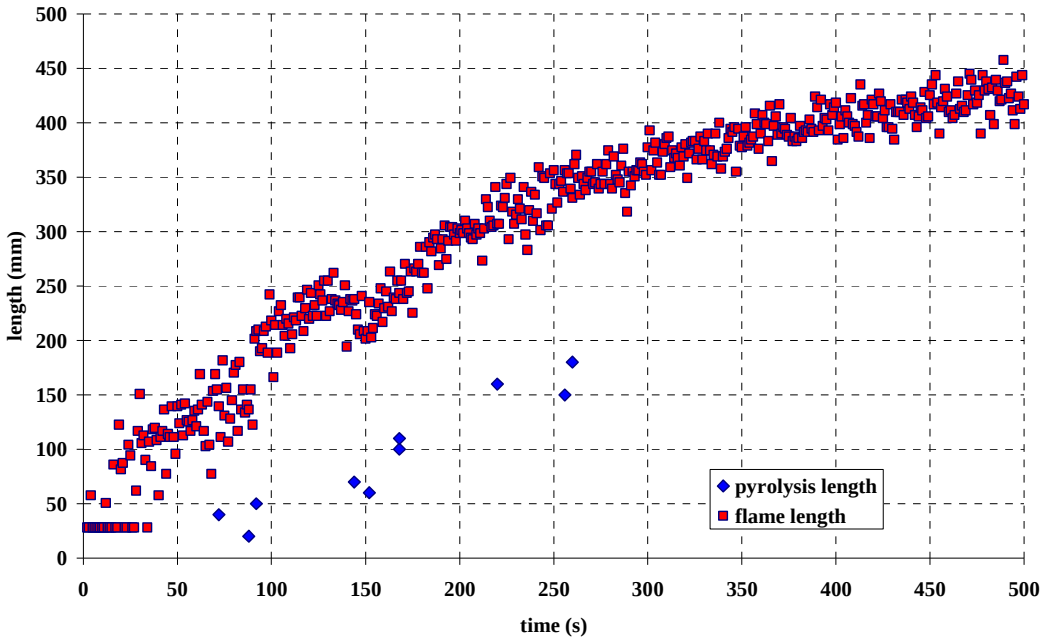

Experiment 10

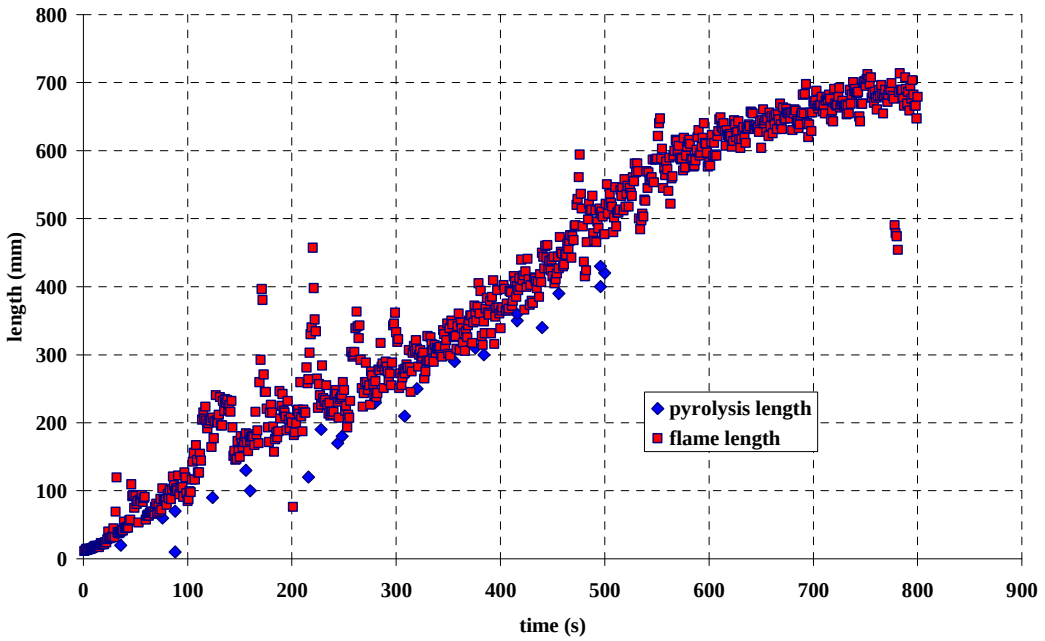

Experiment 11

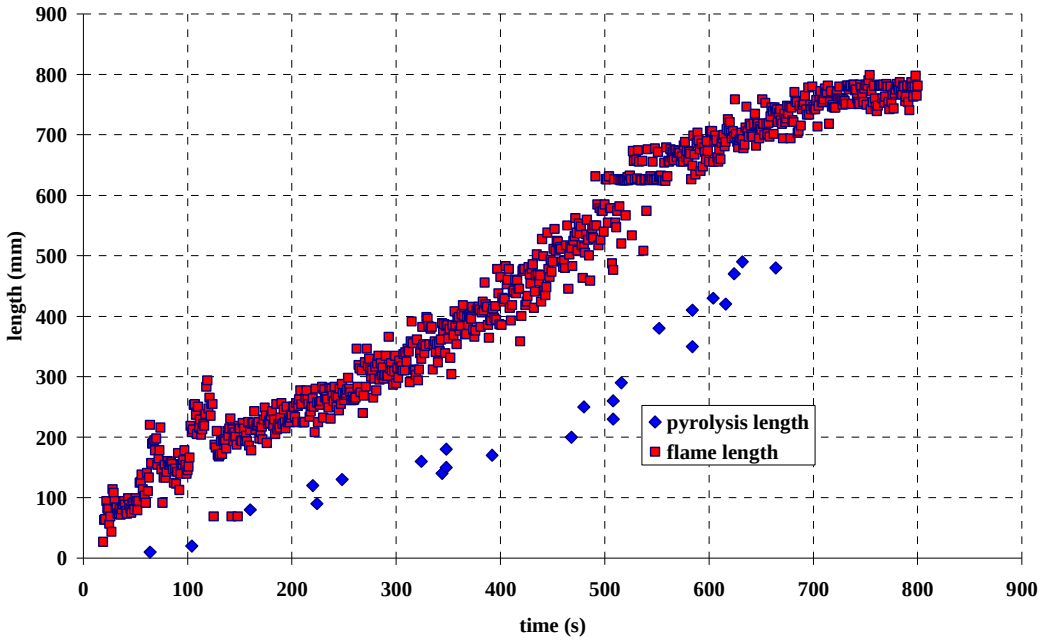

Experiment 12

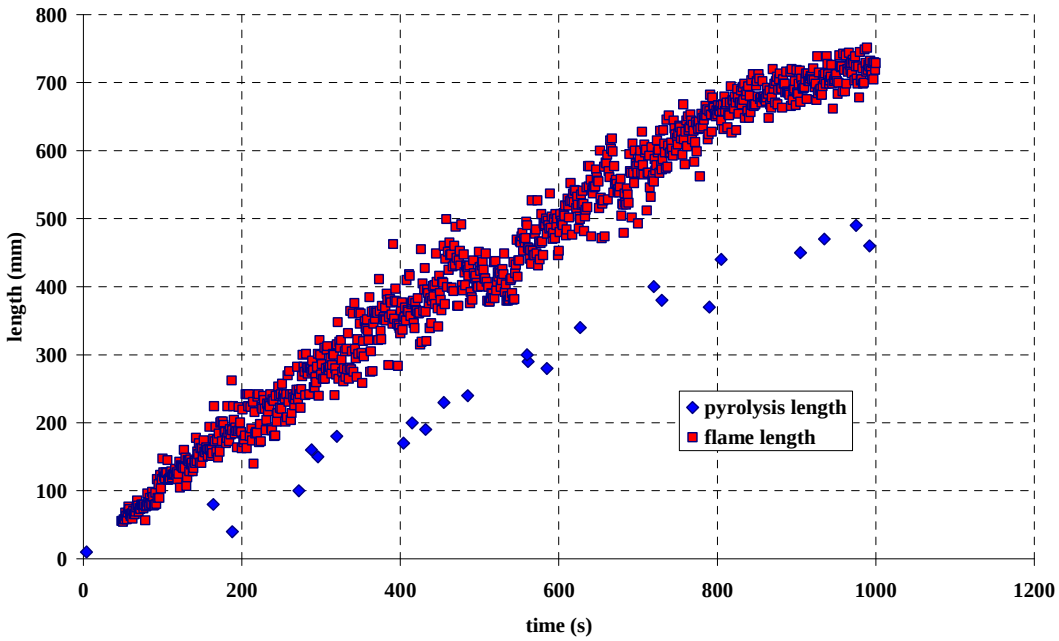

Experiment 13

Ambient Air Velocity Measurements

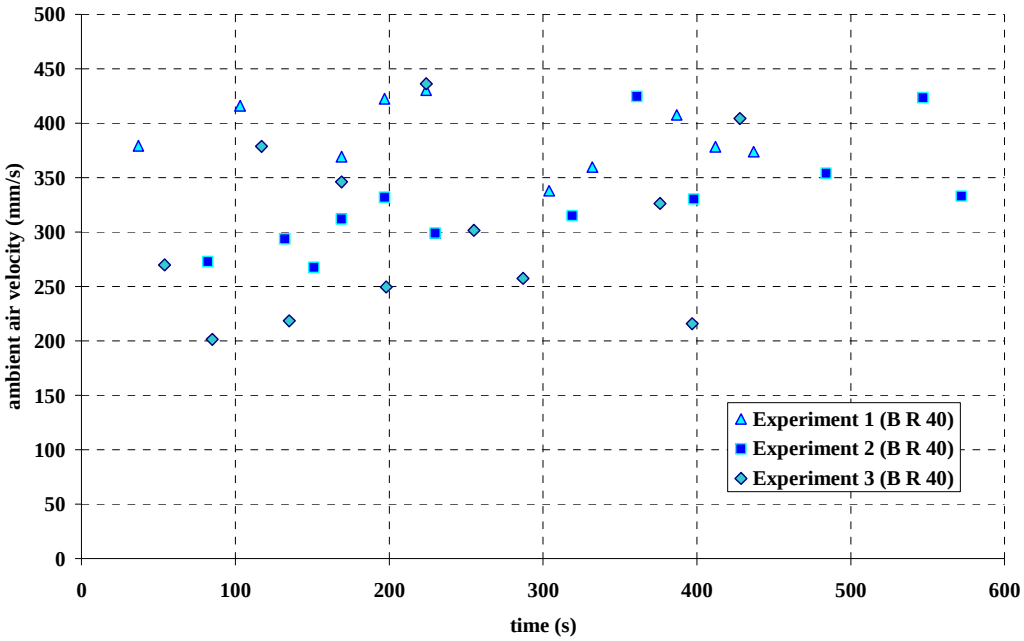

Benchmark Style 200mm Sample Experiments

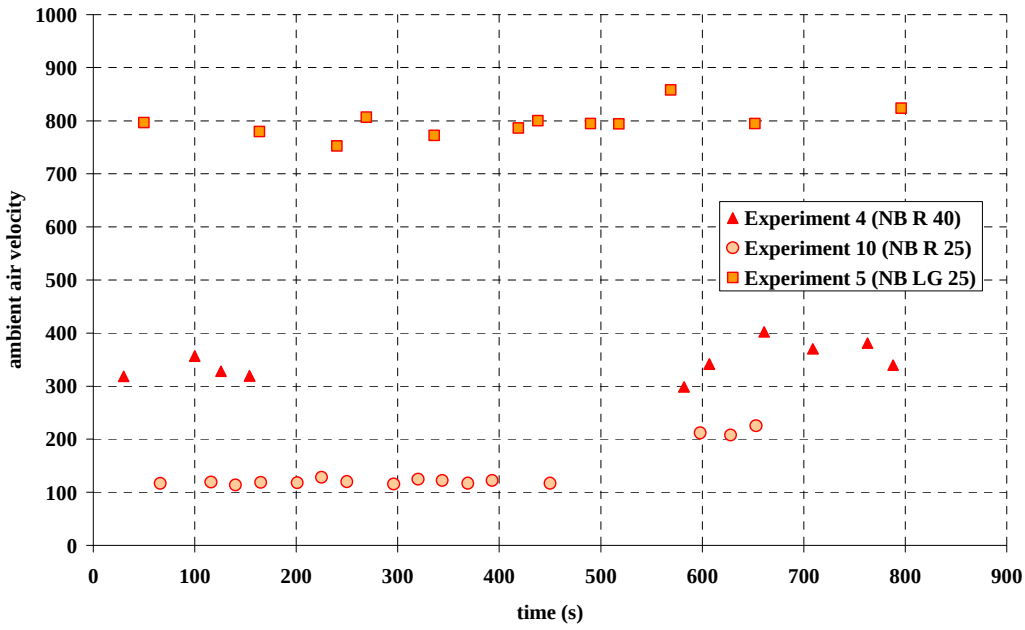

Regular 200mm Sample Experiments

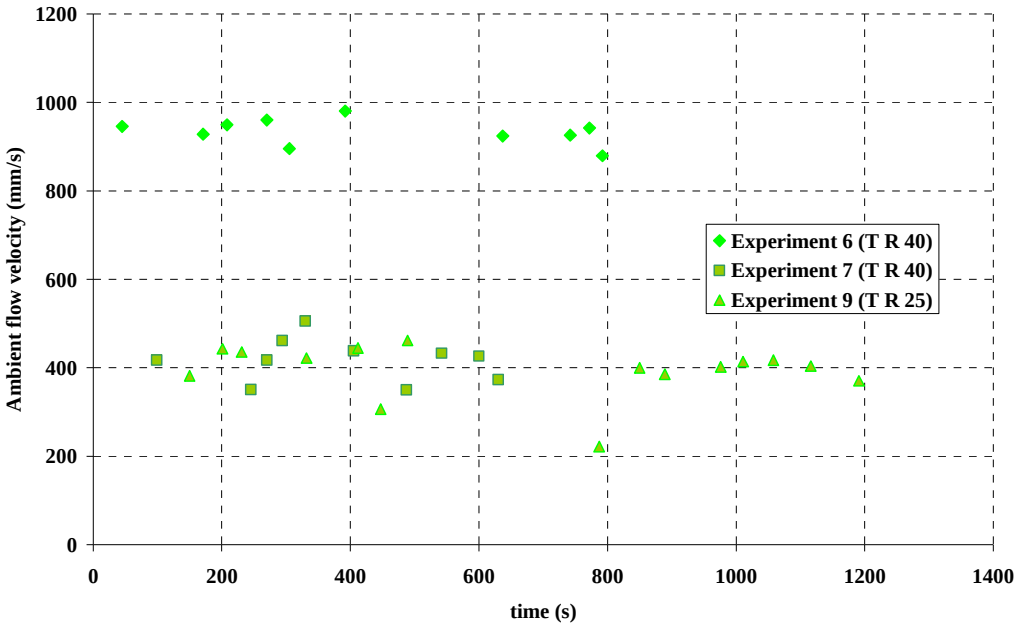

Tilted 200mm Sample Experiments

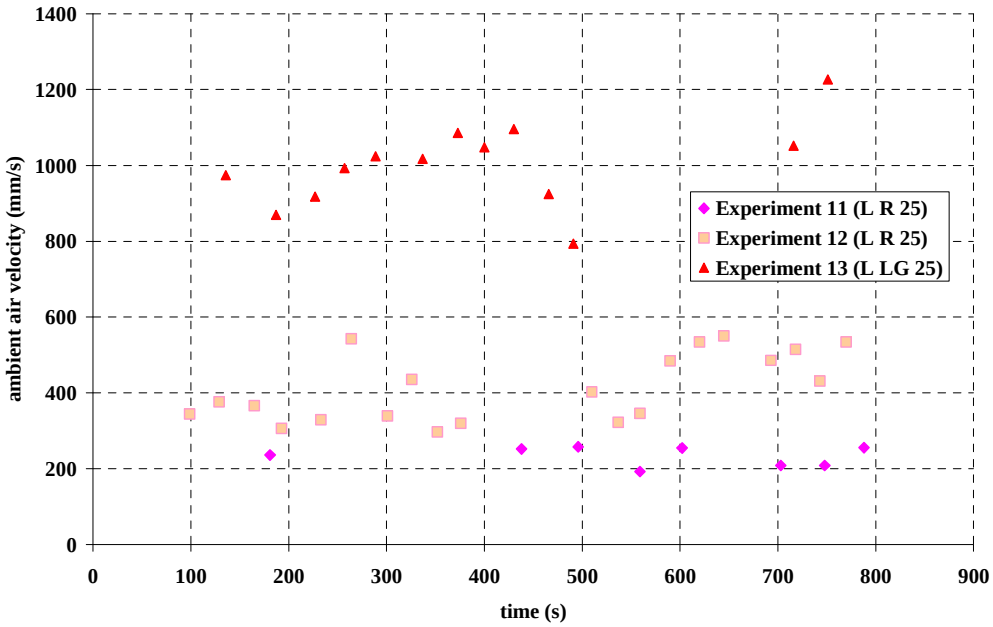

Regular 500mm Sample Experiments

Heat Flux Measurements

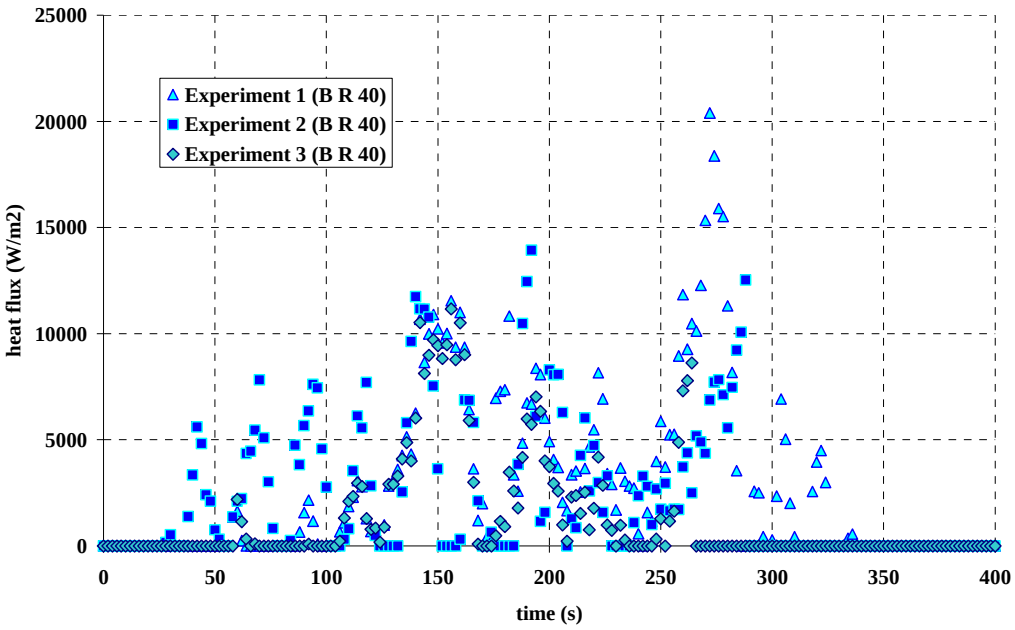

Benchmark Style 200mm Sample Experiments

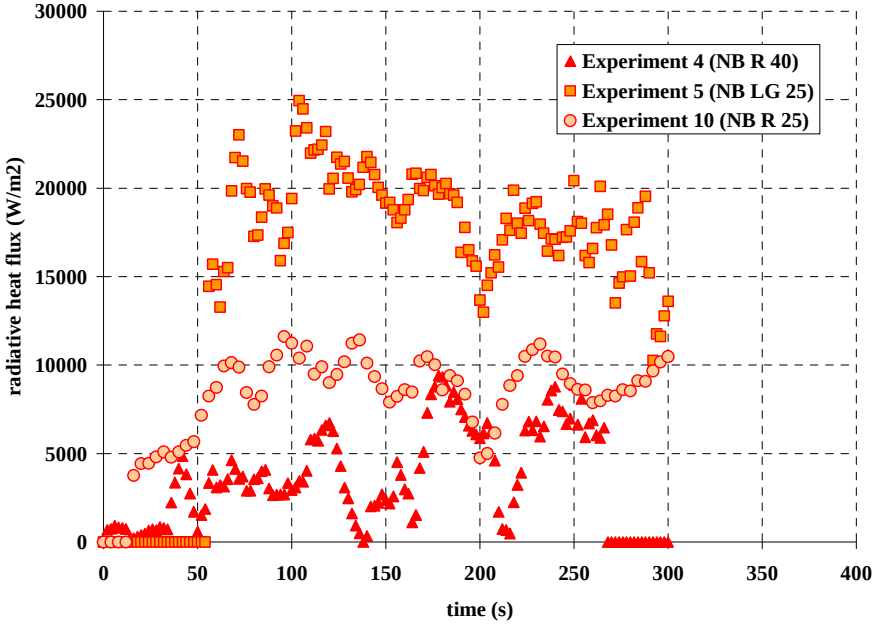

Regular 200mm Sample Experiments

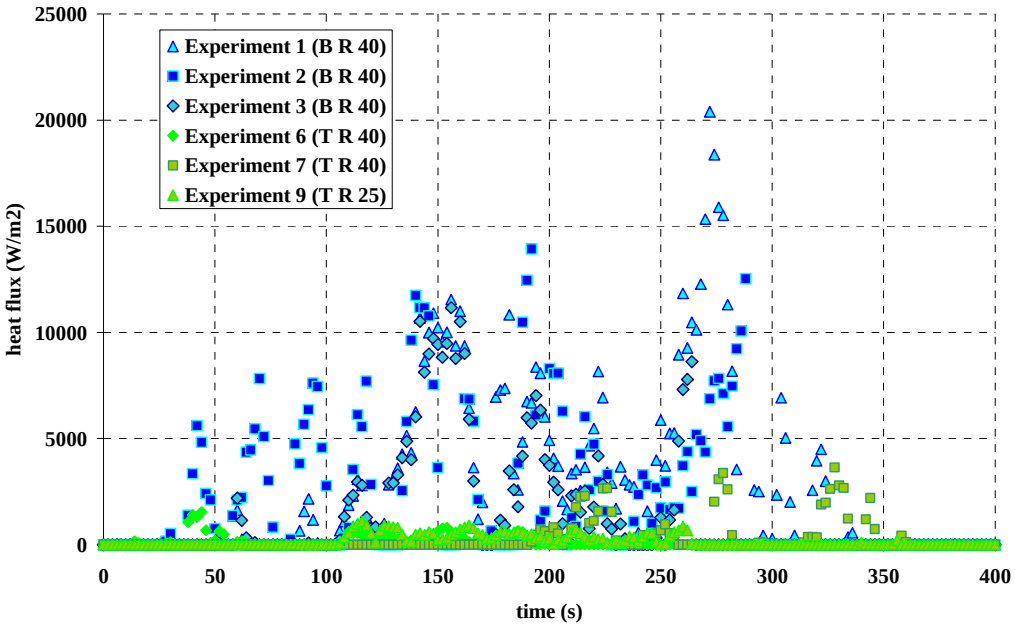

Tilted 200mm Sample Experiments

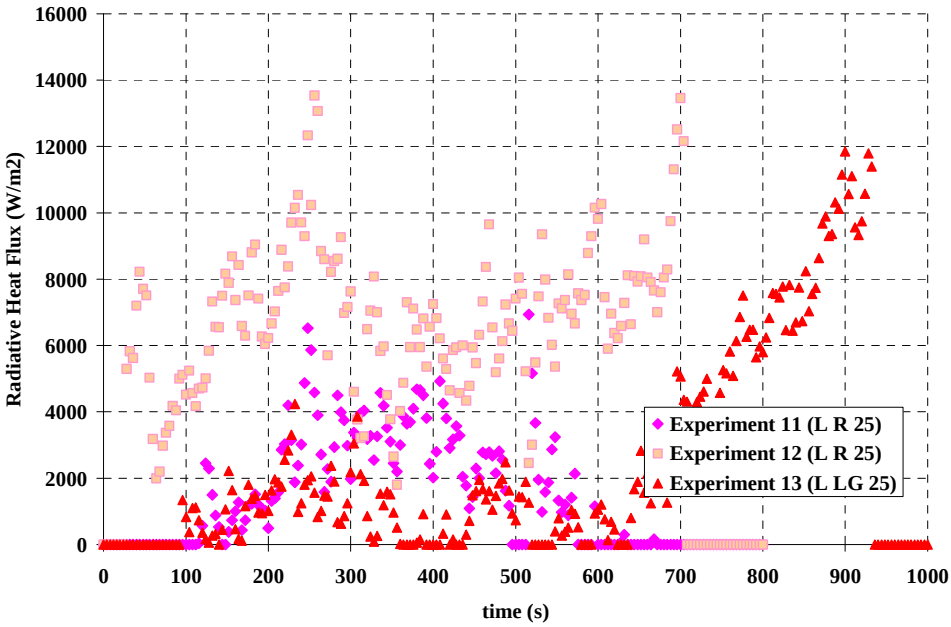

Regular 500mm Sample Experiments

Flame Temperature Measurements

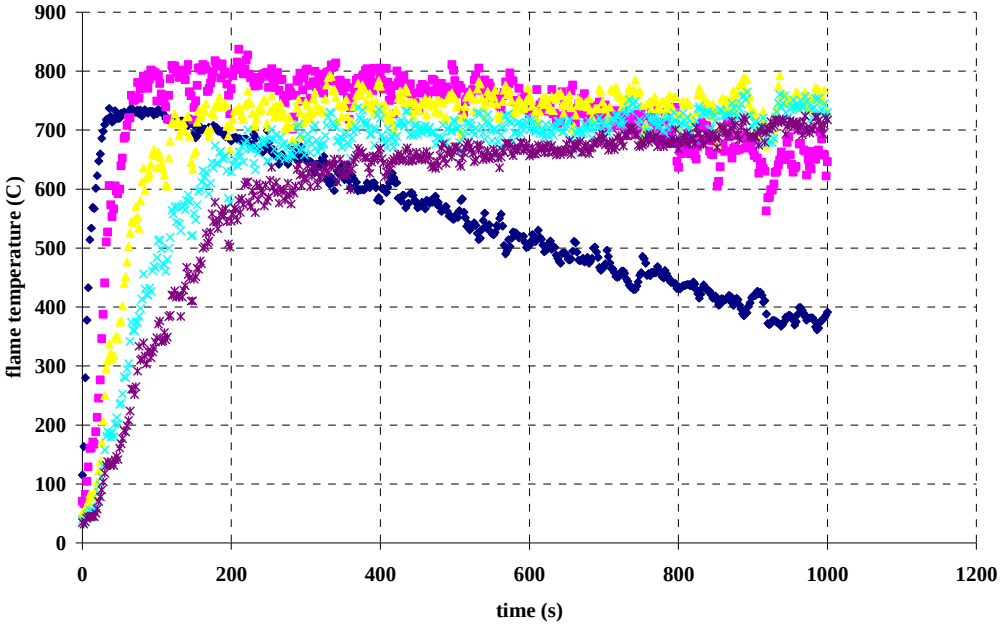

Experiment 1

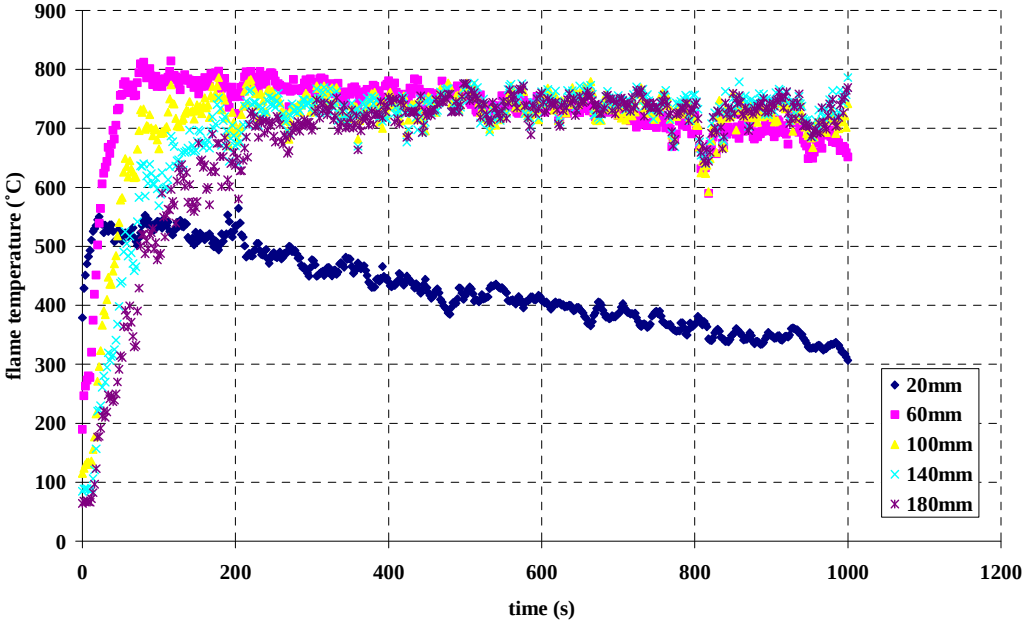

Experiment 2

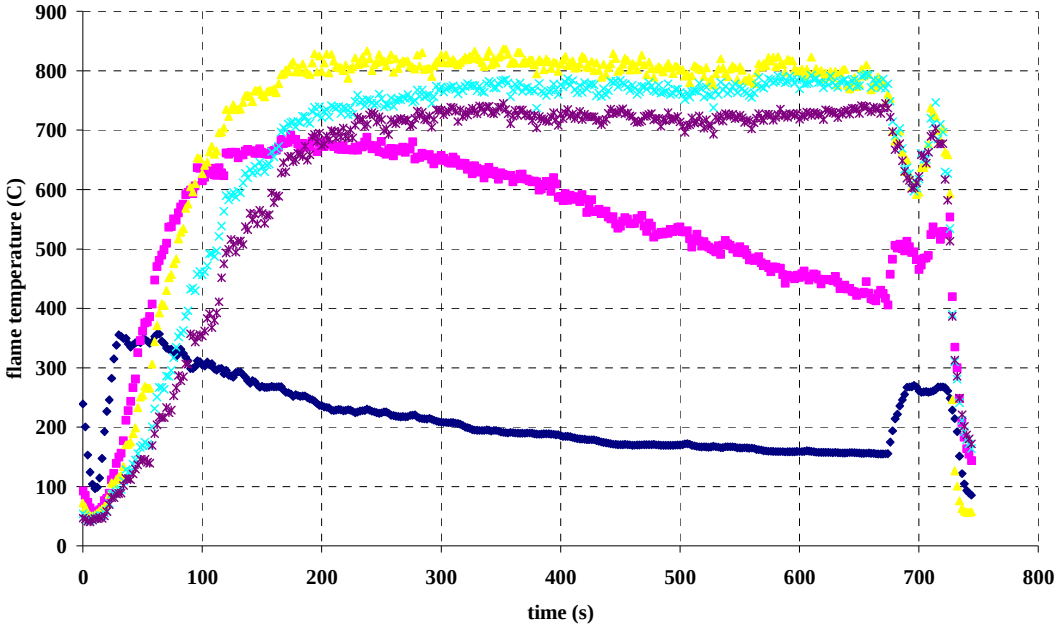

Experiment 3

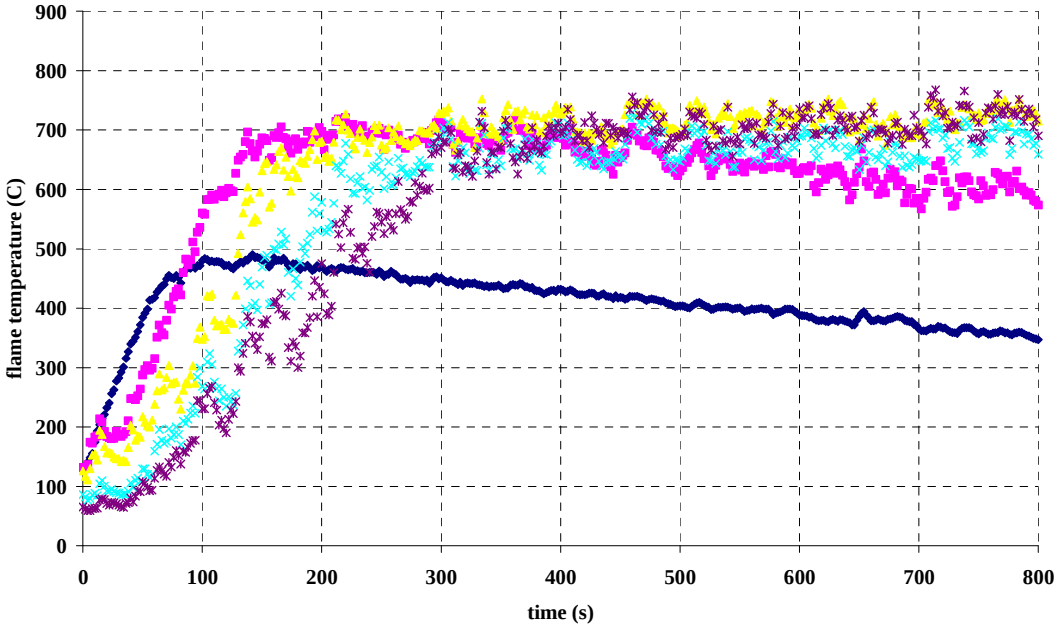

Experiment 4

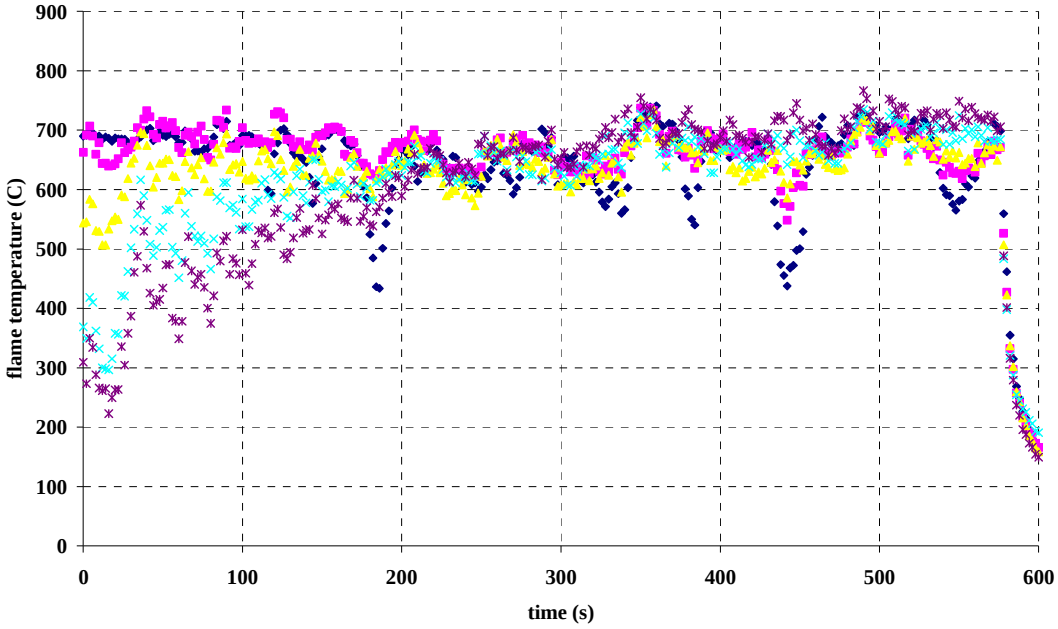

Experiment 5

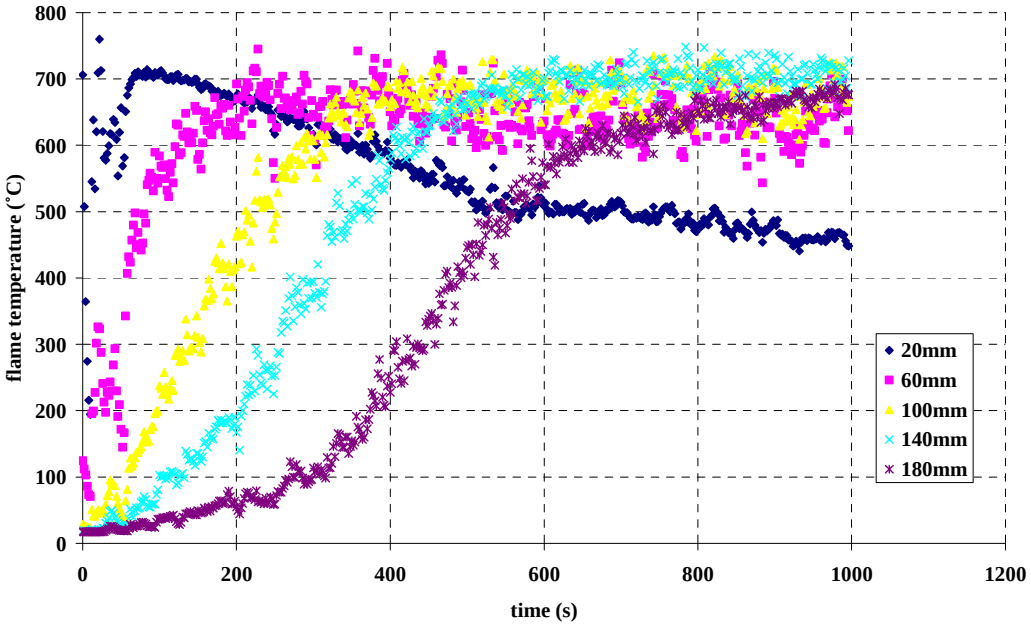

Experiment 6

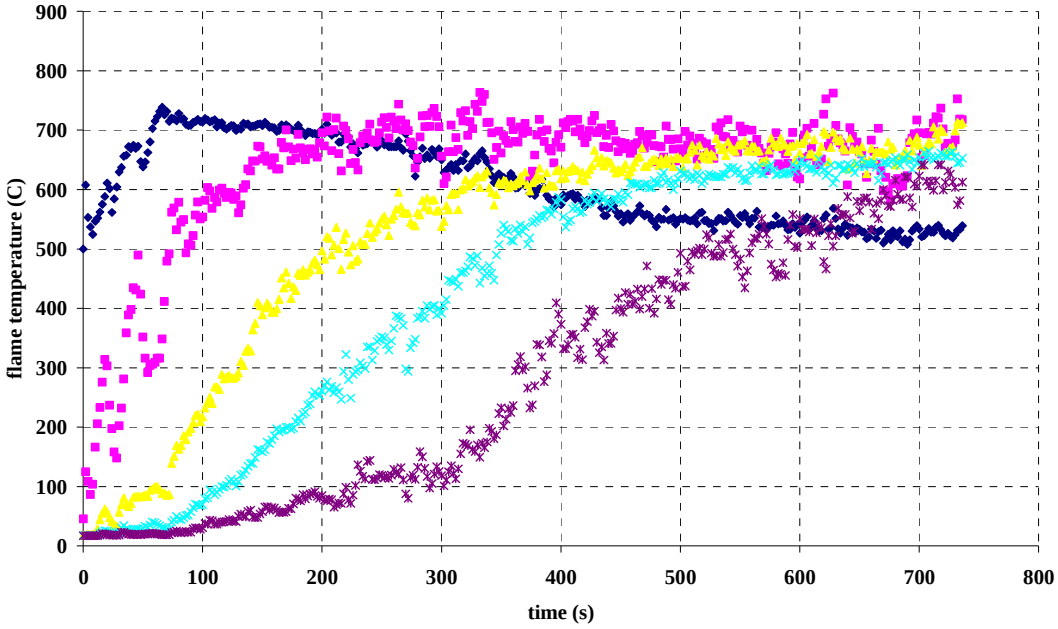

Experiment 7

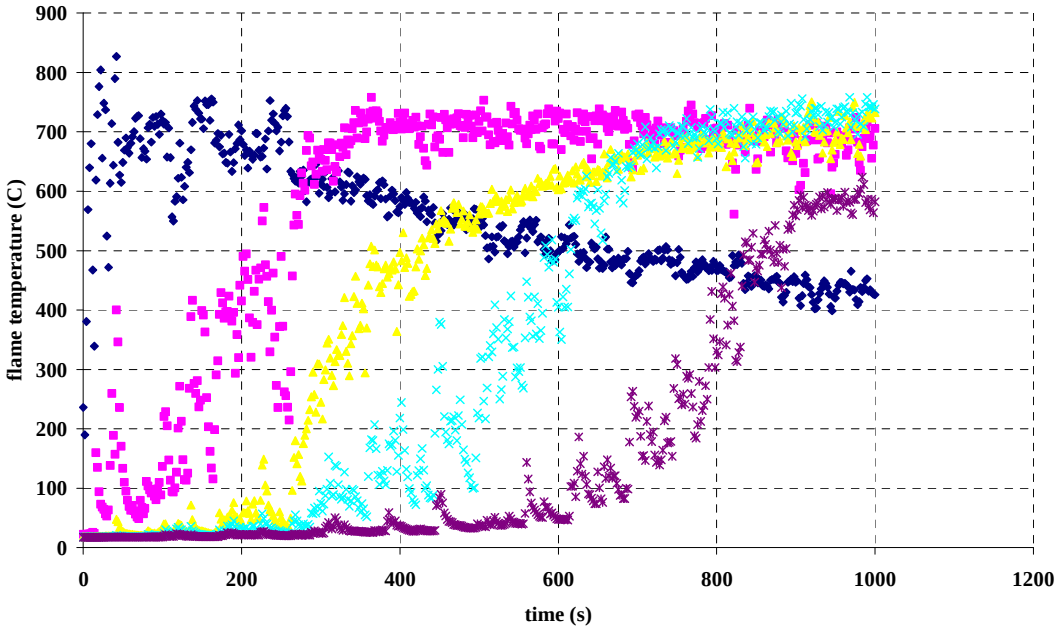

Experiment 9

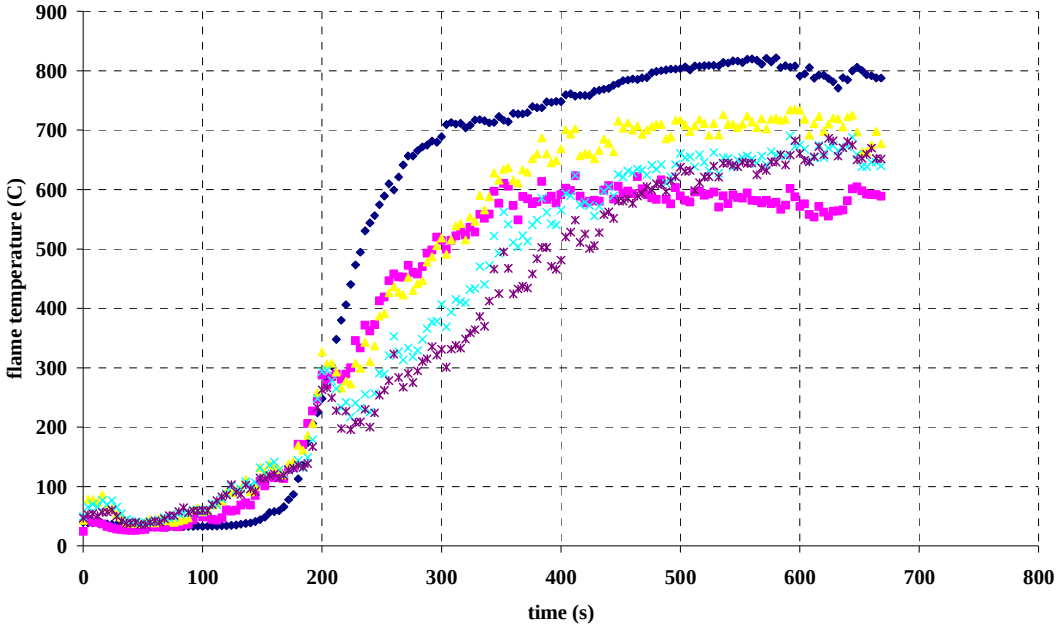

Experiment 10

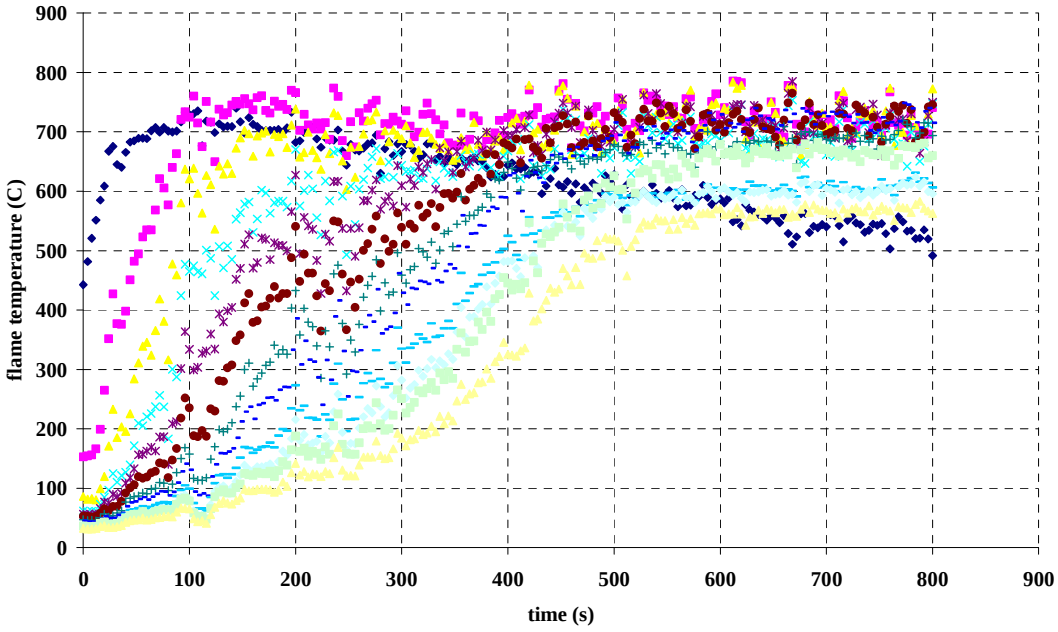

Experiment 11

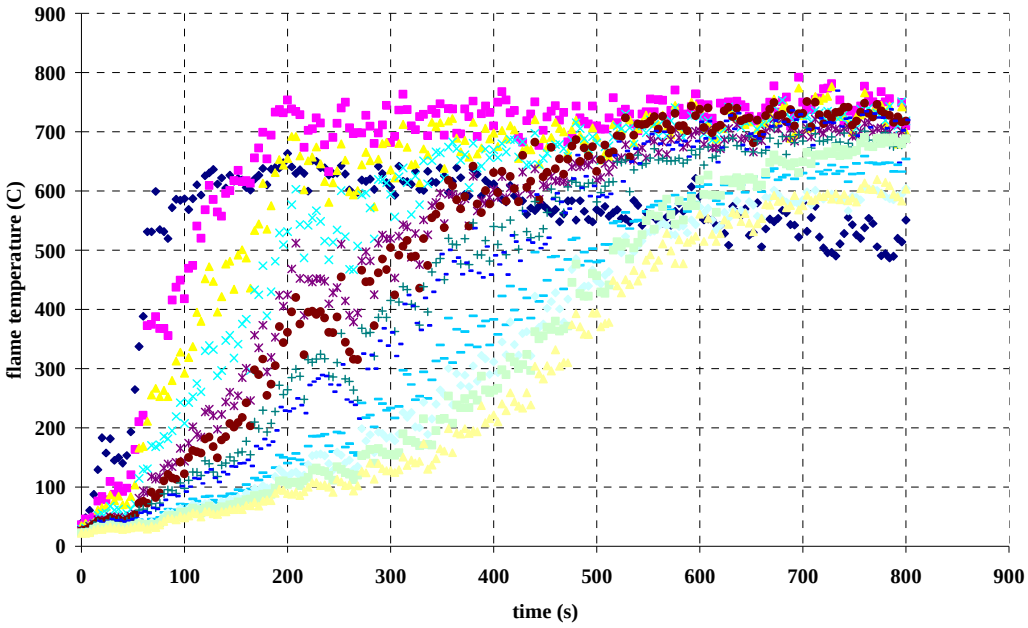

Experiment 12

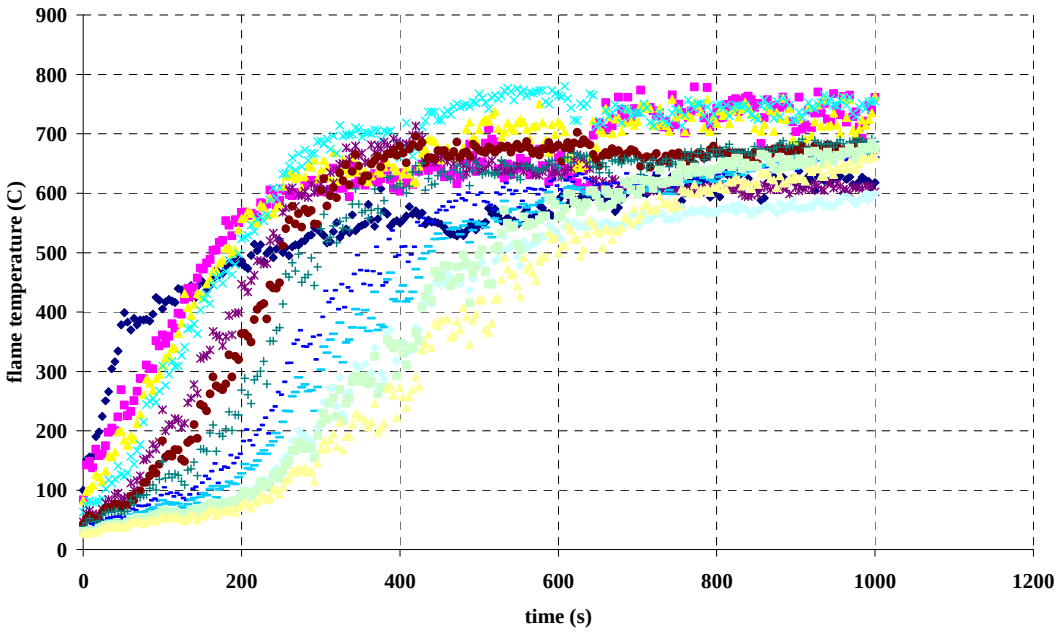

Experiment 13